SCTM 186-59-(14)

THE THEORY AND DESIGN OF THE TRIGGERED SPARK GAP

T. J. Williams - 1451-2

ABSTRACT

The purpose of this paper is to establish the basic theory of operation of the triggered spark gap, and to provide as much qualitative and quantitative engineering design data as the state of the art will allow.

From the basic two-electrode gap, a three-electrode or triggered gap model is established with its static and dynamic triggering characteristics shown. Several geometry conditions such as gap spacing, trigger electrode hole size, and insulator effects are discussed, showing their influence upon the triggering mechanism. A suggested trigger mechanism is given based on that proposed by Sletten and Lewis for the trigatron and modified to fit the present analysis.

Third reprinting
December 7, 1962

Case No. 778.11 * * May 22, 1959

LEGAL NOTICE

This report was prepared as an account of Government sponsored work. Neither the United States, nor the Commission, nor any person acting on behalf of the Commission:

A. Makes any warranty or representation, express or implied, with respect to the accuracy, completeness, or usefulness of the information contained in this report, or that the use of any information, apparatus, method, or process disclosed in this report may not infringe privately owned rights; or

B. Assumes any liabilities with respect to the use of, or for damages resulting from the use of any information, apparatus, method, or process disclosed in this report.

As used in the above, "person acting on behalf of the Commission" includes any employee or contractor of the Commission to the extent that such employee or contractor prepares, handles or distributes, or provides access to, any information pursuant to his employment or contract with the Commission.

Printed in USA. Price $3.00 . Available from the Office of Technical Services, Department of Commerce, Washington 25, D. C.

ACKNOWLEDGMENT

Special thanks are extended to my colleagues at Sandia Corporation, Messrs. K. J. Urquhart, C. I. Votaw, and R. C. Reineke for their encouragement and assistance, and to C. J. Henry and E. J. Szyper, who assisted in many of the laboratory experiments.

To Dr. Ahmed Erteza of the University of New Mexico, sincere appreciation is expressed for his critical review of the manuscript.

TABLE OF CONTENTS

TABLE OF CONTENTS (continued)

LIST OF ILLUSTRATIONS

LIST OF ILLUSTRATIONS (continued)

LIST OF ILLUSTRATIONS (continued)

LIST OF ILLUSTRATIONS (continued)

LIST OF ILLUSTRATIONS (continued)

LIST OF TABLES

THE THEORY AND DESIGN OF THE TRIGGERED SPARK GAP

CH I -- INTRODUCTION

Present day power and electronic requirements are continually increasing the demand for devices employing the electrical breakdown of gases. The application of the spark discharge principle is particularly attractive as a switching component because of its ability to go from a very good insulator to an almost perfect conductor in a fraction of a microsecond and to recover to the insulating state again in an extremely short period. Two-electrode spark gaps have been used as high-voltage voltmeters, electronic switches, and overvoltage protection devices for many years and are still in use. Commercial two-electrode safety gaps are presently available as overvoltage protection devices.

The two-electrode gap has also been used very extensively as a switching device in radar modulator systems and other pulse-forming circuits. In general, the switching action occurs by exceeding the breakdown voltage of the gap until the gap breaks down and conduction occurs. The application of several gaps in series, where the intentional breakdown of one gap set at a low breakdown voltage causes the remaining gaps to be overstressed with a resultant breakdown of the entire chain, has been widely used.

A review of the literature shows that a considerable amount of data have been obtained concerning two-electrode spark discharges, and several theories have been postulated as to the mechanism of breakdown over certain limiting regions. However, this field is still highly emperical since no theory postulated to date fully explains all of the observed phenomena, and there is often incomplete and conflicting data concerning these phenomena. This review of the literature also reveals that only a token amount of work has been published to date on the three-electrode or triggered spark gap.

The original trigatron discussed by Craggs, Haine, and Meek,[1] the recent work by Broadbent of the University of Manchester,[2] the work of Cullington, Chace, and Morgan[3] of the Geophysics Research Directorate, Air Force Cambridge Research Center, the recent work of Sletten and Lewis,[16] and the work of J. Gonz and J. Goldberg[4] of Edgerton, Germeshausen, and Grier, Inc. are the only principal references available to date. Most of the theoretical work done on the triggered spark gap has been for gaps with large gap spacing with holdoff voltages of 20 to 100 kv, while this paper is primarily concerned with gaps with small spacings having holdoff voltages from 3 to 10 kv. Since there is a relatively limited amount of reference material available on the theory of the triggered spark gap, there are many areas that have not been investigated and many areas that require additional and supporting study. The author has investigated many of these areas and the results are reported herein. In brief, the purpose of this paper is to establish the basic theory of operation of the triggered spark gap, and to provide as much qualitative and quantitive engineering design data as the state of the art will allow.

The first chapter of this report reviews some of the possible applications of the triggered spark gap such as a circuit component for pulse generators, protection devices, light-pulse generation, and other laboratory applications where the fast switching of high peak current at high voltage is concerned. The second chapter deals with the analysis of the breakdown of various two-electrode geometries and the correlation of established emperical formulae to the triggered spark-gap problem. After establishing this correlation, Chapter III establishes the basic operation and characteristics of the three-electrode or triggered gap. Based on the results of Chapter III, a static model is established in order to arrive at a means of estimating the dynamic characteristics of the gap. The static model then progresses into the static trigger curve and the various modes of operation showing the characteristic trigger curve for each mode. The effect of the dynamic trigger pulse for various rates of rise of the pulse is given. As will be shown later, the value of the trigger probe breakdown voltage coupled with the capacity level of the trigger circuit plays a major role in the triggering mechanism of the gap. The dynamic characteristics of the various operating modes are discussed, and the resultant influence of the applied gap voltage, pressure, spacing, and other variables is established. Delay time between the initiation of the trigger spark and conduction of the main gap is reviewed along with some of its influencing variables. Chapter IV discusses the important subject of the effect of geometry factors on the triggering and delay time characteristics. Chapter V gives a brief discussion for multiprobe triggered gaps where the initiating trigger signal can be applied to one or more trigger elements.

Chapter IV discusses a few miscellaneous practical design considerations that are important to the design engineer. Chapter VII then concludes the paper with a review of the experimental data and a discussion of the various contributors to the mechanism of breakdown during the triggering cycle. Basically, this mechanism is considered to be primarily attributed to the propagation of a low-density region caused by the heat dissipation of the trigger spark coupled with the space charge effects as a result of the ionization products generated within this region.

Typical Uses of a Triggered Spark Gap

General Considerations

Present day work in the field of electronics requires many applications where a fast switching device is required. For low-power and low-voltage systems, the use of transistors and vacuum tubes is satisfactory in handling currents up to a few amperes. If a few hundred amperes are required, cold-cathode trigger tubes and thyratrons can be used. When the voltages involved become higher and the current required is in the order of 5000 amperes, ignitrons are required. For very high operating voltages and when tens and hundreds of thousands of amperes are required, the triggered spark gap becomes of use. The triggered spark gap is especially suitable when only single pulse currents are required. It has been estimated by workers in the field that there appears to be no real limit to the currents which can be handled by the spark gaps, provided adequate cooling and support of the electrodes is maintained.

Spark gaps, while not only passing extremely high currents with a relatively low voltage drop, can handle high voltages in a small space. The sealed type of spark gap is normally unaffected by variations in ambient temperature, by changes in ambient pressure or by humidity. Practical triggered spark gaps can be made smaller than conventional vacuum tubes for certain applications. They can also be made very rugged, being able to withstand high impact shocks. They require no heater power and are consequently ready for operation at any instant, even after long periods of inactive shelf life. Total delay times of 0.1 μsec or less with jitter of 0.06 μsec are obtainable with proper design.

High-Voltage Equipment Protection Devices

As mentioned above, the early use of the two-electrode spark gap was in the role of a calibrating voltmeter for very high voltage. In present day uses, the two-electrode gap is used to provide overvoltage protection to voltmeters[9] as shown in Fig. 1. If the voltage across the meter exceeds the breakdown rating of the gap, the gap will conduct and remove the high voltage from the meter.

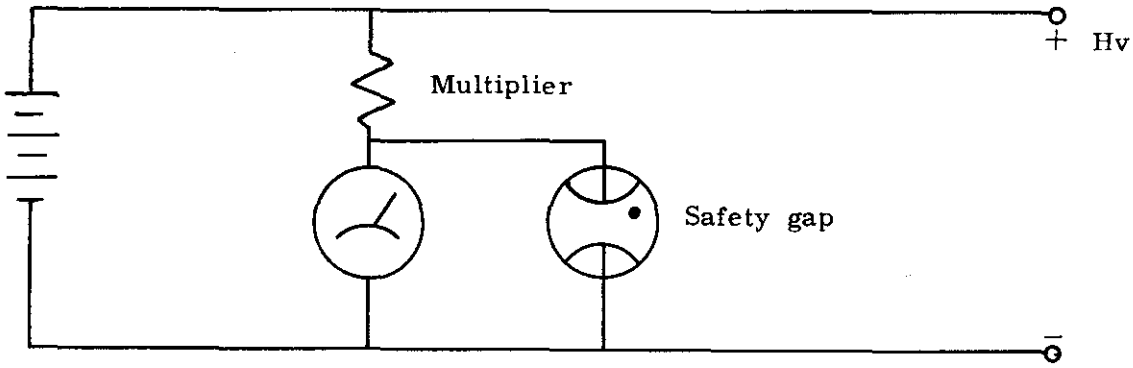

Fig. 1 -- Gap protection circuit

Similar examples are: the use of two-electrode gaps for transformer protection from possible secondary overvoltage in case of load failure, and their use for protecting charging coils and pulse-forming networks from surge damage.

A triggered gap can be used as a protection device as shown in Fig. 2.

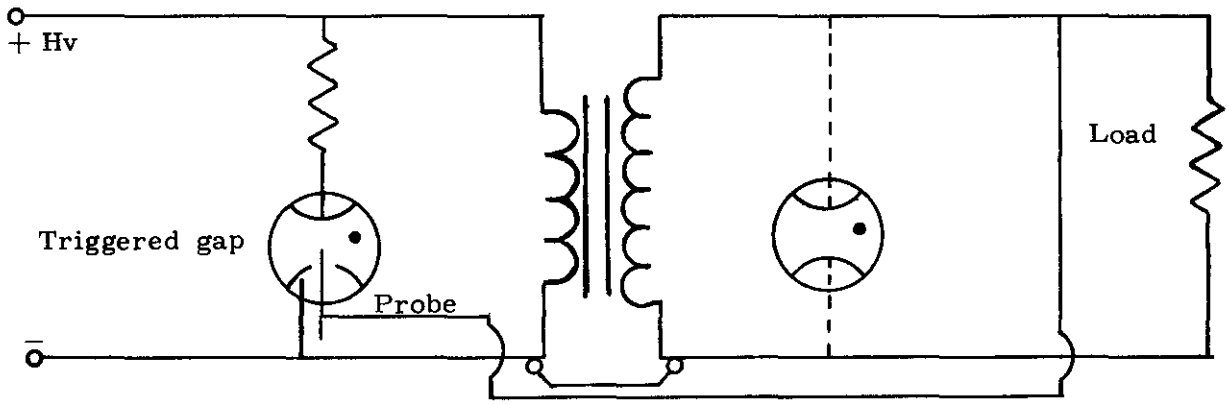

Fig. 2 -- Protective triggered gap circuit

Figure 2 is essentially the same overvoltage protection device for the transformer secondary mentioned above, but providing added protection to the transformer in the event of large current flow. If just the two-electrode gap is used across the transformer secondary, the gap will protect for overvoltages, but will allow a short-circuit current to flow. In certain applications the transformer may be damaged due to excessive current. The use of the triggered gap allows the trigger spark, caused by the probe breakdown due to secondary overvoltage,

to ionize the main gap. When the main gap conducts, the transformer is completely isolated from the input circuit since it is in parallel with the primary terminals.

Figure 3 shows a possible use as an interlock protection for high voltage and lethal energy-storage elements. When the interlock opens, the collapsing field of the primary causes a trigger voltage to be developed at the probe and the trigger spark is formed, the main gap is ionized, and the capacitor then rapidly and safely discharges through the main arc of the gap.

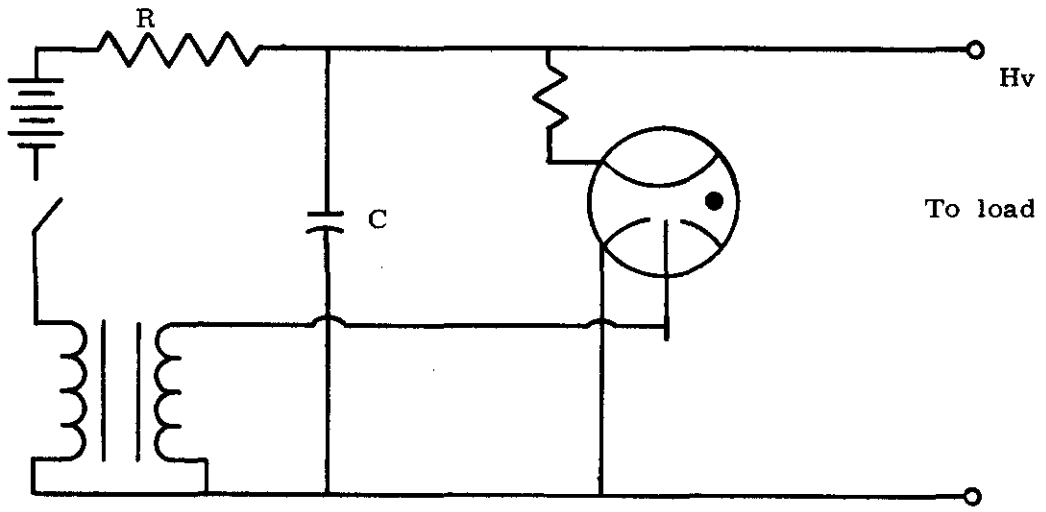

Fig. 3 -- Gap interlock circuit

Switch for Pulse Generators

In certain applications the triggered spark gap can be employed as the switching device for pulse generators. In general, the triggered spark gap could be employed in circuits similar to those employing the conventional thyratron but where the peak current requirements are much higher. A typical pulse generator is shown in Fig. 4.

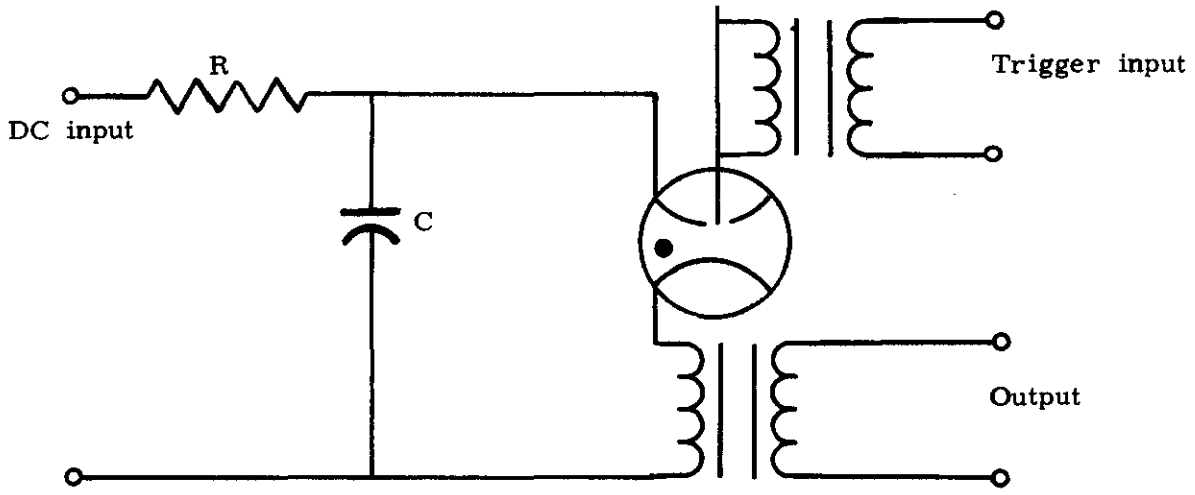

Fig. 4 -- Typical pulse generator circuit

The capacitor is charged to some voltage below the static breakdown voltage of the gap. At the desired time, a trigger signal is applied to the probe causing the probe to break down. The trigger spark then, in turn, causes the main gap to break down and the capacitor discharges through the primary of the output transformer generating the required pulse.

The original triggered spark gap, or trigatron, was developed by Craggs, Haine, and Meek, for use in radar modulators during World War II. The trigatrons were mainly filled with argon, with an addition of 7-percent oxygen to stabilize triggering for high pulse repetition rates. Their operating voltages of several types were from 5 to 24 kv. The pulse rate varied from 400 to 1200 pulses per second with a life of 600 to 2000 hours. The pulse energies varied from 170 to 500 kw and had pulse durations of 1 to 2 μsec. In addition to this original trigatron, later versions have also been operated up to 160 kv.

Typical modulator circuits employing the triggered spark gap are shown in Fig. 5. In the modulating circuit, the triggered spark gap is used to control the discharge of an impedance network, such as an artificial transmission line, to generate a square voltage pulse across a matched load.

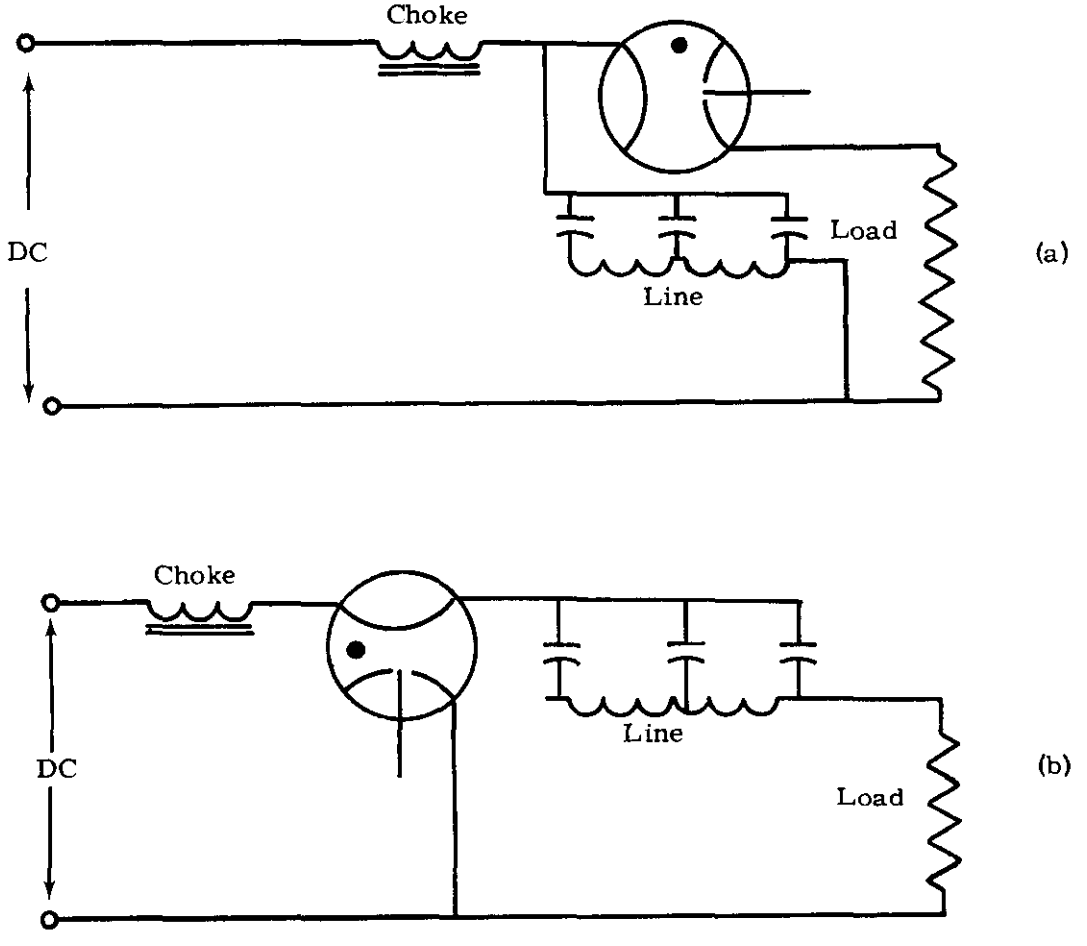

Fig. 5 -- Basic modulator circuits

Several combinations of the triggered spark gap can be employed to good advantage, depending on the requirements of the application. Some typical circuits suggested in the paper by Craggs, Haine, and Meek are shown in Figs. 6, 7, and 8.

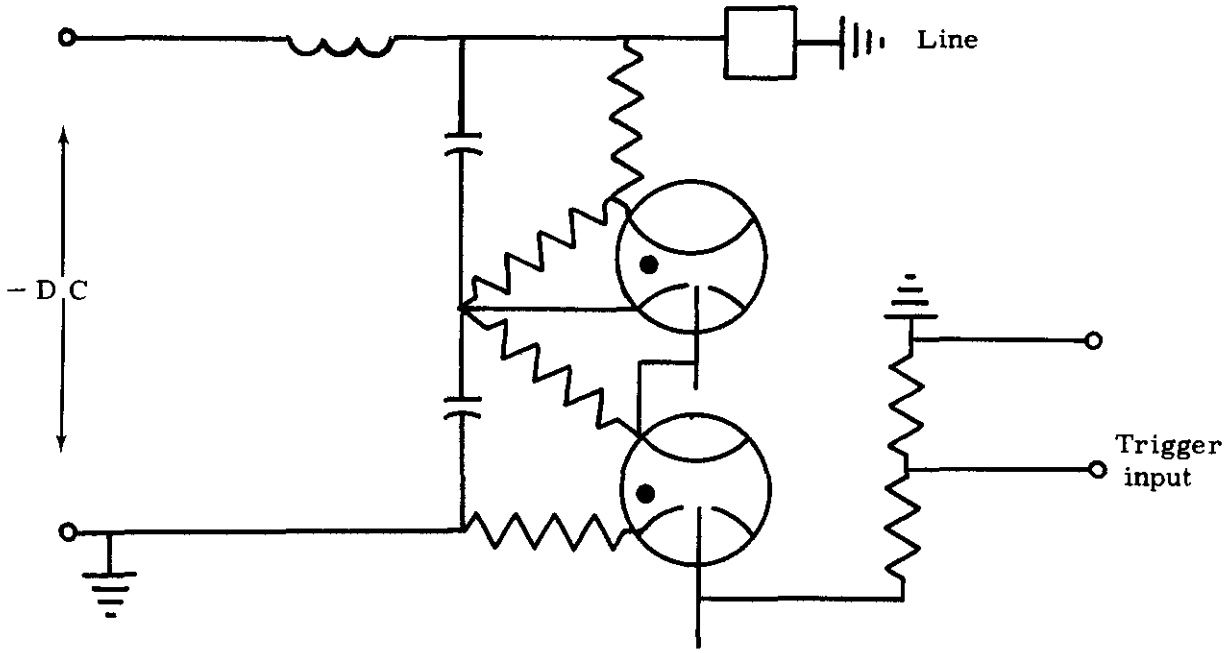

Fig. 6 -- Spark gaps in series

A series combination of two or more gaps allows control of higher voltages than are possible with a single gap. The first gap is triggered by an external pulse, and the second gap is triggered due to a coupling of a pulse from the discharging of the first gap. Such a system operates with a jitter lower than 0.1 μsec.

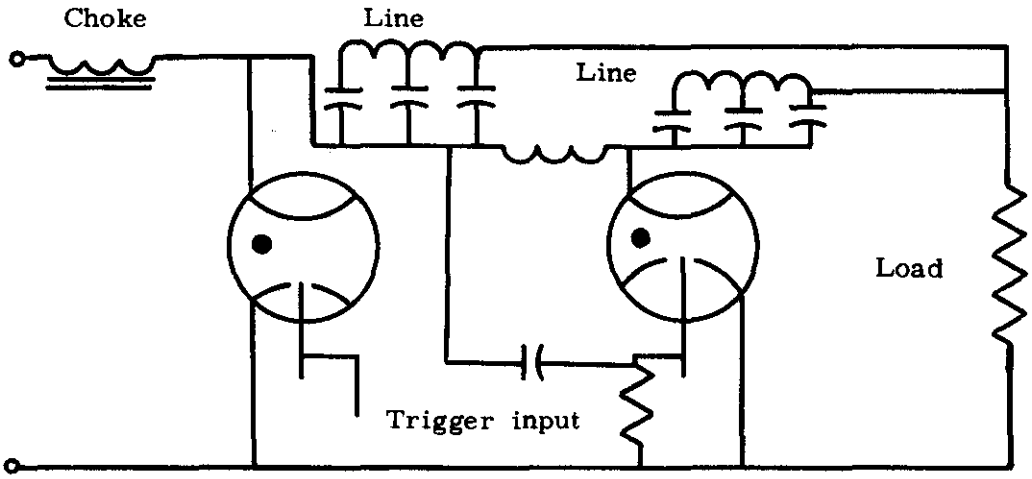

Fig. 7 -- Spark gaps in parallel

If it is desirable to increase the life of the switch tube, two or more gaps can be used in parallel so that the discharge current is shared between the gaps. The circuit of Fig. 7 includes two pulse networks, each of which is discharged by separate gaps. One gap is triggered externally, and the second is triggered by breakdown of the first gap. Figure 8 shows a similar arrangement employing a center-tapped pulse transformer.

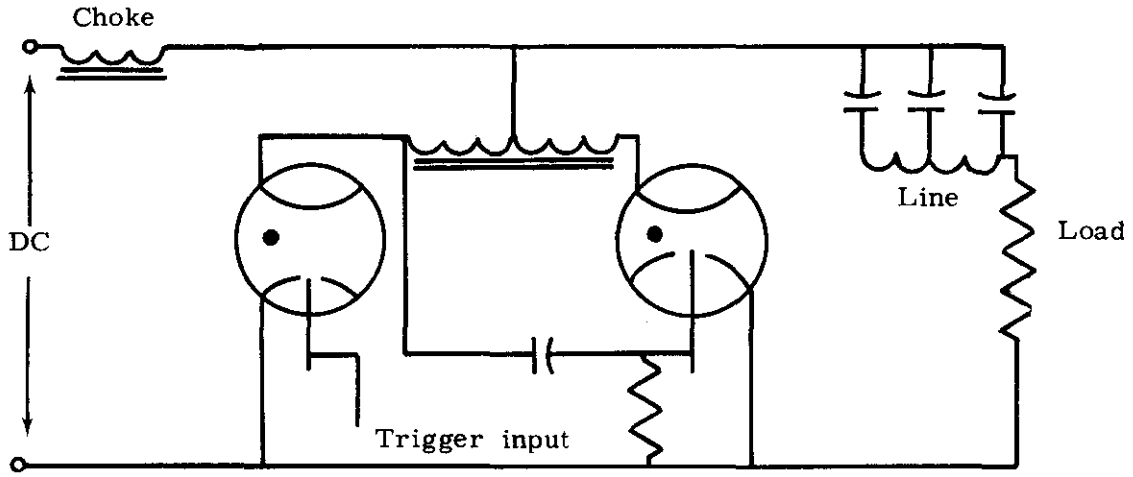

Fig. 8 -- Spark gaps in parallel

The two gaps are triggered as before, one externally and the other due to the breakdown of the first. After breakdown of both gaps, the currents are equalized automatically by the transformer. Since the two halves of the transformer winding are in opposition, the transformer offers a low impedance to the discharge.

Fast-Acting Current Switch for Laboratory Work

The previous sections discussed the triggered gap as a circuit component that would generally be small in size, vacuum-tight, capable of being mass-produced, and capable of passing moderate current reliably many times and at moderate voltages. There is also the very broad field of the triggered spark gap that is used in the laboratory. Whether or not the triggered spark gap is a circuit component or a piece of laboratory equipment, the principles discussed in this paper still apply. The laboratory gap differs from a gap used as a circuit component in several ways. It may be much larger, open to atmospheric variations, demountable for easy reconditioning of the electrode surfaces, operate at higher voltages with wider gap spacings, and pass extremely high currents.

W. Kleen[5] in his experiments with exploding wires employed a test setup as shown in Fig. 9. This arrangement consisted of an AC source charging a 7.2×10^{-2} μf capacitor to approximately 18 kv. A two-electrode spark gap was previously adjusted to have a pulse breakdown voltage of about 18 kv. When the capacitor was charged to 18 kv, the gap broke down, discharging the capacitor into the thin wire. The resultant rapid discharge of energy into the wire then caused it to disintegrate.

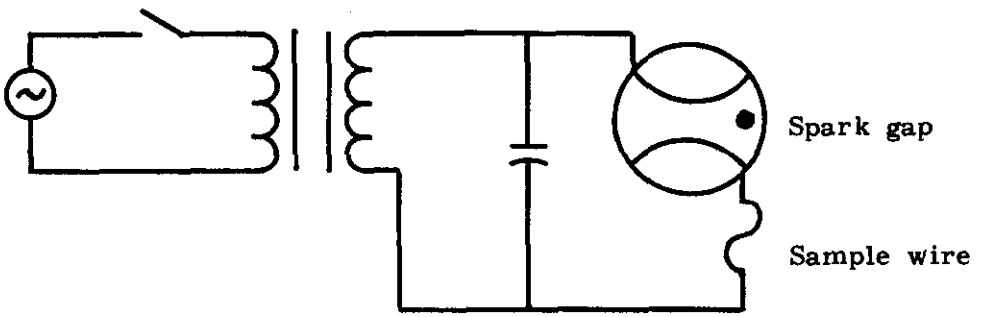

Fig. 9 -- Circuit for investigation of exploding wires

A similar arrangement was employed by Bethge[6] in his investigation of the mechanical deformation of wires by electrical discharges. As seen in Fig. 10, Bethge allowed a capacitor to be charged to some steady voltage below the breakdown voltage of the gap.

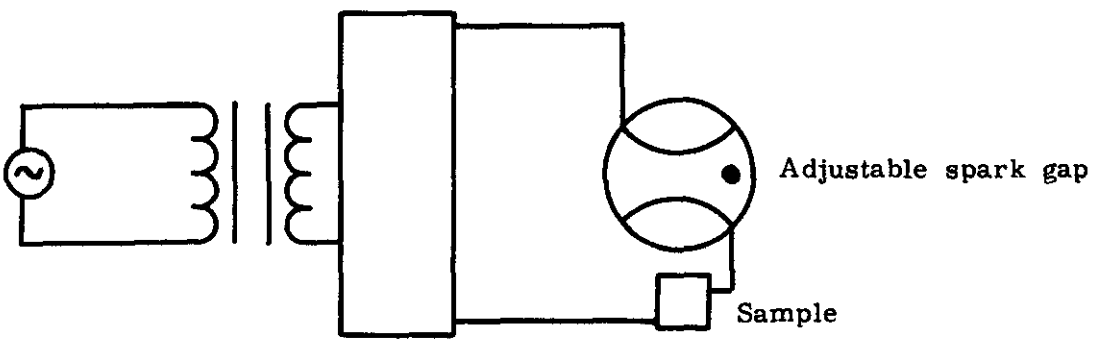

Fig. 10 -- Circuit for investigating deformation of wires electrical discharges

The source and the rectificer were disconnected from the capacitor , and a micrometer connection to one of the electrodes was adjusted, thereby reducing the gap spacing until breakdown occurred. The resultant discharge would then rapidly pass through the wire, causing the wire to take a permanent deformation.

The triggered spark gap could be used to advantage in a similar situation and could be connected as shown in Fig. 11. Use of the triggered gap allows a quick variable adjustment of the capacitor voltage, and rapid and repeatable discharges at voltages much below the static breakdown value of the gap itself. In later work by Zarem, Marshall, and Poole,[7] a triggered spark-gap arrangement similar to Fig. 11 was employed in their investigation of the exploding wire. Also, more recently, Cullington, Chace, and Morgan[3] have used the triggered spark gap in their investigation of the exploding wire. They have termed their gap the "Lovoltatron," which is very similar to the original trigatron, but operates in atmospheric air at lower voltages.

In addition to the above applications, a circuit similar to Fig. 11 could be utilized as a light generation system with rapid initiation speeds and low jitter. More recently, in the work of J. L. Tuck and associates at Los Alamos,[8] the triggered spark gap has been employed in studying the pinch effect. The pinch effect is basically the self-attraction of parallel electric currents. At high currents, fluid metal conductors have a tendency to pinch off. The same basic effect can apply to gases and, in a sustained constricted discharge, extremely high

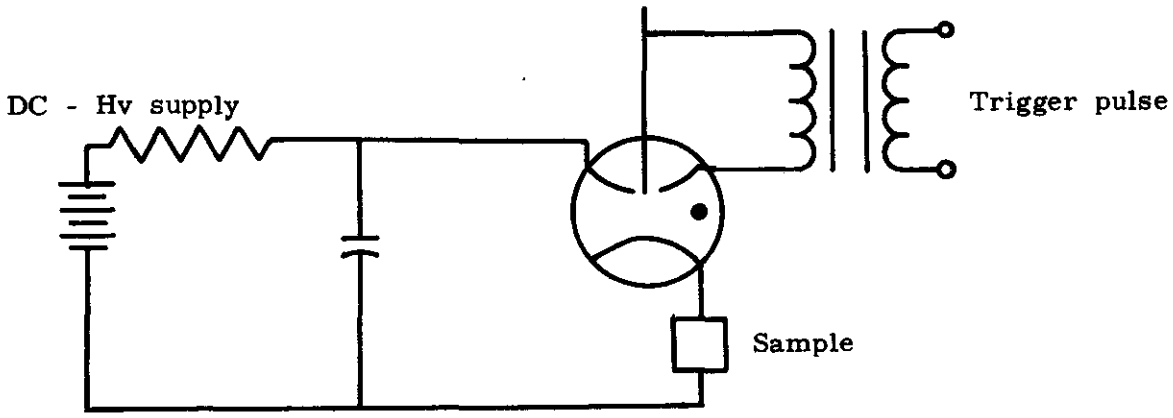

Fig. 11 -- Circuit for investigating exploding wires

temperatures can be obtained. If the temperatures can become high enough, a fusion reaction can take place. One of the methods employed to obtain a pinch discharge is the use of two sphere gaps in series. This is referred to as the straight-type or "Columbus" discharge system between electrodes in a straight tube as contrasted with the "Perhapsatron" or endless discharge system which is excited by magnetic induction in a torus. The straight-type discharge system is shown schematically in Fig. 12.

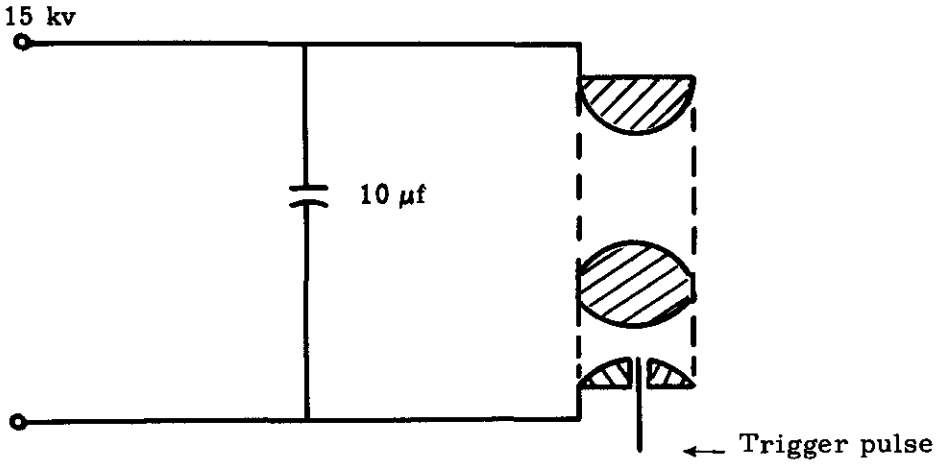

Fig. 12 -- Pinch discharge system

The combination of both gaps in series will hold off the input of 15 kv. When a trigger pulse is applied to the probe of the triggered gap, the gap breaks down, thereby placing the full applied 15 kv across the discharge tube, which in turn immediately conducts, and the discharge is complete.

A similar type of straight pinch discharge tube has been employed by the University of California Ernest O. Lawrence Radiation Laboratory at Livermore, California[10], in its work on the AEC project "Sherwood." Sherwood is the peacetime application of the fusion reaction. The Livermore tube switches 12 μf at 50 kv by means of a spark gap in series with the pinch tube.

Basic Principle of the Triggered Spark Gap

The conventional triggered spark gap is shown in Fig. 13 and consists of two main electrodes and an auxiliary or triggering electrode. The two main electrodes control the holdoff voltage of the gap and carry the current during switching. The triggering electrode, or probe, controls the initiation of the switching action. Upon the application of a suitable pulse to the probe, breakdown occurs and a trigger spark is formed to either the trigger electrode, which contains the probe, or to the main electrode, depending upon the gap design and the applied polarity of the electrodes. The initiation of the low-energy trigger spark then enhances ionization between the main electrodes, causing breakdown and completion of the triggering action.

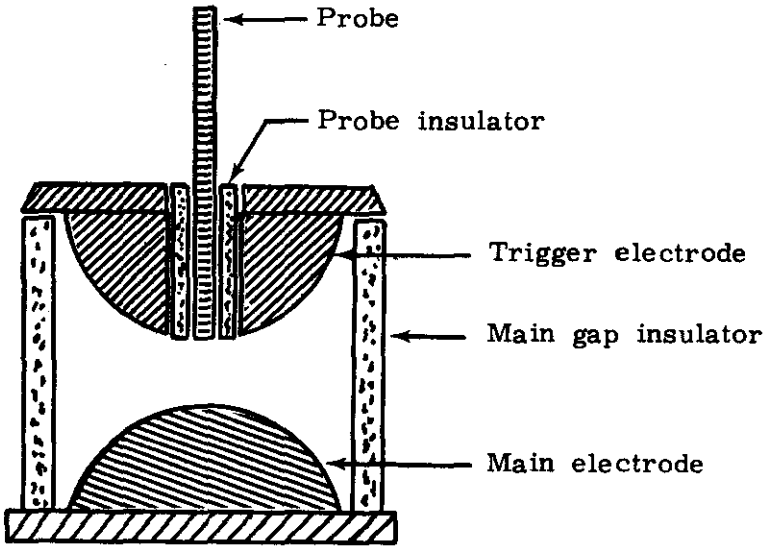

Fig. 13 -- Triggered spark gap

The original trigatron was designed to operate above 15,000 volts, and was originally believed to depend on the generation of corona and field distortion due to the trigger pulse, for its operation. The types of spark gaps investigated by this paper are designed to operate in the range from approximately 800 to 10,000 volts. However, the results obtained here also apply to higher operating voltages. In addition, the initiation of the switching action in these gaps is primarily attributable to the injection of electrons and ions by the trigger spark, with little or no contribution resulting from the corona and trigger pulse field distortion.

After the trigger spark has been initiated, there is a finite time delay between the start of trigger current flow and start of the main current flow. This time delay is termed the delay time of the gap. Dependent on the initial trigger current, the main gap voltage, gap geometry and other considerations, the main current may flow while trigger current is still flowing or it may vary up to several hundred microseconds after the start of trigger current. Delay times greater than this are also possible, but, in general, do not produce repeatable and consistent triggering.

While the basic idea of the triggered spark gap is relatively simple, the design factors for reliable and optimum operation are not so simple and require careful consideration and analysis. Variations of geometry, gas mixture, gas pressure, condition of the electrode surfaces, condition of the insulator surfaces, applied polarity to the electrodes, wave shape and duration of the trigger pulse, natural irradiation of the gap, and other factors all influence the operation of the triggered spark gap. These factors will be considered in more detail in the ensuing discussion.

Schematically, the triggered spark-gap switch in a normal switching application is as shown in Fig. 14. The equivalent circuit now appears as Fig. 15. The spark gap is essentially two switches ganged together, but with a response system in series with these switches. Switch S_1 can be considered the trigger spark, and the switching action is a function of pulse rise time, polarity, amplitude, the gap voltage, and the internal geometry of the probe. Once S_1 is closed, S_2 is closed through the response system and the intended switching action is complete. The response system is a function of the fill gas and pressure, current flow through the trigger spark, applied gap voltage, and the polarization of the gap. This response system will then close S_2 or not close S_2, depending on these parameters. The time required for this closing, in the case of a closure, can vary and will also be a function of the above parameters.

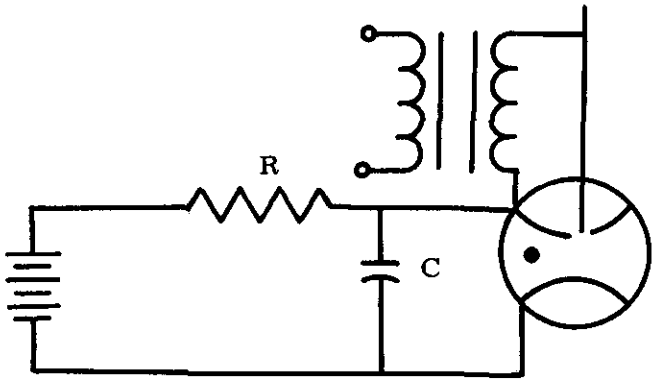

Fig. 14 -- Typical spark gap connection

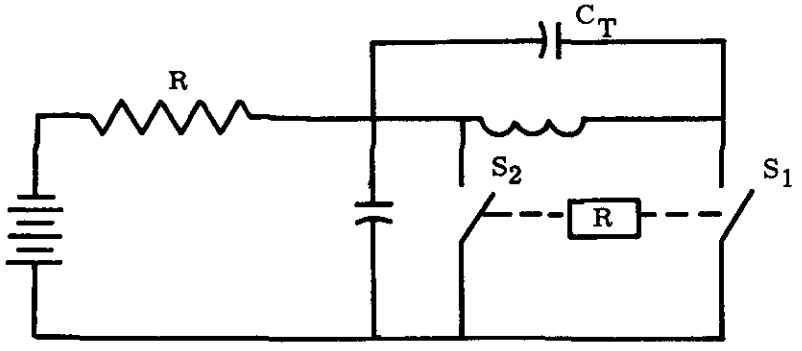

C_T = Secondary distributed capacity, wiring capacity, and probe input capacity

R = Response system

Fig. 15 -- Spark gap equivalent circuit

CH II -- THE TWO-ELECTRODE GAP

Breakdown Characteristics Under Static Conditions

Before the design of single and multiprobe spark gaps can be considered, the basic principles of the conventional two-electrode gaps must be understood. Analysis of symmetrical spherical electrodes will enable the main gap static breakdown to be determined for a given spherical radius, gap spacing, fill pressure, and gas mixture. Analysis of the coaxial wires, parallel wires, and asymmetrical spheres (point to plane) will provide design data for predicting the probe static breakdown voltages. Comparison of observed data will be made with accepted emperical formulae in order to establish the validity of these formulae to our particular application, and then to provide a basis of predicting the results of the more complex field interactions during the triggering interval. In general, the spacings and gas pressures used in the triggered gaps covered by this paper fall in the region that is generally governed by the Townsend Avalanche theory of primary and secondary ionizing mechanisms. There may also be regions of operations, however, where the streamer theory is valid or a combination of both, where an avalanche-to-streamer transition occurs. Once these basic relations are established, the development of the three-electrode or triggered gap can proceed.

Uniform Field - Symmetrical Spheres

The study of the breakdown of a two-electrode gap is a study of the dielectric field generated by the electrode configuration and applied voltage and the dielectric properties of the gas. Consider two large parallel plates where the edge effects are neglected (Fig. 16A).

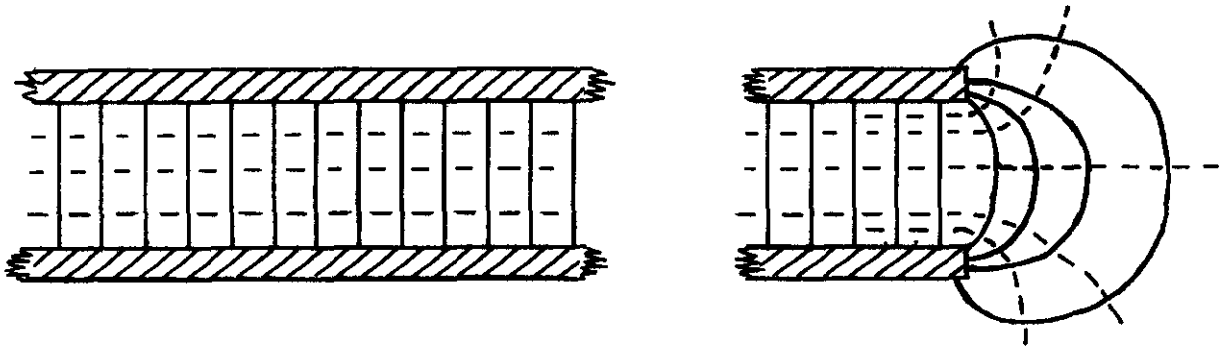

A B

Fig. 16 -- The dielectric field

If a voltage V is applied across the electrodes, a dielectric (or electrostatic) field is set up. These lines of dielectric force are everywhere parallel to each other and enter and leave the metallic conductor at right angles. Perpendicular to these lines of force are the equipotential surfaces which exist between the two conductors.

A given insulation breaks down at any point when the electric gradient at that point exceeds some given value. In order not to overstress the gaps at any point, the gradient should be uniform. Where there is a uniform gradient, the equipotential lines at right angles to the lines of force will be at constant intervals throughout the interelectrode spacing .

The generation of a uniform field by use of infinite parallel plates is not physically realizable, however. Parallel plates of small size could be considered, but they have nonuniform fields at the edges (Fig. 16B). Great concentration at the edges tends to generate higher gradients near the edges than the uniform gradient found between the parallel plates and, consequently, breakdown occurs at reduced voltages. The practical solution is to utilize spheres or portions of spheres which have a large radius compared to the gap spacing (Fig. 17). At the point of minimum gap spacing d, the field is practically uniform. A review of the literature shows that this is the method used by experimenters interested in gas breakdown in uniform fields. The larger the radius of the sphere (approaching infinity) and the smaller the gap spacing, the more uniform is the field.

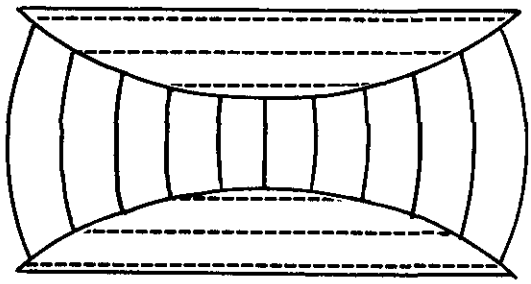

Fig. 17 -- Practical approach to the uniform field

For our considerations, however, we must use portions of spheres having a relatively small radius, with the result that we can only approximate the uniform field.

The holdoff or breakdown voltage of two electrodes generating a uniform field obeys Paschen's law, which states that breakdown is a function only of the product of pressure and spacing. Townsend's equation for conduction of current through a gas and, consequently, the basis for the breakdown criteria in a uniform field, is as follows:[11]

$$I = \frac{I_o e^{\alpha d}}{\left[1 - \left(\frac{\omega}{\alpha}\right)\left(e^{\alpha d} - 1\right)\right]} \qquad (1)$$

where

I = Current at the anode

d = The gap spacing in centimeters

α = Townsend's first coefficient, which is the number of new electron and ion pairs formed by one electron in traveling a distance of 1 cm through a gas

I_o = The initial current at the cathode caused by natural agents such as cosmic rays, ultraviolet radiation, etc.

ω/α = Secondary ionization processes.

α, the number of new electrons formed per electron per centimeter of path, will depend upon the gas, the number of collisions per incident electron traveling a distance d, and upon the energy this electron possesses when it collides with the gas molecules. The number of collisions possible is inversely proportional to the mean free path of the gas or, in other words, directly proportional to the pressure.* Likewise, the energy of a traveling electron will be directly proportional to the electric field intensity E and inversely proportional to the pressure. Thus α is proportional to p and proportional to some function of E/p. Mathematically, this is expressed as

$$\frac{\alpha}{p} = f_1\left(\frac{E}{p}\right). \tag{2}$$

A plot of α/p versus E/p can be found for the various gases in the literature, and some typical curves are shown in Fig. 18.

In addition to the direct formation of electrons by the α mechanism, there is also the contribution of secondary processes β, γ, δ, and ε. β is the coefficient of ionization due to direct ionization of neutral atoms by positive ions; γ is defined as the number of electrons liberated from the cathode per incident positive ion; the number of photoelectrons emitted from the cathode per ionizing collision in the gas is δ/α; and cathode emission caused by incidence of excited atoms is expressed by ε/α. The relative contributions of these processes will vary with the gap parameters but, in general, the γ is probably the most prevalent. ω can be expressed as a function of E/p and therefore

$$\frac{\omega}{\alpha} = f_2\left(\frac{E}{p}\right). \tag{3}$$

Curves for γ plotted versus E/p can be found in the literature for various electrode materials and gases.

*This is a function of density and becomes a function of pressure when the temperature is assumed constant.

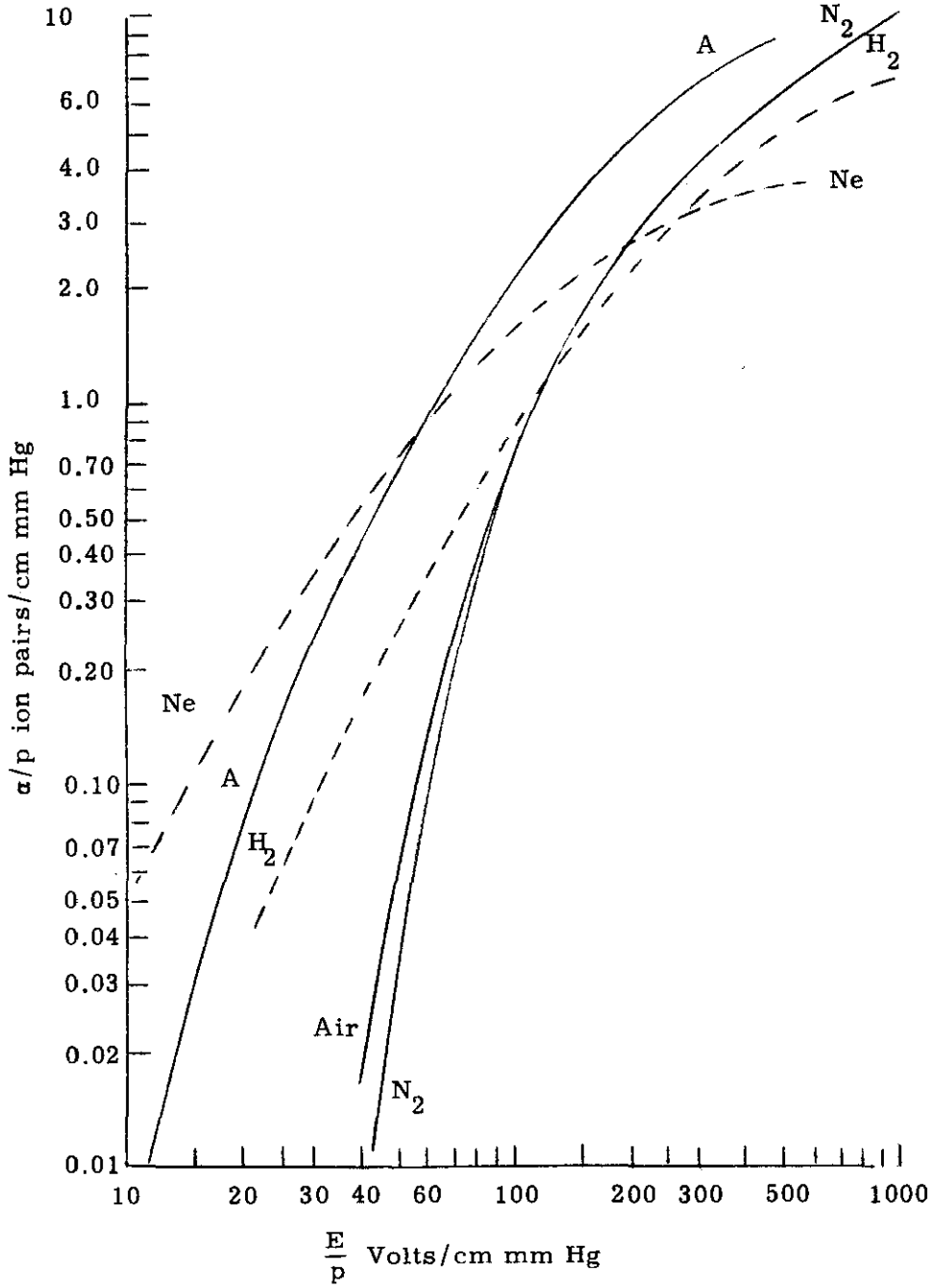

Fig. 18 -- Coefficient of ionization--taken from Gaseous Conductors, J. D. Cobine[17]

Consider Equation (1) above. In order to obtain breakdown, the current at the anode must reach a point where it increases without bound. In order for the current to increase without limit, the denominator must approach zero. That is when

$$\frac{\omega}{\alpha}\left(e^{\alpha d} - 1\right) = 1 . \tag{4}$$

This is Townsend's criterion for the formation of a spark. Since $e^{\alpha d} >> 1$, we can simplify and obtain the following:

$$\frac{\omega}{\alpha}\ e^{\alpha d} = 1 \tag{5}$$

as the sparking criterion. Combining Equations (2) and (3) into Equation (5) gives us the following relationship:

$$f_2\left(\frac{E}{p}\right)e^{pf_1(E/p)d} = 1 \tag{6}$$

If we let the breakdown potential equal V, we can write $Ed = V$. Substituting this into Equation (6) gives us

$$f_2\left(\frac{V}{pd}\right)e^{pdf_1(V/pd)} = 1 . \tag{7}$$

From the above equation, one can see that the breakdown voltage is a function of the product of gap spacing and pressure only. This is known as Paschen's law. This law states, in essence, that if the length of a gap and the gas pressure are altered in such a way that their product is unchanged, the magnitude of the breakdown voltage remains constant. For electrodes of a given area, the volume of gas contained between them is proportional to the separation d. Also, since the concentration is proportional to the pressure, then the product pd is proportional to the number of molecules between the electrodes. In other words, the breakdown voltage depends only upon the total number of molecules of gas between the two electrodes.

A typical pd curve for He is shown below (Fig. 19). This curve, as well as others available on different gases, can be found in Meek and Craggs, Electrical Breakdown of Gases.[12] These curves may be found elsewhere in the literature also. In general, the triggered spark gap is a relatively high-pressure gap, and therefore the pd product above the knee is the main area of interest. Figure 20 shows typical pd curves compiled by the author of spherical electrodes taken in various gases for this pressure region. The electrodes that were used approximate the uniform field and the results are similar to the curve shown in Fig. 19. For the relative breakdown strengths, K, of the various gases compared to air, see page 25.

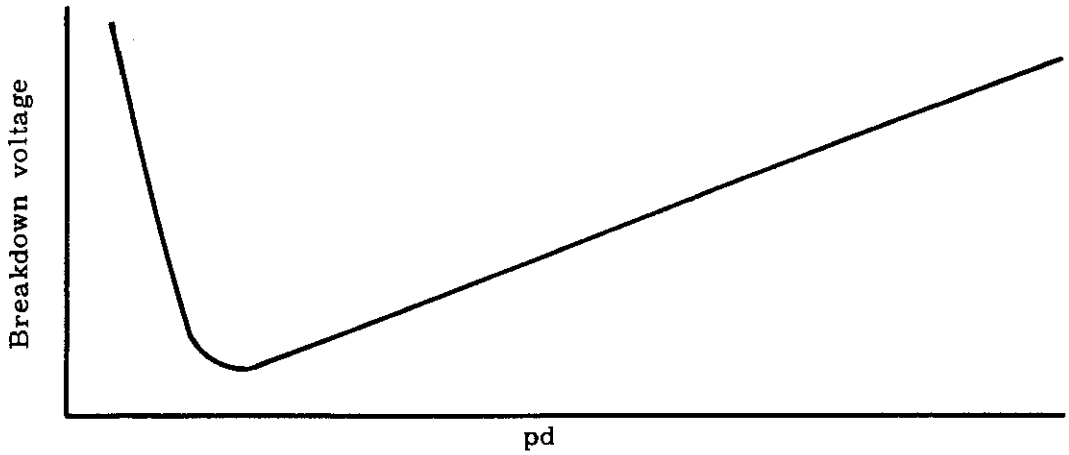

Fig. 19 -- Paschen's breakdown curve

It would be very helpful if an easy and practical method were available to estimate the breakdown value of a gap, given the gas pressure, gas, and gap spacing. Use of the curves in Fig. 20 would give a good estimate rather quickly. One could also calculate the breakdown value, given a definite set of conditions and access to the α curve similar to Fig. 18 for the gas under consideration. Consider the breakdown criterion again

$$\frac{\omega}{\alpha} e^{\alpha d} = 1 . \qquad (5)$$

In the relatively high-pressure region of the spark gap, the effect of ω/α will be small and breakdown is primarily dependent upon αd. With ω/α small, Meek and Craggs[12] report that the empirical value of $\alpha d \approx 20$ is a good estimate required for the relationship $\omega/\alpha\, e^{\alpha d}$ to equal 1. The breakdown criterion is now further simplified to that $\alpha d = 20$. The breakdown value under these conditions can usually be determined within 10 percent. Assume the following conditions:

$$\alpha d = 20 \qquad (8)$$

d = 0.238 cm

E = Electric field in volts/cm

V = Breakdown voltage in volts

p = Pressure of 500 mm of Hg

Gas = Nitrogen

Electrodes = 1.9-cm diameter spheres approximating a uniform field.

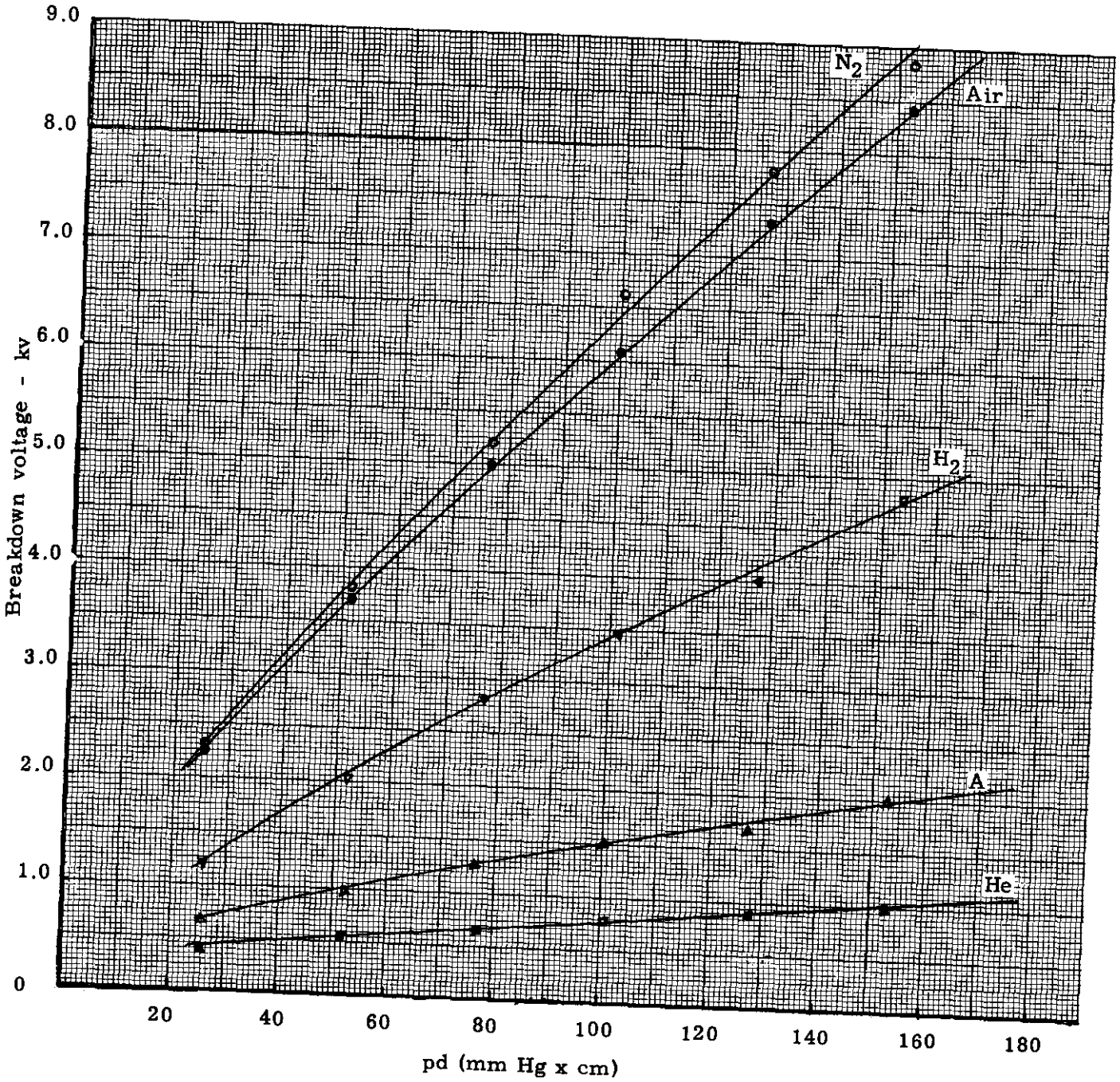

Fig. 20. -- Static breakdown voltage curves in nitrogen, air, hydrogen, argon and helium

$$\alpha d = 20$$

$$\alpha = \frac{20}{0.238} = 84.4$$

$$\frac{\alpha}{p} = \frac{84.4}{500} = 0.169 .$$

From Fig. 18, we obtain

$$\frac{E}{p} = 67 \text{ volts/cm/mm Hg}$$

$$E = (67)(500) = 33{,}500 \text{ volts/cm}$$

$$V = Ed = (33{,}500)(0.238)$$

$$V = 7980 \text{ volts.}$$

From Fig. 20 for $pd = (500)(0.238) = 119$ mm Hg x cm

$$V = 7300 \text{ volts.}$$

The difference from the observed value of 7300 volts and the calculated value of 7980 is about 8 percent, which is certainly close enough. An improved estimate is obtained by utilizing recorded data from page 66 of Meek and Craggs [12] for a value of $\alpha/p = 0.17$. They give $E/p = 60$. Calculating the breakdown voltage as before gives $V = 7140$ volts which is within 3.5 percent of the observed value. Figure 21 is the static breakdown voltage in air for a uniform field observed by Peek [13] in using 0.625-cm diameter spheres at small gap spacings. Shown with it is the calculated curve, using the above approximation that $\alpha d = 20$. Very good agreement is obtained, especially at the higher values of pd. At the low values of pd the calculated curve begins to depart slightly from the observed curve.

Nonuniform Field - Symmetrical Spheres

In the above analysis of the uniform field gap, it was assumed that the radius of the sphere was large compared to the gap spacings; consequently, the ratio of d/r is small, and the breakdown value is a function of pd only and independent of pr. The nonuniform field is obtained when the ratio of d/r is large, and the breakdown value is independent of pd and dependent on pr.

The general law governing the uniform and nonuniform cases is as follows:[14]

(a) Where the ratio of spacing to radius d/r is small, the average gradient E_a is independent of the radius and E_a is a function of the product pd.

(b) Where the ratio of spacing to radius d/r is large, the surface gradient at breakdown E_s is independent of the spacing and E_s is a function of pr.

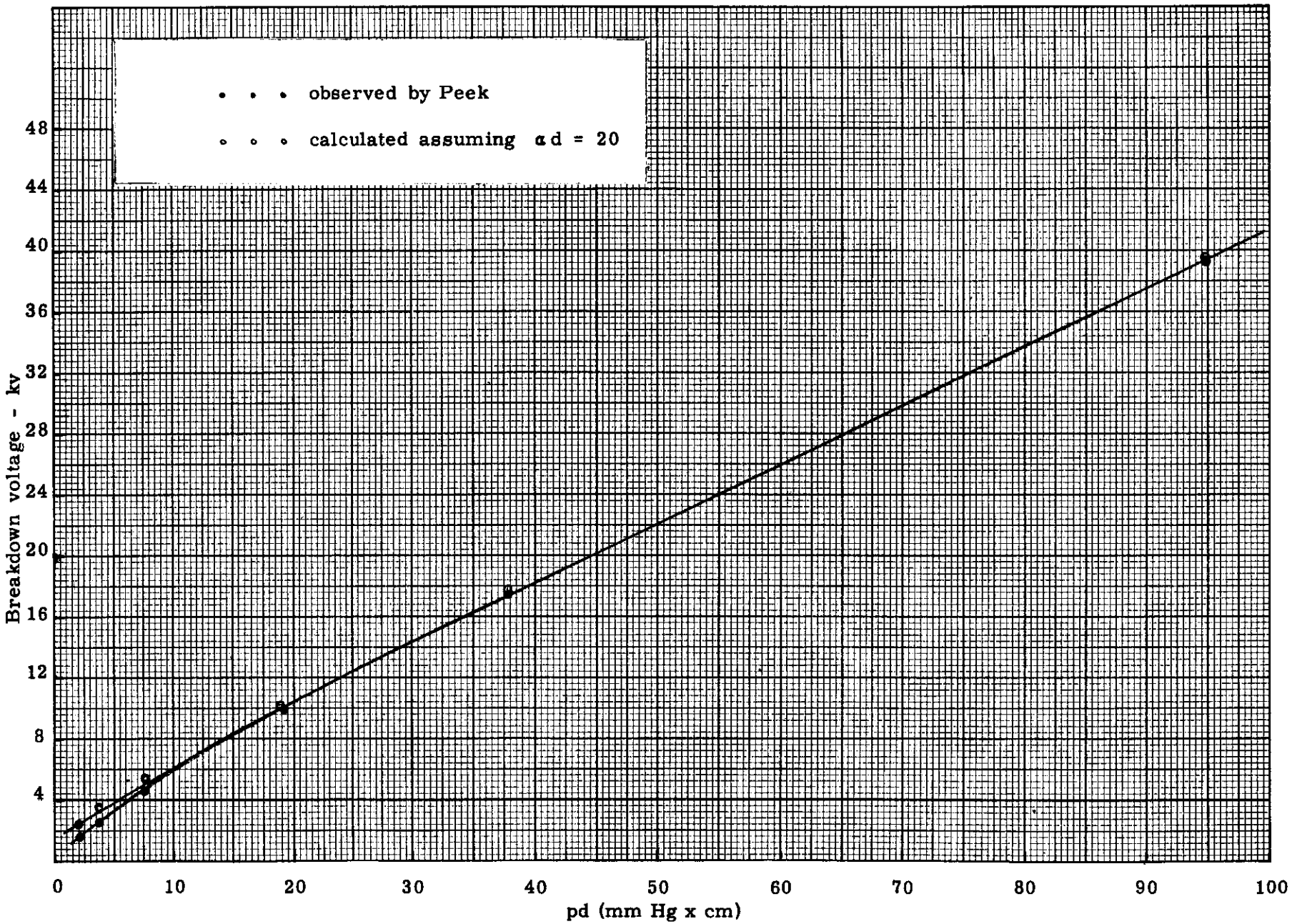

Fig. 21 -- Static breakdown voltage in air for a uniform field (electrode diameter - 6.35 cm)

Assume a uniform field is set up by having a small ratio of d/r. If we keep the gap spacing and fill pressure constant and reduce the sphere radius of curvature, the electric field E_s at the surface of the electrode will increase. The breakdown value will now tend to be influenced by pr as well as pd. As the surface gradient E_s increases, the α mechanism is enhanced and the breakdown value decreases.

In addition to nonuniform fields produced by spheres, the nonuniform fields produced by point-to-plane, point-to-point, point-to-sphere, and other electrode configurations are of interest and are used in the construction of practical triggered gaps. The varying gradient of the nonuniform case tends to complicate analysis of the configuration and calculations are difficult, if not impossible.

We can consider the problems in a general sense as follows: consider the breakdown criterion of Equation (5) for the uniform field,

$$\frac{\omega}{\alpha} \; e^{\alpha d} = 1 . \tag{5}$$

When the field is nonuniform, the electron multiplication is governed by the integral of α over the path traveled. The Townsend breakdown criterion can then be written

$$\frac{\omega}{\alpha} \; e^{\int_0^x \alpha dx} = 1 . \tag{9}$$

$$\int_0^x \alpha dx = \ln \frac{1}{\gamma} \tag{10}$$

If the gradient E as a function of x were known, then α as a function of x could be obtained. This is usually not known and other methods must be employed. Wheatcroft[14] gives the following summary:

> "Townsend and other investigators into the breakdown between point, wires, and similar electrode arrangements have adopted an approximate method which gives a sufficiently satisfactory correlation with experimental results. Where the field is rapidly varying as near the surface of a fine wire or a sharp point, most intense ionization must occur where the field is highest. Farther from the wire or point, where the field is very weak, there is little or no ionization at all. Thus a good estimation for these cases may be made if we suppose that there is no ionization at all over the greater part of the inter-electrode space and make some simple assumption about the breakdown conditions in the remaining portion where the field strength is high.

"It is clear that a region of the discharge in which there is no ionization ($\alpha = 0$) makes no contribution to the integral. It is not, therefore, necessary for the ionization to take place over the whole of the discharge path, provided the breakdown condition is satisfied on the part of the path where ionization does occur."

If we now consider the simplified breakdown criterion on the uniform field

$$\alpha d = 20, \tag{8}$$

then for the nonuniform case, we must make an adjustment to account for an apparent reduction in the spacing over which the uniform field condition of $\alpha d = 20$ is estimated to apply. For $\alpha d = 20$, a reduction of ionized gap length d will give a higher value of α which is expected.

In order to obtain a higher α, we remember that α/p is a function of E/p (Fig. 18). Since p is a constant, the apparent gradient must be much higher than the normal gradient applied in the uniform field case. The problem now is to determine this apparent increase in gradient. Various investigators into breakdown of gases at relatively large spacings have found that, in general, the lowest gradient necessary to cause breakdown in air at atmospheric pressure is about 30 kv/cm. Townsend therefore assumed that the ionization extends from the electrode as far as the point where the gradient falls to 30 kv/cm, and that the average gradient over the ionization zone is the same as that found for a uniform field of the same length.

The results of Peek's[13] work on geometry and breakdown studies were reviewed for a possible solution to our particular problem. Peek observed that the apparent surface gradient for the nonuniform field at breakdown could be expressed as follows:

$$E_s = E_a f = \frac{V_{sbv}}{d} f \text{ kilovolt/cm} \tag{11}$$

where

E_a = average gradient

V_{sbv} = the applied breakdown potential

d = gap spacing

and where f is found to be mathematically and experimentally a function of the ratio of sphere radius and gap spacing.

$$f = f\left(\frac{d}{r}\right). \tag{12}$$

Then f may be calculated by the following simple formula for spheres of equal size:

$$f = \frac{d/r + 1 + \sqrt{(d/r + 1)^2 + 8}}{4}. \tag{13}$$

Table I gives the values obtained from Peek for f, measured and calculated for nongrounded spheres of equal size, and the measured value of fo for one sphere grounded. For the case of one sphere grounded, the shank, connecting leads, ground, etc., have a much greater effect than when both are nongrounded and mathematical values do not check with measured values.

TABLE I

Peek's Field Intensification Factor

d/r	f nongrounded	fo grounded
0.1	1.03	1.03
0.2	1.06	1.06
0.4	1.14	1.14
0.6	1.215	1.22
0.8	1.29	1.31
1.0	1.366	1.41
1.2	1.44	1.51
1.4	1.52	1.62
1.6	1.61	1.73
1.8	1.69	1.85
2.0	1.78	1.97
3.0	2.23	2.59
4.0	2.69	3.21
6.0	3.64	
10.0	5.6	
15.0	8.08	
20.0	10.58	

These points are plotted on Fig. 22 for easy interpretation. For the uniform field case, if we let the ratio of d/r approach zero, we see that f will approach 1 as its limit. From these values for f, we note that the apparent surface gradient at spark-over increases with decreasing radius of the electrodes. As the ratio of d/r becomes larger, the field becomes more nonuniform with the gradient at the surface of the electrodes becoming greater and greater.

Peek gives the following formulae for the surface gradient in volts/cm of various geometries in the nonuniform case for air:

Wire and cylinder $$31\ p\left(1+\frac{0.308}{\sqrt{pr}}\right) \qquad (14)$$

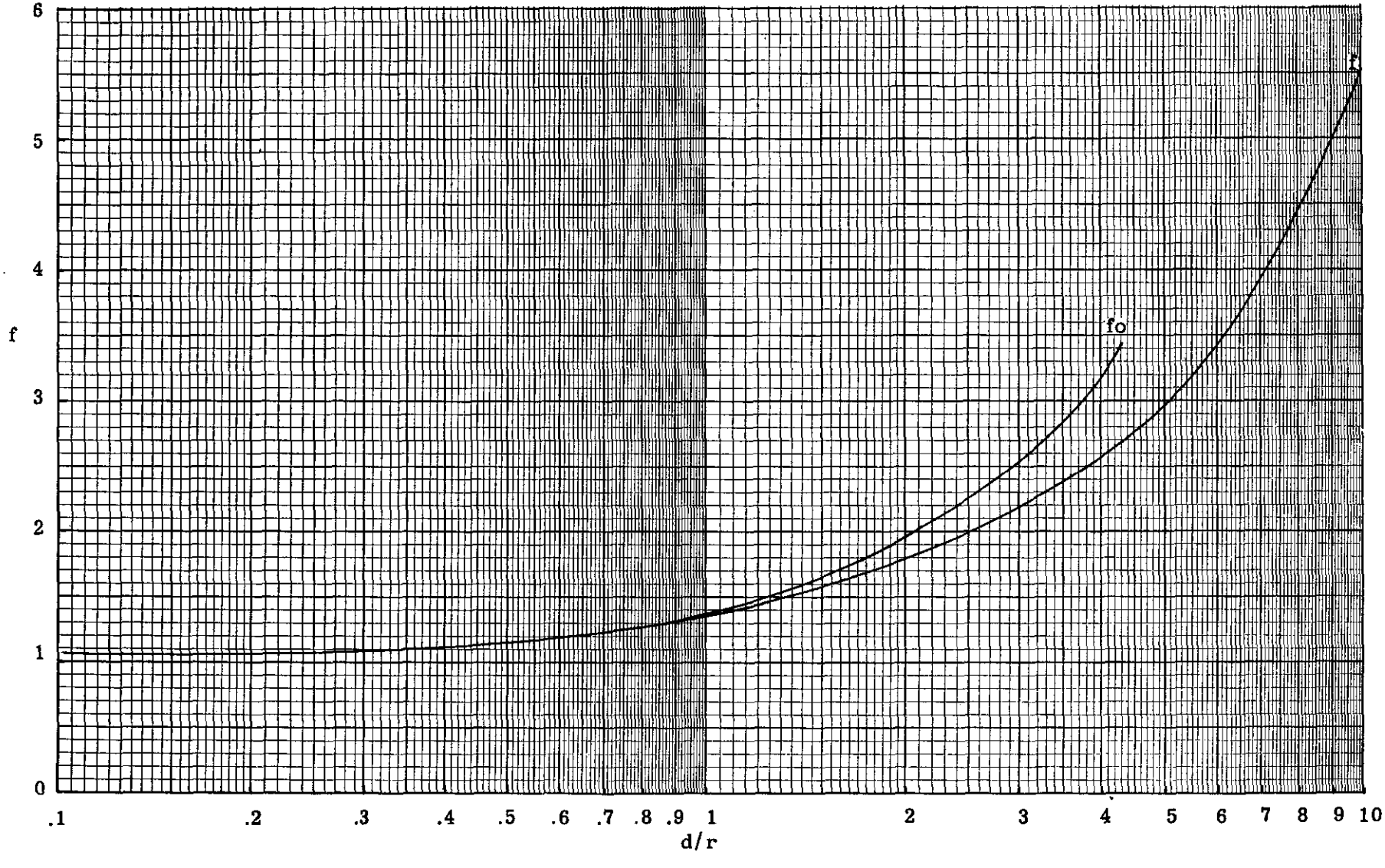

Fig. 22 -- Peek's field intensification factor for spheres of equal size

Parallel wires $$30\ p\left(1 + \frac{0.301}{\sqrt{pr}}\right) \tag{15}$$

Spheres $$27.2\ p\left(1 + \frac{0.54}{\sqrt{pr}}\right) \tag{16}$$

where p is the pressure in atmospheres at normal temperature. A look at these formulae shows that as the radius of the sphere (or wire in the other cases) decreases, the gradient increases. Also, as the pressure decreases, the gradient will decrease for the region above the Paschen minimum which is the area of our interest.

Peek's major work on breakdown criteria was on dielectric phenomena for the purpose of obtaining design information for high-voltage insulation and transmission problems and, consequently, his interest was centered primarily on air at atmospheric pressure. The above equation does take into effect varying pressure, but does not allow for differences in the $\alpha/p = f(E/p)$ curves for different gases. Using the average breakdown gradient of air as a reference and comparing the other gases with it, we can arrive at the following equation:

$$E_s = 27.2\ Kp\left(1 + \frac{0.54}{\sqrt{pr}}\right) \tag{17}$$

where K is now the relative breakdown strength of gases compared to air. These strengths are listed below.[4,15]

TABLE II

Relative Breakdown Strength of Gases

N_2	Air	O_2	H_2	A	He	NH_3	CO_2	CL	SO_2	
1.15	1.00	0.85	0.65	-	-	1.0	0.95	0.85	0.30	Thomson
1.07	1.00	0.91	0.54	0.24	0.07	-	-	-	-	EG&G
1.07	1.00	-	0.56	0.24	0.12	-	-	-	-	Author

Figure 23 shows the observed breakdown curves* in nitrogen and helium obtained in our laboratory with 0.625-cm diameter spheres at a spacing of 0.625 cm. Shown with these curves are our calculated curves for comparison. The agreement is fairly good and is within a 10-percent variation.

*While the constant pd product of the uniform field does not apply for the nonuniform case, we shall continue to use it for comparison purposes. It must be kept in mind that the different arrangements of p and d that give the same pd product do not necessarily have the same breakdown voltage.

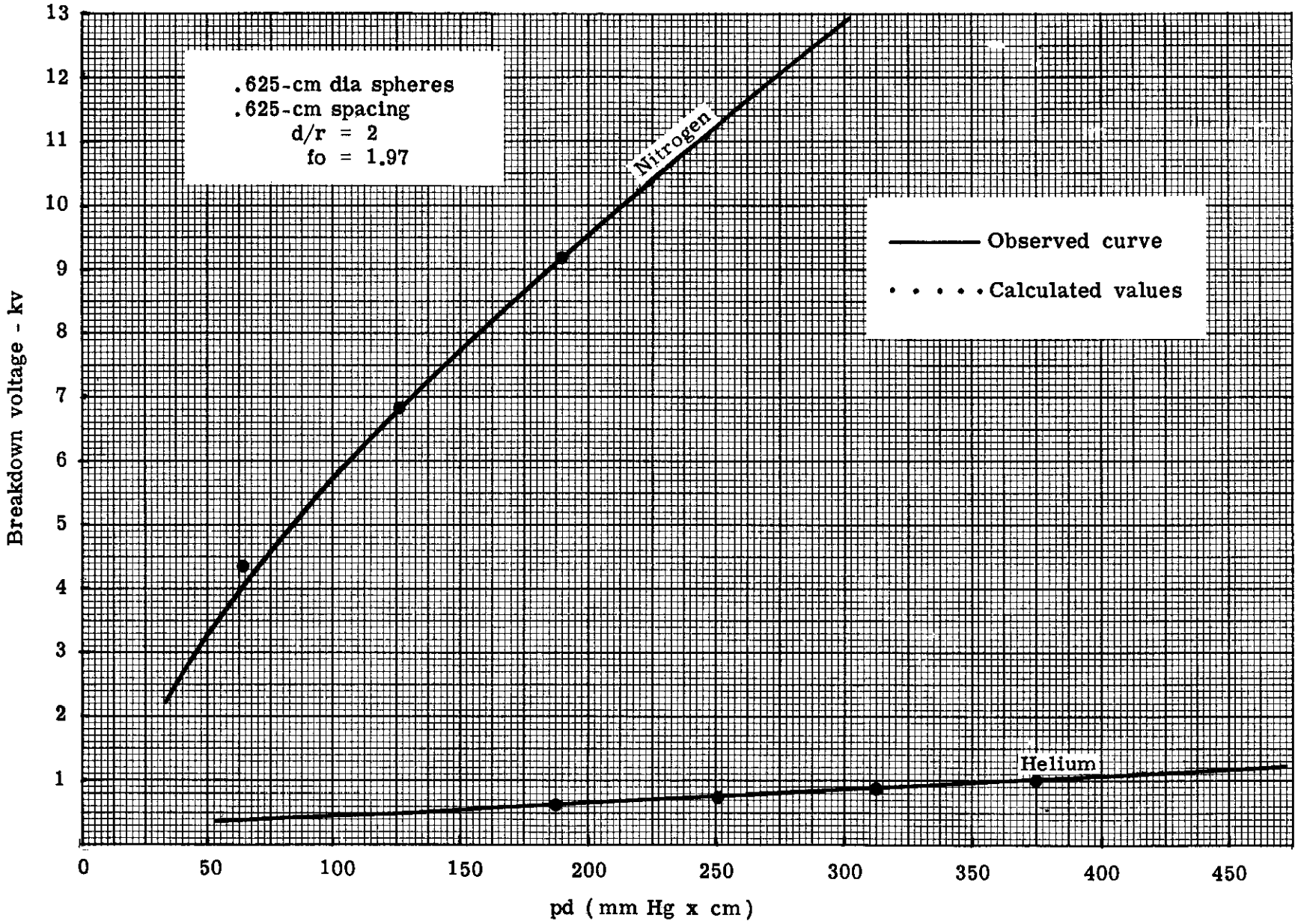

Fig. 23 -- Static breakdown voltage for nonuniform field generated by equal size spheres

Below is a sample calculation for the 0.635-cm-diameter sphere:

$$d = 0.625 \text{ cm},$$

$$r = 0.317 \text{ cm},$$

$$\text{Gas} = \text{Nitrogen},$$

$$K = 1.07, \text{ and}$$

$$p = 30 \text{ cm of Hg pressure} = 0.395 \text{ atmosphere}.$$

The surface breakdown gradient is then estimated to be

$$E_s = (27.2)(1.07)(0.395)\left(1 + \frac{0.54}{\sqrt{(0.395)(0.317)}}\right)$$

$$E_s = 29.0 \text{ kv/cm} .$$

The static breakdown voltage is then estimated to be

$$V_{sbv} = \frac{E_s d}{f} = \frac{(29.0 \text{ kv/cm})(0.625 \text{ cm})}{f}$$

In order to determine f, we calculate the ratio of gap spacing to radius which is

$$d/r = 2 .$$

From Table I we find fo to be equal to 1.97.

$$V_{sbv} = \frac{(29.0 \text{ kv/cm})\ (0.625 \text{ cm})}{1.97} = 9.2 \text{ kv} .$$

A ckeck with Fig. 23 shows very good agreement which, for this value of pd = 188 (mm Hg x cm), gives a breakdown voltage of 9.2 kv.

Nonuniform Field - Asymmetrical Spheres

In the consideration of symmetrical sphere electrodes, it can be shown that if the ratio of d/r is relatively small, where d is the gap spacing and r is the radius of the electrodes, the field approximates a uniform field. Because of this symmetry, it makes no difference which electrode is made positive and which one is negative. To determine the effect of an asymmetrical gap geometry on the breakdown value and the possible influence of polarity, the following experiment was performed.

Several spheres of varying radii were assembled in nitrogen at different gap spacings and fill pressures. The uniform field was approximated by using two spheres with a radius of 1.27 cm separated by a spacing of 0.127 cm. One of the spheres was then replaced by one with a smaller radius. The process was repeated until a range of spheres was obtained with radii varying from 1.27 cm to 0.076 cm. The experiment was then rerun with different gap spacings. Several readings were obtained for each condition and the average value recorded.

Figure 24 shows the breakdown curves at a spacing of 0.127 cm for varying radii. For the 0.952-cm and 0.475-cm radii, there is little variation from the uniform field case. It is reasonable to conclude that if the ratio of gap spacing to radius of the reduced sphere is kept small, then the electrode geometry still approximates the uniform field in the region of the minimum gap spacing and the effect of asymmetry is negligible. Where $r = 0.152$ cm and 0.076 cm, the ratio d/r approaches values equal to or greater than unity, and the geometry now generates a nonuniform field with a resultant lowering of holdoff potential at constant spacings and pressures. The smaller the radius of the smaller sphere, the greater the asymmetry and the lower the breakdown value.

Figure 25 shows the same electrode conditions as above but at an increased gap spacing of 0.254 cm. Here again, the 0.952-cm and 0.475-cm radii do not vary appreciably from the uniform field case, while the 0.152-cm and 0.076-cm radii depart even more from the uniform field than before. For both the 0.127-cm and 0.254-cm gap spacings, there was no effect on breakdown due to polarity on the smaller electrode for the 0.952-cm and 0.475-cm cases. This was to be expected. For the 0.152-cm and 0.076-cm cases, there was a marked effect due to polarity.

Figure 26 shows the 0.152-cm sphere at a spacing of 0.508 cm for both positive and negative polarities. The negative polarity caused the gap to break down 800 volts lower than for a positive polarity. The 0.076-cm sphere differs even more.

Figure 27 shows the breakdown curve for 0.152-cm sphere for spacings of 0.127 cm, 0.254 cm, 0.508 cm, and 0.625 cm. Here again we see that as the ratio of d/r increases, the breakdown voltage decreases. This curve is for a positive smaller electrode.

Figure 28 shows the same condition as above but for a negative smaller electrode. Figure 29 shows the effect of a negative polarity and a 0.076-cm radius sphere on the breakdown curve at different gap spacings.

A study of these asymmetrical geometries brings out a very interesting point. If the gap spacings and sphere radii of the smaller electrode are varied so that the ratio of spacing to radius remains constant, the breakdown value remains constant. This is expected since the field produced should be the same and, consequently, the breakdown would be the same; this also agrees with the Law of Similarity*. Figure 30 shows such a relationship for different combinations of spacings and radii. The curves of equal ratio of d/r give equal breakdown values. Also, here it is clearly shown again that the greater the ratio of spacing to radius, the lower the breakdown value. The effect of polarity for a nonuniform field is very pronounced, as can be seen from these curves. For other geometries, such as wire and cylinder, the breakdown is also lower for negative wire than positive. This has been observed and reported quite extensively in the literature. Meek and Craggs' Electrical Breakdown of Gases discusses this point in some detail.[12]

*The Law of Similarity states that a gap, whose dimensions are reduced by a factor $1/K$ and whose pressure is increased by a factor K, will have the same breakdown voltage as the original gap.

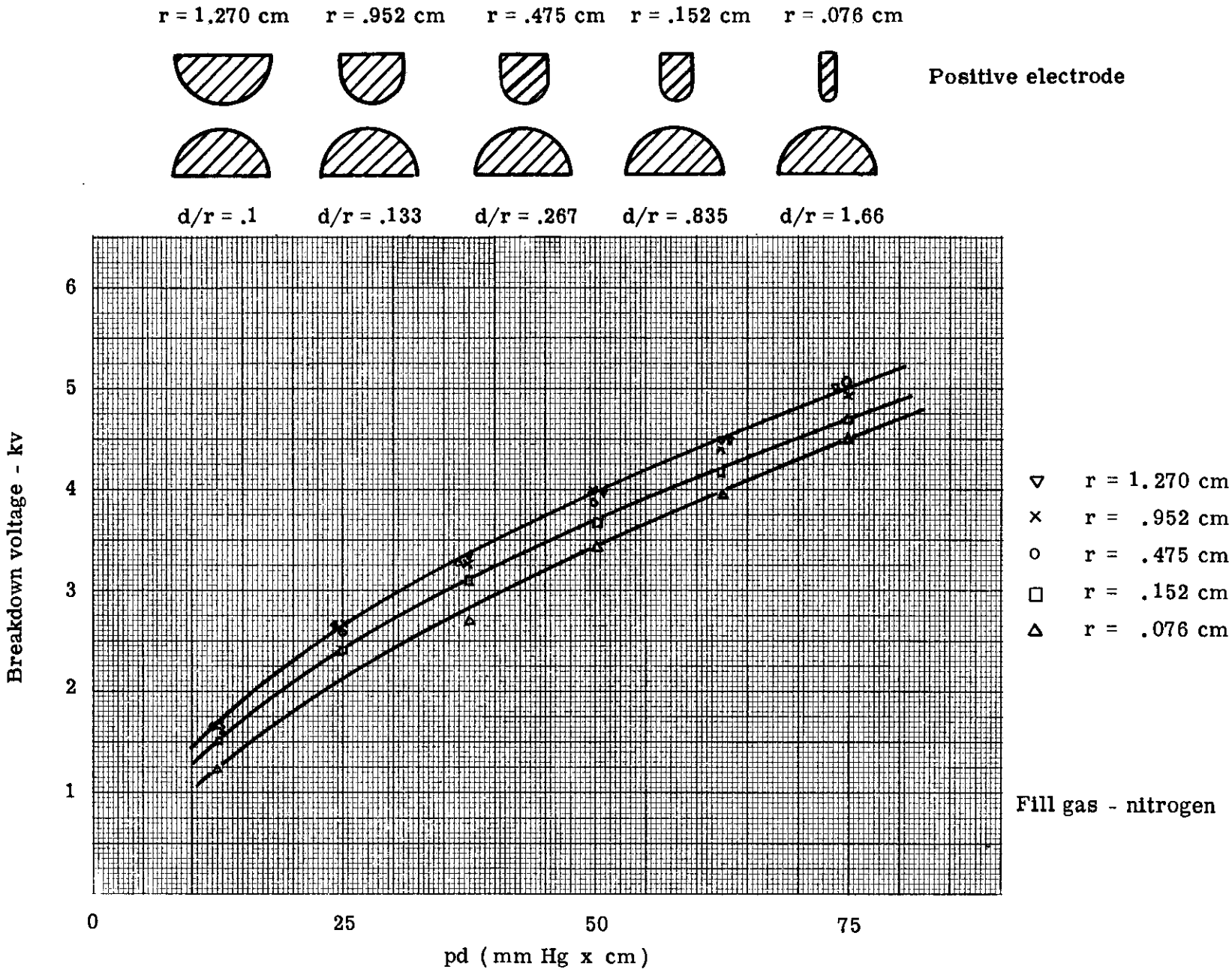

Fig. 24 -- Breakdown curves of asymmetrical electrodes for .127 cm gap spacing

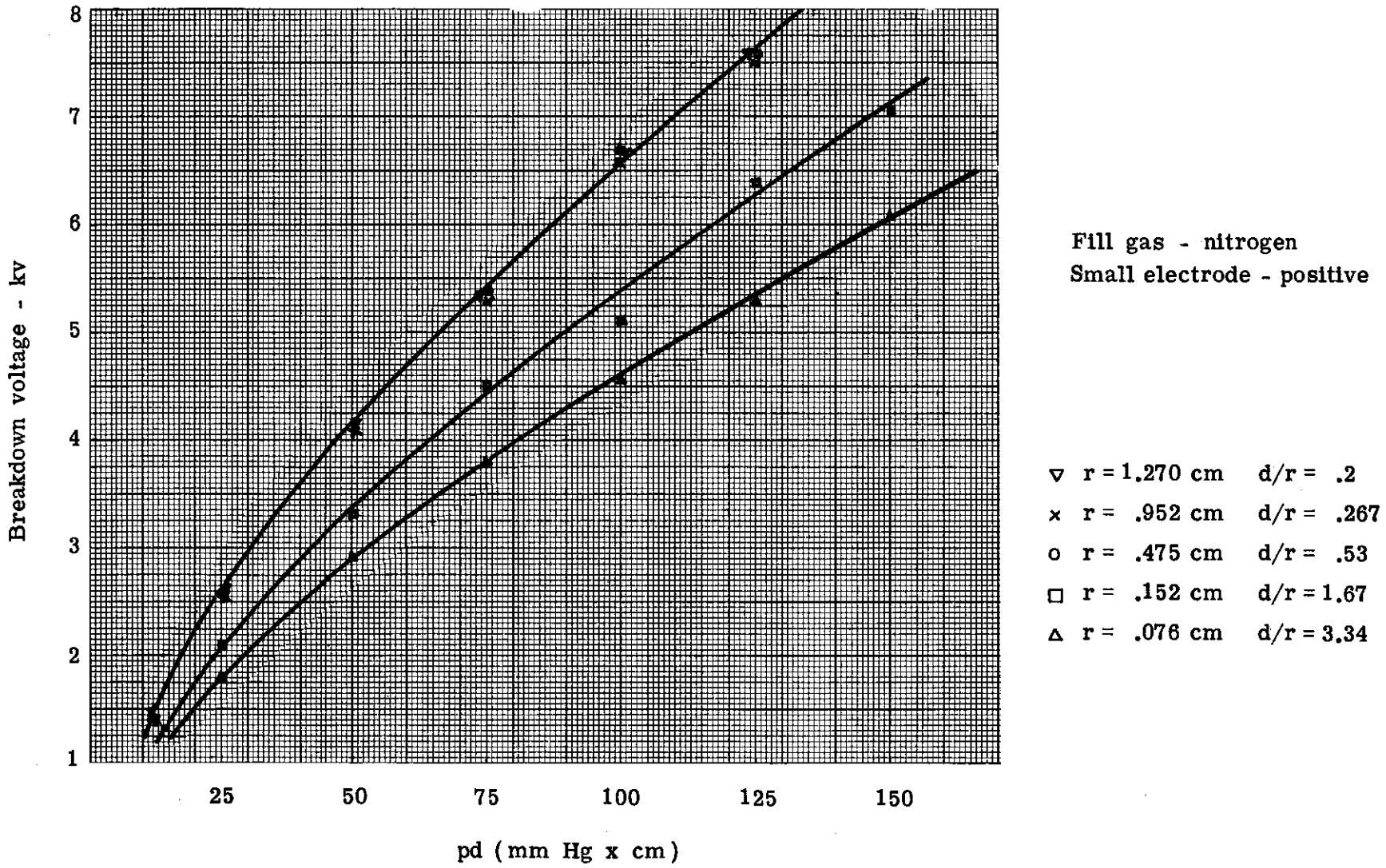

Fig. 25 -- Breakdown curves of asymmetrical electrodes for .254 cm spacing

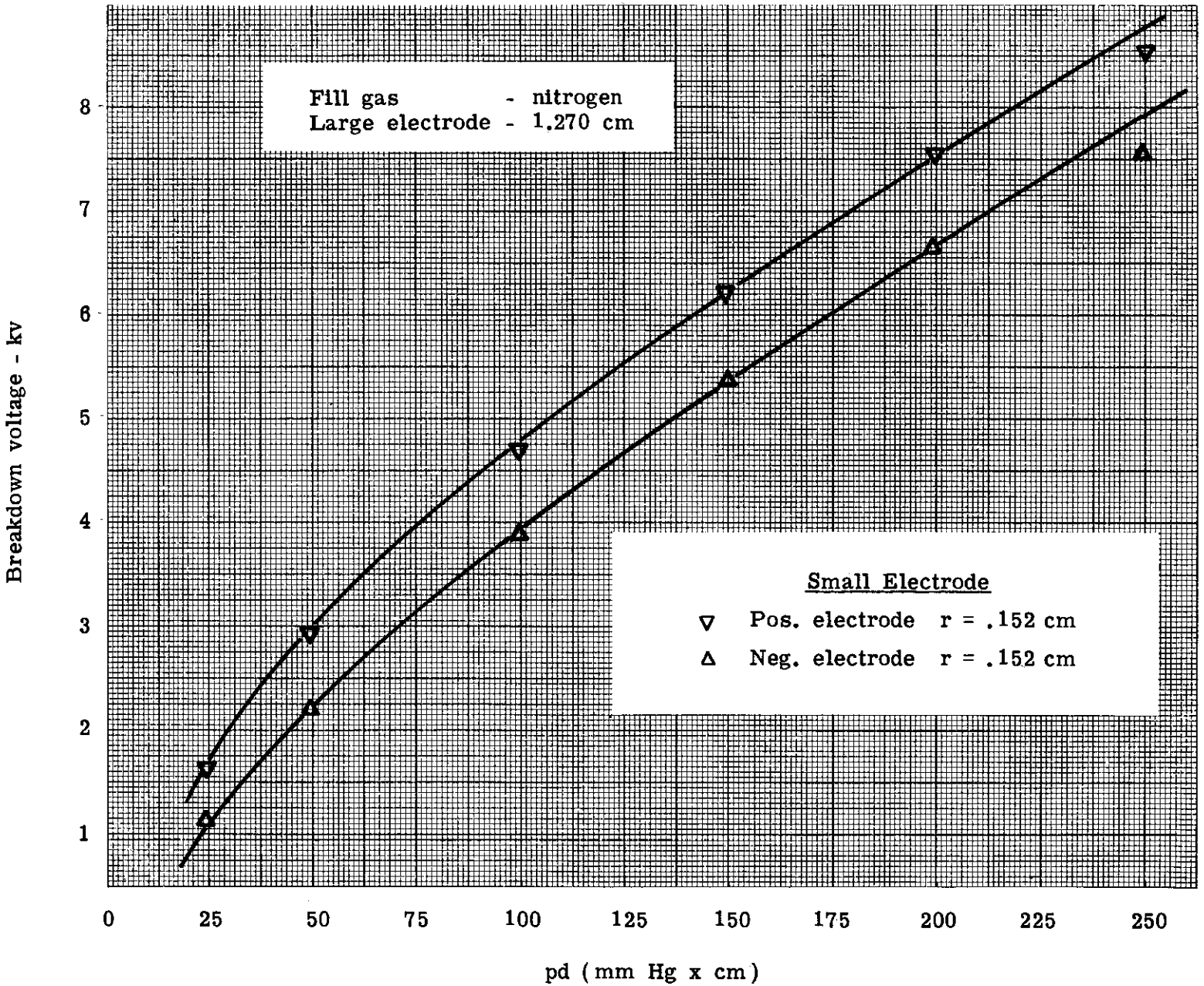

Fig. 26 -- Breakdown curves of asymmetrical electrodes for .508 cm spacing

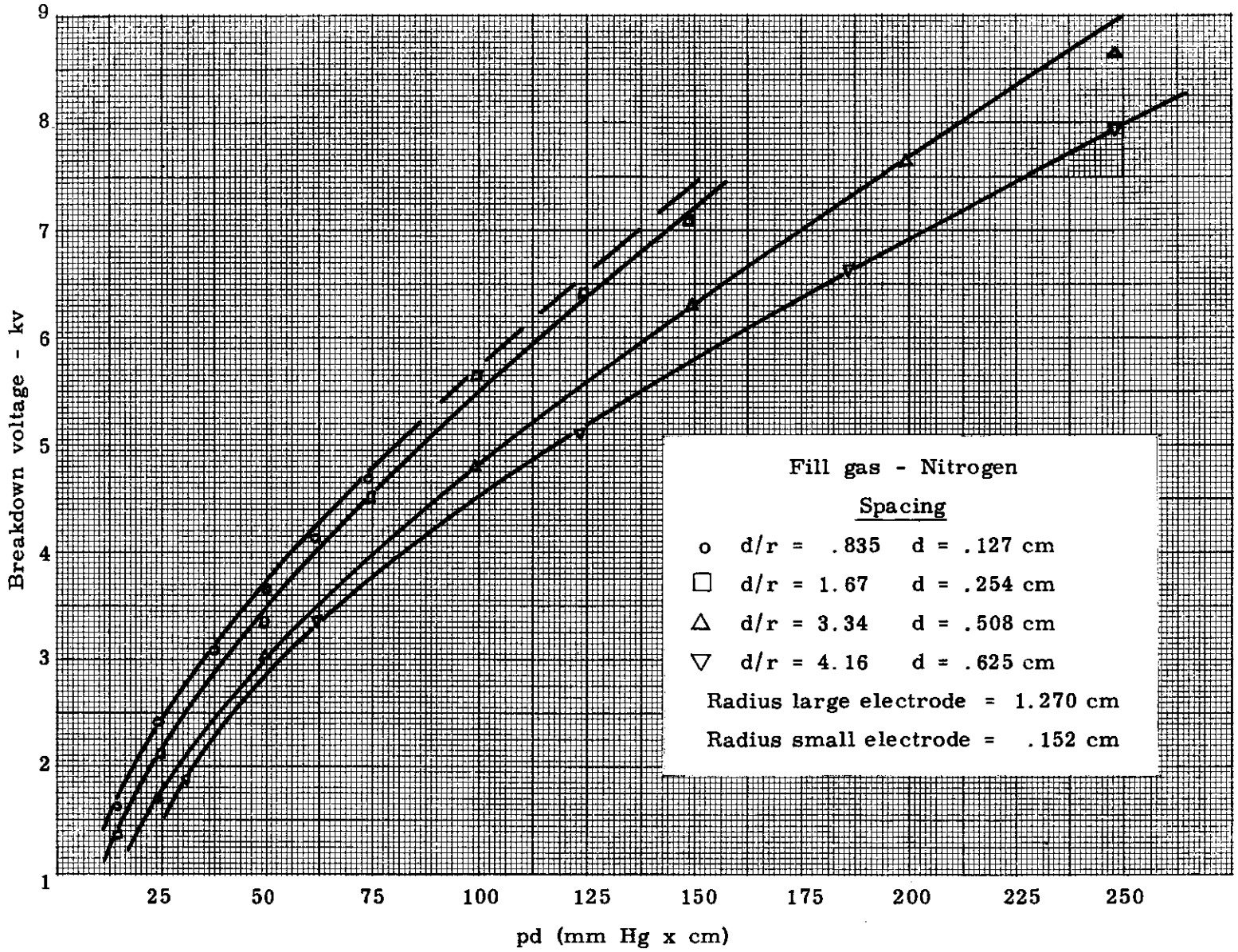

Fig. 27 -- Breakdown curves of asymmetrical electrodes for various gap spacings (small electrode positive)

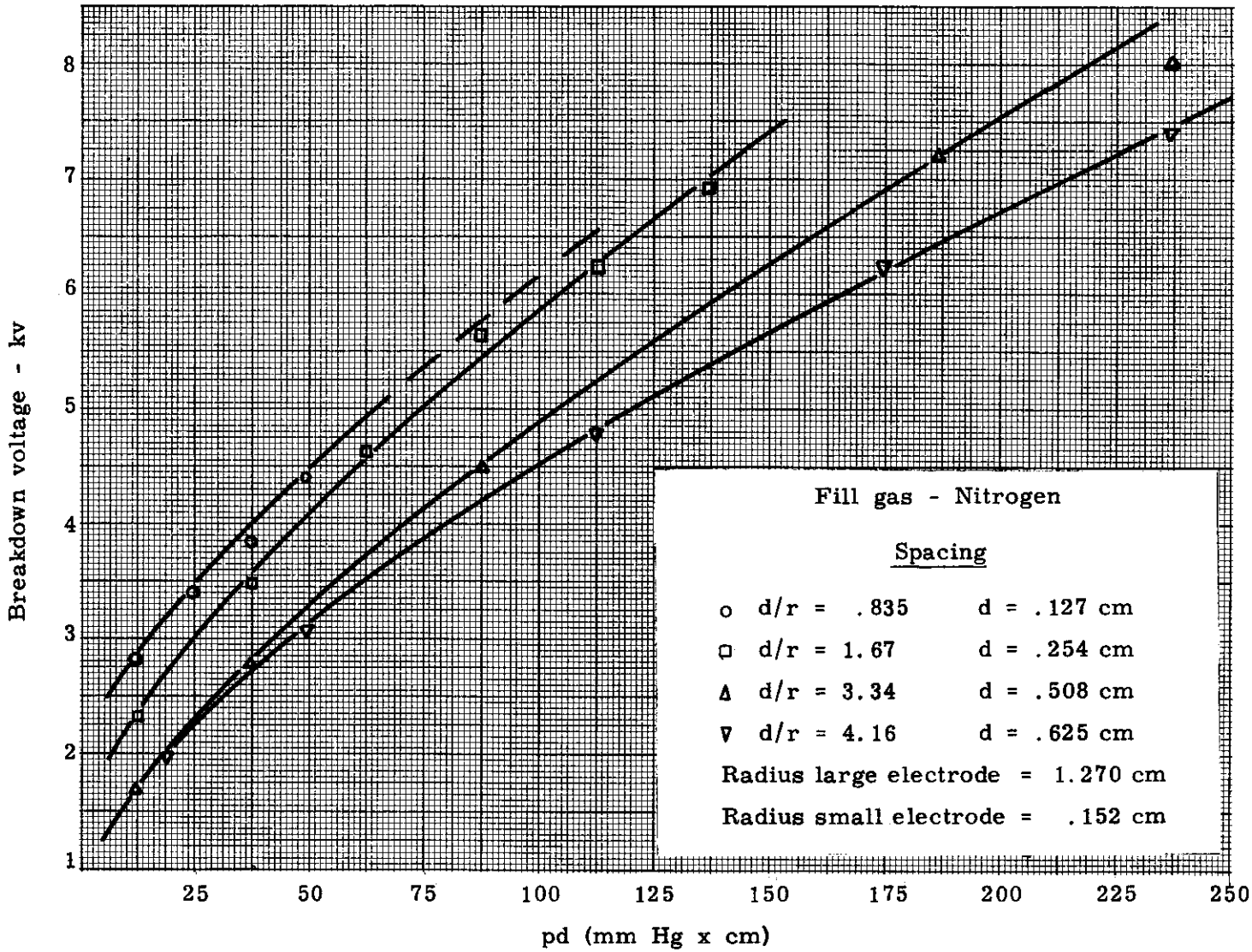

Fig. 28 -- Breakdown curves of asymmetrical electrodes for various gap spacings (small electrode negative)

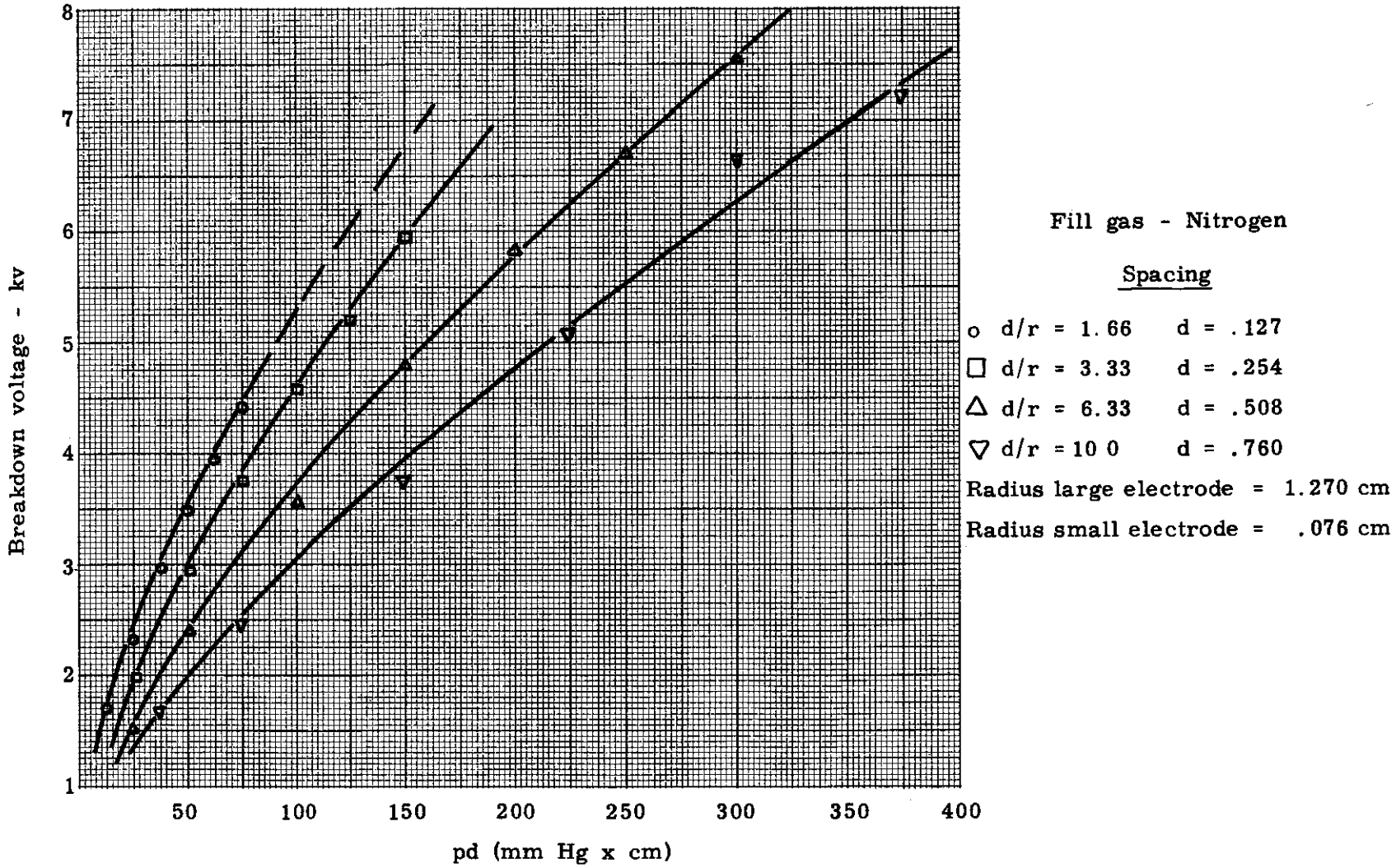

Fig. 29 -- Breakdown curves of asymmetrical electrodes for various gap spacings (small electrode negative)

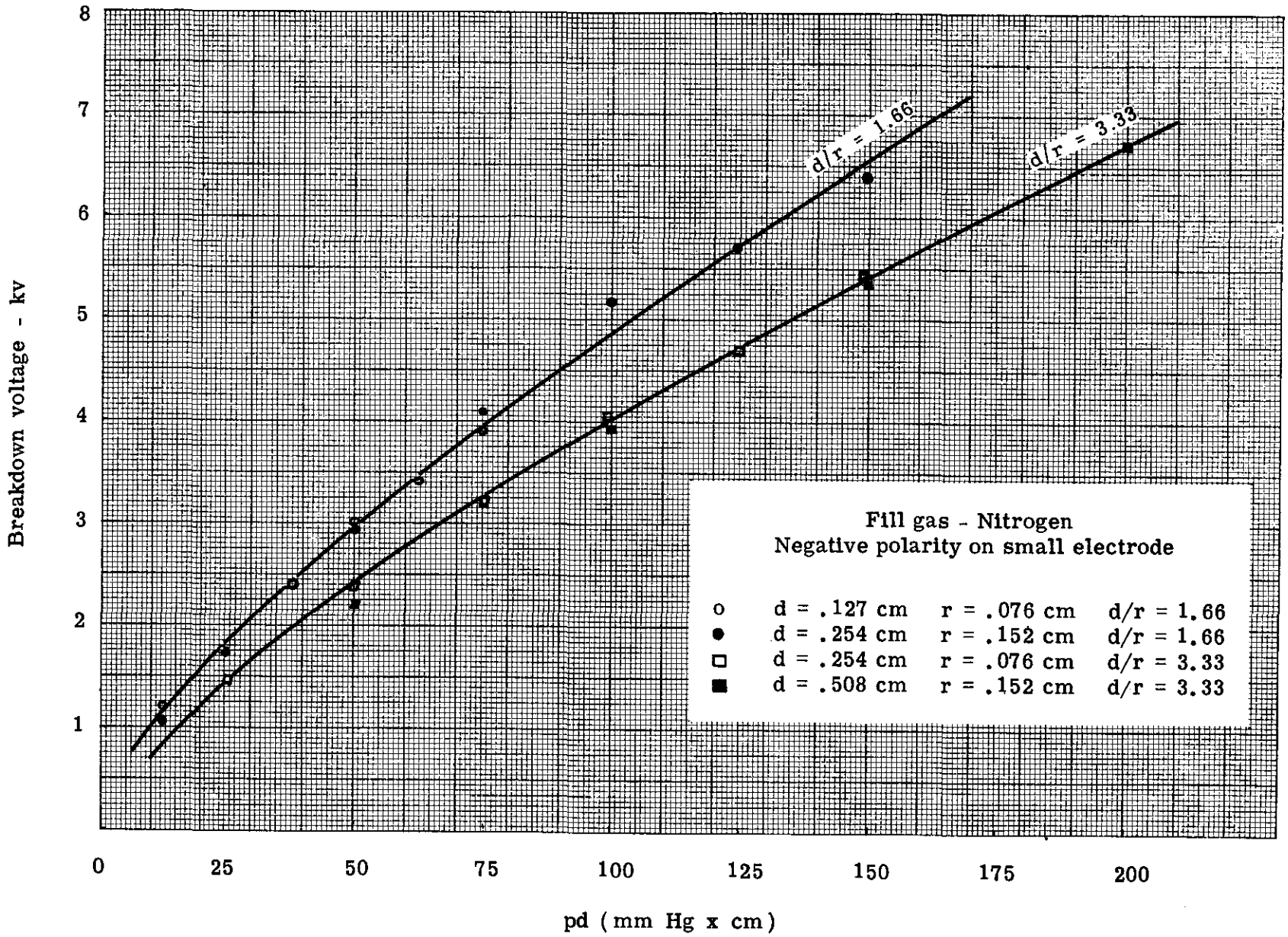

Fig. 30 -- Normalized breakdown curves of asymmetrical electrodes

Nonuniform Field - Point to Plane

If the preceding discussion is carried further where the radius of the smaller sphere becomes smaller and smaller and the radius of the larger sphere becomes larger, the geometry then approaches a point-to-plane configuration. The resultant breakdown curve will then be lower than the curves shown in Figs. 24 and 25. A review of the literature shows that several investigators have studied the breakdown curves for a point-to-plane geometry, but there is very little on the calculations of the breakdown voltage. Wheatcroft[14] reports on an approximate theory of Edmunds concerning the point-to-plane breakdown. The field is based on the point having a hemispherical end, where Edmunds assumes the surface to be a paraboloid of revolution having a focus 1/4 r from the end of the wire where r is the radius of the wire. The resultant formula is therefore

$$V_{sbv} = \frac{E_s r}{4} \ln \frac{8d}{r} \tag{18}$$

where

V_{sbv} is the static breakdown voltage in volts

E_s is the gradient at breakdown at the surface of the conductor in kilovolts/cm

d is the spacing between point to plane in centimeters.

A review of the formula for the wire and cylinder shows that this formula is similar. In fact, as shown experimentally by Wheatcroft (page 97)[14] the surface gradient at breakdown, E_s, for the point to plane has been found to be the same as a wire of radius 1/4 r within a cylinder. We can therefore estimate the breakdown gradient E_s by use of the expression for the wire and cylinder where the ratio d/r of the point-to-plane geometry is relatively large,

$$E_s = 31\ pK \left(1 + \frac{0.308}{\sqrt{p\ 1/4\ r}}\right) \tag{19}$$

or

$$E_s = 31\ pK \left(1 + \frac{0\ 616}{\sqrt{pr}}\right) \tag{20}$$

p is the pressure in atmospheres

K is the relative breakdown strength of the fill gas with respect to air

r is the radius of the point in centimeters.

Figures 31 and 32 show the observed and calculated values for a point of 0.050-cm radius and a sphere of 0.475-cm radius which approximates a plane. Figure 32 is for a fixed gap spacing of 0.127 cm and variations of pressure. Figure 31 shows the breakdown voltage at a fixed pressure of 60 cm of Hg in air with variations of spacings. Figure 33 is both curves plotted as a function of pd to show that, with a nonuniform field, the Paschen law does not hold over all products of pd.

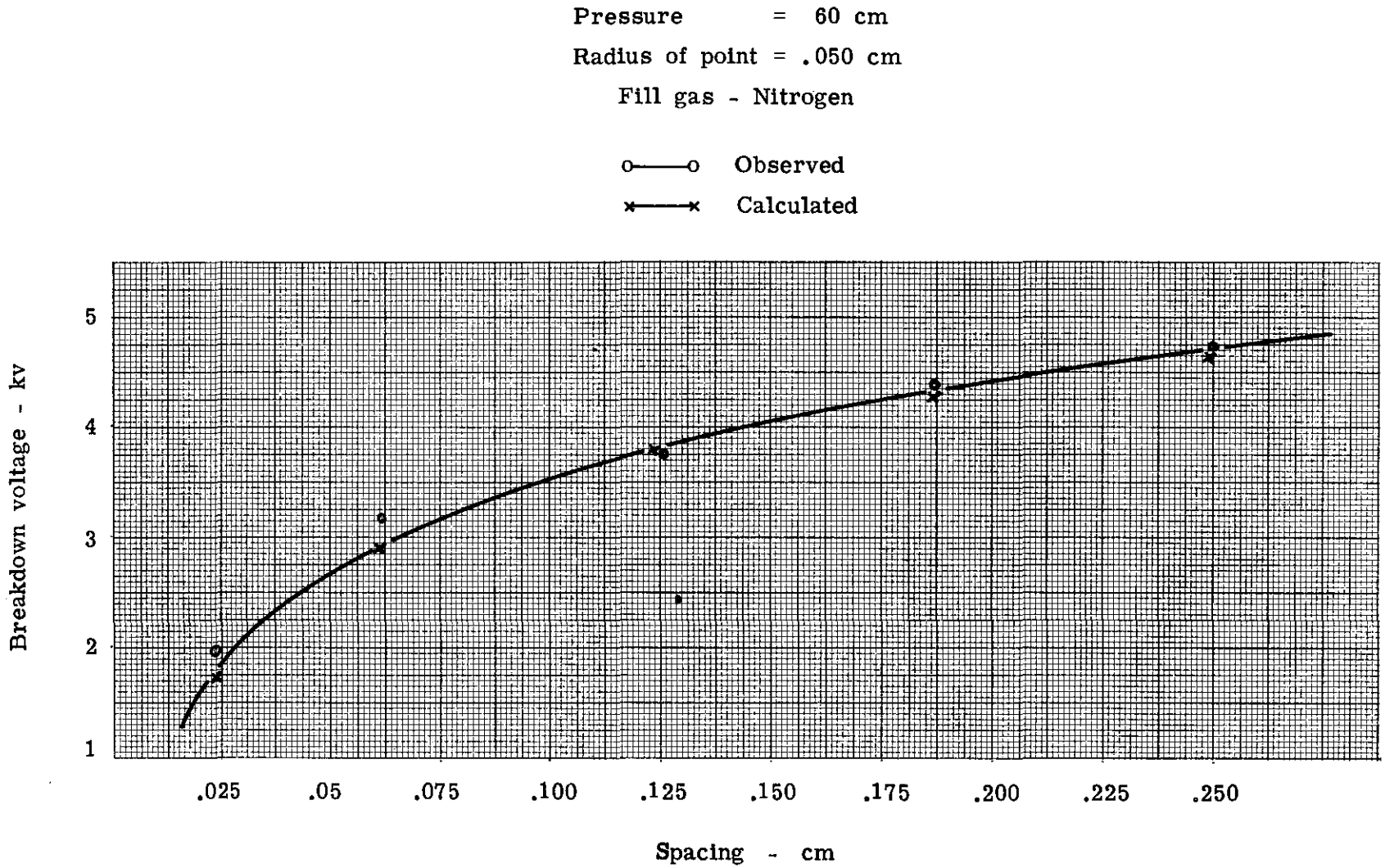

Fig. 31 -- Point-to-plane breakdown voltage for constant pressure and varying spacing

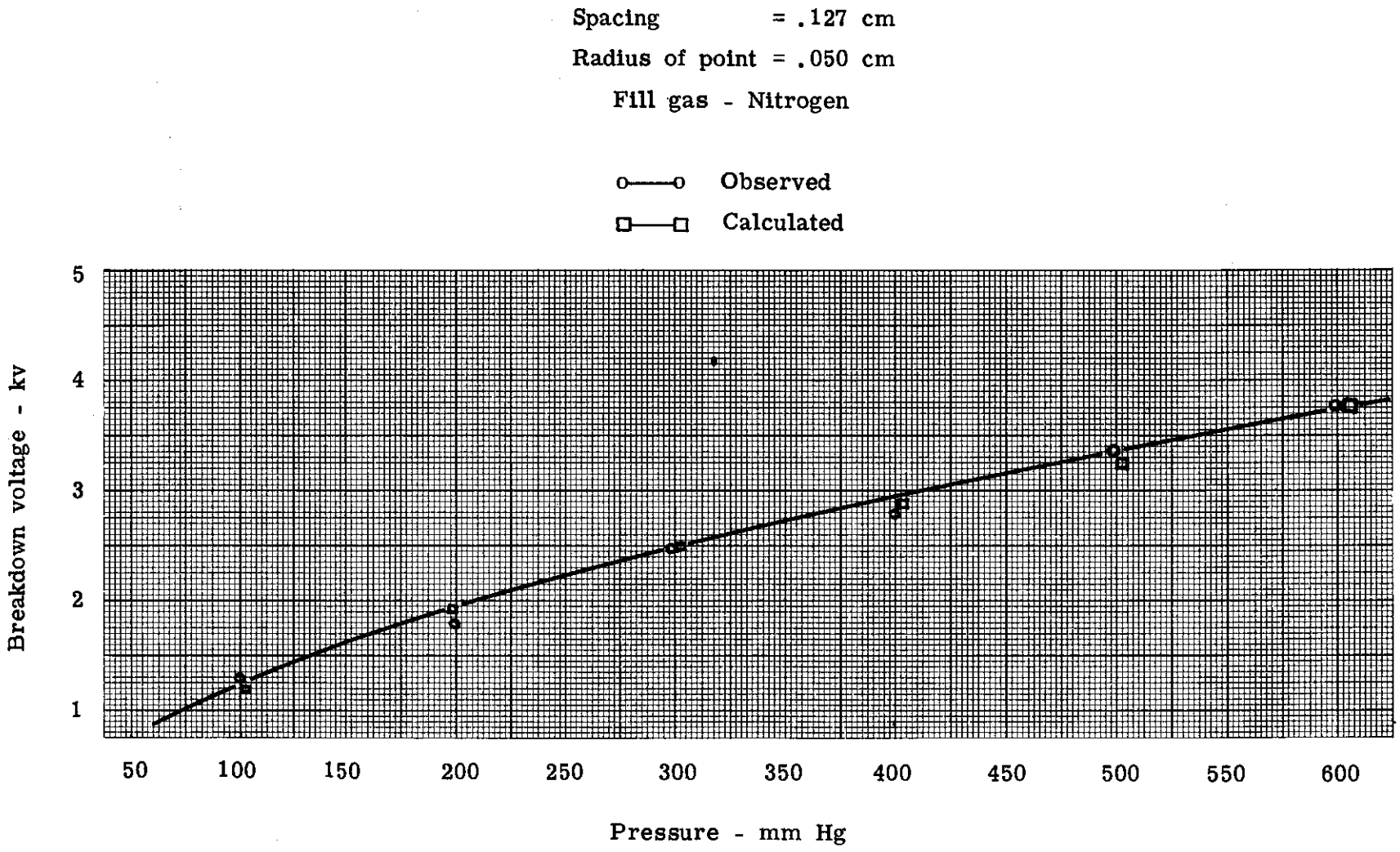

Fig. 32 -- Point-to-plane breakdown for constant spacing and varying pressure

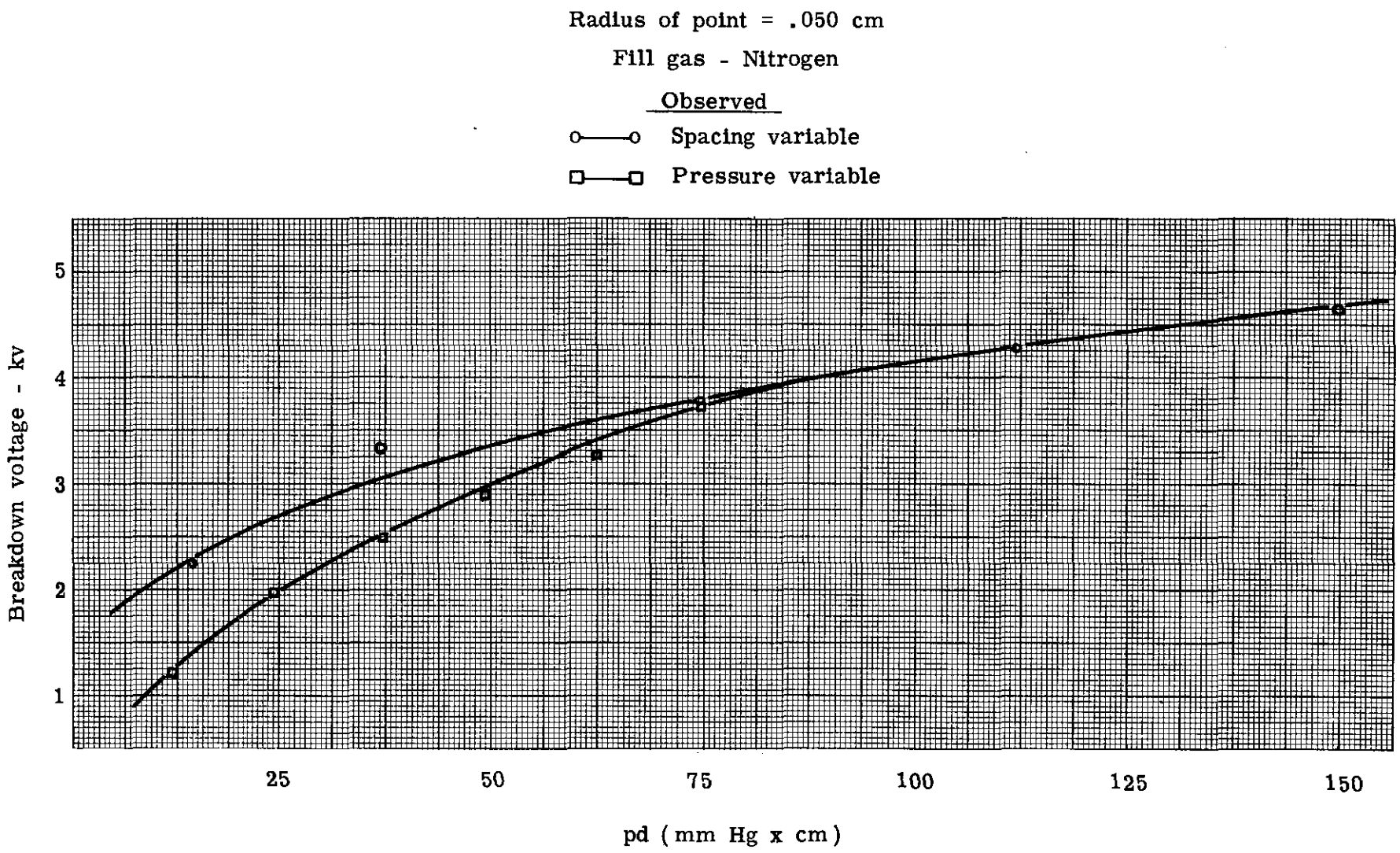

Fig. 33 -- Point-to-plane gap breakdown as a function of pd

The calculated values for Fig. 32 are in good agreement with the observed values, since the spacing of 0.127 cm is sufficient to generate the nonuniform field of the point to plane.

The calculated values for Fig. 31, however, are not quite in exact agreement at the lower gap spacings. The calculated values are lower than the observed values at the smaller gap spacings, indicating that the generated field is approaching a more uniform situation, and the breakdown voltage rises.

Nonuniform Field - Parallel Wires

The apparent breakdown potential for two parallel wires is given in the literature as follows:[13]

$$V_{sbv} = E_s r \ln \frac{d}{r} \text{ in kilovolts,} \tag{21}$$

where

E_s is the gradient at breakdown at the surface of the conductor in kilovolts/cm

r is the radius of the wire in centimeters

d is the spacing between wires in centimeters

The surface gradient E_s at breakdown of the gas also appears to be independent of spacing, except for very short spacings, and is related to the radius of the wire by the following equation:

$$E_s = 30\ pK \left(1 + \frac{0.301}{\sqrt{pr}}\right) \text{ in kilovolts/cm} \tag{22}$$

where

p is the pressure in atmospheres

K is the relative breakdown strength of the fill gas with respect to air

r is the radius of the wire in centimeters.

A review of Equation (21) shows that the smaller the radius, the larger the gradient.

If the ratio of d/r exceeds 5.85, corona will form. The capacity is given by

$$C = \frac{5.55\ k\ 10^{-13}}{\ln\left[\frac{d}{2r} + \sqrt{\frac{(d)^2}{2r} - 1}\right]} \text{ farads/cm} \tag{23}$$

when k is the dielectric constant of the dielectric.

These equations are based on sufficiently long parallel conductors without the influence of the discontinuity of the ends. Our interest, however, in this type of electrode geometry is when the probe-to-probe breakdown of multiprobe gaps is under consideration, and this interest is on the discontinuous ends.

For multiprobe gaps, where the probes are embedded in a common insulator, the probes could be arranged as shown in Fig. 34. This arrangement then approaches the case of two parallel wires, and an estimate of the maximum breakdown value can be obtained from the above equations. It is to be expected that the discontinuity, the surface condition and dielectric constant of the insulator, and the position of the conductors with respect to the insulator (recessed, flush, or protruding) will cause a reduction in the holdoff value of this arrangement. Assuming that for any fixed set of these conditions the effect will be constant, we can obtain an insight into the effect of the ratio of spacing and radius and the direct effect of radius.

Figure 34 shows the comparison between observed and calculated values for 0.102-cm diameter parallel probes that extend beyond the surface of the insulator. The observed values are the averages of several readings. The maximum deviations between the observed curve and calculated curve are 4.2 percent, which is certainly close enough for design purposes. Figure 35 shows the same comparison for 0.050-cm diameter probes that extend only slightly. The maximum variation is about 6.6 percent. Figure 36 shows the same comparisons for 0.102-cm diameter probes that are flush with the insulator surface. The maximum variation is 6.9 percent.

All of these calculated curves show fairly good agreement with the observed values which are always lower than the calculated values. This is due to the reasons stated above. As the pd value increases, the variation between observed and calculated curves also increases. It should be noted that while the average values obtained for the case of the probes that were flush with the insulator compared with the protruding cases, the individual readings of the flush case showed a greater variation between readings. This shows that the conditions of the insulator surface play a very decided role in the breakdown value of this geometry. This present analysis was with a continuous bond between the insulator and the probes, with no voids at either probe. As will be shown in later sections, the effect of voids at the probes or electrodes make a marked reduction in the breakdown value of the combination.

Nonuniform Field - Wire and Cylinder

The apparent breakdown potential for a wire inside a cylinder is given in the literature[13] as follows:

$$V_{sbv} = E_s r \ln \frac{R}{r} \text{ in kilovolts,} \tag{24}$$

where

E_s is the gradient at breakdown at the wire in kilovolts/cm

r is the radius of the wire in centimeters

R is the radius of the cylinder in centimeters .

.102 cm dia Parallel probes

.254 cm Spacing

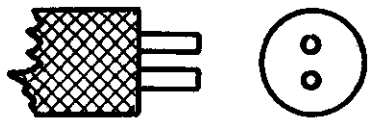

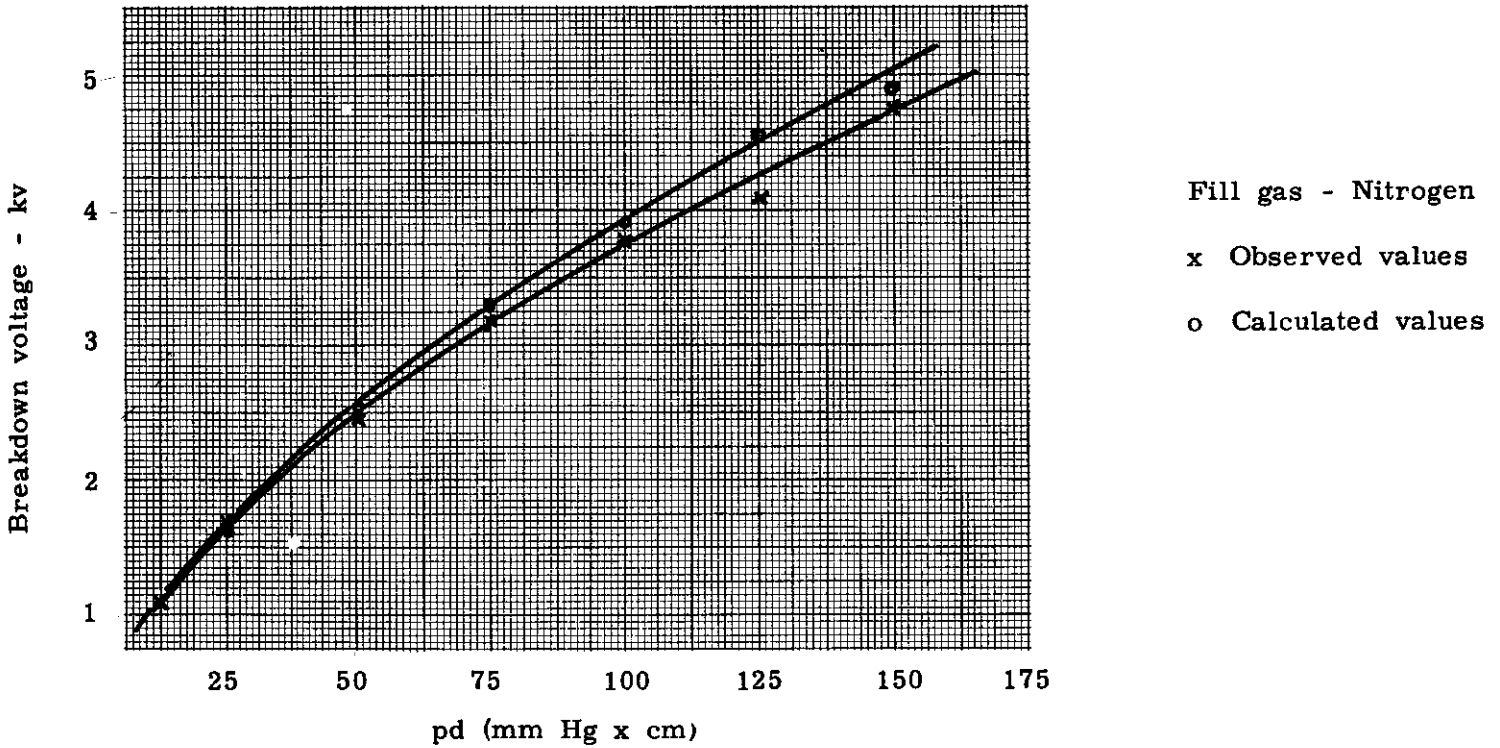

Fig. 34 -- Breakdown curve for parallel probes — .317 cm extension

.050 cm Dia parallel probes

.317 cm Spacing

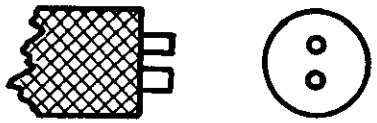

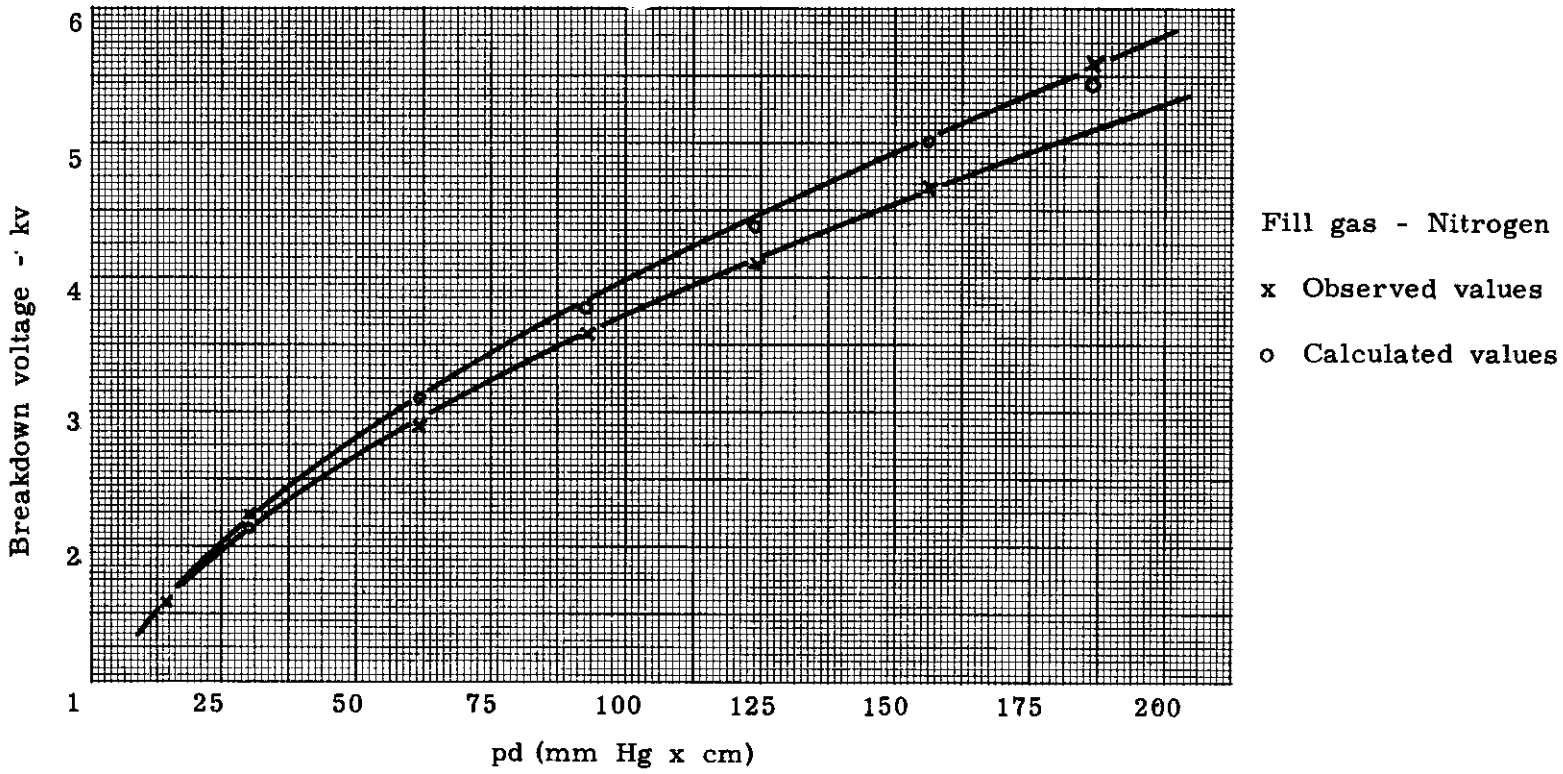

Fig. 35 -- Breakdown curve for parallel probes – .008 cm extension

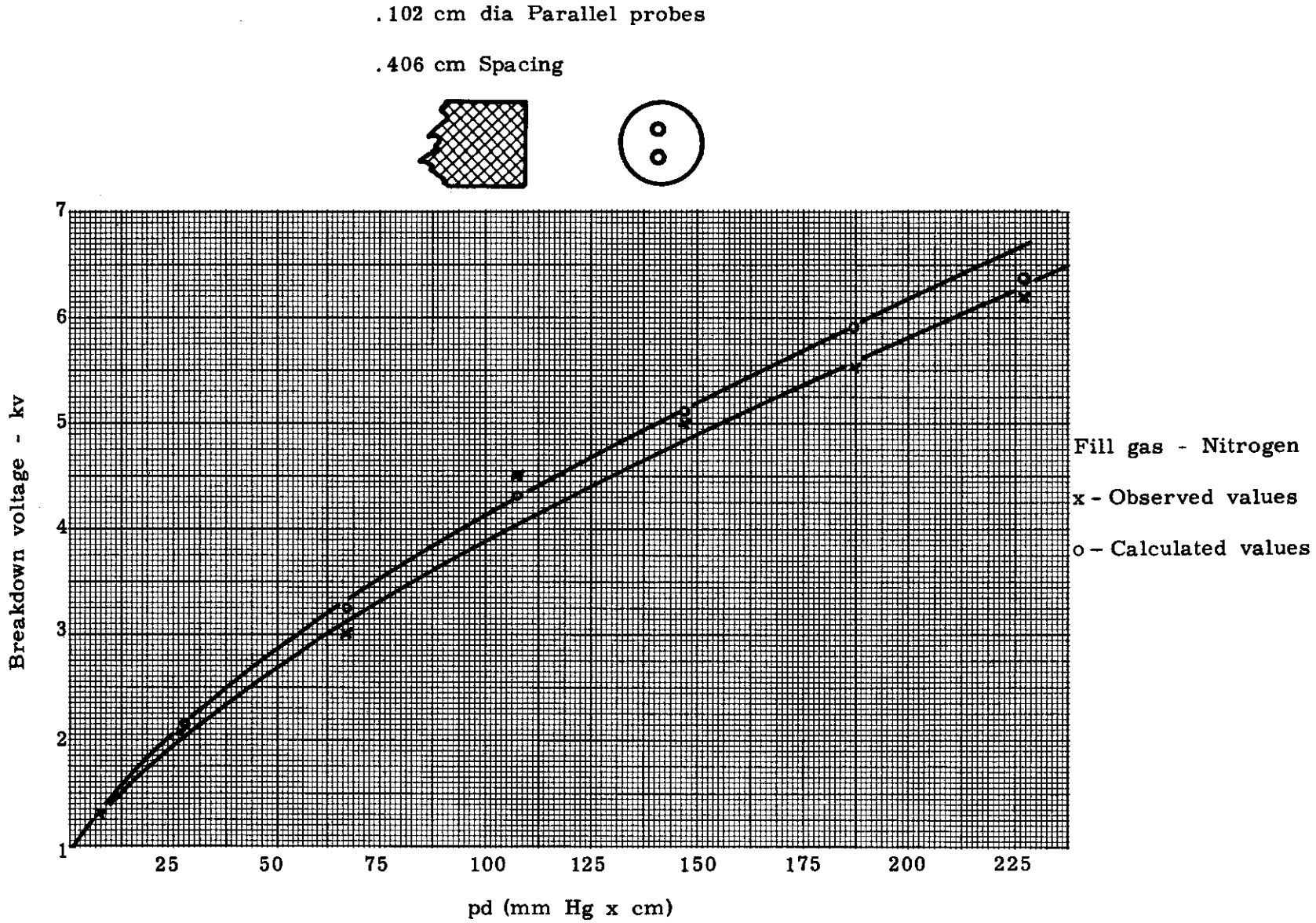

Fig. 36 -- Breakdown curve for parallel probes - no extension

.102 cm dia Wire

.203 cm dia Cylinder

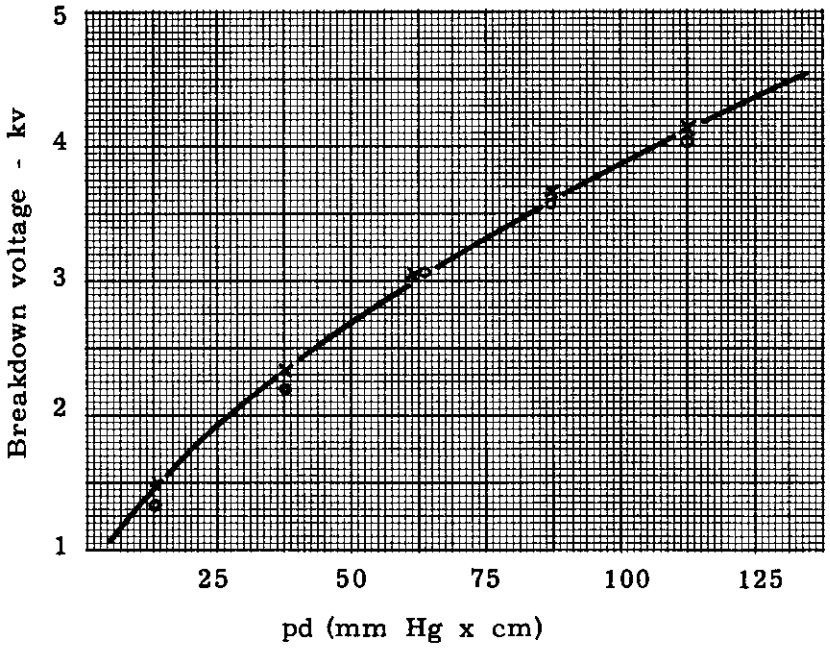

Fill gas - Nitrogen

x - Observed values

o - Calculated values

Fig. 37 -- Breakdown curve for wire and cylinder with bonded glass insulator

The surface gradient E_s at the wire surface at breakdown also appears to be independent of the cylinder radius except for very short radii, and has been shown to be related to the radius of the wire by the following equation:

$$E_s = 31\ pK\left(1 + \frac{0.308}{\sqrt{pr}}\right) \tag{25}$$

where

p is the pressure in atmospheres,

K is the relative breakdown strength of the fill gas with respect to air

r is the radius of the wire in centimeters.

If the ratio of R/r exceeds 2.718, corona will form. The capacity is given by

$$C = \frac{5.55\ k\ 10^{-13}}{\ln \frac{R}{r}}\ \text{farads/cm.} \tag{26}$$

Here again, as in the case of parallel wires, Equation (25) shows that the smaller the wire radius, the larger the gradient.

These equations are also based on sufficiently long cylinders and wires without the influence of the discontinuity of the ends. Our interest, however, in this type of geometry is when the probe-to-trigger-electrode breakdown of single or multiprobe gaps is under consideration, and this interest is on the discontinuous ends.

Figure 37 shows the observed values and calculated values for a 0.102-cm diameter wire and 0.203-cm diameter cylinder; agreement in this case is fairly good. Preliminary data taken for other cases indicate that the observed values are, in general, lower than the calculated values. Evidently the condition of the insulator separating the wire and cylinder can alter the field sufficiently, making it more nonuniform and, consequently, lowering the breakdown value. The sharpness of the probe at the edge will also affect the breakdown characteristics by causing the field to be nonuniform.

The curve of Fig. 37 is for the discontinuity of a wire and cylinder with a glass insulator bonded directly to the wire and the cylinder providing a continuous surface. In order to investigate the breakdown of a similar geometry, but without any intervening insulator between the wire and the cylinder, the geometry shown in Fig. 38 was assembled.

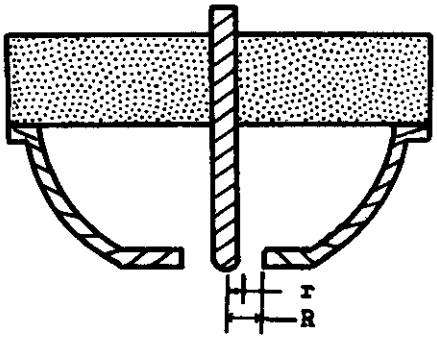

Fig. 38 -- Typical probe assembly

The 0.048-cm radius wire was positioned into a hemispherical dome with a 0.356-cm diameter hole located at the center of the dome. The probe was held in place by the insulator, which is well recessed from the region of interest. The area of spark breakdown is then from near the tip of the wire to the edge of the hole in the dome. This geometry approximates, over a small length, a wire-and-cylinder configuration. The wire has a full radius at the tip. The observed breakdown of this geometry in air at an ambient pressure of 62 cm of Hg is 4000 volts.

Calculating the breakdown for this geometry, the surface gradient E_s at the wire surface at breakdown is given by Equation (25). Therefore,

$$E_s = 31\ pK \left(1 + \frac{0.308}{\sqrt{pr}}\right) \qquad (25)$$

$$E_s = (25.3) \left(1 + \frac{0.308}{\sqrt{0.039}}\right)$$

$$E_s = 63{,}700 \text{ volts/cm} .$$

The breakdown voltage is then given by Equation (24),

$$V_{sbv} = E_s \ln \frac{R}{r} \qquad (24)$$

$$V_{sbv} = 63{,}700 \times 0.048 \times \ln 3.72$$

$$V_{sbv} = 4020 \text{ volts} .$$

The calculated value of 4020 volts is then in good agreement with the observed value of 4000 volts.

In certain applications, the probe will be separated by an insulator with a continuous bond or separated without any insulator at all, while some applications may necessitate use of an insulator with voids at either the probe or the trigger electrode or both. In these arrangements the fields become very complex, and the breakdown voltages will be lower than that predicted for a continuous bond or for no insulator at all. The breakdown for other than a completely homogeneous dielectric will be considered more in detail during the discussion of the static model.

Practical Gaps

In the construction of practical two-electrode gaps and the construction of the main electrodes for triggered gaps, we can only approximate the uniform field by use of symmetrical and spherical electrodes where the radius is usually larger than the gap length. Practical gaps

as circuit components must be made as small as possible; consequently, the electrodes must be made small in diameter. Of course, in using these small diameter spheres, we cannot generate a true uniform field.

A good example of the breakdown of a small practical gap is shown in Fig. 39 which employs spherical, symmetrical electrodes with the gap spacing less than the radius of the sphere. We have investigated the breakdown characteristics of this gap quite extensively, and shown in Fig. 39 are the observed and calculated values. The calculated values were calculated for a uniform field condition, assuming $\alpha d = 20$ for Nitrogen.

Several units were X-rayed to determine their exact spacing, and the gaps were opened to air to allow variations of gas pressure. The average of various spacings and breakdown voltages for these gaps were used. The results of observed and calculated values are in fairly good agreement, except at the lowest values of pd , with the observed values being lower than the calculated values. The reason is probably due to the increased influence of the γ mechanism (secondary emission from the cathode), and the assumption $\alpha d = 20$ is no longer completely valid. The influence of the insulator ring between electrodes on the electric field, the condition of the electrode surfaces, etc., will cause some variation of the breakdown voltage.

Shown in Fig. 40 is the breakdown curve for the gap of Fig. 39 and two 2-electrode safety gaps that tend to produce a nonuniform field by having a very rapidly changing field near the electrodes. From the curves in Fig. 40, one can see that as the ratio of gap spacing to electrode radius increases, the various gaps depart from the uniform field case, and it becomes easier to cause breakdown at any given value of pd. Because of the small gap spacing of the third gap, we were unable to continually increase the pressure to obtain pd values as high as with gaps with larger spacing. This is the reason the pd curve for this gap does not extend beyond a pd value of about 75. The pd curves for Gap 2 and Gap 3 show very markedly how the rapidly varying field near electrodes in nonuniform field gaps affects its breakdown characteristics. If the reduction of the radius is continued even further to the limit of a fine point, the breakdown occurs even lower.

Uniform Field - Gas Mixtures

There are many instances where a gas mixture is employed as the fill gas instead of a single gas. A good example is the use of small amounts of Helium in the fill gas to provide an internal source for Helium leak detection methods. Another use is the inclusion of Oxygen in an Argon fill to quench the residual Argon metastable states for improved trigger operation.

In order to study the effect of gas mixture from the viewpoint of spark gap design, several gases were mixed and the breakdown voltages were recorded. The geometry used consisted of hemispherical electrodes with a radius of 0.457 cm and a gap spacing of 0.127 cm. Figure 41 shows a Nitrogen-Hydrogen mixture, Fig. 42 shows a Nitrogen-Argon mixture, Fig. 43 shows a Nitrogen-Helium mixture, and Fig. 44 shows a Hydrogen-Argon mixture.

The results of these curves indicate that the breakdown voltage of the mixture falls between the breakdown curves of the pure gases as would be expected in the absence of the Penning effect.* The amount of each gas was varied with the resultant breakdown voltages

*The lowering of the breakdown voltage of a gas by a small amount of impurity where the metastable level of the gas is approximately equal to the ionization level of the impurity When excited, atoms having a metastable state have a high probability of transferring this excited energy to another type of atom, if present.

Fill gas - Nitrogen

d = .279 cm

r = .475 cm

o - Calculated

Δ - Observed

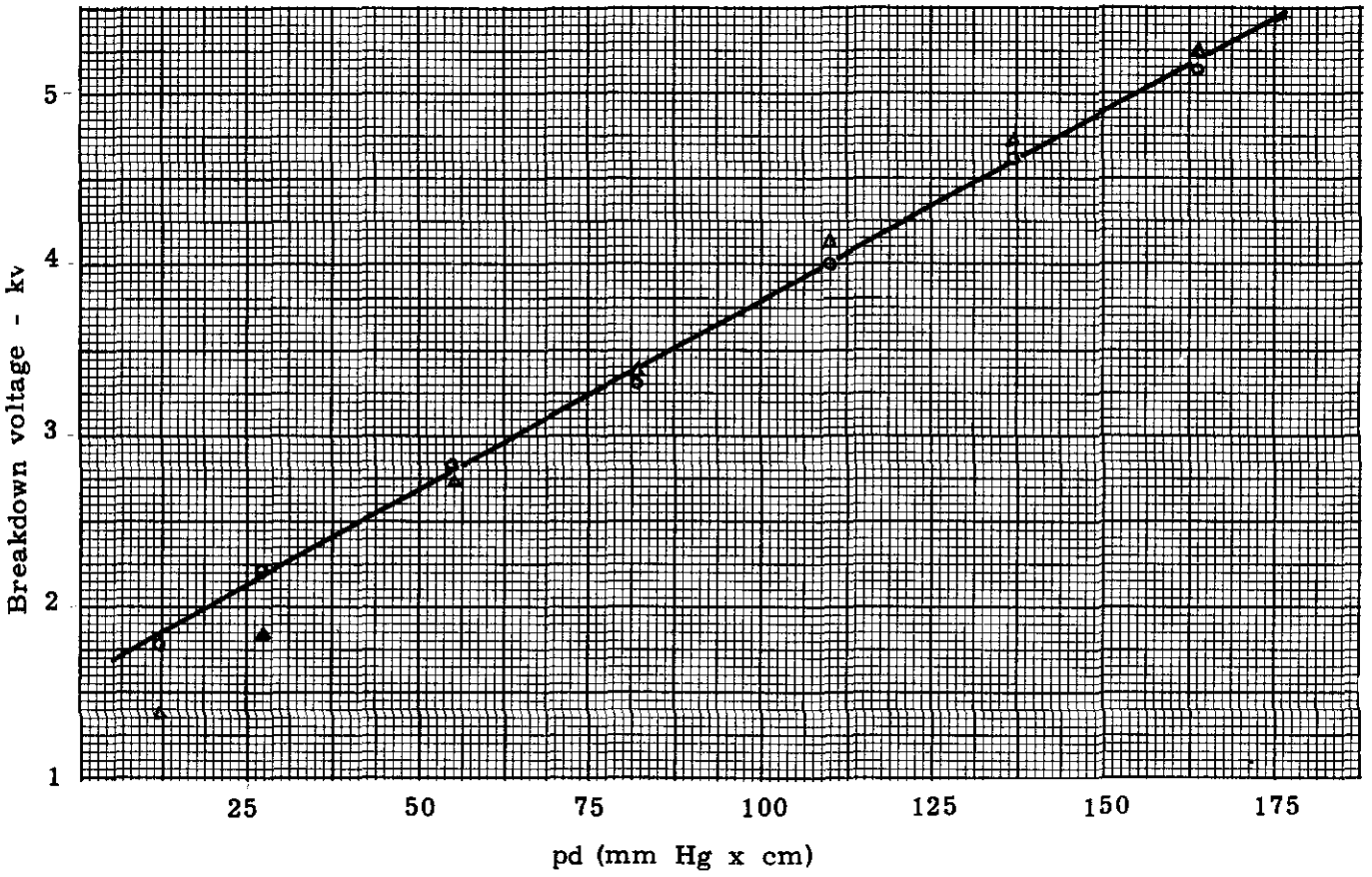

Fig. 39 -- Static breakdown voltage curve for two-electrode gap

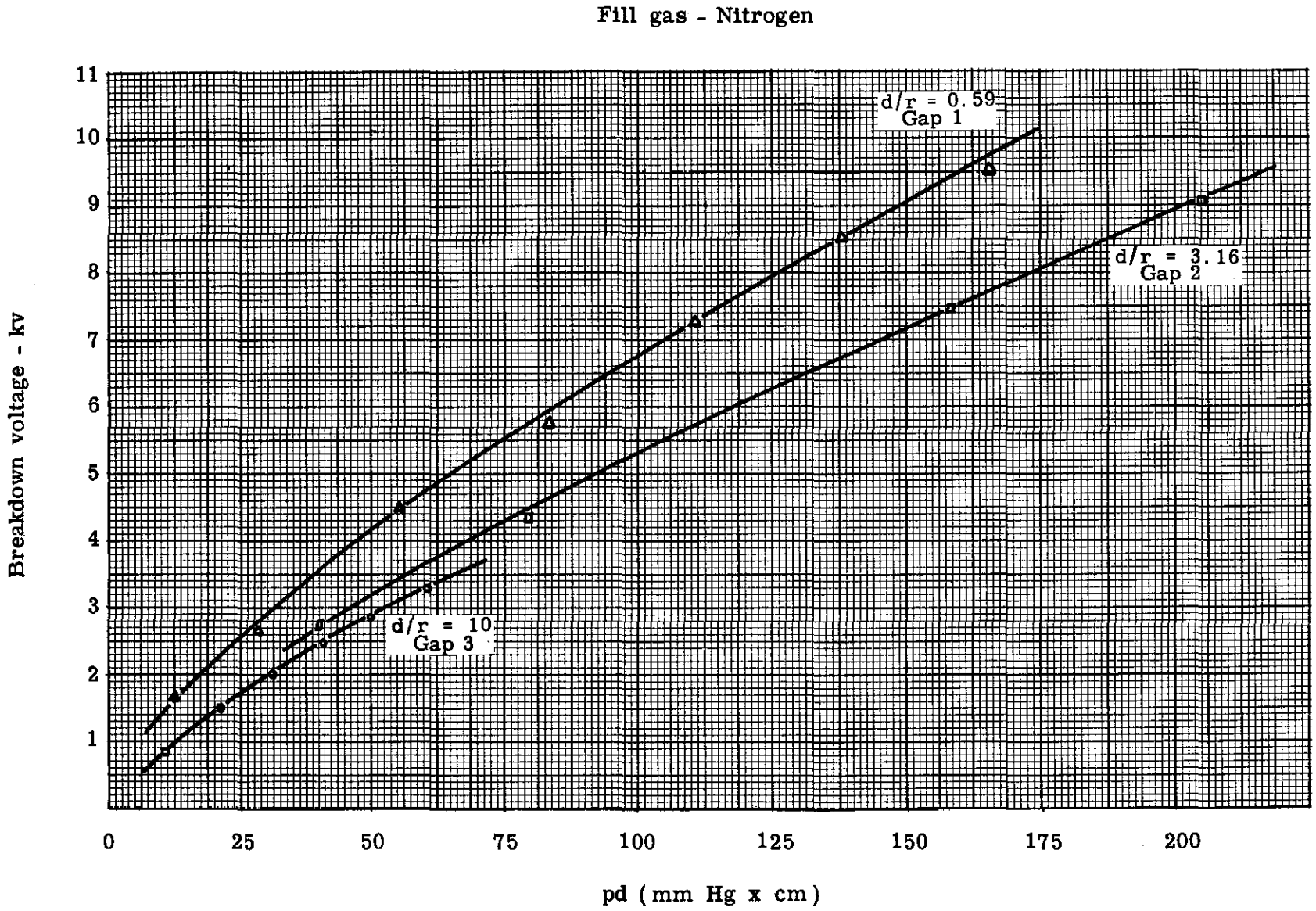

Fig. 40 -- Static breakdown voltage curve for two-electrode gaps showing effect of ratio of d/r

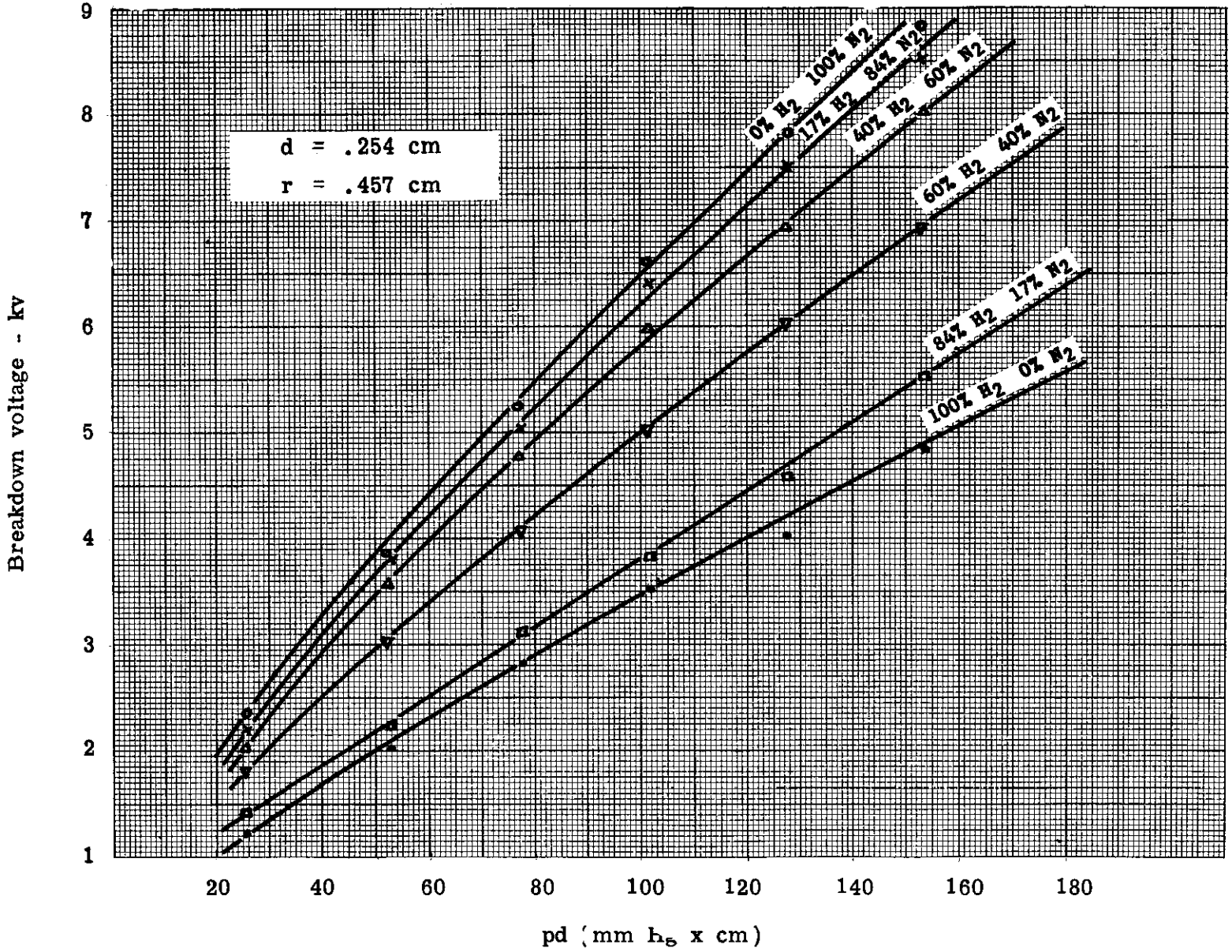

Fig. 41 -- Static breakdown voltage curves in nitrogen-hydrogen mixtures

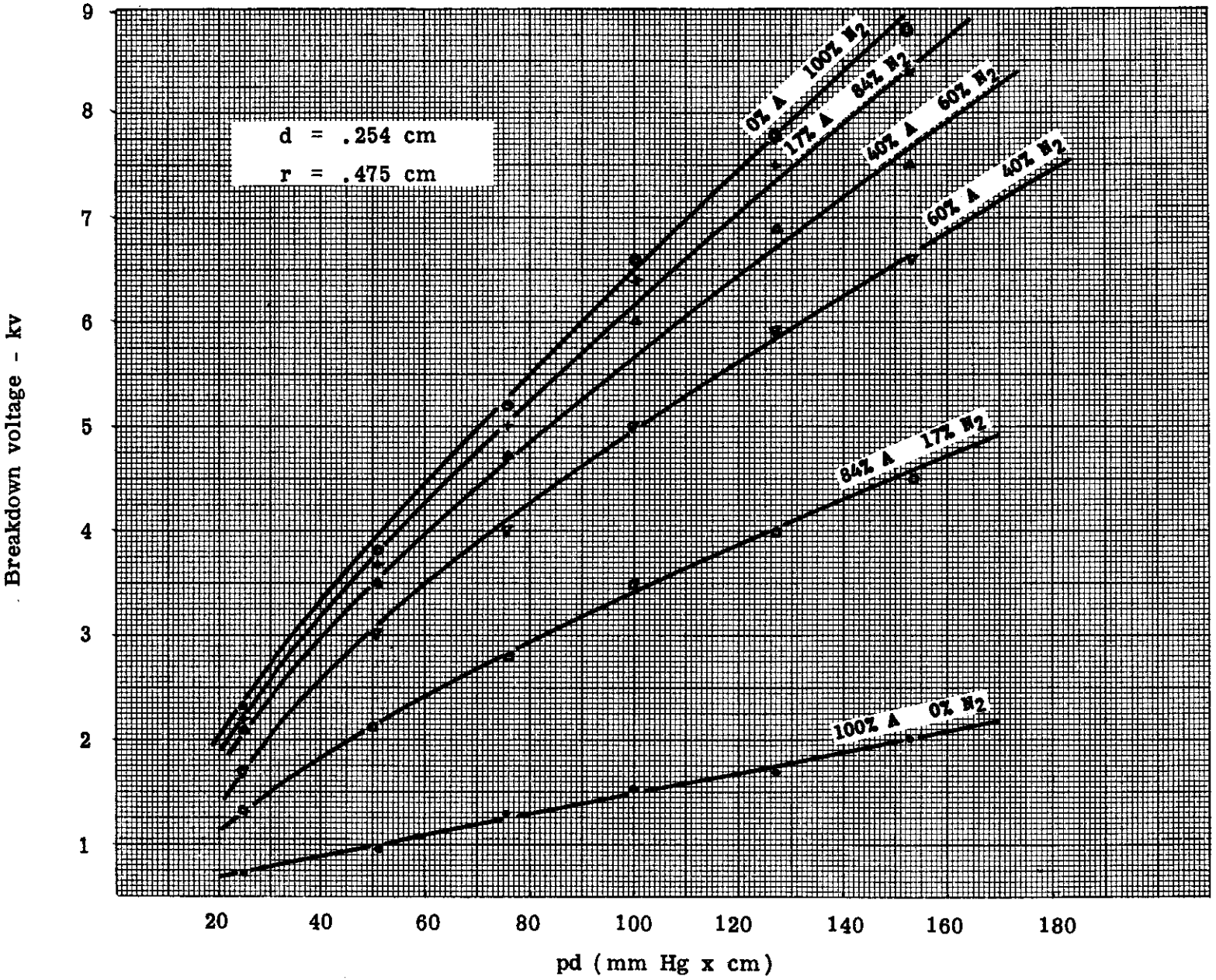

Fig. 42 -- Static breakdown voltage curves in nitrogen-argon mixtures

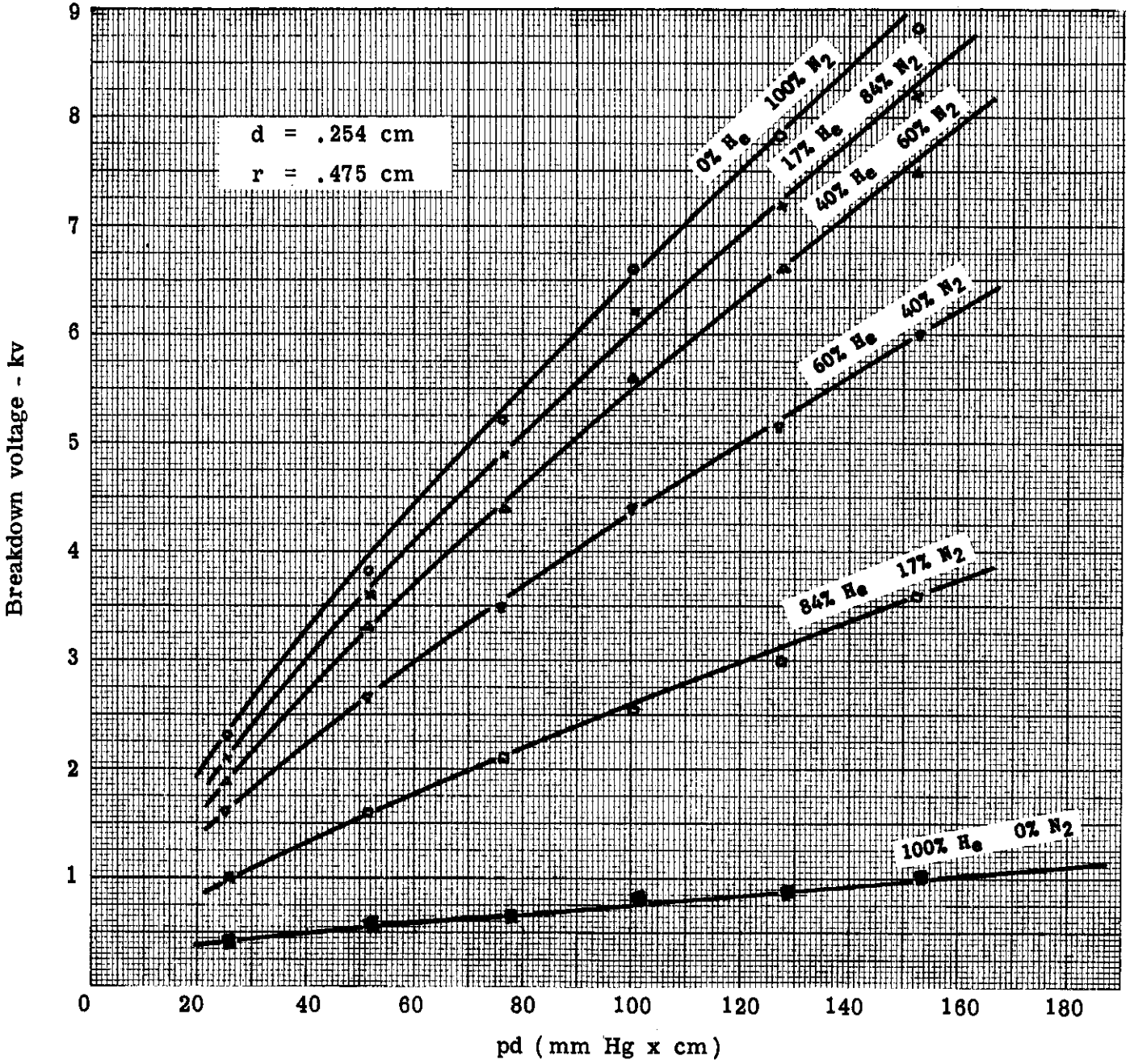

Fig. 43 -- Static breakdown voltage curves in nitrogen-helium mixtures

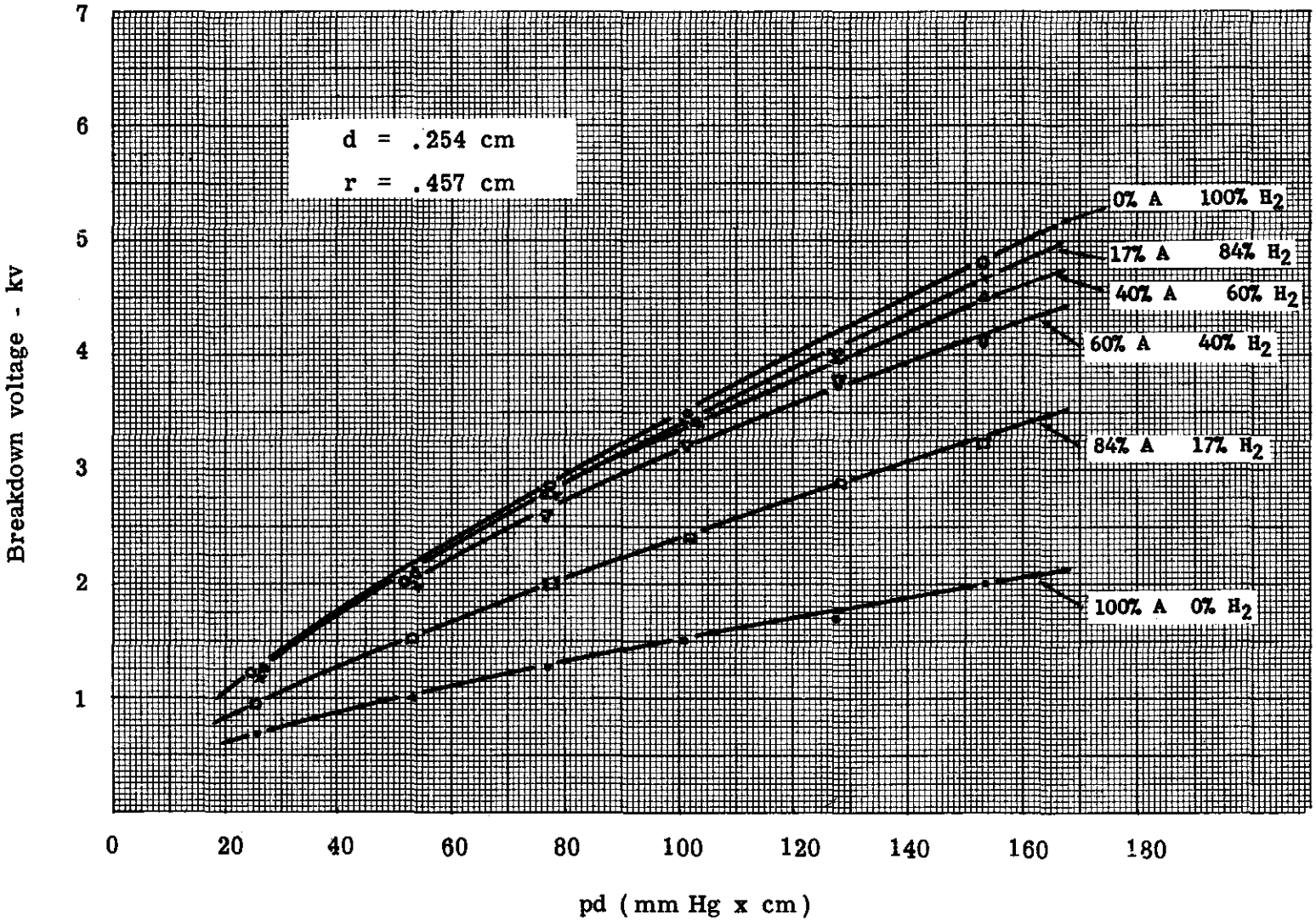

Fig. 44 -- Static breakdown voltage curves in hydrogen-argon mixtures

favoring the breakdown voltage of the higher breakdown gas. For example, in considering the Nitrogen-Argon mixture, a 17 percent contribution of Nitrogen has a greater effect than does a 17 percent contribution of Argon.

Further consideration of these curves indicates that the contribution to the total breakdown of each constituent gas is related to the partial pressure of each gas in the mixture. For example, let us consider the various mixtures for the pd product of 153 mm Hg x cm . For this pd product the total pressure is 600 mm Hg. The partial pressure of each gas was determined and the breakdown voltage of each gas at the revised pd product of partial pressure and gap spacing was recorded. The sum of the breakdowns of the partial pressures was tabulated and compared with the breakdown voltage of the combination. These results are shown in Table III.

TABLE III

Comparison of the Breakdown Voltages for Partial Pressures of Gas Mixture with the Breakdown Voltage of the Total Combined Mixture

Mixture-%		Pressure-mm Hg		Pd-mm Hg x cm		SBV-volts		SBV-volts	SBV-volts
N_2	He	N_2	He	N_2	He	N_2	He	N_2 + He	observed
17	84	100	500	25.4	127.0	2300	900	3200	3600
40	60	240	360	61.0	91.5	4450	750	5200	6000
60	40	360	240	91.5	61.0	6000	600	6600	7500
84	17	500	100	127.0	25.4	7800	400	8200	8200
N_2	A	N_2	A	N_2	A	N_2	A	N_2 + A	Observed
17	84	100	500	25.4	127.0	2300	1700	4000	4500
40	60	240	360	61.0	91.5	4450	1450	5900	6600
60	40	360	240	91.5	61.0	6000	1150	7150	7500
84	17	500	100	127.0	25.4	7800	700	8500	8400
N_2	H_2	N_2	H_2	N_2	H_2	N_2	H_2	N_2 + H_2	Observed
17	84	100	500	25.4	127.0	2300	4000	6300	5500
40	60	240	360	61.0	91.5	4450	3200	7650	6900
60	40	360	240	91.5	61.0	6000	2300	8300	8000
84	17	500	100	127.0	25.4	7800	1200	9000	8500
H_2	A	H_2	A	H_2	A	H_2	A	H_2 + A	Observed
17	84	100	500	25.4	127.0	1200	1700	2900	3200
40	60	240	360	61.0	91.5	2300	1450	3750	4100
60	40	360	240	91.5	61.0	3200	1150	4350	4500
80	17	500	100	127.0	25.4	4000	700	4700	4700

From the results of Table III, we can conclude that a fairly close approximation of a gas mixture where the Penning effect is not operating is to obtain the sum of breakdown voltages of each gas for the partial pressure of each gas.

The relative breakdown strength, K , of these gas mixtures is of interest and is shown below in Table IV.

TABLE IV

The Relative Breakdown Strength of Various Gas Mixtures .

Nitrogen-Hydrogen		Nitrogen-Argon		Nitrogen-Helium		Hydrogen-Argon	
Mixture	K	Mixture	K	Mixture	K	Mixture	K
$17\%N_2$-$84\%H_2$	1.01	$17\%N_2$-84%A	1.00	$17\%N_2$-$84\%H_e$	.97	$17\%H_2$-84%A	.56
$40\%N_2$-$60\%H_2$	.95	$40\%N_2$-60%A	.89	$40\%N_2$-$60\%H_e$	.89	$40\%H_2$-60%A	.53
$60\%N_2$-$40\%H_2$	.82	$60\%N_2$-40%A	.78	$60\%N_2$-$40\%H_e$	.71	$60\%H_2$-40%A	.49
$84\%N_2$-$17\%H_2$	.65	$84\%N_2$-17%A	.54	$84\%N_2$-$17\%H_e$	.43	$84\%H_2$-17%A	.38

CH III -- THE THREE-ELECTRODE GAP

Methods of Triggering

As has been shown, a two-electrode spark gap can be constructed that will hold off all voltages up to its designed critical breakdown value. The problem now is to devise some means of causing this gap to change from a very good insulator at some given voltage below its hold-off value, to a conductor allowing the switching of peak currents of up to about 100,000 amperes. The method of performing this switching is accomplished by causing sufficient ionization of the gas between the electrodes and allowing the gap to breakdown. The following are methods that may be used to accomplish this breakdown:

1. Sudden increase of voltage across the gap
2. Sudden reduction in gap spacing
3. Sudden reduction in gas density
4. Natural radioactive irradiation of the gap
5. Ultraviolet irradiation of the gap
6. Injection of ions and/or electrons into the gap
7. Heated filament in the gas dielectric
8. Distortion of the electric field

The method of ion and electron injection is the most practical, and provides rapid and reliable triggering with low delay times and a relatively low applied gap voltages. This injection of electrons and ions is obtained by generating an auxiliary spark inside the gap. This auxiliary spark is then a reservoir of electrons and ions and the source of a low-density region due to the energy dissipated by the trigger spark. These ions and electrons are then acted upon by the accelerating field of the applied voltage. Consequently, in their travel across the gap behind the propagating low-density region the, α , mechanism is enchanced causing complete ionization of the gas and formation of the arc. In addition to this source of electrons and ions, the auxiliary spark is also a source of photon or ultraviolet irradiation of the gap.

Effect of Trigger Probe Hole

If one of the spheres is modified by having a hole drilled through it, there is a marked lowering of its holdoff ability. The sharp corners of the hole distort the electric field thereby producing a nonuniform field condition and, as we have seen earlier, the nonuniform field tends

to cause higher surface gradients with resultant lower breakdown voltages. If the probe is now inserted into this hole along with the insulator, the static breakdown value increases to approximately its original value. This indicates that the insulator obtains a surface polarization charge and the gap geometry again appears as a uniform field and the breakdown value goes up. Since the probe is normally connected to the trigger electrode through the trigger transformer, this further tends to cause the field to be uniform.

Figures 45 and 46 show the results of two sets of electrodes with holes of varying diameters drilled into one of the electrodes. The hole diameters were so chosen so that they were a certain percentage of the electrode diameter for comparison purposes. The holes chosen represent up to 30 percent of the electrode diameter.

These curves clearly show that the larger the hole with respect to the electrode diameter, the more nonuniform the electric field becomes and the lower the breakdown voltage. The points plotted represent the average of five readings.

From the standpoint of gap design, it is clear that the smaller the probe hole with respect to electrode diameter, the less the effect on influencing and lowering the breakdown voltage. Also, there is a greater reduction in breakdown voltage for the large trigger electrode holes when the main gap spacing is large.

The result of inserting an insulator and a probe into the trigger electrode hole is to cause the gap to resume approximately its original static breakdown voltage; the smaller the gap spacing, the closer the breakdown returns to the original value. From the standpoint of gap design, it is seen that if the hole is filled with the probe wire and the insulator, and the reference potential of the probe is the same as the trigger electrode, then the holdoff voltage of the triggered gap will essentially be that of a two-electrode gap. If no insulator is inserted in the region of the probe tip, the static breakdown voltage of the gap will then be reduced from that of a two-electrode gap.

This general effect has been reported earlier in the EG&G report.[4] This additional work was performed to obtain more data on this characteristic, especially with respect to the effect of variations of hole diameter within a given sphere, which was not covered by the EG&G report.

The Static Model

In initiating the triggering action the first step is, of course, to establish the trigger spark by applying a trigger pulse of sufficient amplitude.

The electric gradients internal to the gap will determine the value of pulse breakdown for a given rise time, and whether the trigger spark forms to the trigger electrode or to the main electrode. As will be shown later, the initial path of the trigger spark plays an importa part in the triggering characteristics.

It is of interest to consider the static triggering of the three-electrode triggered spar gap. Consider a spark gap as shown in Fig. 47. The main gap is composed of portions of spheres where the ratio of d/r is small, thereby generating a fairly uniform electric field. The holdoff capability of the main gap can therefore be established by the considerations discussed in Chapter II . It now becomes the problem of establishing the proper probe diamete and probe hole in the upper electrode for a given main gap spacing and intended trigger spar

Hole Diameter

0.000 cm 0% of sphere dia
0.127 cm 10% of sphere dia
0.254 cm 20% of sphere dia
0.380 cm 30% of sphere dia

Fill gas - Nitrogen
Pressure - 60 cm Hg
Spacing - variable

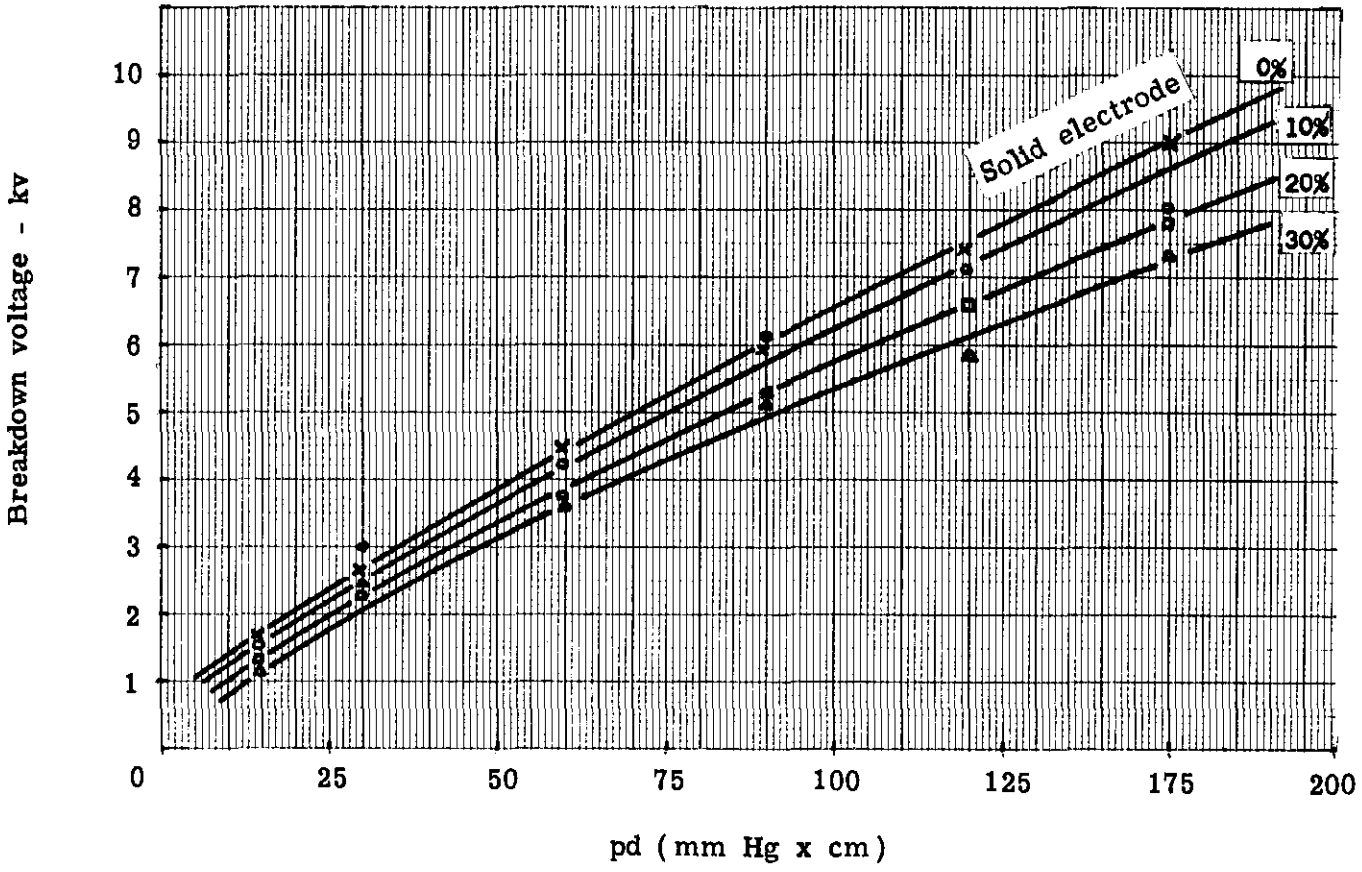

Fig. 45 -- Breakdown curves of 1.270-cm dia spheres with various probe hole diameters

Fill gas - Nitrogen
Pressure - 60 cm Hg
Spacing - variable

Hole Diameter	
0.000 cm	0% of sphere dia
0.093 cm	10% of sphere dia
0.190 cm	20% of sphere dia
0.287 cm	30% of sphere dia

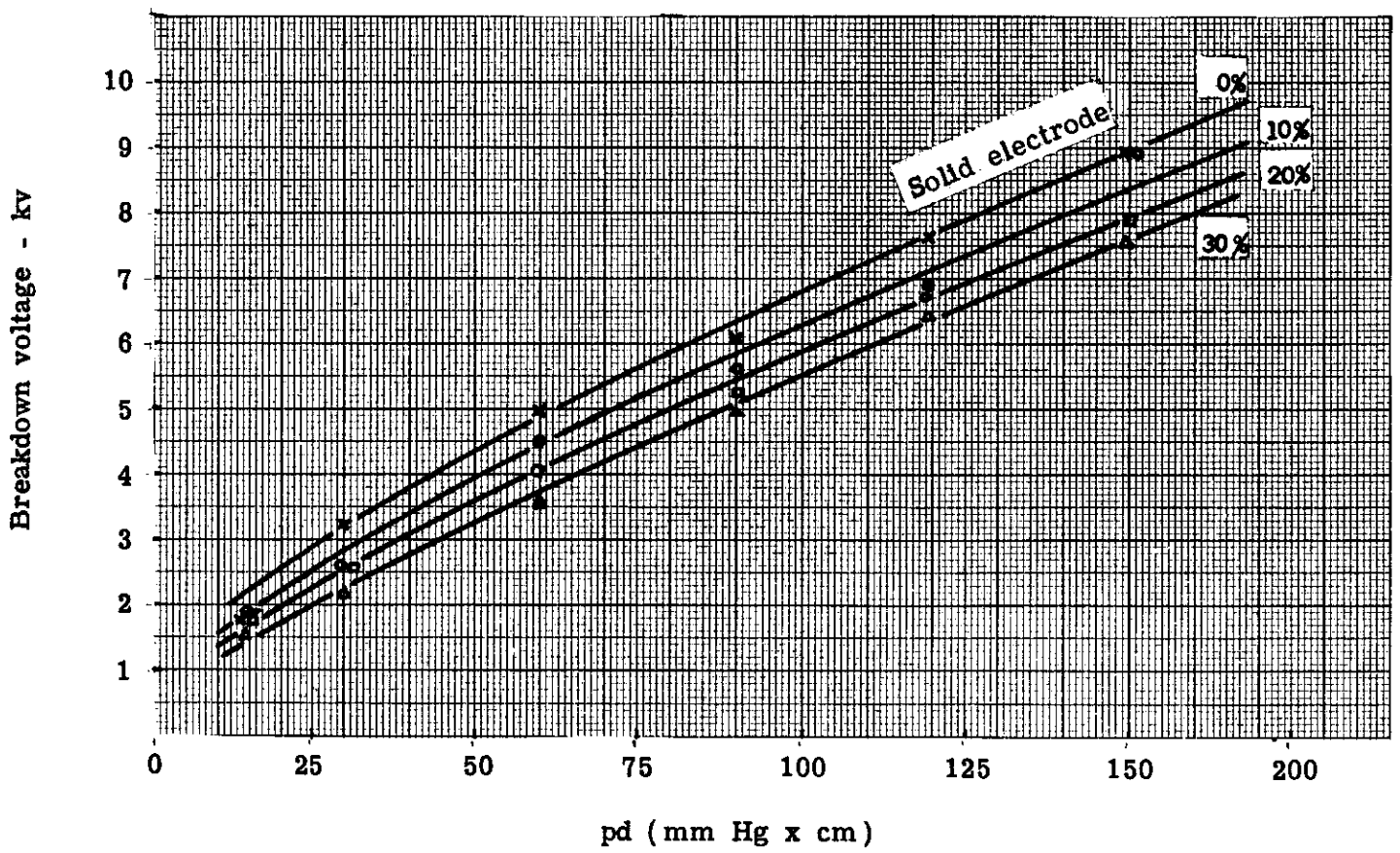

Fig. 46 -- Breakdown curves of 0.952-cm dia spheres with various probe hole diameters

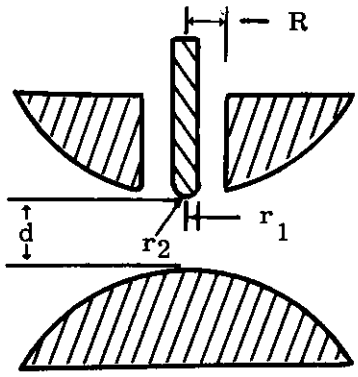

Fig. 47 -- Geometry for the static model

path. If the trigger spark is desired to cross the main gap rather than to the adjacent electrode, the gradient setup between probe-to-main electrode must be, therefore, greater than for the gradient from the probe to the trigger electrode for any given applied voltage to the probe.

Observation of the spark gap of Fig. 47 suggests that the probe-to-main electrode gradient can be approximated by the point-to-plane gap, while the probe-to-trigger electrode can be approximated by the coaxial wire and cylinder gradients. For the present, we will assume the hemispherical radius of the probe to be that of the radius of the wire. From the discussion in Chapter II , we have the following approximation to the breakdown values of the probe. The dielectric of the insulating medium is assumed to be air,

$$\epsilon = 1 .$$

The breakdown voltage of the coaxial arrangement is

$$V_1 = r_1 E_1 \ln \frac{R}{r_1} \tag{27}$$

while the breakdown voltage of point-to-plane is

$$V_2 = \frac{r_2 E_2}{4} \ln \frac{8d}{r_2} \tag{28}$$

Therefore, the ratio of probe-to-trigger electrode breakdown to probe-to-main electrode breakdown is then the ratio of the coaxial breakdown voltage and the point-to-plane breakdown. This ratio, K_p is given below as

$$K_p = \frac{V_1}{V_2} = \frac{r_1 E_1 \ln \frac{R}{r_1}}{\frac{r_2}{4} E_2 \ln \frac{8d}{r_2}} \tag{29}$$

However, in practical use, the radius of the wire used in the point-to-plane geometry and the radius of the wire in the wire and cylinder geometry are generally the same. Therefore,

$$r_1 = r_2 = r$$

and now

$$K_p = \frac{4E_1 \ln \frac{R}{r}}{E_2 \ln \frac{8d}{r}} . \tag{30}$$

As discussed earlier, the surface gradient E_1 at the breakdown value of the gas appears to be independent of spacing, except for very short spacings, and is related to the radius of the wire by the following equation:

$$E_1 = 31\ pK \left(1 + \frac{0.308}{\sqrt{pr}}\right) \text{ in kilovolts/cm,} \tag{25}$$

where

p is the pressure in atmospheres

K is the relative strength of the fill gas with respect to air

r is the radius of the wire in centimeters .

As mentioned above, the point of radius r_2 opposite a plane should breakdown with the same surface gradient as a wire of $1/4\ r_2$ within a cylinder.

Therefore, if we want to determine the surface gradient of the point to plane, we take one-fourth of the radius of the point, and take this figure and apply it into the expression for the coaxial case. In the design of triggered gaps, the radius may be the same for both configurations and, therefore, the surface gradient at breakdown for the probe-to-main electrode (point-to-plane) geometry will be higher than for the probe-to-trigger electrode (wire and cylinder) geometry.

If we now substitute into the expression for K_p the expressions for E_1 and E_2 :

$$K_p = \frac{(4)(31\ pK)\left(1 + \frac{0.308}{\sqrt{pr}}\right) \ln \frac{R}{r}}{31\ pK \left(1 + \frac{0.308}{\sqrt{pr/4}}\right) \ln \frac{8d}{r}} \tag{31}$$

simplifying we obtain:

$$K_p = \frac{4\left(1 + \frac{0.308}{\sqrt{pr}}\right) \ln \frac{R}{r}}{\left(1 + \frac{0.616}{\sqrt{pr}}\right) \ln \frac{8d}{r}} \tag{32}$$

by a simple algebraic manipulation, then:

$$K_p = 2\left(1 + \frac{1}{a}\right) \frac{\ln \frac{R}{r}}{\ln \frac{8d}{r}} \tag{33}$$

where

$$a = 1 + \frac{0.616}{\sqrt{pr}}$$

Assuming various values of R/d for a given probe radius, r, we obtain the curves of K_p versus R/d shown in Figs. 48 and 49.

From the above expression or from the curves of Figs. 48 and 49, the relative static breakdown of probe-to-main electrode and probe-to-trigger electrode can be determined and to what electrode the trigger spark will form to. Depending upon the application of the triggered spark gap and the required operating characteristics, it may be desirable to have the probe-to-trigger electrode holdoff voltage much higher than the probe-to-main electrode holdoff and vice versa. While the influence of the interaction of the fields of the two geometries, the applied reference potential, and the polarity of the electrodes will all influence the relative breakdown ratio, the present expression nevertheless gives an approximation to establishing the necessary spacings and geometry to satisfy the static breakdown requirements of the various electrodes.

It should be kept in mind that this type of probe geometry, with a substantial hole in the trigger electrode, will result in the breakdown voltage of the main gap being lowered, as discussed in the preceding section. In addition, the interaction of the main field and the probe field causes a slight increase in the probe-to-trigger electrode breakdown, as the main gap spacing is made smaller.

The Effect of the Probe Insulator

On Probe-to-Trigger Electrode Breakdown

In many practical applications there is usually an insulator other than air or gas to separate the probe from the trigger electrode. In some cases there may be a continuous, homogeneous bond between the probe and the trigger electrode. There may also be a void of variable width adjacent to the electrode or the probe or both. Referring to Chapter II, if there is continuous bond, the observed breakdown value is fairly close to the calculated value. (Discontinuity effects may be present, however.)

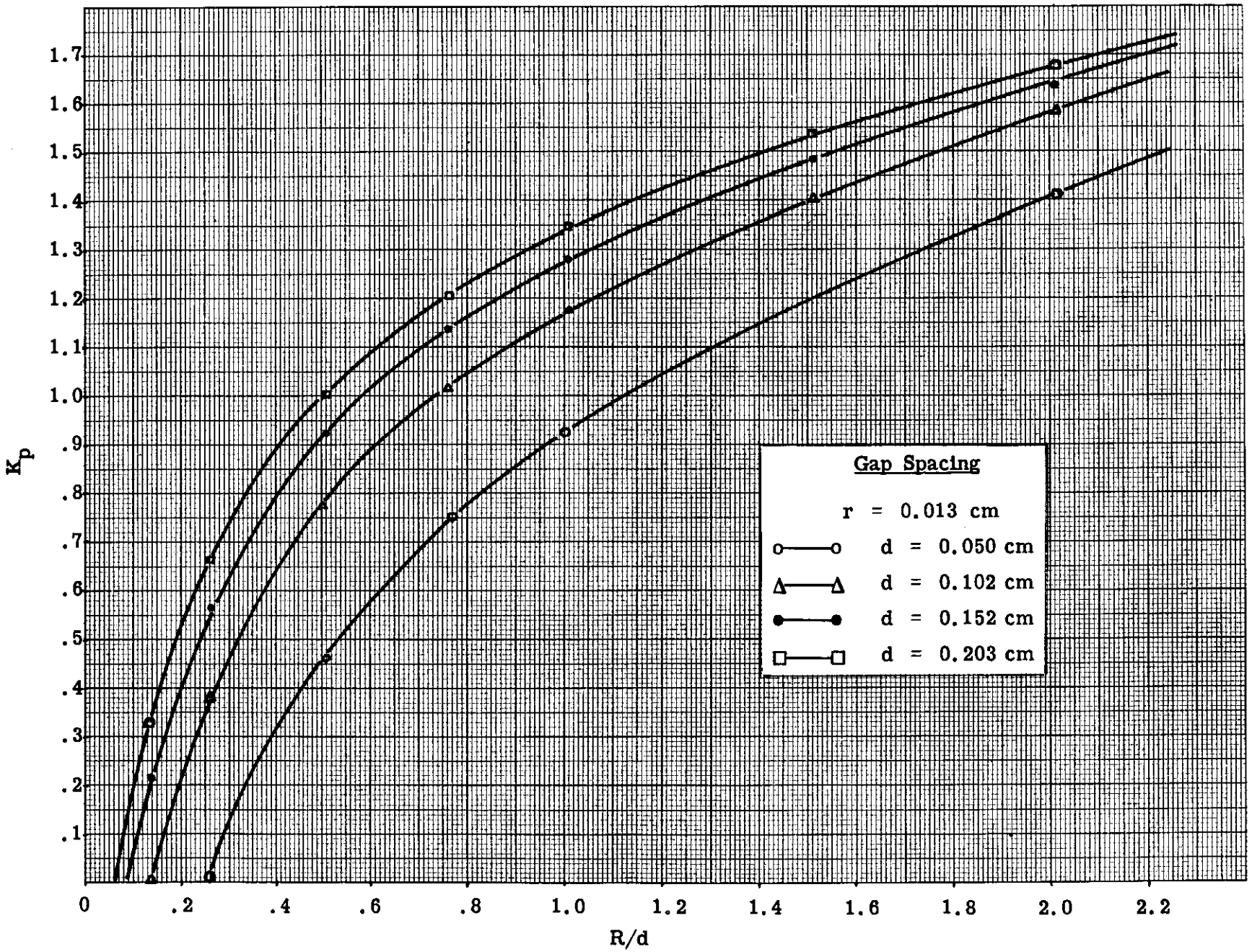

Fig. 48 -- Static breakdown ratio, K_p, as a function of R/d

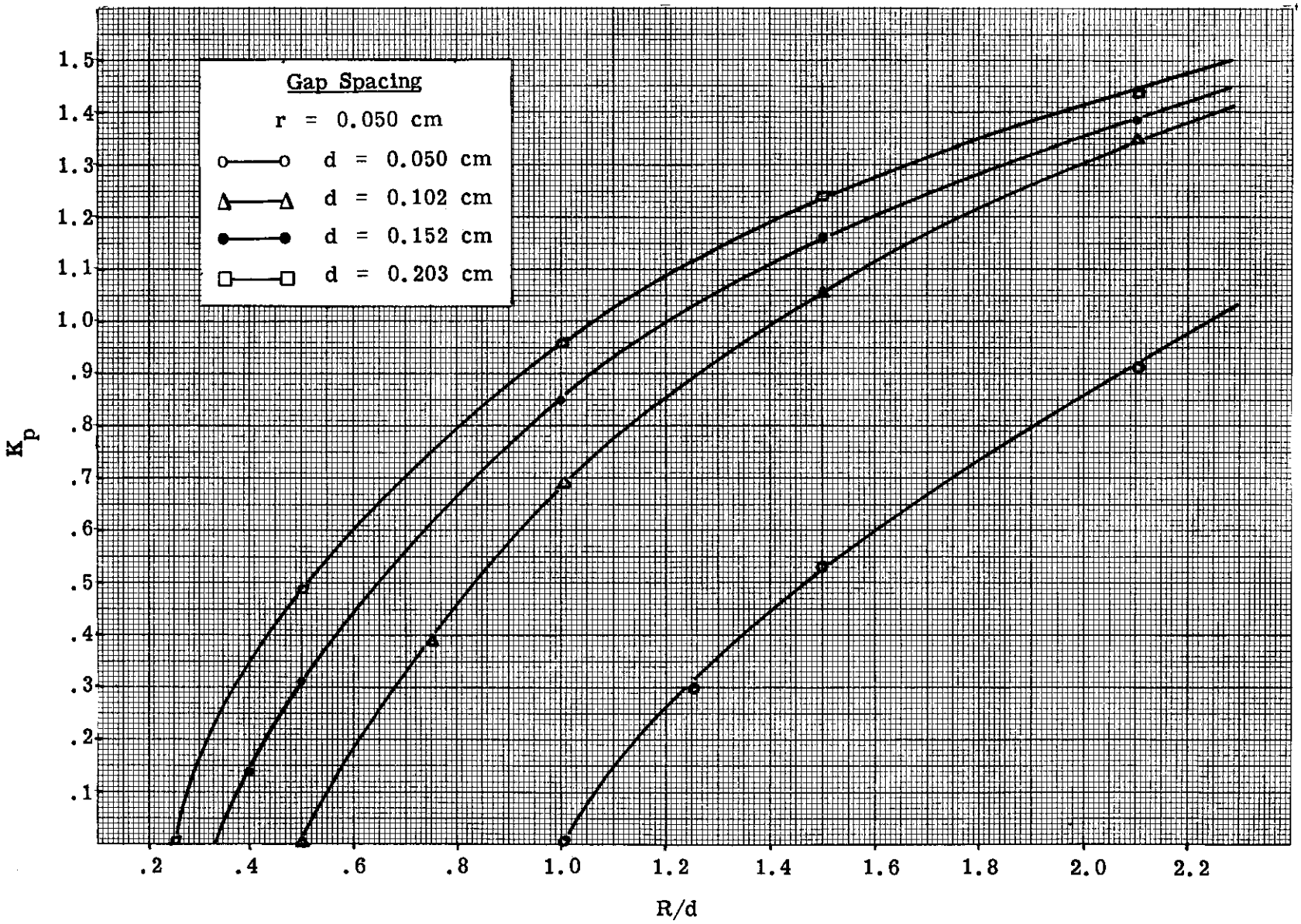

Fig. 49 -- Static breakdown ratio, K_p, as a function of R/d

If a small gas void is present between the insulator and electrodes, it is well known that the gas dielectric will be overstressed by the influence of the higher dielectric constant insulator. The result of this intensified electric field stress in this region is to reduce the holdoff voltage of the geometry. The amount of voltage reduction is then a function of the void spacing and the dielectric constant of the insulator with respect to the gas voids. For a coaxial probe arrangement as shown in Fig. 50, the resultant gradient can be shown to be as follows[13]:

$$E'_x = \frac{V}{r_x K_x \left(\frac{1}{K_a} \ln \frac{r_2}{r_1} + \frac{1}{K_b} \ln \frac{r_3}{r_2} + \frac{1}{K_c} \ln \frac{r_4}{r_3} \right)} . \qquad (34)$$

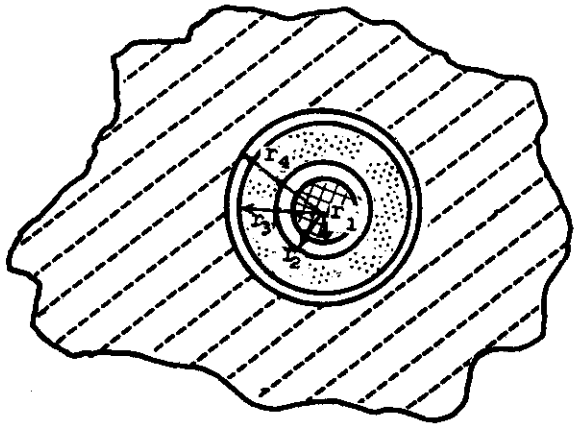

Fig. 50 -- Coaxial probe arrangement

Where

V = Applied voltage

K_a = Dielectric constant of medium 1, r_1-r_2

K_b = Dielectric constant of medium 2, r_2-r_3

K_c = Dielectric constant of medium 3, r_3-r_4

r_1 = Radius of probe

r_2 = Inner radius of insulator

r_3 = Outer radius of insulator

r_4 = Radius of trigger electrode

Where E_x = electric field at radius r_x in a medium of dielectric constant K_x.

If we assume the original case of a single homogeneous dielectric between the probe and the trigger electrode, $r_2 = r_3 = r_4$ and, therefore,

$$E_{r_1} = \frac{V}{r_1 \ln \frac{r_4}{r_1}} . \tag{35}$$

Since $r_1 = r$ and $r_4 = R$, we have the case previously discussed of a coaxial geometry with no discontinuities.

The relative increase in electric field due to the insertion of gas voids between an insulator and the probe, and trigger electrode is then given by the following expression

$$A = \frac{E'_{r_x}}{E_{r_x}} = \frac{\ln \frac{r_4}{r_1}}{K_x \left(\frac{1}{K_a} \ln \frac{r_2}{r_1} + \frac{1}{K_b} \ln \frac{r_3}{r_2} + \frac{1}{K_c} \ln \frac{r_4}{r_3} \right)} \tag{36}$$

Since we have a discontinuous geometry at the probe-to-trigger electrode region, we have the field distribution just inside the interface surface of the void affecting the field just outside of the surface in the main gap region. While the spark that forms between the probe and trigger electrode is entirely outside of the insulator surface, the effect of the field in the void regions inside this surface influences the ionization processes in that region, resulting in a lowering of the holdoff voltage of the combination. The most important practical considerations are as follows:

1. Overstressing of the gas in the void at the probe due to the void at the probe.

2. Overstressing of the gas in the void at the probe due to the void at the probe and the void at the trigger electrode.

3. Overstressing of the gas in the void at the trigger electrode due to a void at the trigger electrode.

4. Overstressing of the gas in the void at the trigger electrode due to a void at the trigger electrode and a void at the probe.

Other changes of the field for a continuous bond at the probe or trigger electrode, or in the insulator, are not important, since they cannot contribute to the breakdown path of the trigger spark.

Consider Case No. 1 where the insulator is bonded to the trigger electrode and a void occurs at the probe. The relative increase in the field in this void is then of interest and since $K_x = K_a = 1$ for air, $r_3 = r_4$ and $K_c = K_b$, our expression reduces to the following

$$A = \frac{\ln \frac{r_4}{r_1}}{\left(\ln \frac{r_2}{r_1} + \frac{1}{K_b} \ln \frac{r_4}{r_2} \right)} \tag{37}$$

if we allow r_2 to approach r_1, the relative field increase, A, approaches K_b as the limit. While the field intensity increases at the probe as r_2 approaches r_1, the effective area over which this high field region applies is correspondingly reduced. If the electric field in this region is increased sufficiently, the breakdown gradient of the fill gas at a given pressure may be exceeded, causing the region to become conductive. This conductive region enhances complete breakdown of the probe by effectively shortening the spacing and providing a supply of electrons and ions to stimulate the avalanche mechanism.

It can also be seen that if there is no void present, $r_2 = r_1$ and K_a no longer equals 1 but equals K_b. Therefore, for a continuous, homogeneous material between the probe and trigger electrode, the relative increased factor, A, equals 1 regardless of the insulating medium employed.

If we consider Case No. 3 in the manner discussed above, we find that the expression for A reduces to

$$A = \frac{\ln \frac{r_4}{r_1}}{\frac{K_c}{K_b} \ln \frac{r_3}{r_1} + \ln \frac{r_4}{r_3}} \tag{38}$$

and as r_3 approaches r_4, A again approaches K_b as the limit since $K_c = 1$. If we consider the field at the trigger electrode due to a void at the probe as well as at the trigger electrode, we obtain

$$A = \frac{\ln \frac{r_4}{r_1}}{\left(\ln \frac{r_2}{r_1} + \frac{1}{K_b} \ln \frac{r_3}{r_2} + \ln \frac{r_4}{r_3} \right)} \tag{39}$$

since $K_a = K_c = 1$.

Again as r_2 approaches r_1 and r_3 approaches r_4, A approaches K_b. In general, for equal small spacings of r_3 to r_4 and r_1 to r_2, the contribution of $\ln r_4/r_3$ to the field is less than for $\ln r_2/r_1$. Therefore a void occurring at the probe reduces the field in the void at the trigger electrode approximately by a factor of $\ln r_2/r_1$. If the field is evaluated at the probe for voids at the probe and the trigger electrode, we obtain the following expression

$$A = \frac{\ln \frac{r_4}{r_1}}{\left(\ln \frac{r_2}{r_1} + \frac{1}{K_b} \ln \frac{r_3}{r_2} + \ln \frac{r_4}{r_3}\right)}$$

which is the same as the previous expression. In the consideration of the increased field in the void at the probe, a large void at the trigger electrode would result in a considerable reduction of the probe field regardless of how small the void surrounding the probe became, while a small void at the trigger electrode would not greatly influence the field at the probe.

In order to show the relative increase in field strength in the void at the probe and at the trigger electrode due to the overstressing by the dielectric constant of the insulator, the normalized curves of Figs. 51 and 52 are plotted. Two dielectric strengths are chosen and the voids are expressed as a percentage of the wire radius, r_1. Various curves are then shown for selected ratios of cylinder radius, r_4, to wire radius, r_1. Each figure is for the condition that there is no void at the other electrode, but that only the void under discussion is present.

While the preceding formulas and the normalized curves give the effect of the increased field strength in the various voids due to the effect of the intervening insulator, they do not in themselves give a predicted value of the breakdown voltage of a geometry containing such voids. In order to understand this effect in more detail, a study of the breakdown voltages of several geometries with varying voids and cylinder radii, R, was undertaken. The ability to control the probe-to-trigger electrode breakdown is important not only from the actual breakdown value view point, but also from the affect this breakdown value has on the trigger spark requirements.

The results of the study showed that for small voids at the probe with no void (or very small voids) at the trigger electrode, there was a slight reduction of breakdown voltage from the geometry having no insulator or with a continuous homogeneous insulator. If the void at the probe is increased, the breakdown voltage is decreased even further. However, there is a minimum void distance that results in a lowering of the breakdown voltage. If the void is increased further, the breakdown voltage of the geometry is increased. If the voids at both the trigger electrode and the probe are varied, the problem becomes more complex.

Based on the results obtained from this study, an approximate analysis of the breakdown voltage of a coaxial geometry with an intervening insulator is presented. Consider the typical cross-sectional view show in Fig. 53.

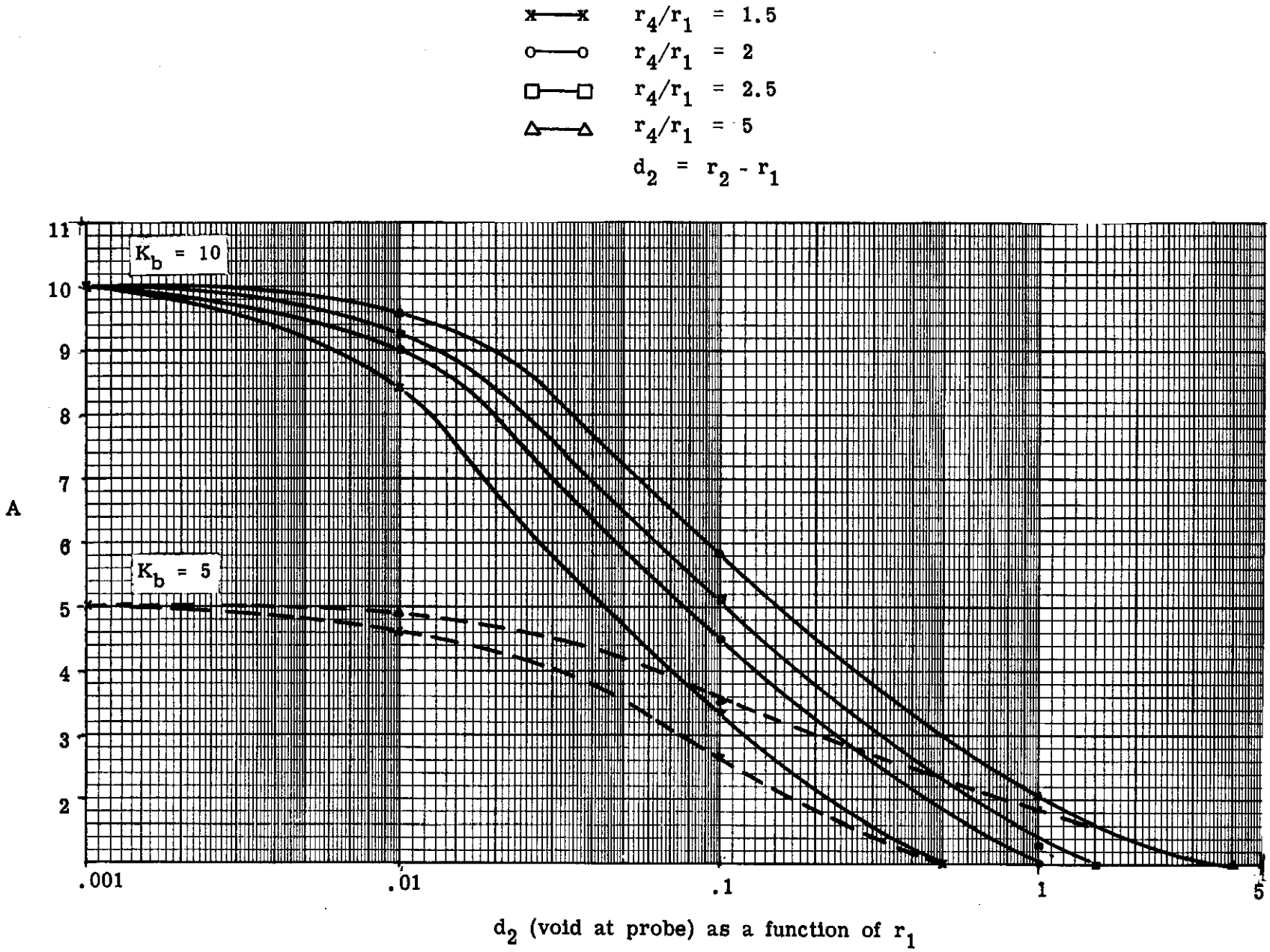

Fig. 51 -- Relative increase in field strength, A, as a function of void spacing at the probe

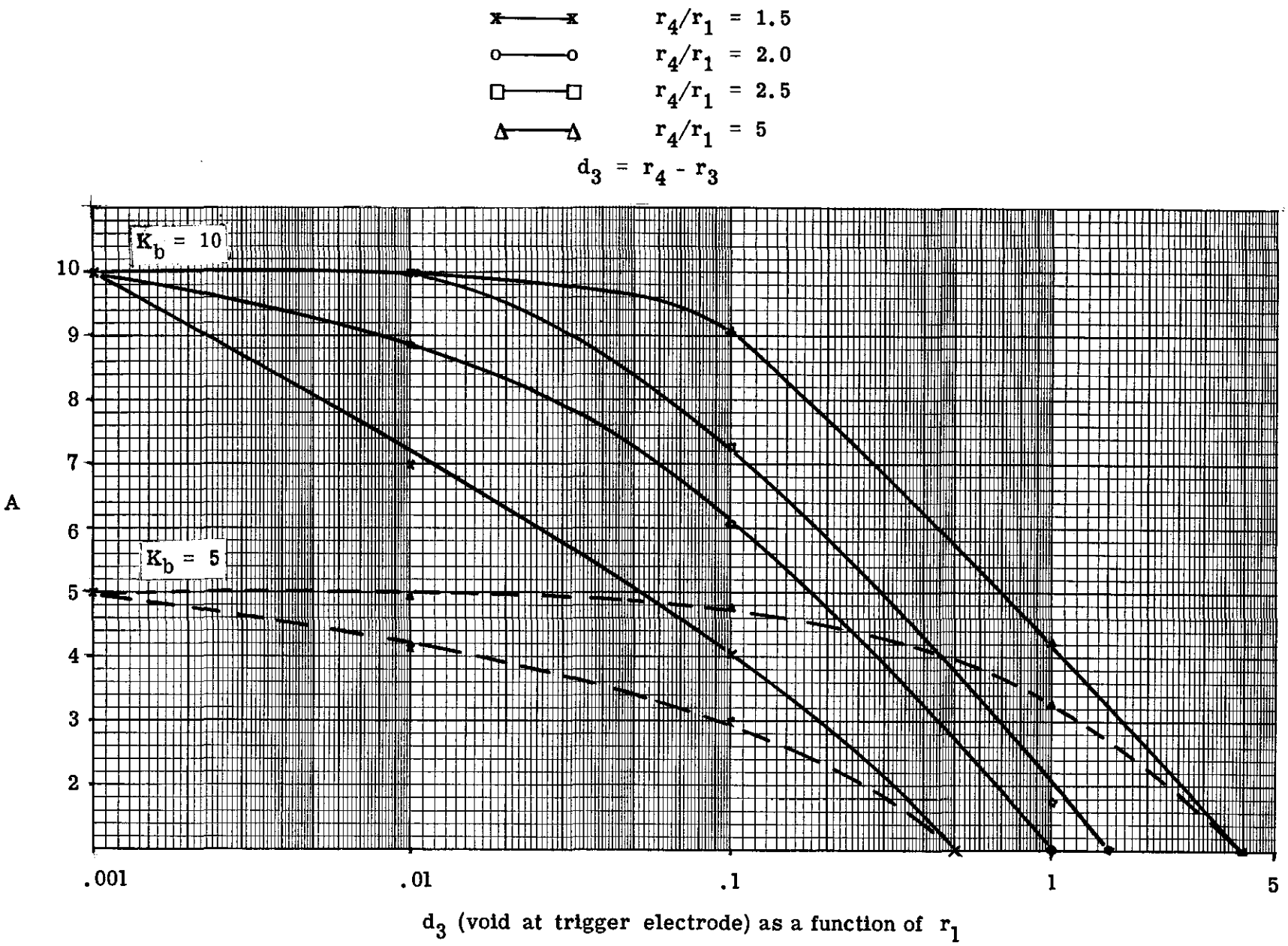

Fig. 52 -- Relative increase in field strength, A, as a function of void spacing at the trigger electrode

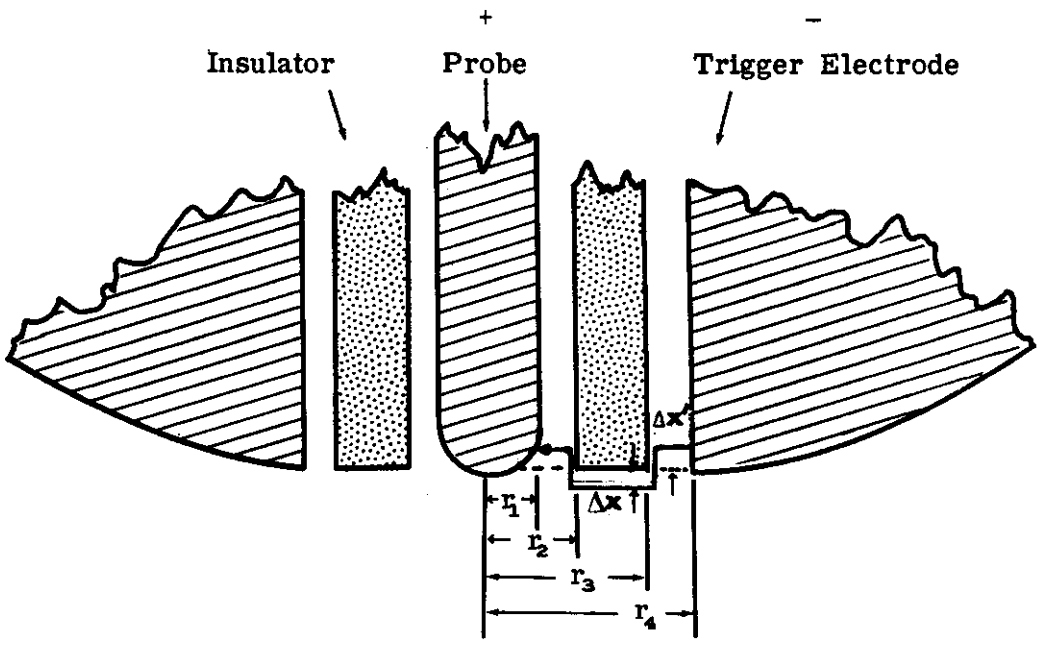

Fig. 53 -- Trigger electrode assembly

Let us consider the discharge path as being along the path between probe and the trigger electrode at a distance ΔX from the projected surface of the insulator. If now an electron is released from the surface of the trigger electrode, and we consider that it is a distance $\Delta X'$ inside the void, it will be accelerated by the overstressed field in the void between r_4 and r_3. The amount of cumulative ionization will then be a function of the electric field and the distance over which this field applies. There would also be cumulative ionization along a path ΔX into the main gap volume, but the field in this region would be the lower unstressed field due to the homogeneous dielectric of the fill gas. When the avalanche reaches r_3, we will assume that it is now only influenced by the unstressed field existing in the path a distance ΔX from the insulator surface. This field will then be active over the region between r_2 and r_3. When the avalanche reaches r_2, it is now accelerated by the increased field along a path a distance $\Delta X'$ into the void adjacent to the probe.

The final magnitude of the avalanche is expressed as

$$I = I_o \, e^{\int_o^x \alpha dx} \tag{40}$$

Since α is a function of the electric field, the amount of cumulative ionization is proportional to the electric field and the distance over which the field applies. Thus the breakdown criteria would be a function of the summation of the ionization over the total path.

Employing a method similar to the method used by Townsend in analyzing the breakdown of nonuniform fields, we will assume a uniform field over a limited region and determine an average field just sufficient for ionization to result in breakdown. This method was originally discussed in Chapter II. The radius at which the field is just sufficient to support ionization is then determined. The effective path length will then be the difference from this radius and the radius of the wire. The average field over this distance is now assumed to be the applied

uniform field. Over the remaining distance it will be assumed that there will be no contribution to the ionization process. Three examples showing three different geometry combinations will demonstrate this analysis, as seen in Figs. 54, 55 and 56.

EXAMPLE 1

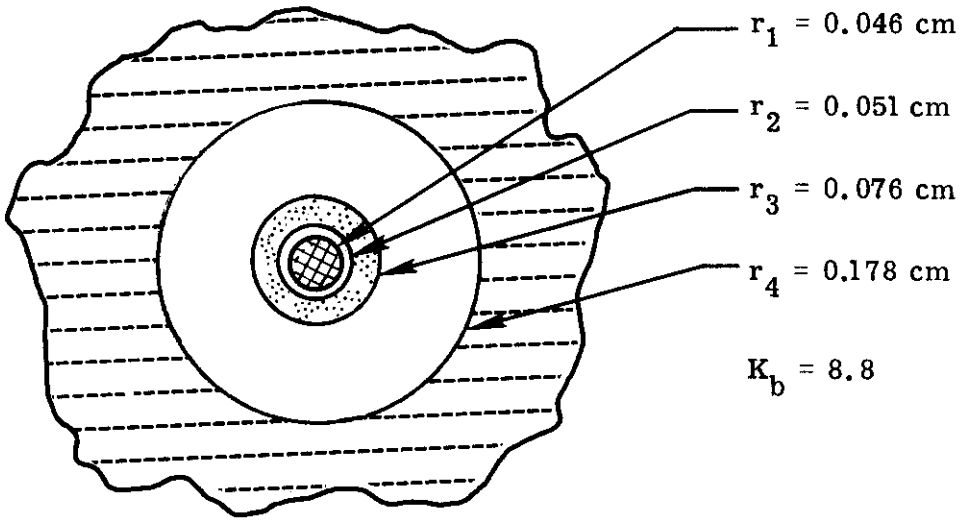

Fig. 54 -- Trigger electrode assembly with a small void at the probe and a large void at the trigger electrode

This example is for a 0.046-cm radius wire in a 0.178-cm radius cylinder with a small void at the probe and a large void at the trigger electrode. The gas dielectric is air with a dielectric constant of 1. The solid insulator is an alumina body with a dielectric constant of approximately 8.8. The observed and calculated value with only a gas insulator between the probe and the trigger electrode is 4000 volts. With the insulator and resultant voids, the observed breakdown voltage is 3500 volts. Calculation of the unstressed field at the probe can be obtained by use of Equation (27). Therefore,

$$E_{r_1} = \frac{V}{r_1 \ln \frac{r_4}{r_1}} = \frac{3500}{0.046 \ln 4.1} = 57{,}000 \text{ volts/cm} .$$

Since the electric field at any radius r_x is given by

$$E_{r_x} = \frac{r_1 E_{r_1}}{r_x} , \tag{41}$$

we can determine the unstressed electric field at the various radii representing the discontinuities of the dielectric between the probe and the trigger electrode. These are as follows:

$$E_{r_2} = \frac{0.046}{0.051}\ (57{,}000) = 51{,}200 \text{ volts/cm}$$

$$E_{r_3} = \frac{0.046}{0.076}\ (57{,}000) = 34{,}200 \text{ volts/cm} .$$

In order to determine the stressed electric field, E'_{r_x}, the relative increase in the electric field must be determined. Therefore, by Equation (36) we have

$$A = \frac{E'_{r_x}}{E_{r_x}} = \frac{\ln \frac{0.178}{0.018}}{\left(\ln \frac{0.051}{0.046} + \frac{1}{8.8} \ln \frac{0.076}{0.051} + \ln \frac{0.178}{0.076}\right)} = 1.36 .$$

From this factor we can then estimate the stressed electric field at the various radii; hence,

$$E'_{r_1} = (1.36)(57{,}000) = 77{,}500 \text{ volts/cm}$$

$$E'_{r_2} = (1.36)(51{,}200) = 70{,}000 \text{ volts/cm}$$

$$E'_{r_3} = (1.36)(34{,}200) = 46{,}600 \text{ volts/cm}$$

The pressure in which this geometry was maintained was 620 mm Hg. From emperical data available in the literature, the critical electric field required for cumulative ionization is approximately 25,300 volts/cm. There can be ionization at lower electric fields, but the resultant ionization is considered to be negligible for the purposes of estimating breakdown. Determining the radius at which the stressed field drops to this value, we have

$$r'_x = \frac{r_1 A E_{r_1}}{25{,}300} = \frac{(0.046)(1.36)(57{,}000)}{25{,}300} = 0.140 \text{ cm} .$$

The effective spacing over which the uniform field approximation will apply will be

$$r'_x - r_1 = 0.140 - 0.046 = 0.094 \text{ cm} .$$

Several methods can be used to estimate the uniform field gradient required for breakdown for a spacing of 0.094 cm. The αd approximation from Chapter II could be employed or the breakdown gradient could be estimated from published curves of breakdown versus pd

In addition, an estimate of the breakdown field strength may be found from the Townsend empirical breakdown equation[17] of

$$E_s = 30 + \frac{1.35}{d} \text{ kv/cm (atmospheric pressure, } 25^{o}\text{C)} . \qquad (42)$$

The above equation can be modified for variation of operating pressure as mentioned above. Using these methods of estimating the required breakdown gradient for the uniform field approximation results in an estimate of 39,650 volts/cm.

Since,

$$E_x = \frac{E_{r_0} r_0}{r_x} = \frac{K_0}{r_x} ,$$

where

$$K_0 = E_{r_0} r_0$$

is a constant (Eq (41)), the average electric field between various radii is found by integrating the electric field over this region and dividing by the length. For example, the average field between r' and r_3 is

$$E'_{av}\left(r'-r_3\right) = \frac{K_3}{r'-r_3}\int_{r_3}^{r'} \frac{dr}{r} = \frac{K_3}{r'-r_3}\left[\ln r_3 - \ln r'\right]$$

$$E'_{av}\left(r'-r_3\right) = \frac{3550}{.064}\left[-1.96611 + 2.57702\right] = 34{,}000 \text{ volts/cm} .$$

Likewise:

$$E_{av}\left(r_3 - r_2\right) = 38{,}500 \text{ volts/cm}$$

$$E'_{av}\left(r_2 - r_1\right) = 73{,}000 \text{ volts/cm} .$$

If we now weigh these averages in proportion to the distance over which they contribute to the ionization process and take the summation over the total spacing, we obtain

$$E_{av} = \left(\frac{0.064}{0.094}\right)(34{,}000) + \left(\frac{0.025}{0.094}\right)(38{,}500) + \left(\frac{0.005}{0.094}\right)(73{,}000)$$

$$E_{av} = 37{,}400 \text{ volts/cm} .$$

This result then shows that breakdown occurred with the resultant average electric field being approximately equal (within 5%) to the uniform field approximation for a distance of 0.094 cm.

EXAMPLE 2

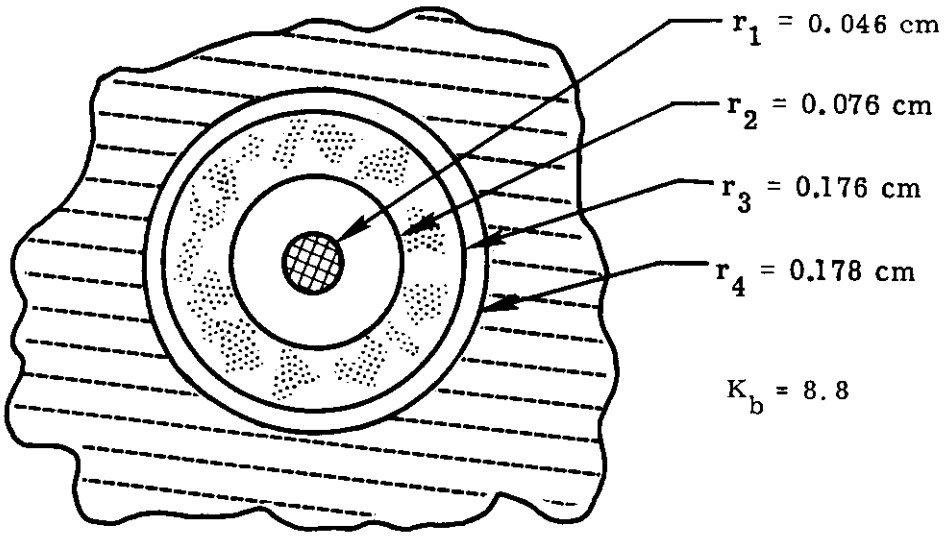

Fig. 55 -- Trigger electrode assembly with a large void at the probe and a small void at the trigger electrode

This example is for a 0.046-cm radius wire in a 0.178-cm radius cylinder with a small void at the trigger electrode and a large void at the probe. The observed breakdown voltage for this geometry is 2600 volts. Performing the analysis similar to Example 1, the following results are obtained for the applied voltage of 2600 volts.

$$E_{r_1} = 40{,}000 \text{ volts/cm}$$

$$E_{r_2} = 24{,}300 \text{ volts/cm}$$

$$E_{r_3} = 10{,}700 \text{ volts/cm} .$$

The increased electric field factor, A , equals 2.25; hence,

$$E'_{r_1} = 90{,}000 \text{ volts/cm}$$

$$E'_{r_2} = 54{,}600 \text{ volts/cm}$$

$$E'_{r_3} = 24{,}000 \text{ volts/cm} .$$

Since E_{r_2} and E'_{r_3} are below the critical ionization gradient, all cumulative ionization must occur between r_1 and r_2 due to the stressed field in this region. The average electric field over this region is then found to be 69,200 volts/cm. The breakdown gradient for a uniform field over the same spacing is approximately 67,000 volts/cm.

EXAMPLE 3

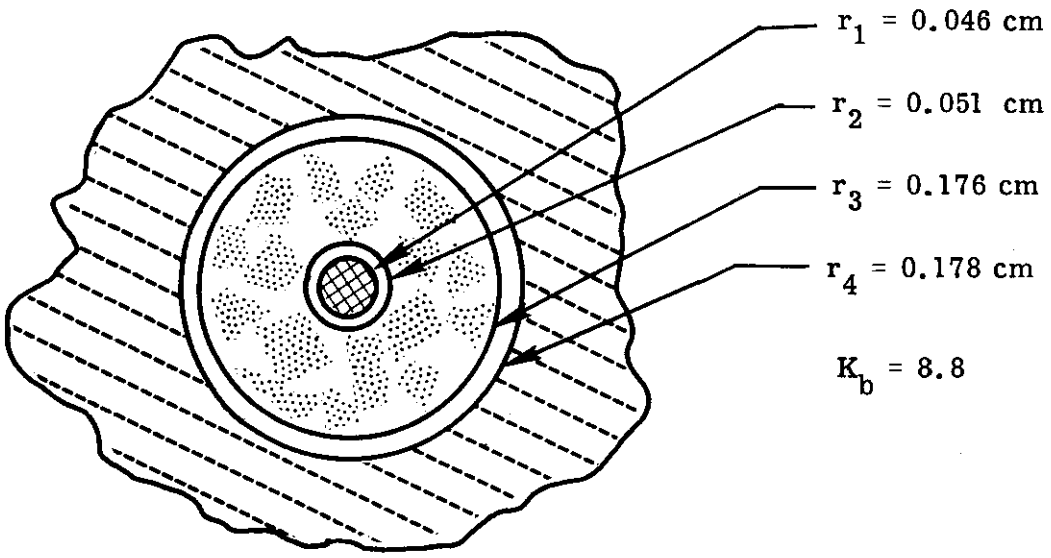

Fig. 56 -- Trigger electrode assembly with small voids at the probe and at the trigger electrodes

This example is for a 0.046-cm radius wire in a 0.178-cm radius cylinder with a small void at the trigger electrode and a small void at the probe. The observed breakdown voltage at a pressure of 620 mm Hg in air is 3500 volts. Therefore, for 3500 volts at the probe, we obtain

$$E_{r_1} = 54{,}000 \text{ volts/cm}$$

$$E_{r_2} = 48{,}500 \text{ volts/cm}$$

$$E_{r_3} = 14{,}200 \text{ volts/cm} .$$

The increased electric field factor, A , equals 5.6; therefore,

$$E'_{r_1} = 301{,}000 \text{ volts/cm}$$

$$E'_{r_2} = 269{,}000 \text{ volts/cm}$$

$$E'_{r_3} = 79{,}000 \text{ volts/cm} .$$

Neglecting any ionization contribution due to the small void at the electrode, we then determine the radius at which the unstressed gradient ceases. The radius is 0.098 cm. The summation of the weighted averages over this region is then

$$E_{av} = \left(\frac{0.047}{0.052}\right)(34,800) + \left(\frac{0.005}{0.052}\right)(285,000) = 58,400 \text{ volts/cm}$$

The corresponding breakdown gradient for a uniform field over the same spacing is 53,500 volts/cm.

While the foregoing analysis is not rigorous, it does give an insight to the approximate fields in the various regions and their relation to the breakdown gradient of the geometry. By trial and error then, the breakdown voltage of any complex geometry can be calculated. A breakdown voltage is assumed, the electric field is calculated at the different radii, and a critical radius, r', is determined which provides the minimum critical electric field required for cumulative ionization. The weighted summation of these electric fields over the critical distance is made and compared to the uniform field gradient having the same critical length $(r' - r_1)$. The process is repeated until the two critical fields are approximately equal. The assumed voltage is the breakdown voltage of the geometry.

On Probe-to-Main Electrode Breakdown

The insulator surrounding the probe also affects the point-to-plane breakdown but in an entirely different manner. If the point-to-plane configuration of Chapter II is again considered, but now with a ceramic insulator surrounding the point, we obtain the breakdown curves of this geometry for variations of gap spacing and fill pressure as shown in Figs. 57 and 58. With this new curve is also shown the original curve for comparison purposes. A review of these curves shows that with addition of the insulator surrounding the probe the breakdown value has increased. The effective radius with the insulator is now the radius of the insulator. If the breakdown curve is calculated using the 0.076 and 0.102-cm radius instead of the 0.050-cm radius of the wire alone, we obtain fairly good agreement with the observed values. This clearly indicates that with the slow application of voltage to the probe the insulator has sufficient time to accumulate surface charge by leakage from the probe. The accumulation of charge effectively increases the size of the point to that of the outside diameter of the insulator. Therefore, calculating the point-to-plane breakdown using this effective point radius gives good agreement with observed values.

As will be shown later, if a rapid application of voltage is applied to the probe, for example a pulse voltage, the point will obtain full voltage before any appreciable charge can collect on the surface of the insulator. The resultant breakdown then approaches the original point-to-plane breakdown value. However if the rate of rise of the applied pulse is high enough, the breakdown of the geometry will increase due to the formative and statistical time lag theory. This will be discussed in more detail later on.

On the Static Model

From the preceding results, we see that the insertion of a solid insulator surrounding the probe affects both the probe-to-main electrode breakdown as well as the probe-to-trigger electrode breakdown. If the solid insulator is homogeneous without any voids, the breakdown of the probe-to-trigger electrode is not altered from the breakdown that would be obtained for a gas dielectric. The probe-to-main electrode will be increased by the rate the leakage charge

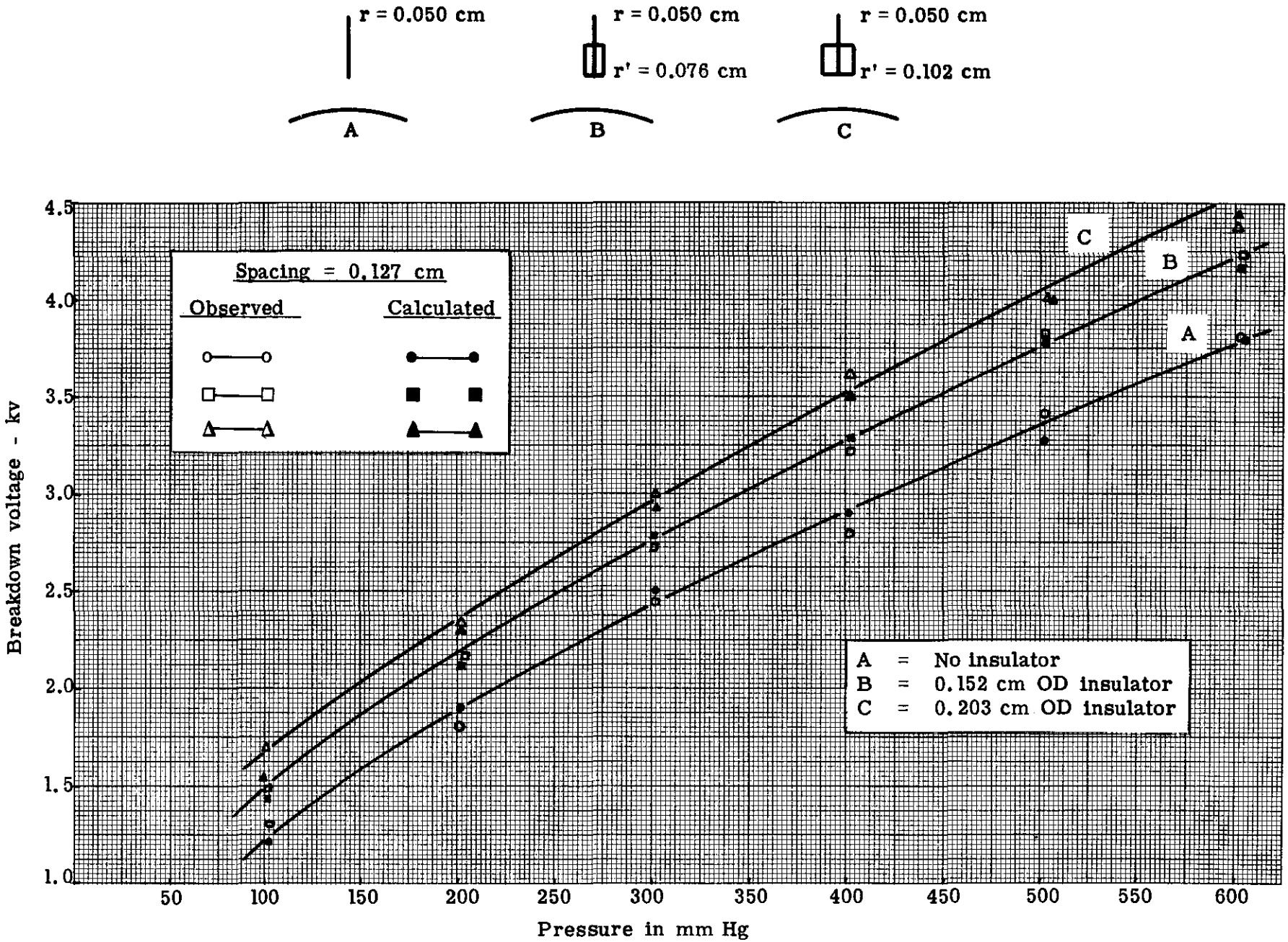

Fig. 57 -- Effect of probe insulator on point-to-plane breakdown (pressure variable)

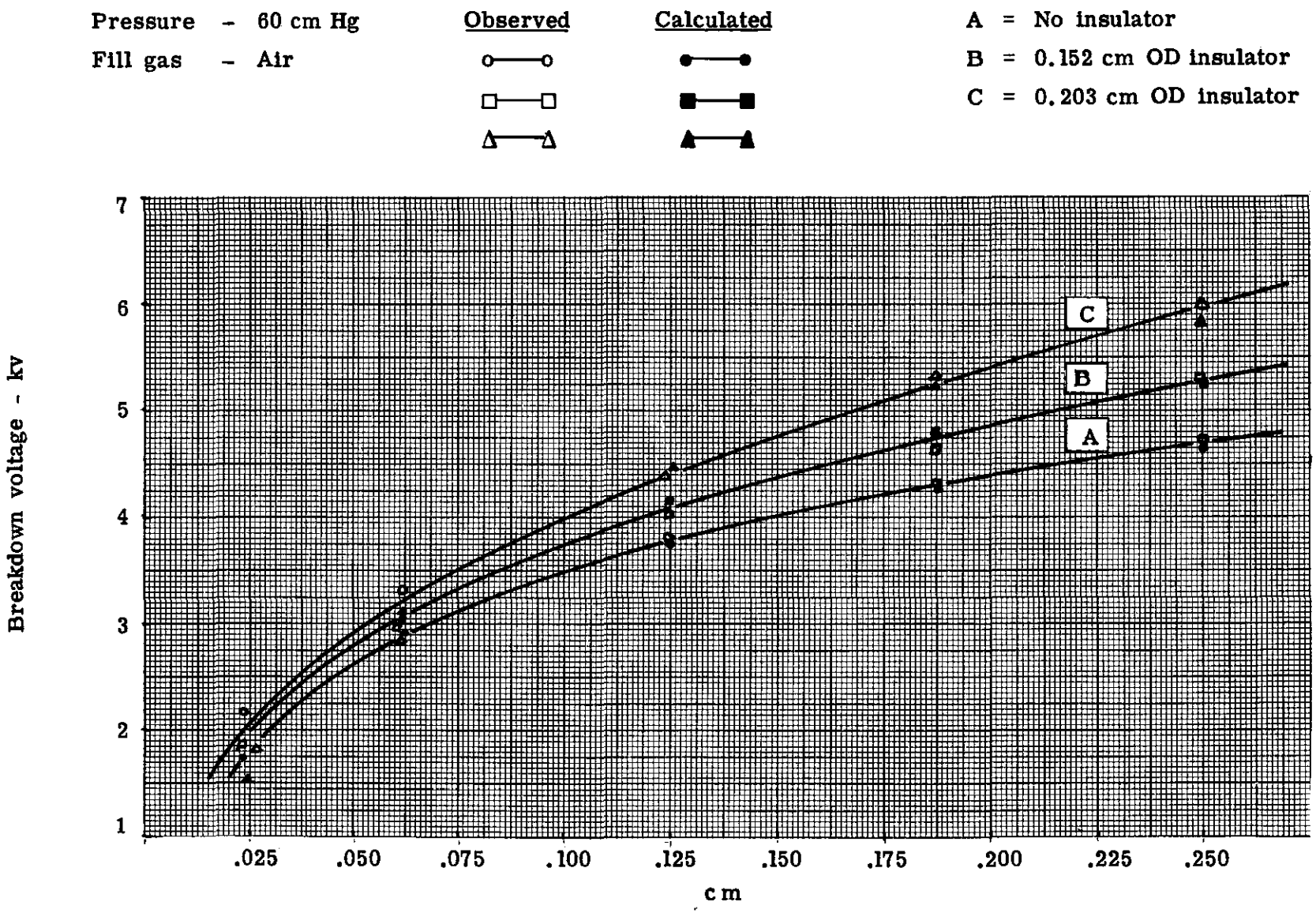

Fig. 58 -- Effect of probe insulator on point-to-plane breakdown (spacing variable)

accumulates on the insulator which changes the effective radius of the probe. This effective radius then can approach the radius, R , of the trigger electrode hole. If R is relatively small, the factor K_p (ratio of probe-to-trigger electrode breakdown to probe-to-main electrode breakdown) will become:

$$K_p = \frac{4\left(1 + \frac{0.308}{\sqrt{pr}}\right) \ln \frac{R}{r}}{\left(1 + \frac{0.616}{\sqrt{pr}}\right) \ln \frac{8d}{R}} \tag{43}$$

If R is relatively large, the static breakdown of the probe-to-opposite electrode will be approximately equal to static breakdown voltage of the main gap. Hence, K_p is given by

$$K_p = \frac{31\ pK\left(1 + \frac{0.308}{\sqrt{pr}}\right) \ln \frac{R}{r}}{V_{sbv}} \text{ kilovolts} \tag{44}$$

or

$$K_p = \frac{31\ pK\left(1 + \frac{0.308}{\sqrt{pr}}\right) \ln \frac{R}{r}}{30d + 1.35} \text{ kilovolts} \tag{45}$$

using the uniform field approximation.

For the case where voids are present, the problem becomes more complex and the only approach is to use Equation (36) as an estimate in determining the breakdown by trial-and-error methods.

The Static Trigger Curve and Operating Modes

Considering the individual static breakdown voltages of the probe-to-trigger electrode and probe-to-opposite electrode, a static trigger curve can be predicted. This static curve then forms the limit of the dynamic curves when the rise time of the dynamic pulse is allowed to approach the slowly applied voltage of static voltage (DC). If we consider the trigger electrode to be the reference electrode, there are then four basic operating modes of the triggered spark gap. These four modes are shown below in Fig. 59.

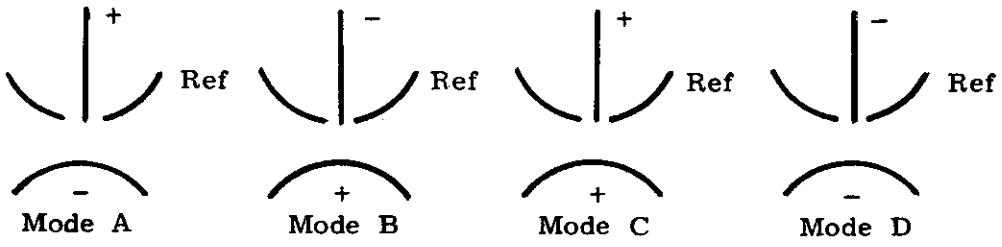

Fig. 59 -- Operating modes of the triggered spark gap

For Modes A and B, there are then two possible paths the trigger spark may take depending on the relative spacings of the various electrodes and the applied gap voltage. The trigger spark may either form to the trigger electrode or across the gap to the main electrode. For Modes C and D, the trigger spark always forms to the trigger electrode.

In practical applications the reference electrode can be grounded or have either a negative or positive applied voltage. In most practical applications the trigger pulse is supplied by means of a suitable transformer. In these cases the static probe voltage is the same as the reference voltage, since the secondary of the transformer is returned to this electrode as shown in Fig. 60.

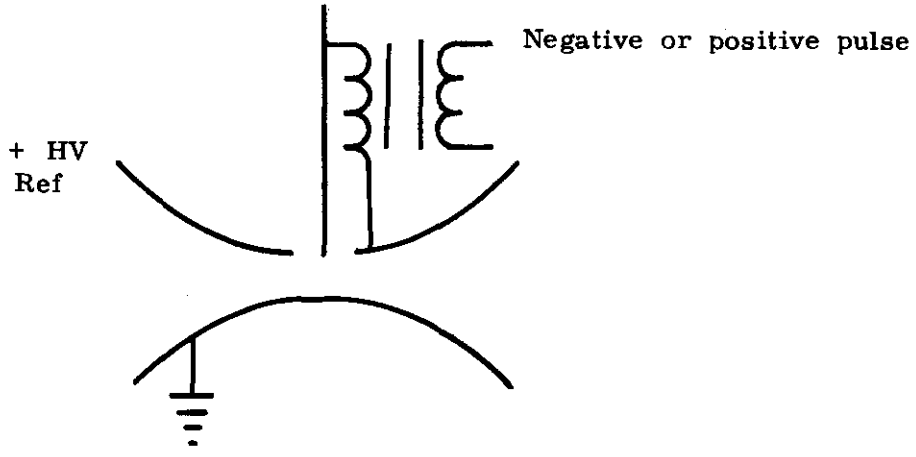

Fig. 60 -- Transformer connection with the trigger electrode as reference

However, if the probe-to-trigger electrode static breakdown voltage is always higher than the intended operating voltage of the main gap, the probe could be maintained at the voltage of the opposite electrode as shown in Fig. 61.

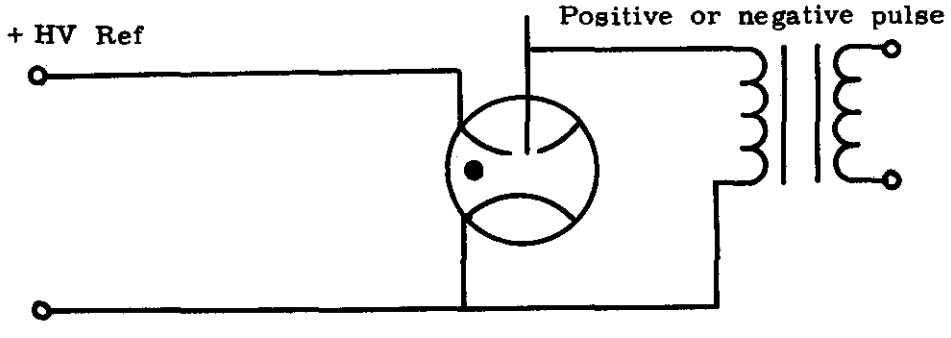

Fig. 61 -- Transformer connection with the main electrode as reference

The static trigger curve can be obtained for any gap by use of the following circuit (Fig. 62):

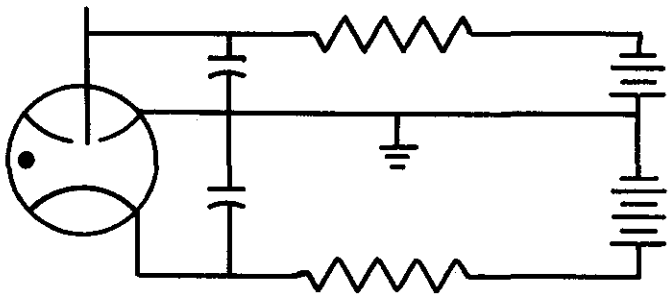

Fig. 62 -- Static trigger curve circuit

The power supply to the probe is set at zero and the applied voltage of the main gap is gradually increased until the static breakdown is obtained. The main gap voltage is then reduced a given increment, and the applied voltage on the probe is gradually increased until the probe breaks down, thereby causing the main gap to breakdown. The main gap voltage is then reduced another increment and the process repeated.

Considering Mode A operation on a gap with a gap spacing of 0.140 cm, we can plot the static trigger curve shown in Fig. 63. The static breakdown of the main electrodes is 5050 volts, static breakdown of probe-to-main electrode is also about 5000 volts, and the probe-to-trigger electrode static breakdown voltage is 2250 volts. If the main gap voltage is reduced, we expect then that the potential of the probe must be increased by a like amount so that total potential is now equal to the original static breakdown voltage of the probe. If the reduction of gap voltage and the corresponding increase in probe voltage is less than the static breakdown voltage of probe-to-trigger electrode, then the static trigger spark forms to the main electrode. We would then expect a linear relation between the static probe voltage and the applied gap voltage. This linear relation should then hold until the reduction in main gap voltage equaled the probe-to-trigger electrode static breakdown voltage. At this point the trigger spark should form to either electrode with equal frequency. If now the main gap voltage is reduced even further, the controlling breakdown voltage will now be the probe-to-trigger electrode and will remain constant for further reduction of main gap voltage. A review of Fig. 63 shows good agreement at each end, but tapers off at the transition point falling slightly below the predicted curve.

Figure 64 shows the static trigger curves for a similar geometry where the probe-to-trigger electrode breakdown is 2800 volts and the probe-to-main electrode breakdown is approximately 5400 volts. This curve shows Mode A, Mode B, and Mode C operation. Mode A is an aiding field situation for the probe. Likewise, Mode B is an aiding field, but since the probe of Mode B is negative, the resultant breakdown is much lower, as previously shown. The main gap breakdown will remain the same, since a symmetrical system is essentially unaffected by polarity. The resultant probe-to-main electrode gradient for a negative point provides a lower breakdown voltage than probe-to-trigger electrode voltage, and as the main gap voltage is reduced, the probe breakdown is always to the opposite electrode and consequently a transition point does not occur.

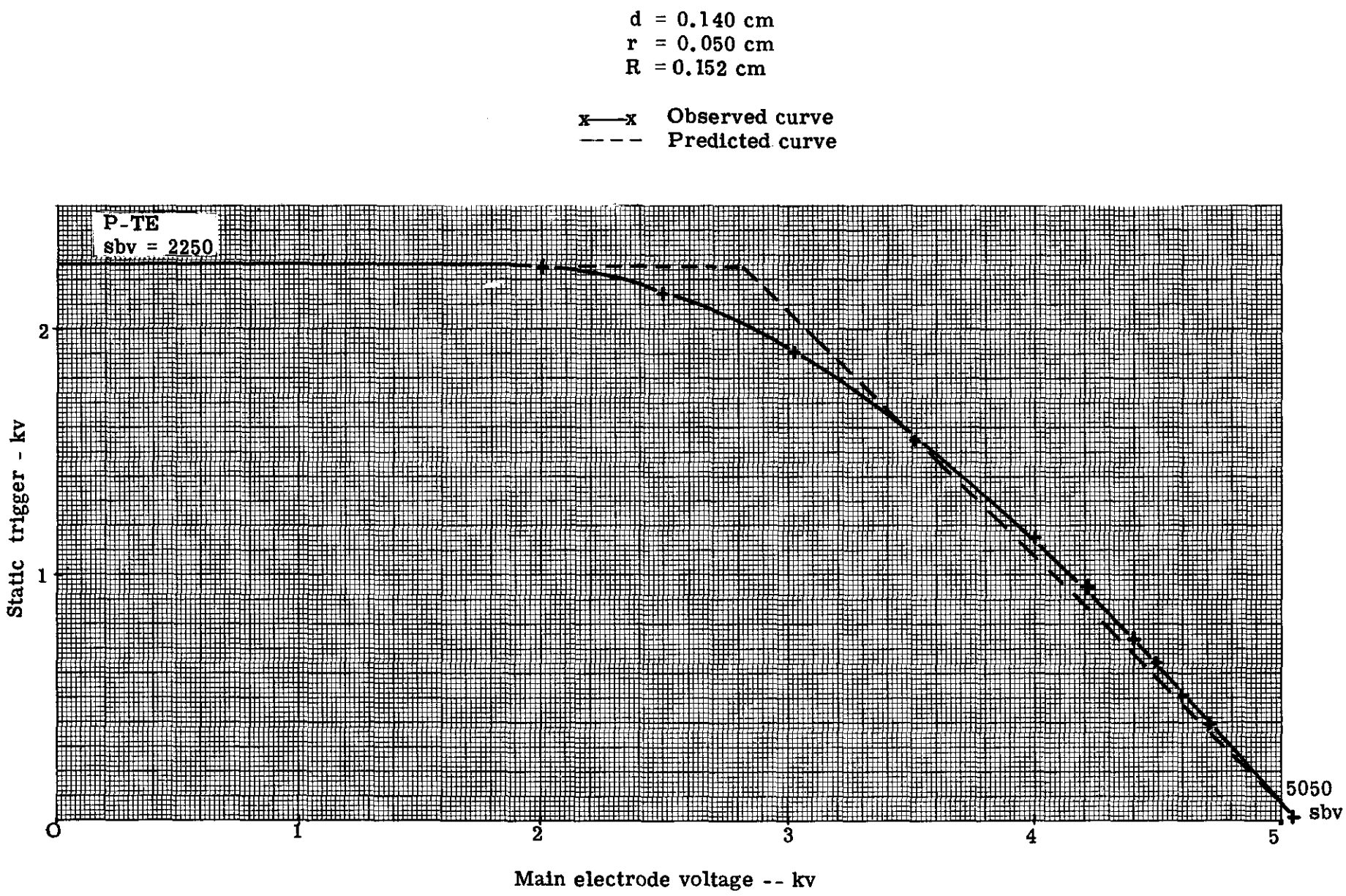

Fig. 63 -- Typical static trigger curve--Mode A Operation

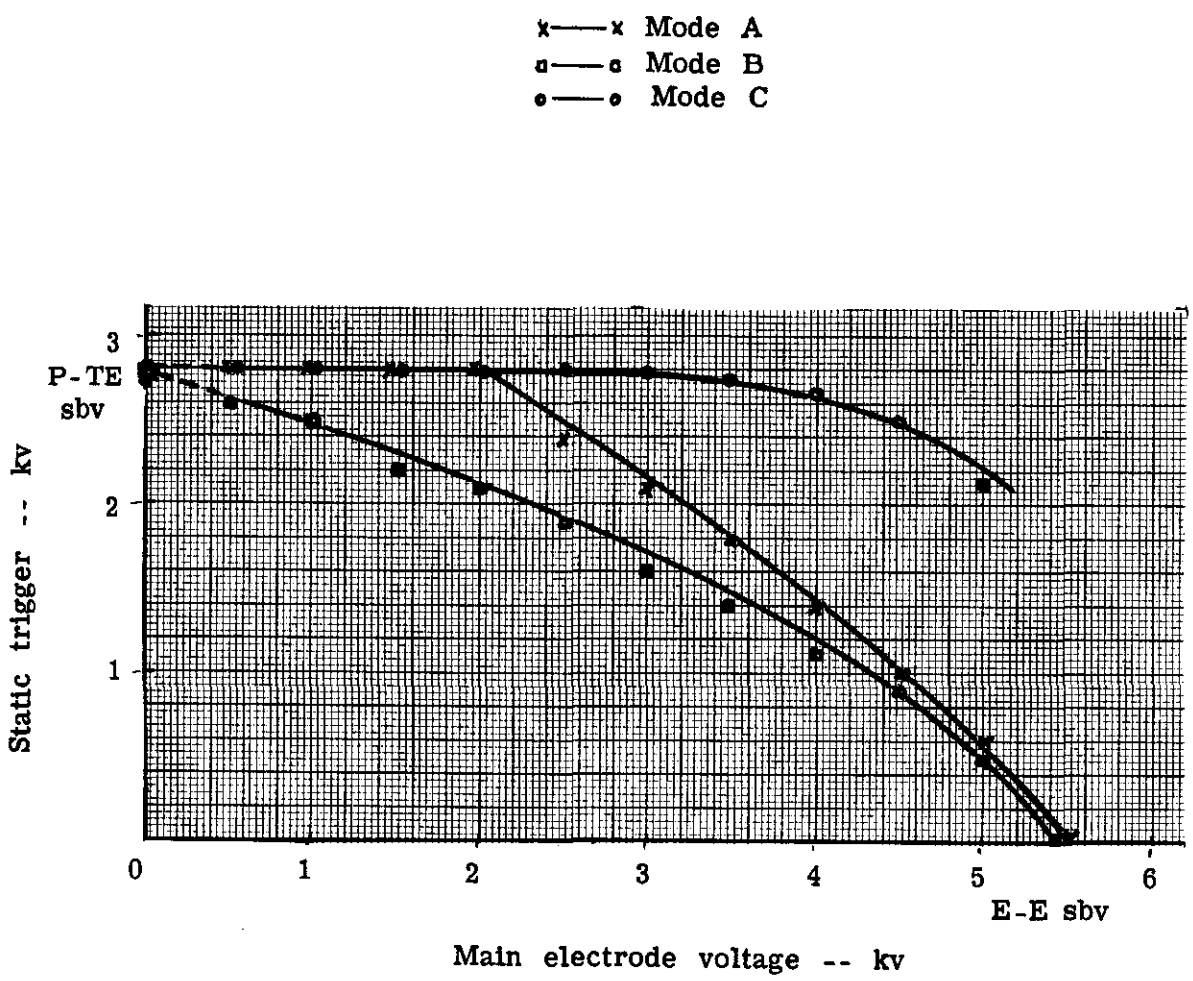

Fig. 64 -- Static trigger curve

For the aiding field cases of Modes A and B, the internal electric field is the result of the various voltages that can be applied to the three electrodes. Any change in the combination of these voltages will alter the distribution of this field over the intended path of the discharge. The geometry of these electrodes is fixed and the fill pressure is fixed; therefore, the probe will breakdown when the summation of the electric field across this path reaches the required level for breakdown. As these voltages are varied this field will become more nonuniform, causing a concentration of field such that the summation of field across the path gives the necessary total. This interdependency of electrode voltages will then account for the fact that the observed curves fall below the curve that would be predicted, on the basis that the probe-to-trigger electrode, sbv, at no-gap voltage and probe-to-main electrode, sbv, at no-gap voltage were independent variables.

For Modes C and D operation, the gap field is a repelling field to the probe field, and for large gap spacings, the probe-to-trigger electrode breakdown predominates and is almost independent of main gap voltages. For smaller gap spacings, the probe breakdown voltage is influenced somewhat at the higher main gap voltages causing the probe breakdown voltage to drop. This is shown in Fig. 64 and 65. Figure 65 is a static trigger curve for a gap of 0.165-cm gap spacing and 0.050-cm probe radius with a continuous seal to the trigger electrode. Figure 66 is the static trigger curve for a gap with 0.254-cm gap spacing, a probe radius of 0.050 cm, and a hole radius in the trigger electrode of 0.152 cm with a small void at the trigger electrode, but with no void at the probe.

In order to study the effect of variation of pressure and gap spacing on the static trigger curve, an experiment was performed employing a fixed probe and trigger electrode assembly. The gap spacing is adjusted by a micrometer movement controlled from outside of the bell jar. The internal pressure is then varied from 10 to 60 cm. The fill gas is ambient air. The probe assembly consists of a 0.046-cm radius probe, with a 0.102 cm ID x 0.152 cm OD ceramic insulator. The radius of the main spheres is 0.475 cm. Figure 67 shows the effect of gap spacing at a constant pressure on Mode A operation, and Fig. 68 shows the effect of fill pressure at a constant gap spacing on Mode A operation. For the variation of gap spacing, the static breakdown voltage increases for increasing gap spacing as predicted. The linear relation below the transition point still holds with increasing gap spacing. Since this linear relation still holds, the transition point between probe-to-main electrode breakdown and probe-to-trigger electrode increases with increasing gap spacing. Simply the gap transition point can be expressed as

$$V_t = V_{sbv} - \left(P \text{ to } TE_{sbv}\right). \tag{46}$$

There is a noticeable effect of probe-to-trigger electrode breakdown with respect to gap spacing. As the gap spacing becomes smaller, the probe-to-trigger electrode, sbv, becomes higher. This indicates a rearrangement of the gap's internal field due to the proximity of the lower electrode to the probe-to-trigger electrode configuration. This effect has also been noted when there was no applied voltage across the main gap and the trigger and opposite electrodes were at ground potential. If the opposite electrode was fairly close to the trigger electrode, the static breakdown between probe and the trigger electrode increased. As mentioned earlier, this increase is also influenced by the size of the trigger electrode hole.

For the variation of pressure at a fixed gap spacing and fixed probe geometry, the main electrode breakdown and probe-to-trigger electrode breakdown voltage increase with an increase in pressure. This is shown in Fig. 68. The shape of the curve for varying pressure is essentially unchanged. However, since the increase in the main gap breakdown is greater for increasing pressure than that for the probe-to-trigger electrode breakdown, the transition

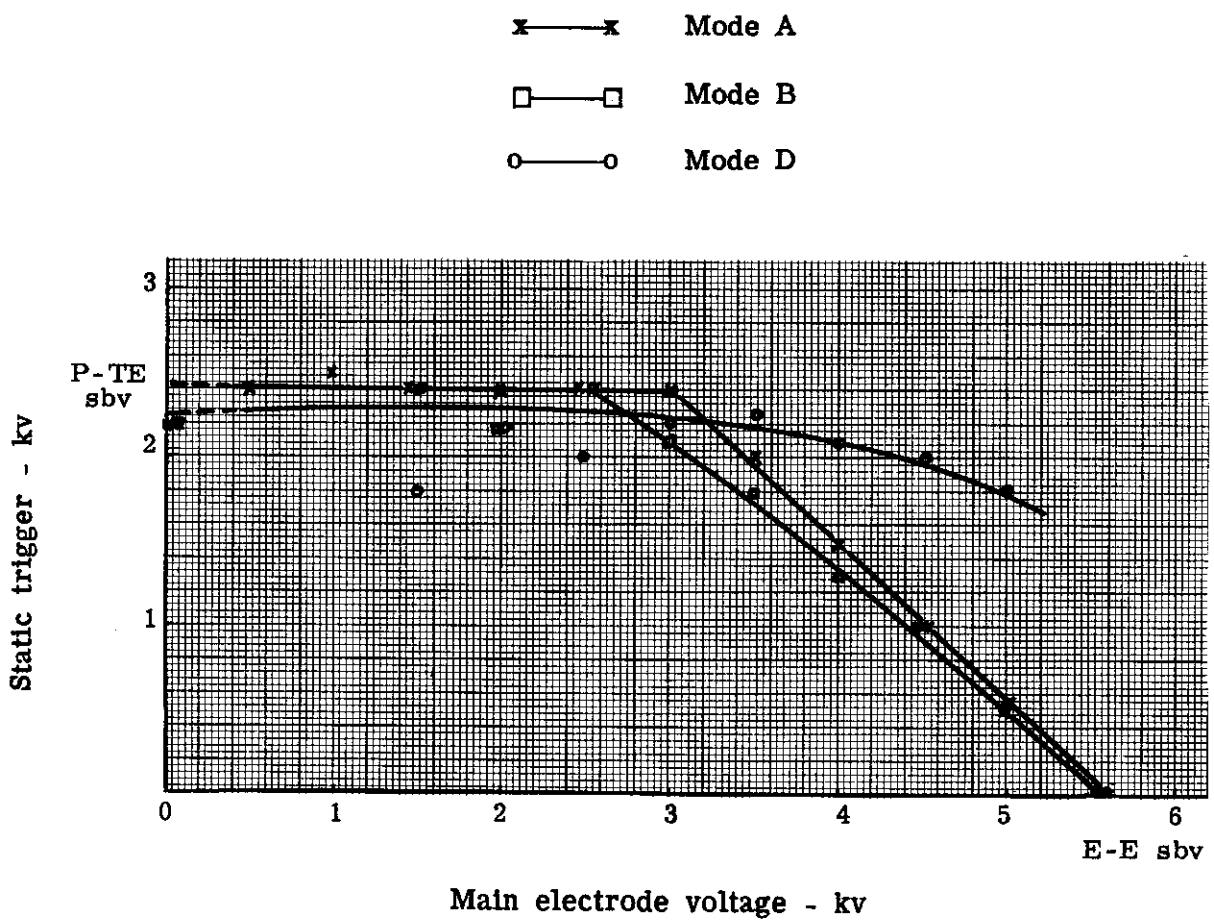

Fig. 65 -- Static trigger curve

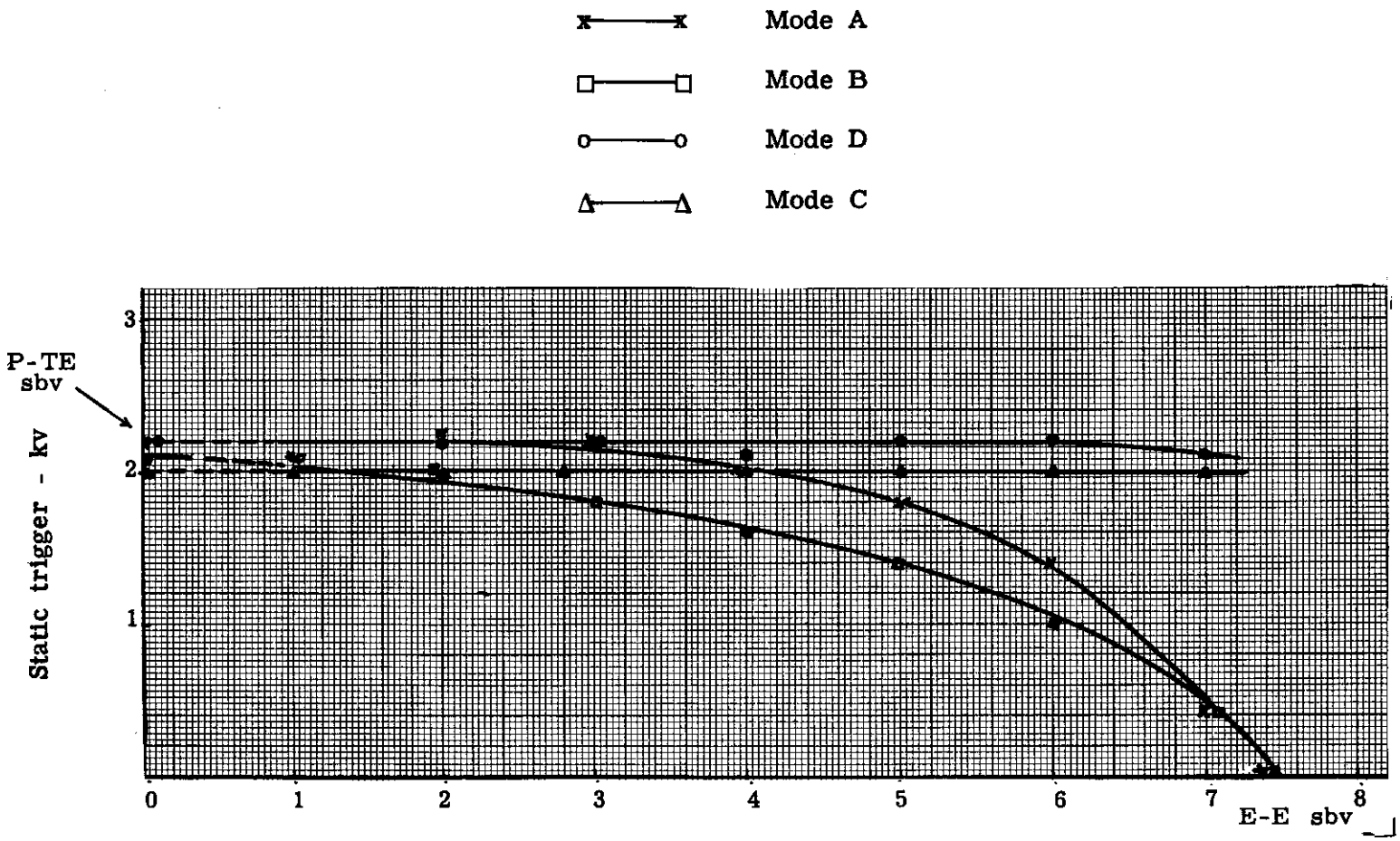

Fig. 66 -- Static trigger curve

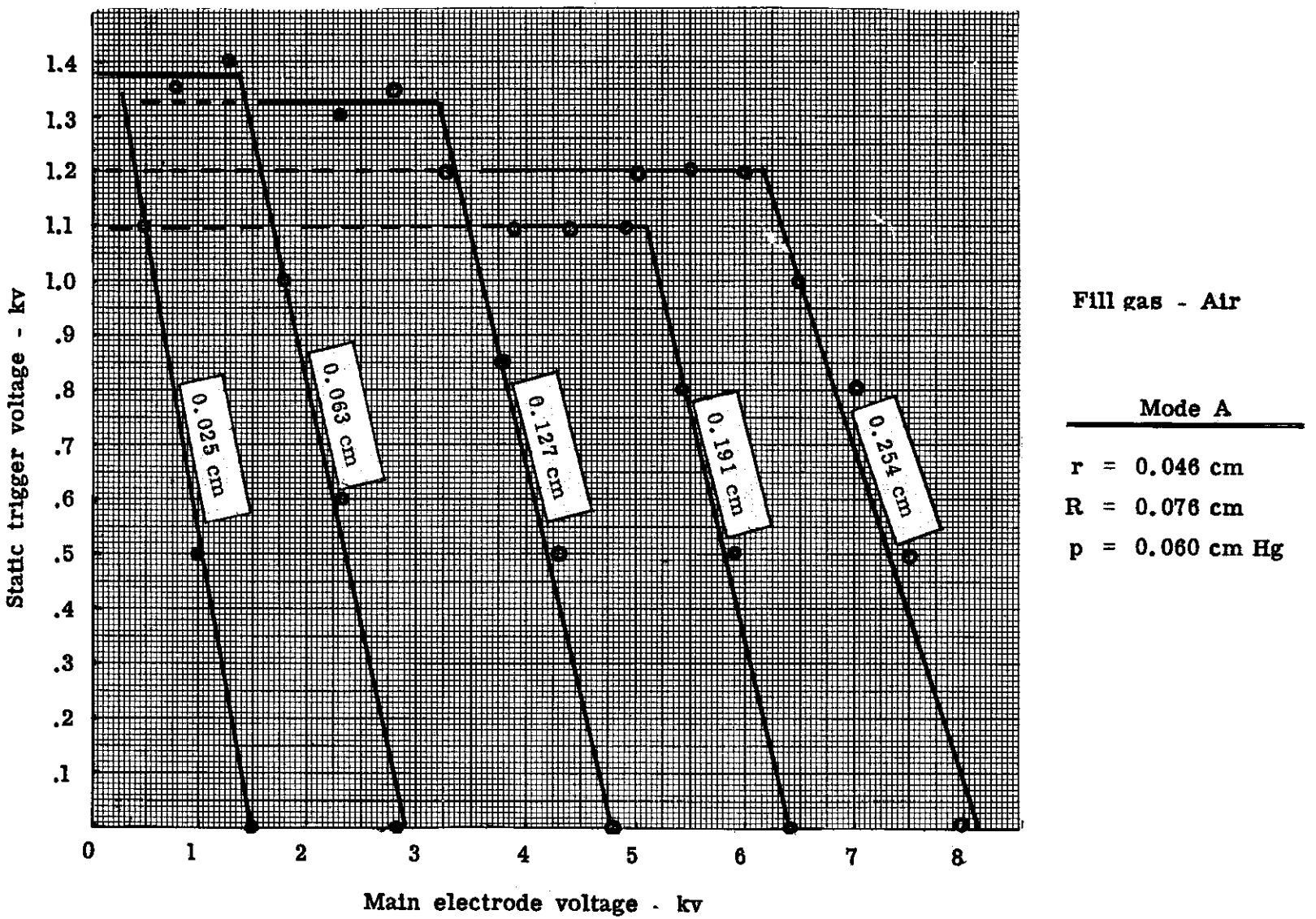

Fig. 67 -- Static trigger curves for varying gap spacing

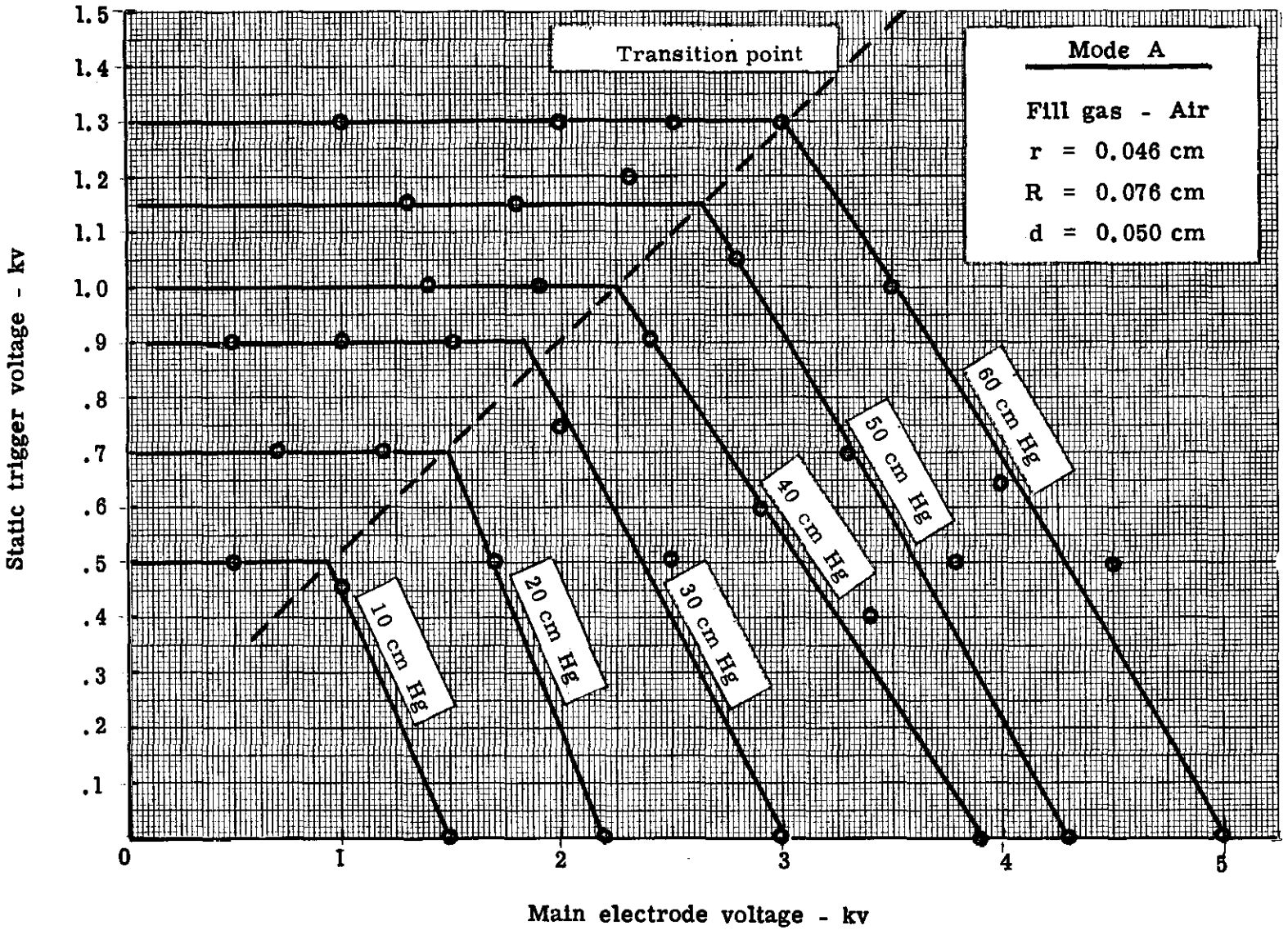

Fig. 68 -- Static trigger curves for varying pressure

point also increases for increasing pressure. A good example is shown in Fig. 69 where the probe-to-trigger electrode and probe-(with surrounding insulator)-to-main electrode breakdown as a function of pressure are given. As indicated, the variation for probe-to-trigger electrode increases at a slower rate than for probe-to-main electrode. This is especially true where there are voids at the probe. The breakdown curves are slightly lower than that predicted since the probe did not have a full radius, but a rather sharp taper into a flat surface. The high probe-to-main electrode breakdown is influenced by the surrounding insulator as mentioned earlier. Whenever possible, in considering the static trigger curve for either single or complex geometries, the use of an analog field plotter to study the resultant electric fields is recommended. Also in constructing practical gaps, such factors as the microgeometries and finish of the metal electrodes, surface condition of the insulators, presence of voids, oxide layers, etc., will affect the static and pulse trigger curves and must be carefully controlled.

Pulse Triggering

The static curves give a glimpse of how the trigger characteristics may vary for different polarities and gap structure. They would represent the limit of pulse voltages as the pulse is varied from a fast rising pulse to a slow rising pulse approaching a 60-cycle or DC condition. In order to investigate the trigger curves for various pulses of different rise times, three transformers were used. One transformer gave a 10 to 90-percent rise time of 150 μsec, another gave a rise of 2 μsec, and a third gave a rise of 0.5 μsec. The corresponding rates of rise are 366 volts/μsec, 2750 volts/μsec, and 11,000 volts/μsec, respectively. These pulses were applied to the probe of a typical gap for all possible polarity cases (Modes A through D) and with varying gap voltages. The curves obtained were then compared with the static curve for the various cases. Figures 70, 71, 72, and 73 show these comparisons. It should be pointed out that at this stage we are only interested in the pulse conditions required for probe breakdown and not in whether the main gap broke down. The circuit used to obtain those pulses is shown in Fig. 70 where the probe battery and capacitor of the static trigger curve have been replaced by the transformer as a voltage generator. The C_d is the distributed secondary capacity, wiring capacity, and probe input capacity.

These curves show that in general the pulse conditions follow the static cases fairly closely. The comparison for Modes B, C, and D are quite good, while in Mode A there is more variation. It should be pointed out that the values obtained are the average of ten observations taken on a 545 Tektronix scope with a calibrated capacity-divider input.

At fast rise times, as for the example of the 0.5-μsec pulse, the variation of breakdown voltage is very pronounced. As the rise time becomes slower, the repeatability improves. For the fast rising pulses where any delay at all is experienced in establishing the avalanche mechanism of the trigger spark, the fast rise of the pulse would carry the trigger pulse another 500 volts or so. Undoubtedly the condition for breakdown is satisfied earlier at a lower voltage but, because of the time required to form this spark (this time may vary with the number of firings, condition of the probes and electrodes after each shot, the initial ionization state of the gas, and the time between trigger attempts), the applied voltages will overshoot. At slower rises this variation or overshoot becomes less, and the pulse voltage at breakdown is more repeatable.

Figure 70 for Mode A shows that as the rate of rise increases, the pulse voltage at breakdown increases. The sharp break of the static case is not clearly repeated in the pulse condition, but the breakdown value is still a function of the applied voltage on the gap; the trigger voltage decreasing with increasing gap voltage. Where the static case falls approximately linearly to zero, as the gap voltage approaches the main gap sbv value, the pulse case does not and approaches some finite pulse limit instead.

Fill gas - Air

Sphere radius - 0.475 cm

r = 0.046 cm

R = 0.076 cm

d = 0.127 cm

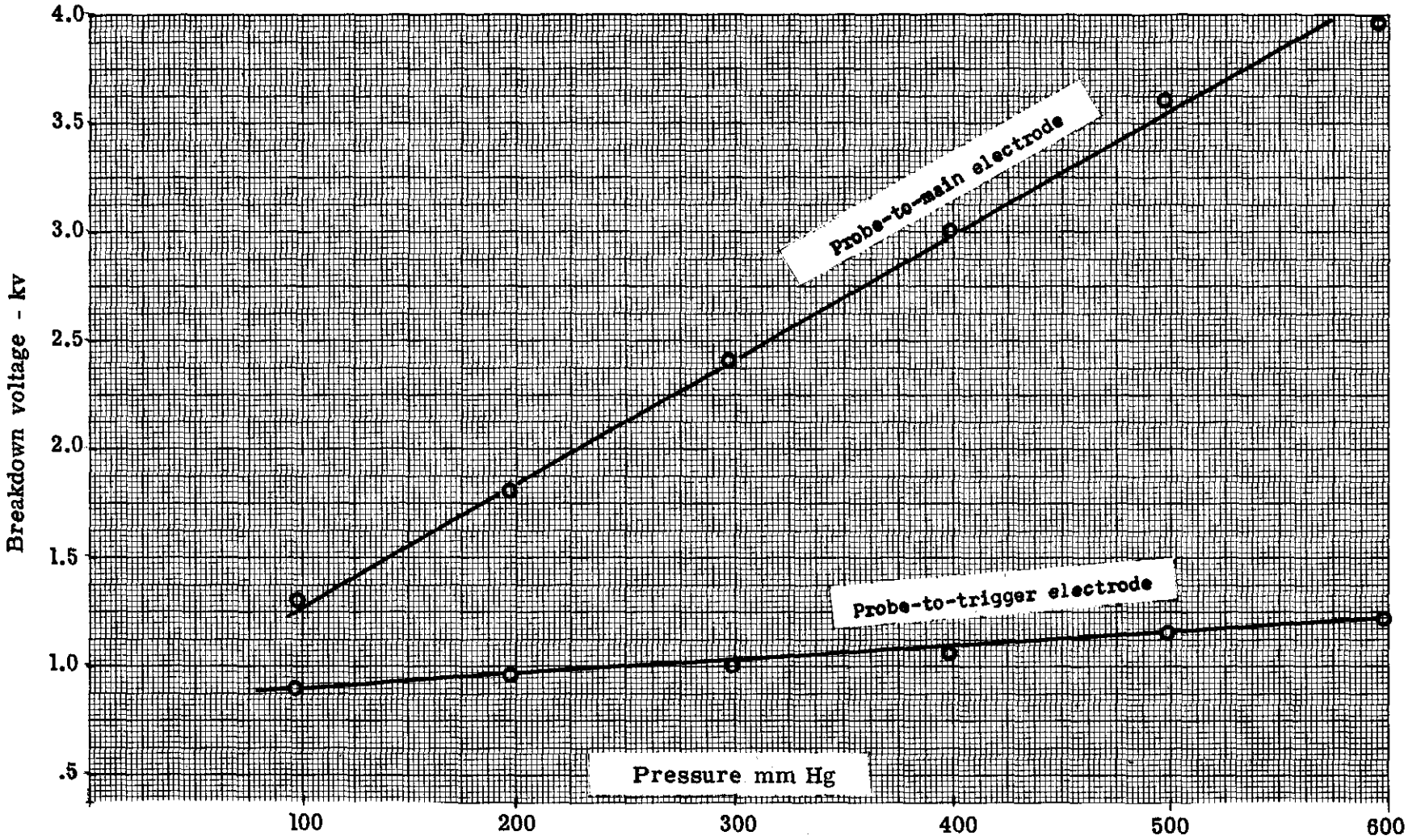

Fig. 69 -- Breakdown curves probe-to-trigger electrode and probe-to-main electrode

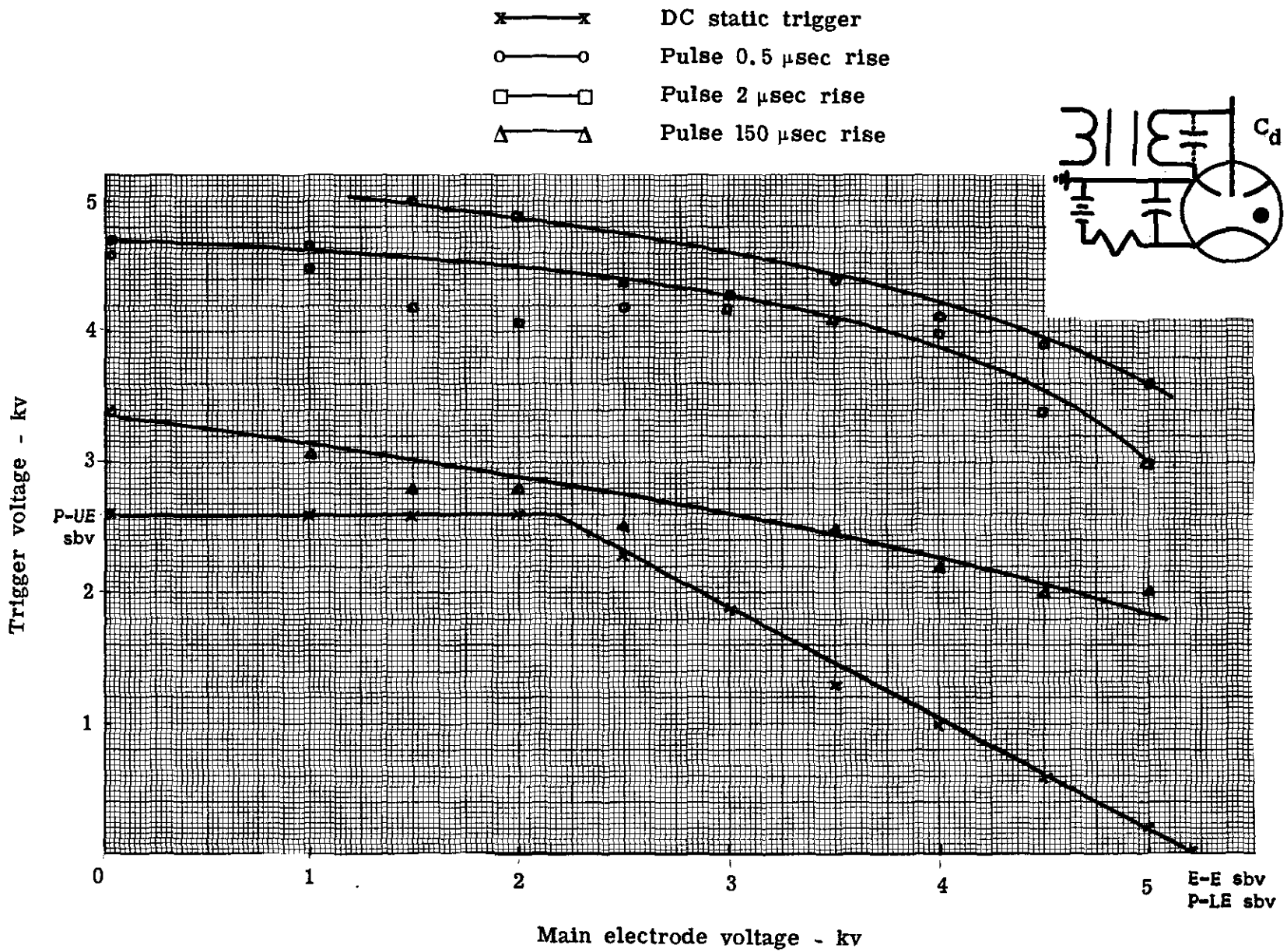

Fig. 70 -- Pulse trigger curves for trigger Mode A

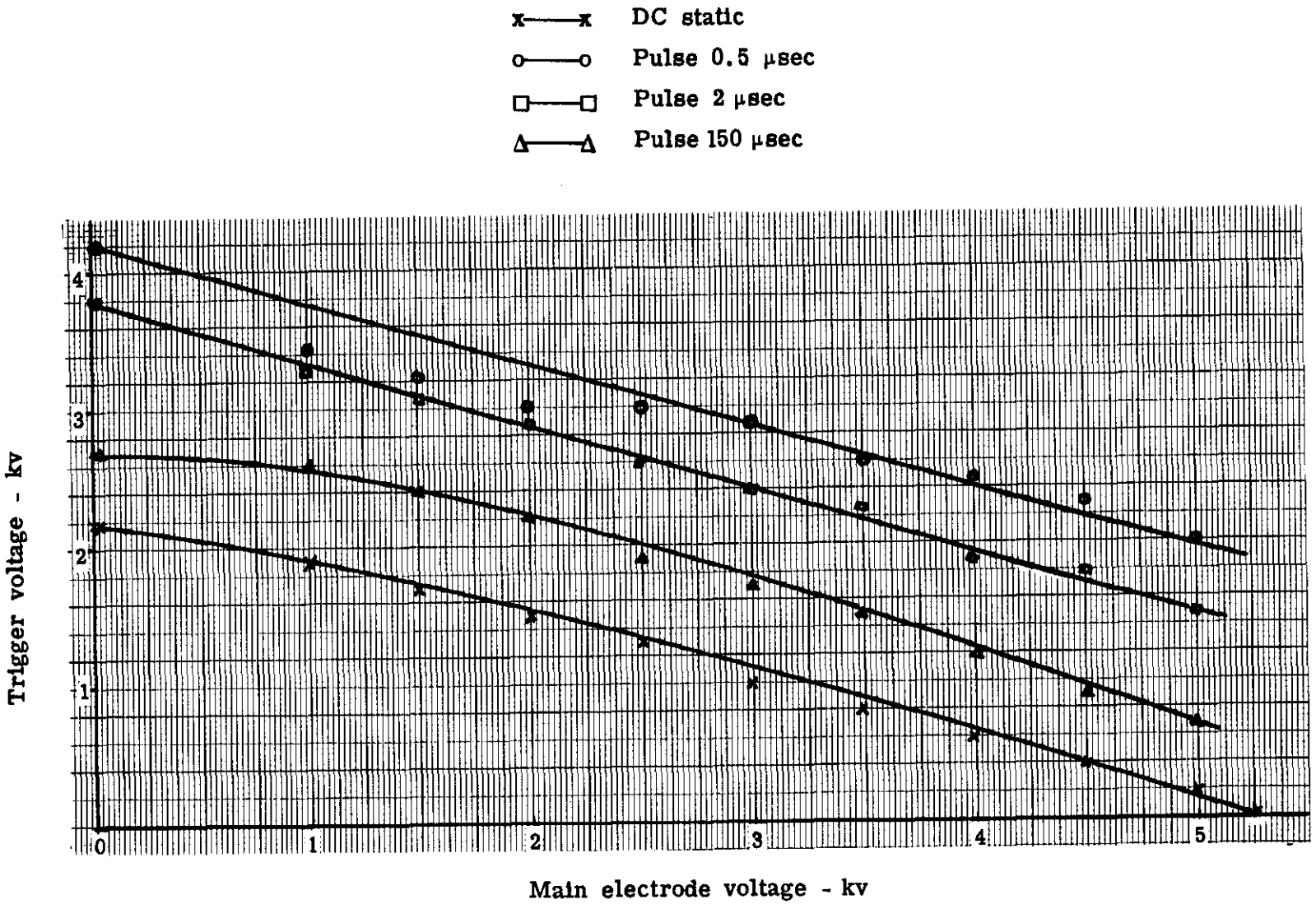

Fig. 71 -- Pulse trigger curves for trigger Mode B

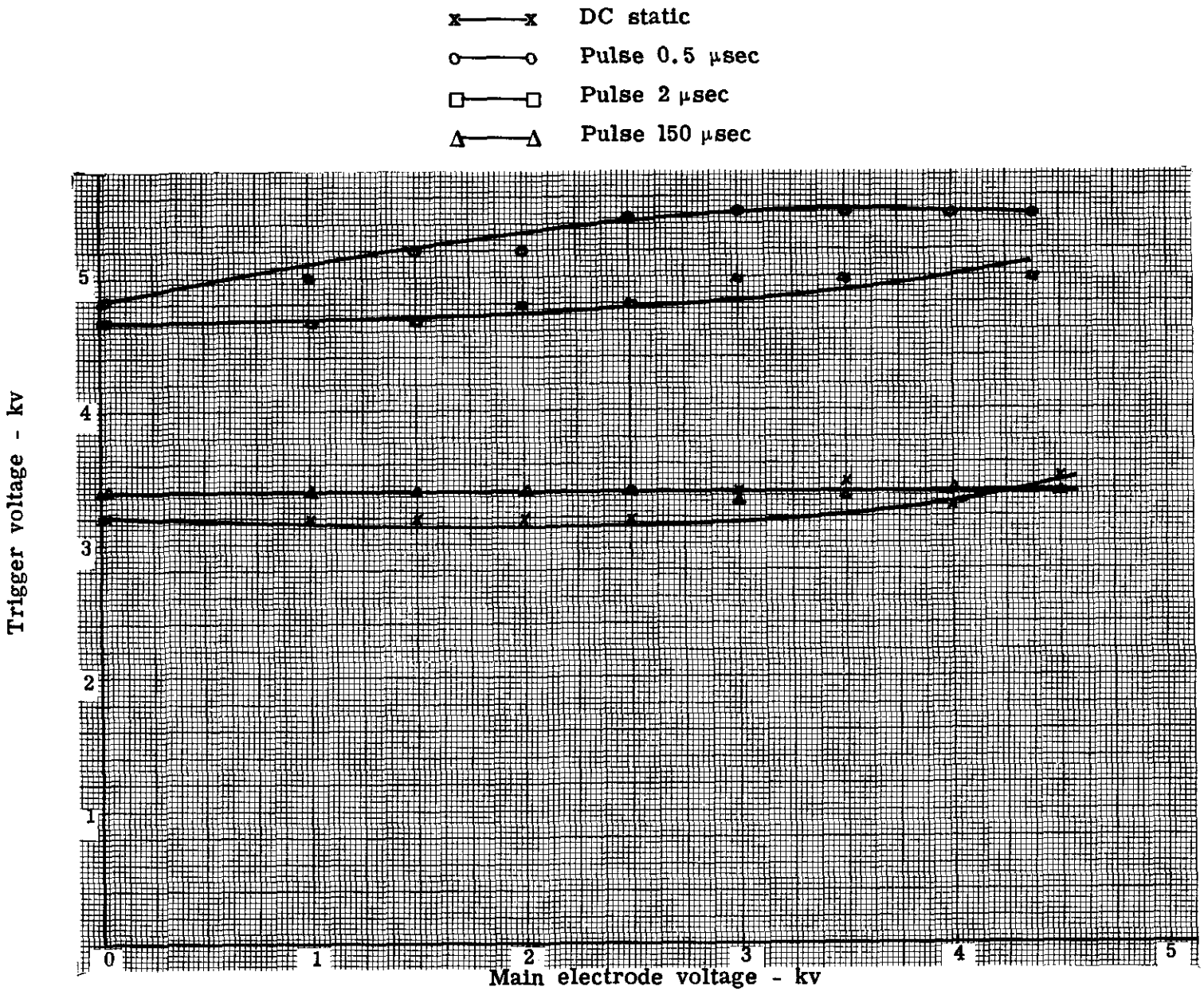

Fig. 72 -- Pulse trigger curves for trigger Mode C

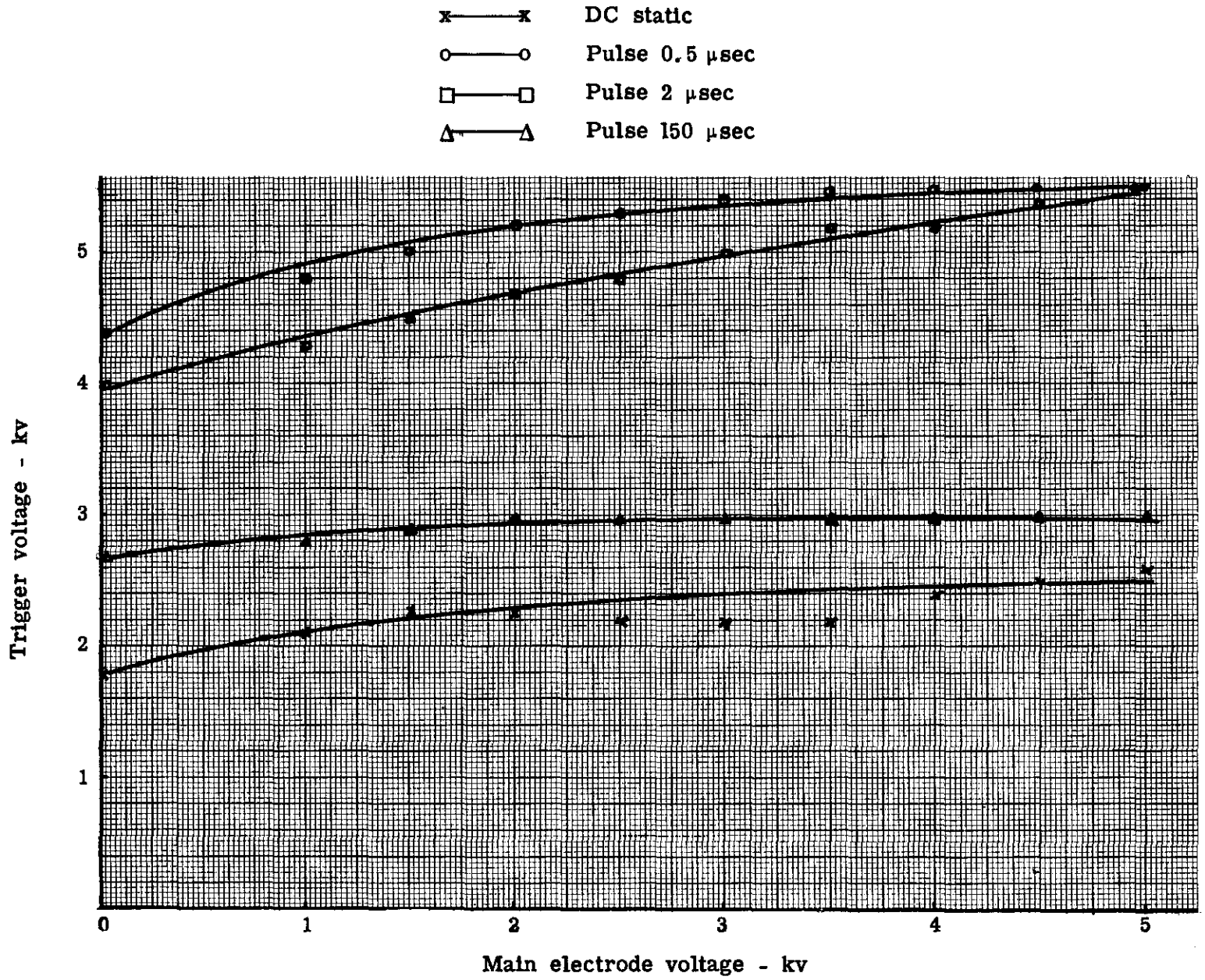

Fig. 73 -- Pulse trigger curves for trigger Mode D

As the rate of rise of the applied pulse increases, the pulse breakdown at zero gap voltage increases. This increase would tend to move the knee to the left, and if high enough compared to the probe-to-main electrode breakdown, the knee would not appear at all. A good example of the shifting of the knee is shown in Fig. 74, for a different type of gap than the one discussed in Figs. 70 through 73. The static breakdown of the probe-to-trigger electrode is 600 volts, and the pulse breakdown for a 2-μsec pulse is 1800 volts. The knee was consequently moved to the left. First consider the static case. The probe-to-main electrode static breakdown is 5500 volts. As we lower the gap voltage, as in the earlier discussion of the static trigger, the probe voltage increases approximately linearly until the probe-to-trigger electrode, sbv , is reached, and it then remains constant as the gap voltage is lowered.

For the pulse case, the probe-to-trigger electrode breakdown has increased to 1800 volts, while the pulse breakdown of the probe-to-main electrode has decreased to 4200 volts. When the static voltage on the probe is gradually increased, the insulator bonded to the probe gains surface charge. While the insulator is not a good conductor, it will slowly accumulate or "conduct" charge away from the probe along the surface of the insulator if the applied voltage rise is slow. This has the effect of effectively increasing the probe diameter, tending to make the field more uniform as previously shown in Chapter III . This effect appears to be more prevalent for point-to-plane geometries than for coaxial geometries with a homogeneous insulator. As the field becomes more uniform, the resultant probe-to-main electrode breakdown voltage is higher. Now when a fast rising pulse is applied to the probe, the probe will come to that voltage rapidly while the accumulated charge on the insulator will accumulate slowly; the effective probe diameter is then smaller, the field becomes nonuniform, and the breakdown value is lowered. Since the ratio of probe-to-trigger electrode pulse breakdown to probe-to-main electrode pulse breakdown has increased, the knee has been shifted accordingly.

If the same geometry of probe-to-main electrode is placed in the bell jar without the probe insulator, the static breakdown would be lower than this pulse value. Studies have shown that the breakdown value for any electrode arrangement without insulator effects such as point-to-plane, parallel wires, etc., is higher under pulse conditions than static conditions. Meek and Craggs discuss this point to some extent in their book Electrical Breakdown of Gases[12], and our data are in agreement with the following theory:

> "The time which elapses between the instant of application of a voltage to a gap and the occurrence of breakdown is known as the time lag and consists of two separate parts:
>
> 1. The statistical time lag caused by the need for an electron to appear in the gap during the period of application of the voltage in order to initiate the discharge.
>
> 2. The formative time lag corresponding to the time required for the time required for the discharge, once it has been initiated, to develop across the gap.
>
> The statistical time lag is clearly a variable quantity which depends on the amount of preionization, or irradiation, of the gap. Such irradiation may be produced by ultraviolet light, radioactive materials, or other methods. A gap subjected to an impulse voltage may break down if the peak voltage reaches the DC breakdown value provided that the irradiation is sufficient to cause an electron to be present to initiate the breakdown process. With less irradiation present the voltage must be maintained above the DC breakdown value for a longer period before an electron appears. Therefore, to cause breakdown of a gap with an impulse voltage of defined wave shape, increasing values of peak voltage are required as the amount of irradiation is decreased so that the voltage is in excess of the DC breakdown value for increasingly long time intervals."

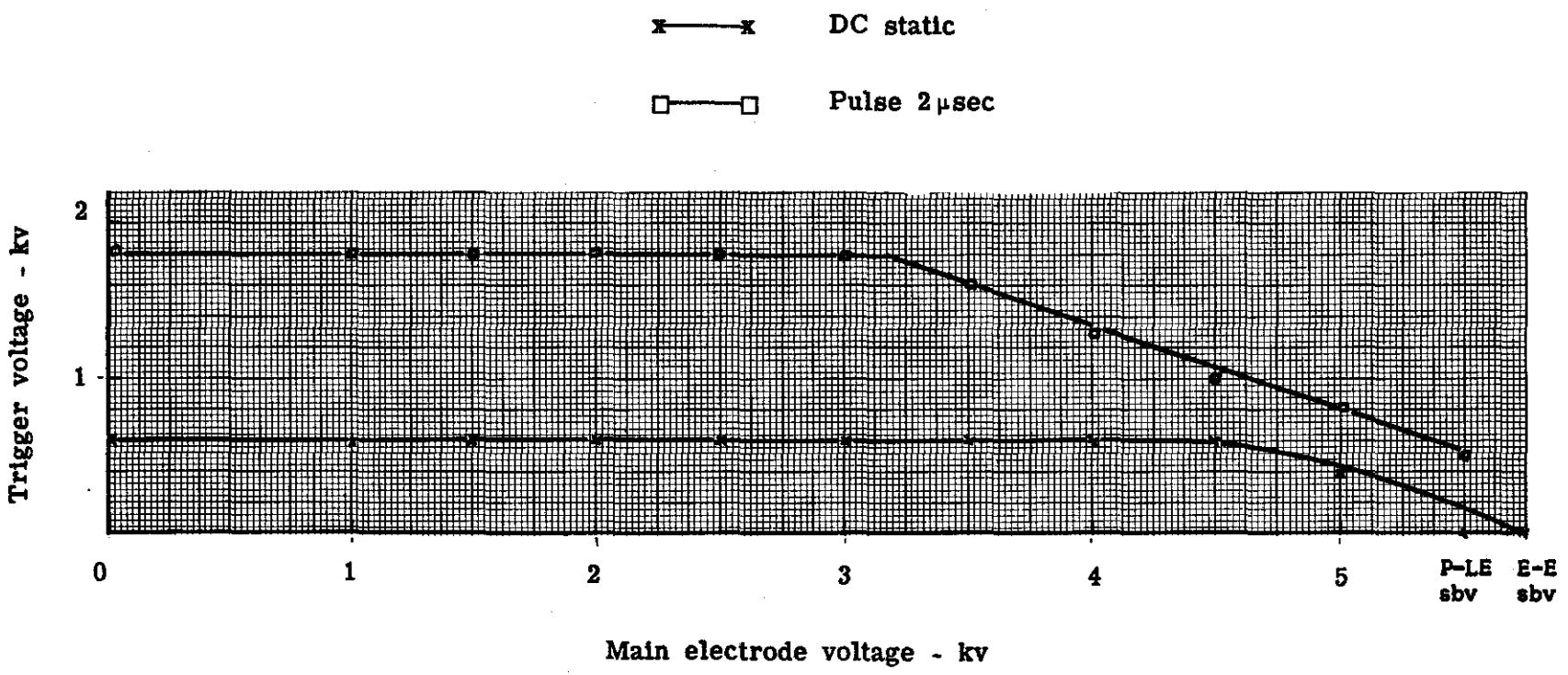

Fig. 74 -- Pulse trigger curve for trigger Mode A

Likewise, Figs. 71, 72, and 73 for these typical gaps show the trigger breakdown curves for the other three modes. In general, the pulse breakdown voltages follows the slope of the static curves. The faster the rate of rise, the higher the breakdown value. Where the polarity and geometry of the gap are chosen so that the trigger spark must form to the trigger electrode, there is a gradual upward slope of the trigger pulse breakdown for increasing gap voltage. This occurs for both the static and pulse conditions, and is due to the repelling field distribution caused by the potentials applied to the various electrodes.

A figure that might be employed to advantage which relates the pulse breakdown for different rise times to the static breakdown is the impulse ratio. This ratio will be defined as:

$$I_p = \frac{\text{Pulse breakdown voltage}}{\text{Static breakdown voltage}} .$$

These impulse ratios for the four polarity cases of the gap geometry of Figs.70 through 73, at an applied gap voltage of 1500 volts, are plotted in Fig. 75. They indicate the pulse trend and give an insight to predicting pulse breakdown values. In general, if the slope of the trigger curves follows the slope of the static curve (as it does in Modes B, C, and D for this particular geometry), the impulse ratio remains constant. For Mode A the impulse ratio will vary with the gap voltage.

In order to obtain statistical data on this parameter, several sealed gaps were tested using the 2-μsec rise pulse. In this test the static and pulse breakdown values were obtained for a positive-going probe with no gap voltage applied. Values for probe-to-trigger electrode and probe-to-main electrode were obtained. These gaps represent a sample size of 36 probes. Figure 76 shows this distribution for the case of probe-to-trigger electrode. The mean, $\overline{X}$, is 1.6 while the deviation, σ , is 0.26. Therefore $\overline{X} \pm 2\sigma$ will enclose 95 percent of the data and give the upper and lower limit of 2.12 and 1.08, respectively. For the case of probe-to-main electrode, $\overline{X}$ = 0.78, σ = 0.097, $\overline{X} \pm 2\sigma$ = 0.683 to 0.877. Figure 76 also shows graphically the breakdown voltages of the various rates of rise of these pulses.

To show the statistical variation of pulse triggering on sealed enclosed gaps, the pulse readings for different modes are shown in Fig. 77. The sample sizes vary from 12 units on Mode D to 76 units on Mode B. The variation of readings are shown as well as the averages. The readings were for a rise time of 0.5 μsec and are compared with typical curves taken for 2-μsec and 150-μsec rise times. The gap represented has a probe diameter of 0.102 cm, gap spacing of 0.165 cm, and a continuous bond between the probe and trigger electrode at a spacing of 0.127 cm .

Up to this point in the discussion, only the impulse ratios of gaps having continuous homogeneous bonds to the probe and trigger electrode have been considered. If the probe insulator has a void at the trigger electrode or at the probe or both, the problem becomes more complex and is not completely understood. Generally, the presence of a void, especially at the probe allows a corona discharge to take place in the void region prior to the pulse reaching the spark discharge voltage. As discussed earlier, this predischarge is the result of field intensification in the void caused by the overstressing of the gas by the higher dielectric constant of the insulator. Due to the irradiation of the gap from this preionization source, there are then sufficient initiatory electrons available, as the applied pulse voltage is increasing so that the breakdown process is initiated as the pulse voltage reaches the DC breakdown value. Thus, the statistical time lag is eliminated and, since the formative time lag is usually small, the pulse breakdown equals the DC breakdown and the impulse ratio then equals unity. For sufficient void spacings then there should not be any noticeable effect on the pulse breakdown due to the rate of rise of the applied pulse. This is, in general, borne out in practical designs

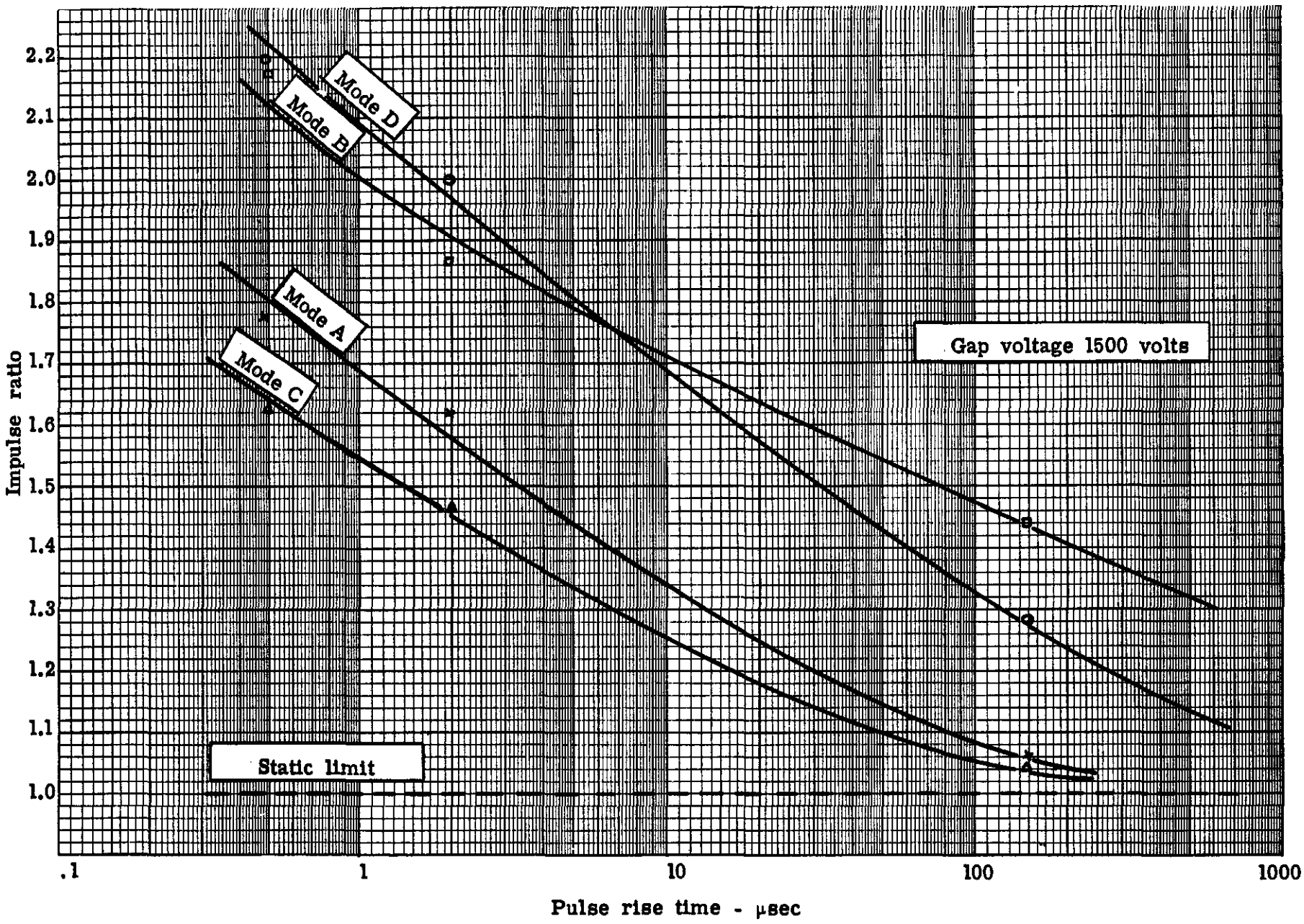

Fig. 75 -- Curves of typical gap trigger impulse ratios

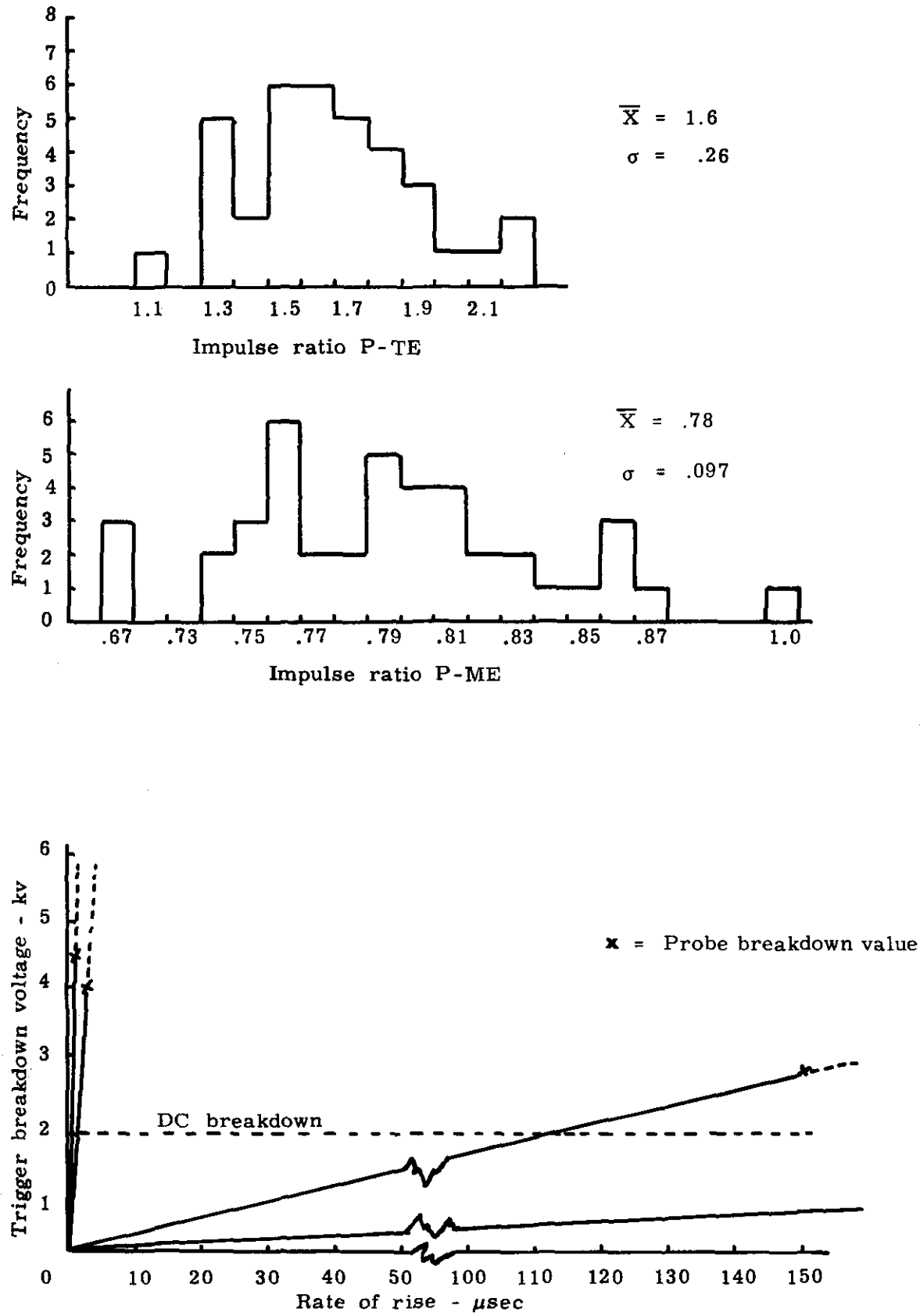

Fig. 76 -- Probe-to-trigger electrode

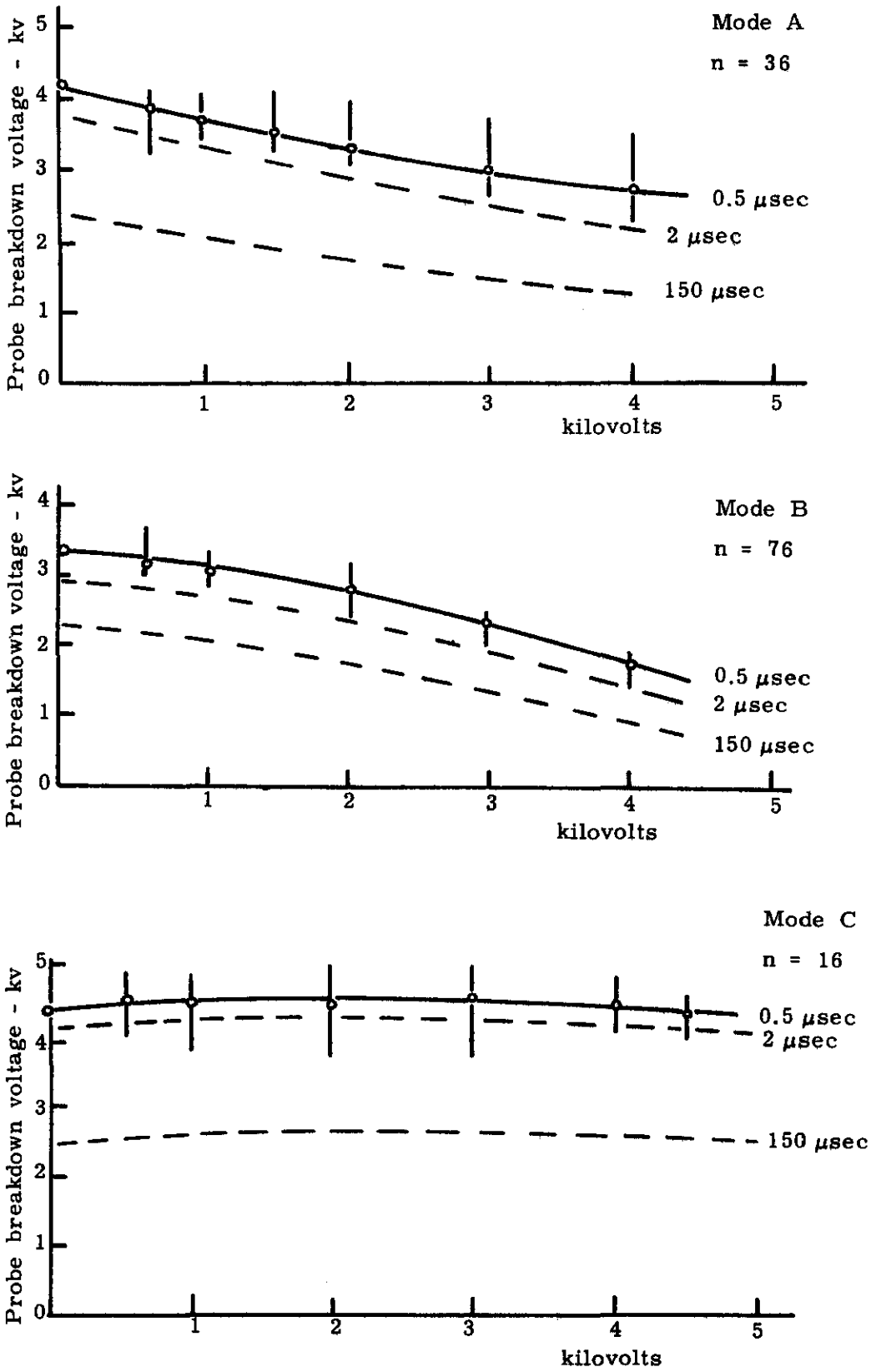

Fig. 77 -- Electrode-to-electrode voltage - kv

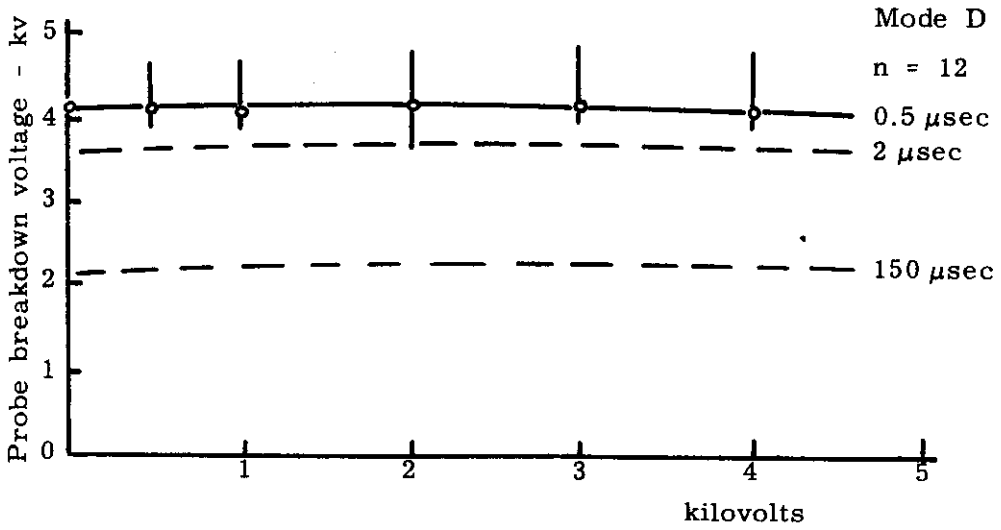

Fig. 77 (cont) -- Electrode-to-electrode voltage - kv

as shown in Figs. 78 and 79. Figures 78 and 79 show the pulse breakdown frequency distribution for a large number of gaps having a void at the probe for a 0.5- and 30-μsec rise time pulse, respectively. In general the distributions are about equal. If the voids are made very small or very large so that there is essentially no preionization and consequently no strong irradiation of the gap, then the impulse ratio will be less than or greater than 1 depending upon the rate of rise of the pulse coupled with whether it is a point-to-plane geometry or a coaxial geometry.

To estimate the pulse breakdown voltage of a given geometry, the static breakdown voltage of the geometry can be estimated by methods mentioned previously and by multiplying this value by the impulse ratio, I_p, for the given pulse under consideration. Therefore, for the two cases of interest, namely the point-to-plane (probe-to-main electrode) and the wire and cylinder (point-to-trigger electrode), the estimated pulse breakdown voltage will be for a gaseous dielectric, as follows:

Probe-to-trigger electrode

$$V_{pulse} = I_p \; 31 \; pK \left(1 + \frac{0.308}{\sqrt{pr}}\right) r \; \ln \frac{R}{r} \text{ kilovolts} \tag{47}$$

Probe-to-main electrode

$$V_{pulse} = I_p \; 31 \; pK \left(1 + \frac{0.616}{\sqrt{pr}}\right) \frac{r}{4} \; \ln \frac{8d}{r} \text{ kilovolts} \tag{48}$$

For the case of probe-to-main electrode breakdown with an insulator surrounding the probe, the breakdown can be expressed in two ways. The first is the same as the above Equation (48) where the static breakdown is estimated assuming the surface charge of the insulator does not exist, and the impulse ratio, I_p, is based on the static breakdown of the point-to-plane without the insulator present. The other method is to use the actual static breakdown value due to the surface charge effect of the probe insulator and the modified impulse ratio, I'_p, which is

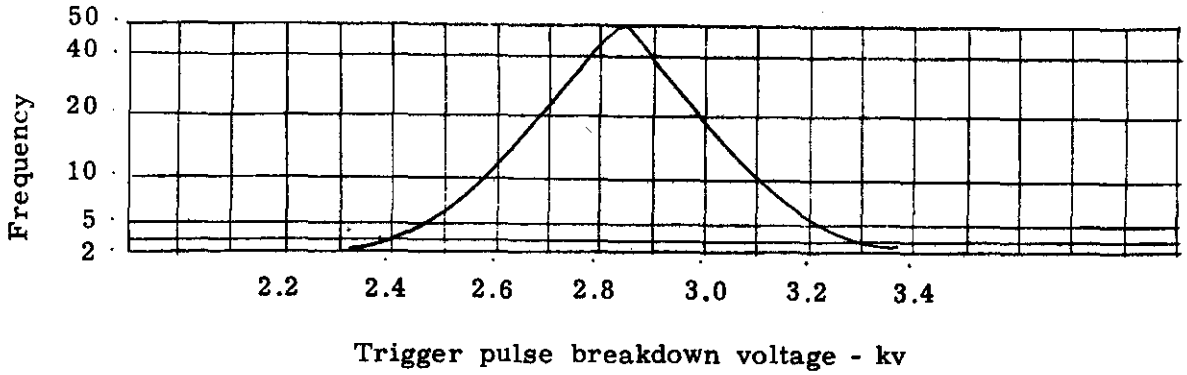

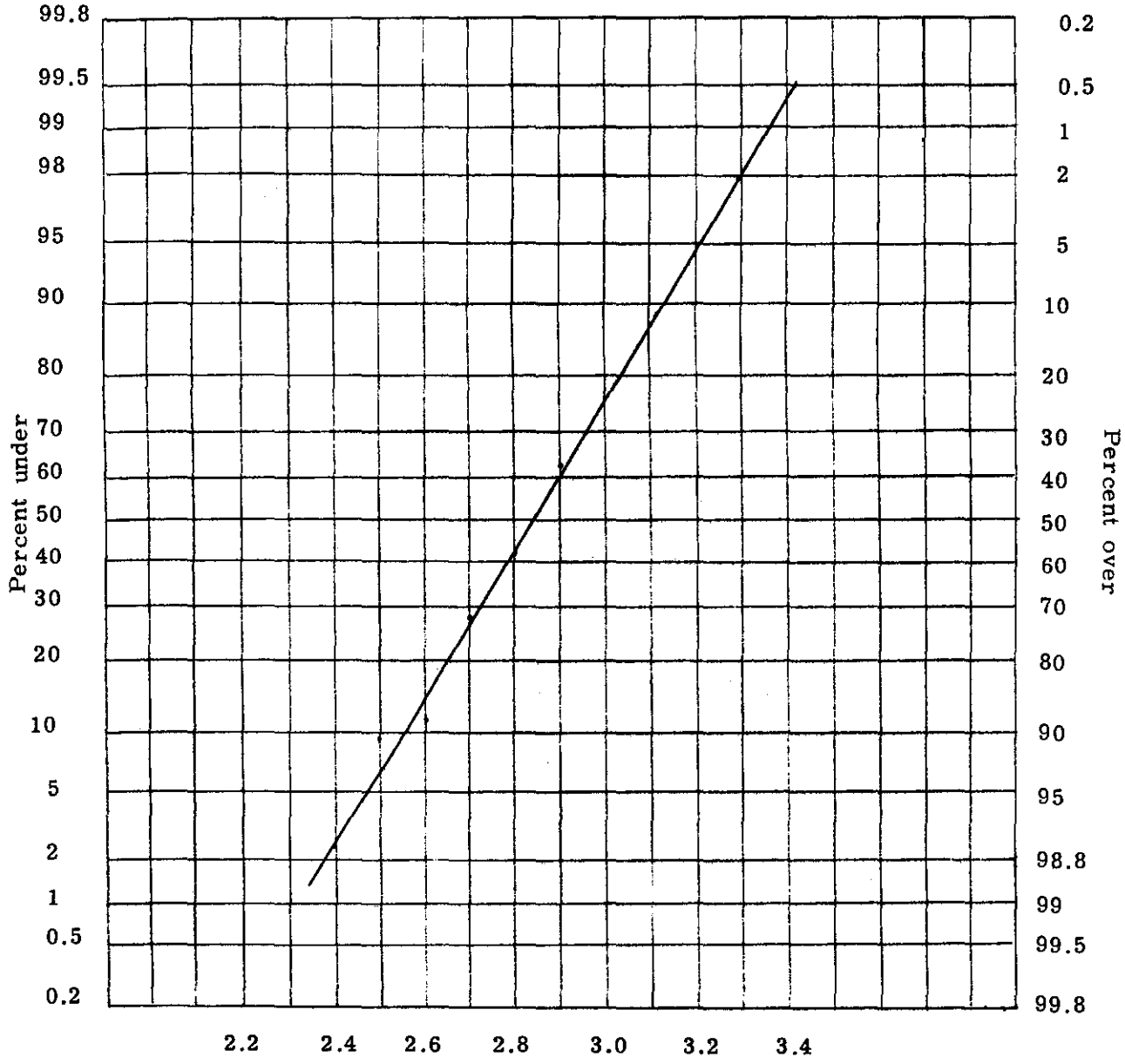

Fig. 78 -- Curve of frequency distribution of trigger pulse breakdown voltage

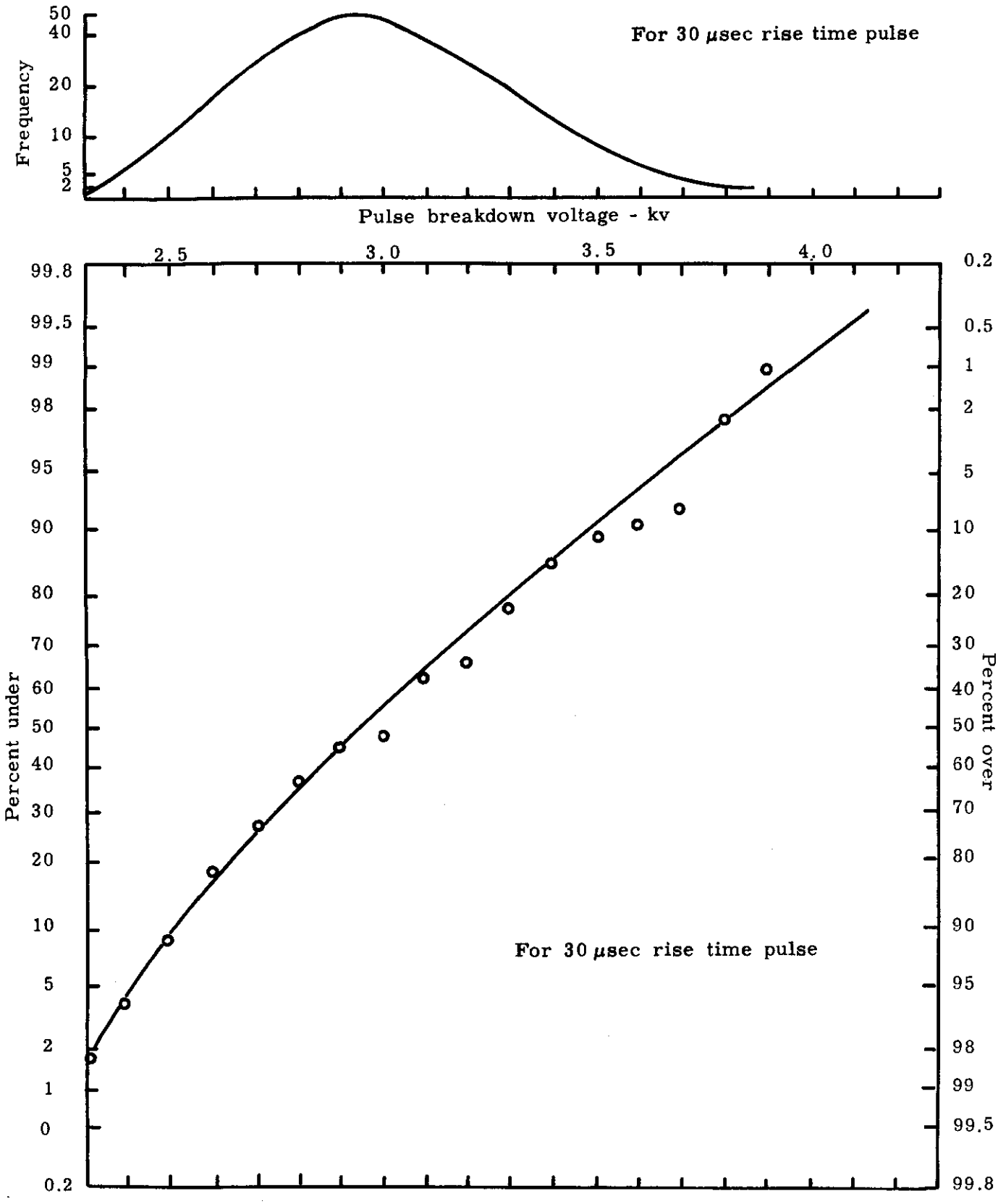

Fig. 79 -- Distribution of pulse breakdown averages for isolated probes

also based on the static breakdown voltage with the insulator present. For the case of probe-to-trigger electrode breakdown for voids at these electrodes, the problem becomes more complex, and the impulse ratio must be based on previously observed data.

The impulse ratio for the probe-to-main electrode geometry is not the same as the impulse ratio for the probe-to-trigger electrode for the same applied pulse. Therefore, the combination of the two geometries in forming the static model would be modified by the ratio of the impulse ratios for the two geometries for a given wave input. The static model for the gaseous dielectric can then be modified for the pulse condition as follows:

$$K_p = 2\left(1 + \frac{1}{a}\right) \frac{I_{p_1} \ln \frac{R}{r}}{I_{p_2} \ln \frac{8d}{r}} \tag{49}$$

where I_{p_1} is the impulse ratio for probe-to-trigger electrode, and I_{p_2} is the impulse ratio for probe-to-main electrode. Therefore, if the trigger spark is required to form to a given electrode, not only must the static conditions be satisfied, but the impulse ratio must be lower for the desired path.

Some data on the impulse ratio for various geometries can be found in the literature but, in general, the available data are limited and only cover certain limited regions.

The general trend of the impulse ratios, I_p, for probe-to-trigger electrode (wire and cylinder), probe-to-main electrode (point-to-plane), and probe-to-probe (parallel wires) where there is a solid insulator of various kinds between probes and between the probe and trigger electrode, is as follows:

A. Probe-to-Trigger Electrode

1. Where there are voids present, I_p is high at high pressures, decreases at moderate pressures, increases again at low pressures. Where there are no voids, I_p increases with increasing pressure.

2. I_p increases with increasing rates of rise of the applied voltage where there are no voids (or very small voids) at the probe.

3. With no void at the probe, and for a fixed r, I_p increases with increasing R.

4. With a void at the probe and for a fixed r, I_p decreases with increasing R.

5. With no voids at the probe, I_p is always one or greater than one.

6. With voids at the probe, I_p may be less than one, equal to one, or greater than one depending upon the magnitude of the void, rate of rise of the pulse, and the geometry.

B. Probe-to-Main Electrode

1. I_p increases with increasing pressure where there are no voids present. With a void at the probe, I_p appears to be independent of pressure.

2. I_p is greater than one where there are voids present.

3. I_p is usually less than one where there are no voids present.

4. I_p is high at small gap spacings, and decreases with increasing spacing. I_p then levels off and even increases as the gap spacing increases further.

5. I_p is less for a negative probe than for a positive probe.

6. I_p increases with increasing rate of rise of applied voltage.

C. Probe-to-Probe

1. I_p increases for increasing pressure.

2. I_p increases for increasing spacing between wires.

A summary of the observed impulse ratios for various geometries is given in Table V.

General Trigger Spark Requirements

Basic Considerations

The use of the triggered spark gap within 60 to 90 percent of its natural holdoff voltage offers no problem to the ability of generating a trigger spark capable of providing reliable triggering of the main gap on every attempt. This is true for any of the four possible modes of operation. If the operating range of the gap is required to extend down to voltages of 40 to 20 percent of the natural holdoff voltage of the gap, the problem of reliable triggering becomes more acute. The problem is not merely that of providing sufficient overvoltage to the trigger probe and thereby causing breakdown, but also of the follow through of the trigger spark required. For a fixed trigger input there will be a minimum gap voltage at which reliable triggering will occur. If the gap voltage is reduced, the trigger input must be increased. This minimum gap voltage at a given trigger input is termed the cutoff point of the gap. At all operating gap voltages above this cutoff value, the reference trigger input will then always fire the gap.

It is often possible to cause triggering below the cutoff voltage for a given trigger input, but this triggering is intermittent and unreliable. In the region just below cutoff, the ability to trigger appears to be statistical in nature. Consider a trigger circuit consisting of a low impedance input connected to a pulse transformer which in turn is connected to the trigger probe of the gap. The gap is being operated at approximately its cutoff voltage as previously determined from the trigger circuit under test. The input of the trigger circuit is then reduced to a value where the open-circuit voltage is just sufficient to cause probe breakdown. At this input and other increments of input up to the point providing minimum cut off of the gap, the number of successful firings out of a considerable number of attempts is recorded. The distribution of such a test is shown in Fig. 80. This distribution then shows the variation between 0 and 100 percent triggering as a function of trigger input.

TABLE V

Impulse Ratios of Various Geometries in Nitrogen

Probe to Trigger Electrode

Geometry					Pressure					
Voids	Insulator	r (cm)	R (cm)	Pulse (v/cm)	60 cm Hg	50 cm Hg	40 cm Hg	30 cm Hg	20 cm Hg	10 cm Hg
None at probe Small at TE	Glass	0.076	0.178	300	1.83	1.75	1.56	1.72	1.78	1.75
None at probe Small at TE	Glass	0.076	0.178	800	2.14	2.40	2.15	2.12	2.05	2.50
None at probe Small at TE	Glass	0.076	0.178	1,200	2.30	2.24	2.34	2.25	2.34	3.05
None at probe Small at TE	Glass	0.076	0.178	3,000	2.68	2.50	2.25	1.88	1.98	2.90
None at probe Small at TE	Glass	0.076	0.178	20,000	2.24	2.17	2.35	2.10	2.43	3.35
None at probe Large at TE	Glass	0.076	0.241	300	2.16	1.94	2.20	2.16	3.34	4.06
None at probe Large at TE	Glass	0.076	0.241	800	2.76	2.52	2.96	3.04	4.06	5.00
None at probe Large at TE	Glass	0.076	0.241	1,200	2.40	2.03	2.60	2.50	3.24	4.35
None at probe Large at TE	Glass	0.076	0.241	3,000	2.00	1.73	2.13	1.80	2.54	2.89
None at probe Large at TE	Glass	0.076	0.241	20,000	2.13	1.81	2.26	2.29	3.18	3.90
None	Glass	0.102	0.305	300	1.09	1.14	1.30	1.30	1.88	2.58
				800	1.07	1.18	1.33	1.33	1.65	2.17
				1,200	1.08	1.09	1.25	1.46	1.59	1.74
				3,000	1.40	1.49	1.56	1.92	2.39	3.00
Small voids at probe and TE	Lava	0.025	0.152	300	0.70	0.75	0.69	0.63	0.69	0.84
Small voids at probe and TE	Lava	0.025	0.152	800	0.76	0.76	0.77	0.70	0.76	0.84
Small voids at probe and TE	Lava	0.025	0.152	1,200	0.84	0.83	0.78	0.67	0.71	0.76

TABLE V (continued)

Probe to Trigger Electrode

Geometry					Pressure					
Voids	Insulator	r (cm)	R (cm)	Pulse (v/cm)	60 cm Hg	50 cm Hg	40 cm Hg	30 cm Hg	20 cm Hg	10 cm Hg
Small voids at probe and TE	Lava	0.025	0.152	3,000	1.01	0.92	0.96	0.85	0.74	0.97
Small voids at probe and TE	Lava	0.025	0.152	20,000	0.95	0.97	0.99	0.73	0.82	1.17
Small voids at probe and TE	Alumina	0.050	0.165	300	0.72	0.70	0.69	0.74	0.94	0.95
Small voids at probe and TE	Alumina	0.050	0.165	800	0.83	0.95	0.81	0.88	0.91	0.97
Small voids at probe and TE	Alumina	0.050	0.165	1,200	1.04	1.12	1.05	0.96	0.99	1.48
Small voids at probe and TE	Alumina	0.050	0.165	3,000	1.19	1.26	1.09	1.03	1.23	1.76
Small voids at probe and TE	Alumina	0.046	0.076	200	1.31	1.16	1.24	1.34	1.54	1.71
Small voids at probe and TE	Alumina	0.030	0.132	300		1.08				
Small voids at probe at TE	Alumina	0.046	0.76	300	1.23					
Small voids at probe at TE	Alumina	0.046	0.120	300	1.13					
Small voids at probe and TE	Alumina	0.046	0.127	300	1.16					
Small voids at probe and TE	Alumina	0.046	0.152	300	0.30*					
Small voids at probe and TE	Alumina	0.046	0.178	300	1.07					
Probe to Main Electrode										
Small at probe	Ceramic (surrounding probe)	0.046	0.013	200	1.60					

*Insulator made of two concentric ceramic tubing with a void at the center.

TABLE V (continued)

Probe to Main Electrode

Geometry					Pressure					
Voids	Insulator	r (cm)	R (cm)	Pulse (v/cm)	60 cm Hg	50 cm Hg	40 cm Hg	30 cm Hg	20 cm Hg	10 cm Hg
Small at probe	Ceramic (surrounding probe)	0.046	0.025	200	1.18					
Small at probe	Ceramic (surrounding probe)	0.046	0.013	200	1.75*					
Small at probe	Ceramic (surrounding probe)	0.046	0.025	200	1.30*					
Small at probe	Ceramic (surrounding probe)	0.046	0.038	200	1.06*					
Small at probe	Ceramic (surrounding probe)	0.046	0.050	200	1.00*					
Small at probe	Ceramic (surrounding probe)	0.046	0.127	200	1.12*					
Small at probe	Ceramic (surrounding probe)	0.046	0.191	200	1.15*					
Small at probe	Ceramic (surrounding probe)	0.046	0.127	200	1.14	1.08	1.15	1.12	1.04	1.31
None	Glass (surrounding probe)	0.050	0.165	3,000	0.73	0.79	0.81	0.86	0.94	1.18
None	Glass (surrounding probe)	0.050	0.165	3,000	-0.63	-0.67	-0.75	-0.75	-0.88	

*Air instead of N_2

TABLE V (continued)

Probe to Probe (Parallel wires for multiprobe gaps)

Geometry					Pressure						
Voids	Insulator	r (cm)	R (cm)	Pulse (v/cm)	60 cm Hg	50 cm Hg	40 cm Hg	30 cm Hg	20 cm Hg	10 cm Hg	5 cm Hg
None	Glass (surrounding probe)	0.050	0.254	1,200	1.42	1.65	1.65	1.59	1.63	2.26	2.56
None	Glass (surrounding probe)	0.050	0.419	1,200			1.65	1.60	2.34	2.96	3.70
None	Glass (surrounding probe)	0.050	0.610	1,200				1.74	2.20	3.15	3.60

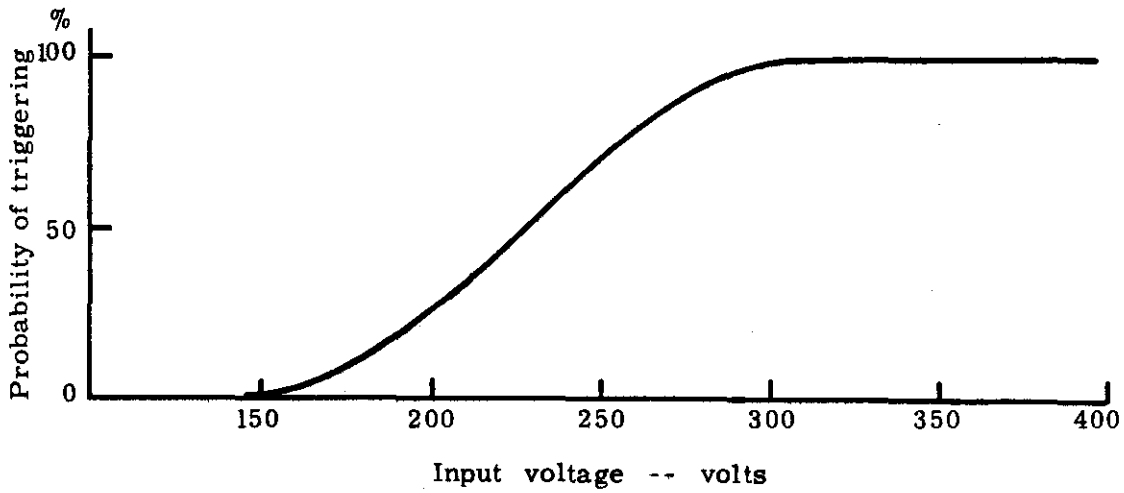

Fig. 80 -- Probability of triggering curve

One could also obtain a similar curve for a constant trigger input but for a variation in applied gap voltage over a range of gap voltages giving 0 to 100 percent firings. This is very pronounced for Modes A and D and to a much lesser extent for Modes B and C.

Investigation of pulse transformers used in triggering spark gaps shows that the ability to trigger the spark gap is influenced by the trigger circuit impedance, especially the capacitance of the trigger circuit. As will be shown later, the delay time between the trigger spark and the main gap breakdown is influenced by the magnitude of the trigger spark. It has also been observed that some gaps, which require a high pulse breakdown from a fixed triggering source, give more reliable triggering at a lower gap operating voltage than gaps of a similar geometry with a probe whose pulse breakdown voltage is low. This clearly illustrates the need to be able to control probe breakdown voltage reliability. The influence of the gap geometry also plays an important role in ease of gap triggering. It can also be shown that in the case of trigger transformers that the range of the gap operating voltage is extended at the lower gap voltages if an external capacitance of about 50 to 100 $\mu\mu$f is put across the terminal of the secondary output of the transformer. This improvement is obtained only as long as the open-circuit pulse voltage is not lowered or the rise time affected in such a way as to cause a reduction of probe breakdown voltage.

In order to determine the minimum trigger spark requirements the circuit of Fig. 81 was employed. In addition to this circuit, the static trigger circuit of Fig. 62 was employed to obtain the static trigger curve as a reference. The idea of this trigger circuit is that a variable lumped capacitance can be charged to a given DC voltage. The capacitor is then switched directly to the probe. Since at the time the capacitor is switched to the probe it is removed from the charging source, the total input for complete triggering can be determined. By varying the capacitance and the voltage, the minimum capacitance-voltage relationship for triggering can be determined.

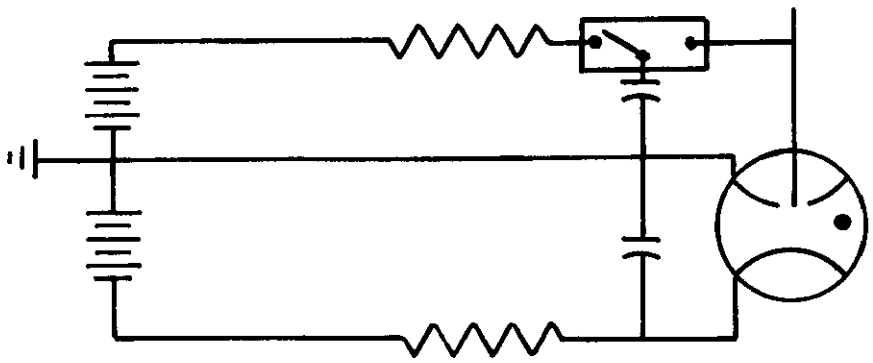

Fig. 81 -- Circuit for measuring minimum trigger requirement

At the moment just prior to switching, the probe potential is zero. At a small time after switching the probe is now at the potential of the capacitor and the resultant wave shape is essentially a step input, since the probe will usually break down before any appreciable charge has leaked off of the capacitor. The impulse theory mentioned earlier will also apply to this case, as far as the time required for the probe to break down at any given voltage. The higher the voltage on the capacitor above the DC static breakdown voltage, the shorter the statistical and formative time lag will be, and the sooner the probe will break down from the time of application of the applied pulse. Figure 82 below demonstrates this characteristic.

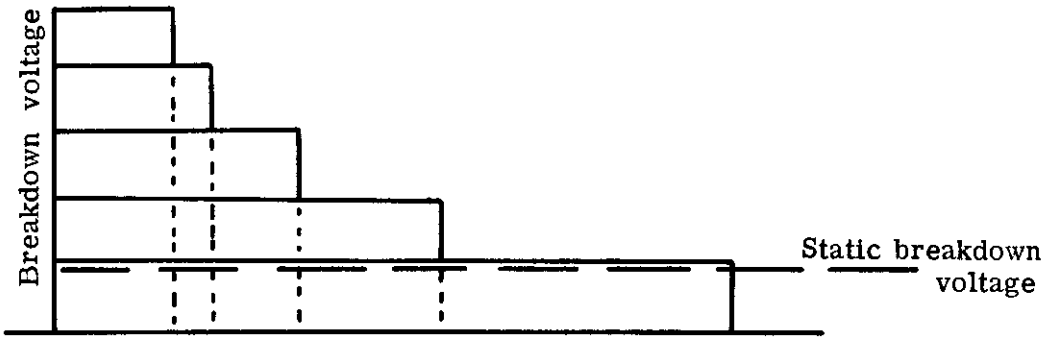

Fig. 82 -- Step input voltage to the probe

The main point of our interest, however, is the fact that we have a step input and can maintain voltages at the probe in excess of the static breakdown value. This would not be possible if a pulse were used with a finite rise time, since the probe would break down along the leading edge and therefore would not reach the peak voltage intended. With the use of the charged capacitor we essentially then have a known DC voltage applied to the probe at the instant of the probe breakdown.

After performing the initial test, it was soon evident that the test circuit was not supplying the input voltage to the probe as required. A close look at the test circuit showed that, instead of the charged capacitor switching directly to the probe, it was in reality charging another capacitor through some small resistance. The second capacitor consists of the probe input capacity of approximately 5 $\mu\mu$f plus the wiring capacity and switch capacity of approximately 13 $\mu\mu$f. The equivalent circuit would then be as shown in Fig. 83.

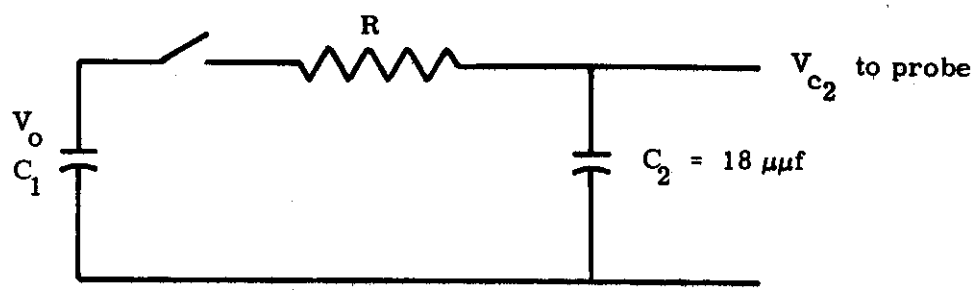

Fig. 83 -- Minimum trigger equivalent circuit

It can be shown then that the voltage appearing across the 18 $\mu\mu f$ or probe capacity is as given by the following expression

$$V_{c_2} = \frac{1}{c_2}\int_o^t idt = \frac{1}{c_2}\int_o^t \frac{V_o}{R}\, e^{-\lambda t} \tag{50}$$

$$V_{c_2} = \frac{V_o\, C_1}{C_1 + C_2}\left[1 - e^{-\lambda t}\right] \tag{51}$$

where

$$\lambda = \frac{1}{R}\left(\frac{C_1 + C_2}{C_1\, C_2}\right)$$

and C_1 is charged to V_o and C_2 is zero at time $t = 0$.

For very small values of R (as in our case being only the wiring resistance) and for steady state conditions, $t \to \infty$, the maximum resultant voltage on C_2 is now

$$V_{c_2} = \frac{V_o\, C_1}{C_1 + C_2}$$

From this expression we can see that if $C_1 \gg C_2$, the resultant voltage is essentially that of the applied voltage. However, to obtain the minimum trigger conditions the input capacitance, C_1, must be made smaller and smaller. If $C_1 = C_2$, then it is easily seen that only one half of the input voltage reaches the probe. Also if the probe does break down at this voltage, the resultant trigger circuit capacity is now $C_1 + C_2$ charged to the resultant voltage. With this expression, a corrected voltage and capacitance combination can be obtained for any input combination.

Mode A Operation

If a typical gap, such that the gap geometry allows the trigger spark to form to the main electrode, is triggered by using the charged capacitor circuit, the trigger characteristics obtained for Mode A operation are shown in Fig. 84. As the applied gap voltage is reduced slightly below its static breakdown value, the probe voltage for the various capacitor levels is that of the voltage obtained for the static trigger. As the gap voltage is reduced further, this relationship continues to hold until a gap voltage of less than 3 kv is reached. It is evident then that, when the trigger spark forms across the gap to the main electrode, the voltage required for breakdown at the level of a 39 $\mu\mu$f or above is sufficient to obtain complete transfer. Since the lowest possible combination of capacity that could be obtained with the present circuit and associated high-voltage power supply is 39 $\mu\mu$f, the true minimum requirements in this region could not be determined. The voltage could not be reduced, since it would then fail to cause probe breakdown and the trigger spark would not form.

As the gap voltage is reduced even further below its natural holdoff value, the minimum requirements for triggering are not met by the probe breakdown voltage and the minimum capacity of 39 $\mu\mu$f. In order to cause transfer then, either the probe voltage must be increased for the minimum capacity available or else the available capacity must be increased for the minimum probe breakdown voltage or a combination of both. As the gap voltage is decreased further, the effect becomes more pronounced for the minimum trigger capacity and consequently requires higher input voltages to effect triggering.

The point at which the required trigger voltage departs appreciably from the static curve is described at the "gap cutoff" (V_ℓ) voltage for the given capacity level.

It should also be mentioned that this gap cutoff value must be restricted to a finite delay time as well as a main gap voltage point, since two combinations of capacity levels at the same main gap voltage level will give complete triggering but with different delay times. The lower capacity level would give longer delay times than the higher capacity levels. In general, a delay time of under 100 μsec should be used when defining cutoff. The gap should normally be operated above the cutoff value, and delay times should then be well under 10 μsec for an optimum gap and trigger circuit design.

When the gap voltage is reduced below 2 kv, the static trigger voltage is about 2750 volts and the trigger spark now forms to the trigger electrode. For the 127 and 167 $\mu\mu$f capacity levels, the minimum probe breakdown voltage is still sufficient to cause triggering, while the 64 and 39 $\mu\mu$f require higher and higher probe voltages. Eventually the gap voltage becomes so low that the 167 $\mu\mu$f capacity level fails to trigger the gap. For the 64 $\mu\mu$f capacity level, we see that the effective operating range is 2 kv to the sbv of 5.4 kv or a range of about 3.4 kv. The 2-kv cutoff occurs at a reduction of 63 percent from the sbv value of the gap. To increase the operating range by 1 kv would require reducing the cutoff voltage to 1 kv by doubling the capacity level to 127 $\mu\mu$f. Cutoff would then occur at an 82 percent reduction from the sbv of the gap. Obviously the higher the ratio of gap operating voltage to its natural static breakdown voltage, the easier the triggering becomes.

Figure 85 shows a similar trigger curve for a different gap geometry where the relative cutoff values are determined by the different capacity levels. Figure 86 is a single curve for a third gap geometry showing the cutoff characteristics for a 70 $\mu\mu$f capacity level. The operating range is approximately 4 kv, and the cutoff occurs at a reduction of 67 percent from the static breakdown value of the gap. The curves for Mode B, which is also an aiding field case, are not shown but would essentially have a similar curve.

Fill gas – Nitrogen

r = 0.050 cm

R = 0.140 cm

d = 0.165 cm

p = 540 mm Hg

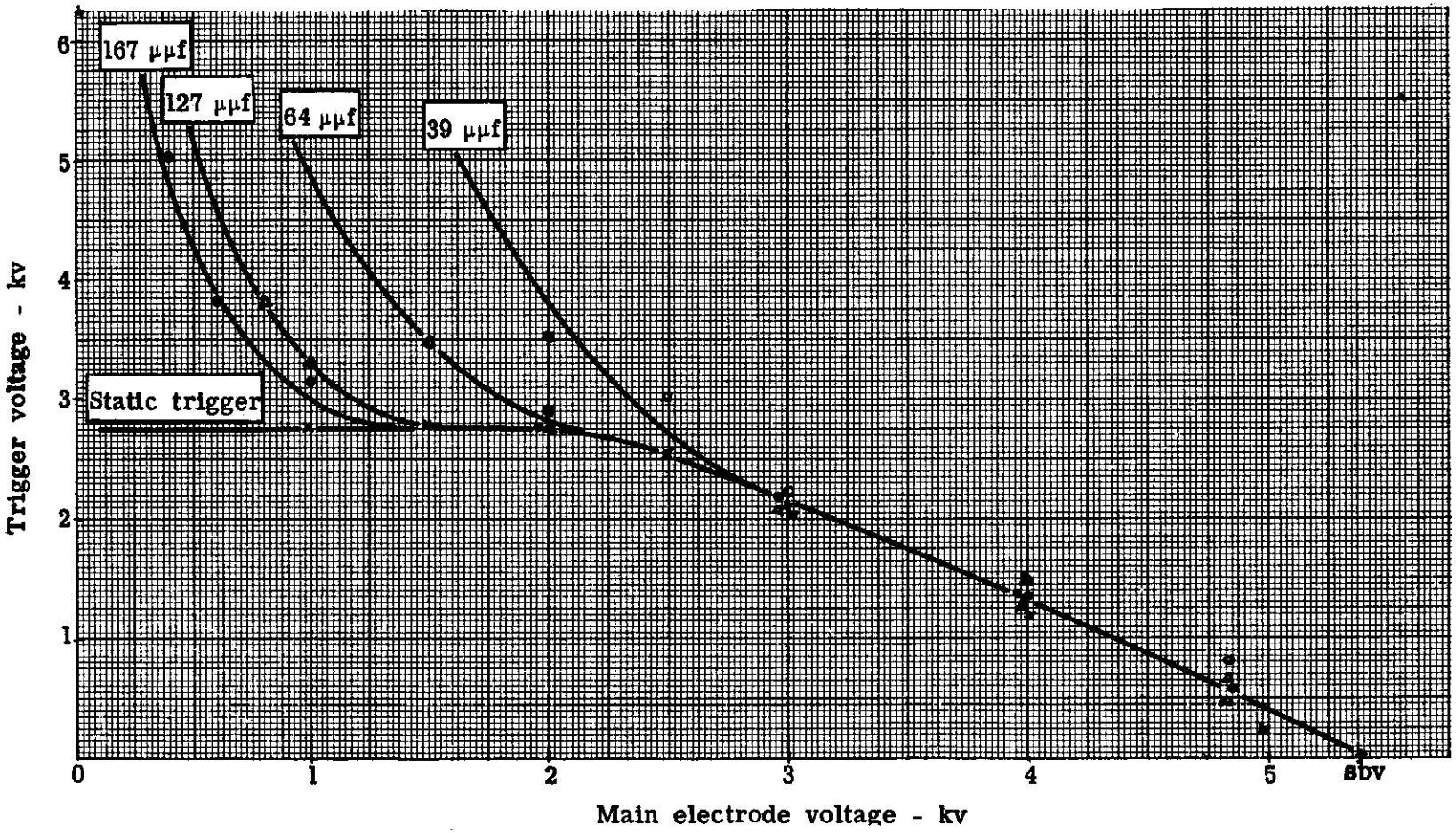

Fig. 84 -- Trigger voltage required for gap breakdown vs main electrode voltage -- for different trigger capacity

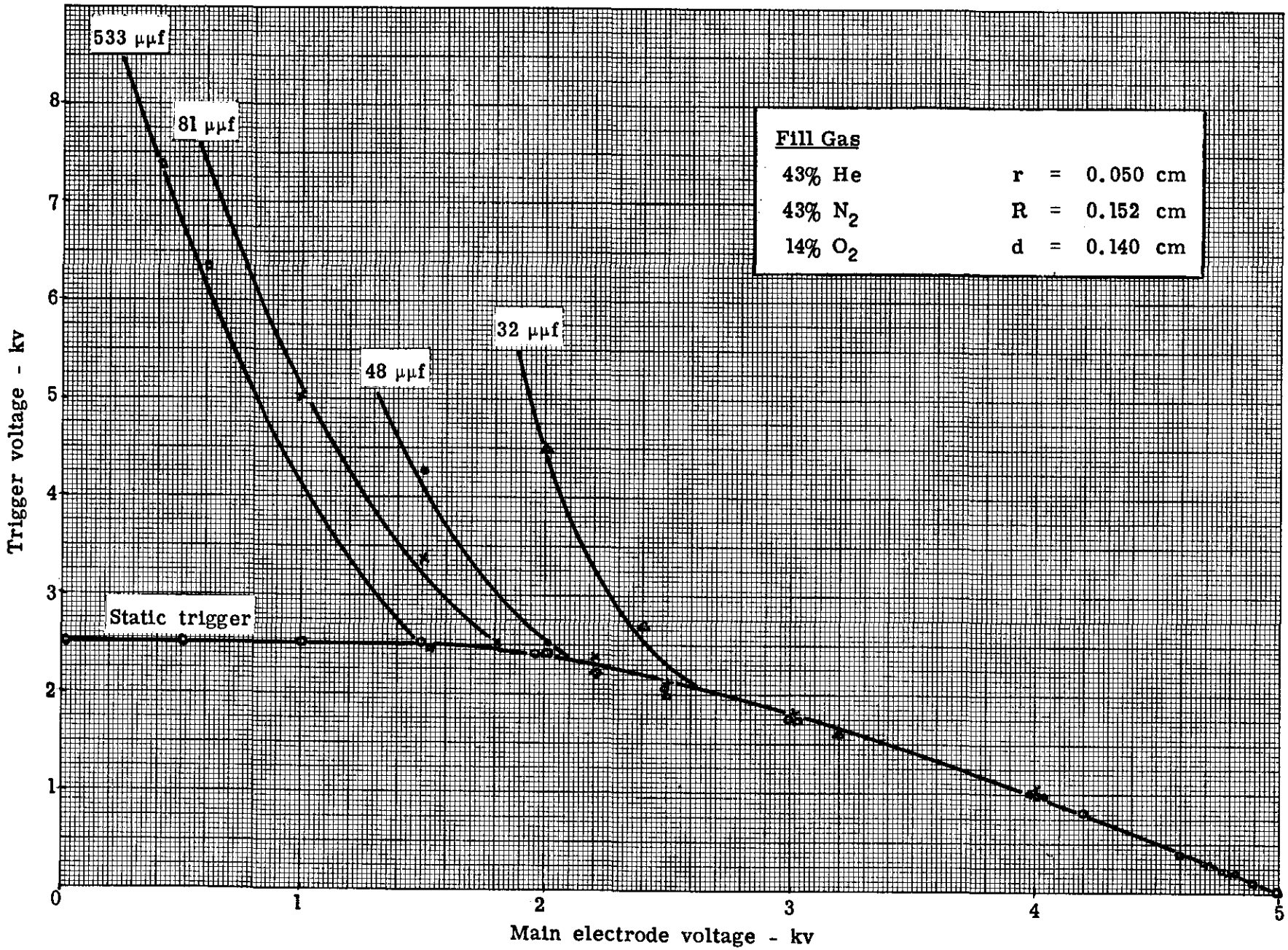

Fig. 85 -- Trigger voltage required for gap breakdown in Mode A operation vs main electrode voltage -- for variation of trigger capacity

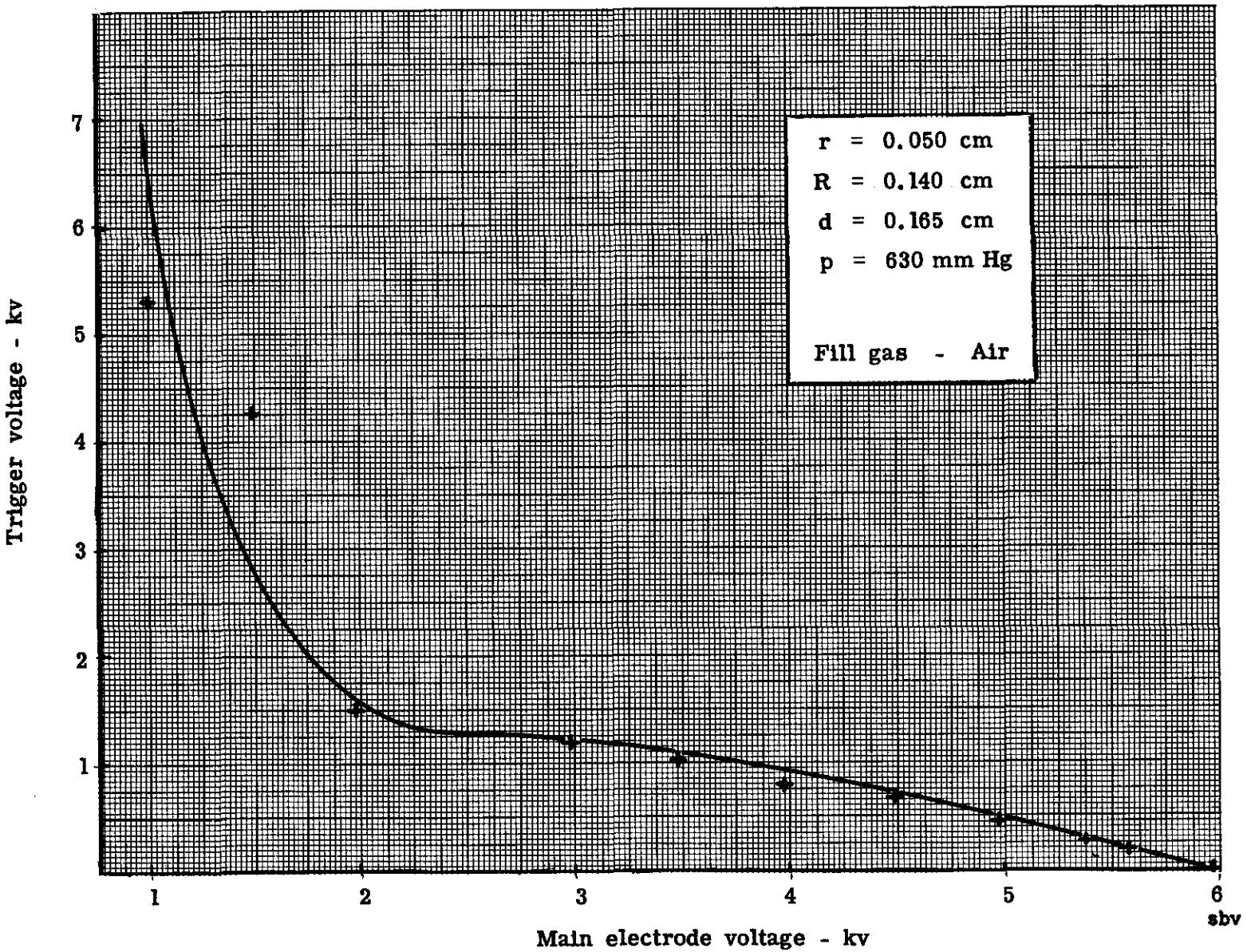
r = 0.050 cm
R = 0.140 cm
d = 0.165 cm
p = 630 mm Hg
Fill gas - Air
Trigger voltage - kv
Main electrode voltage - kv
sbv
1
2
3
4
5
6
7

Mode C Operation

A similar analysis on the same gap geometry can be made for Mode C which is a repelling main field. Figure 87 shows the trigger and static curves for a typical gap geometry. In the Mode C operation for this particular geometry, the principal trigger spark path is probe-to-trigger electrode. As the gap voltage is lowered below its sbv value, the trigger voltage is independent of gap voltage and is approximately equal to the probe-to-trigger electrode breakdown voltage. For the 467 $\mu\mu$f capacity level, the minimum probe breakdown voltage is sufficient to cause triggering down to about a cutoff value of 1 kv. The lower capacity levels have higher cutoff values as would be expected but, in addition, the trigger voltage level is higher than the static trigger curve. In this case, the gap cutoff voltage has to be redefined as the gap voltage where the trigger voltage increases above a constant value characteristic to its capacity level. Here at the lower capacity levels, an interchange of capacity and voltage can be made to effect triggering. The 73 and 43 $\mu\mu$f are not shown because of the exceedingly high input voltages required to obtain the necessary probe voltages for this capacity level. Comparison of this mode of operation with Mode A, for the same gap geometry, shows that the voltage-capacity combination required for triggering is higher for Mode C than Mode A. However, as will be shown later, Mode C for other geometries can be easier to trigger than Mode A.

Pressure Variation

For a fixed gap geometry, the variation of pressure on the gap breakdown and trigger characteristics are important. Figure 88 shows the variation of trigger characteristics for variations of pressure for a capacity level of 467 $\mu\mu$f. Except at the gap cutoff voltage of 600 volts, the trigger curves follow the outline predicted by the static trigger curves. Since the probe-to-trigger electrode spacing and probe-to-main electrode is fixed, the increase in pressure causes the respective static breakdown values to increase. This increase gives an increased operating range, but also higher trigger voltages. The capacity level is sufficient for the resultant trigger voltage to cause triggering for all gap voltages above approximately 1 kv.

If a lower capacity level is used in the trigger circuit the results shown in Fig. 89 are obtained. The capacity level shown is 93 $\mu\mu$f. The cutoff value for the lower capacity levels occur at higher gap voltages as would be expected. Since the capacity is low, the minimum static breakdown voltage is not sufficient to cause triggering and higher trigger voltages are required. With this higher voltage, the characteristic static plateau is not observed and represents a more accurate estimate of the trigger requirements.

In order to obtain a better comparison between the trigger curves at different pressures, the curves of Figs. 88 and 89 are normalized in Figs. 90 and 91, by plotting trigger voltage as a function of the ratio of main gap voltage to its natural static breakdown voltage. For the 467 $\mu\mu$f capacity level, the characteristic static plateau is still present when the probe-to-trigger electrode breakdown voltage is reached which is, of course, different for the different fill pressures. As the pressure increases, the plateau level is increased proportionally. In the region of probe-to-main electrode breakdown, the breakdown curves for the various pressures essentially follow the same sloping curve, but at higher levels for higher pressures.

The curves of Figs. 92, 93, and 94 show the Mode A trigger characteristics for the various capacity levels for three different fill pressures, 20-cm Hg, 40-cm Hg, and 60-cm Hg, respectively. The static curves are essentially those of Fig. 88, and the trigger curves at the lower capacity levels are similar to Fig. 89.

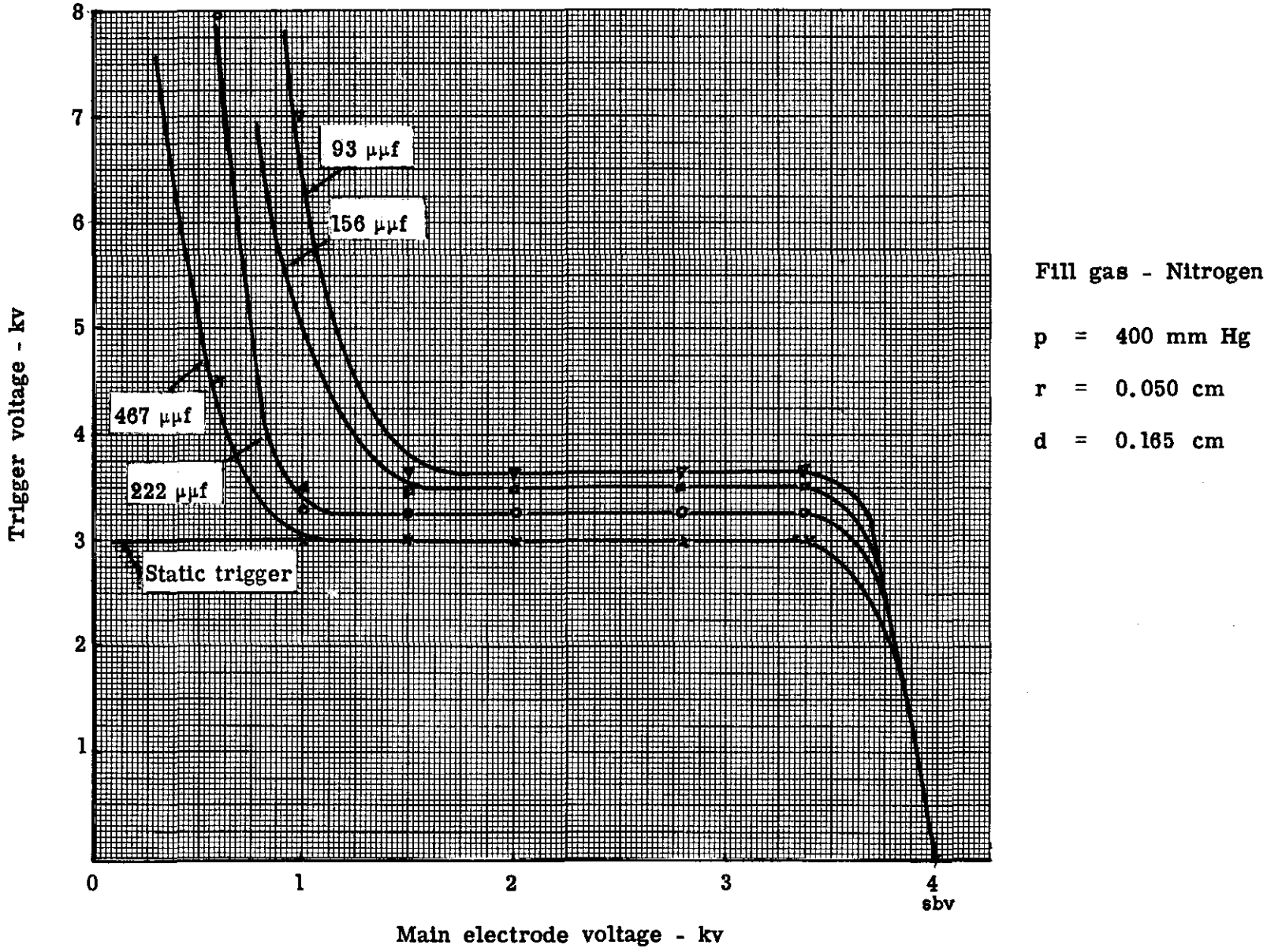

Fig. 87 -- Trigger voltage for gap breakdown in Mode C operation for varying trigger circuit capacity

Mode A Operation

r = 0.050 cm

Constant gap spacing - 0.065 in.

x——x 100 mm Hg

△——△ 200 mm Hg

o——o 300 mm Hg

■——■ 400 mm Hg

●——● 500 mm Hg

▽——▽ 600 mm Hg

Fill gas - Nitrogen

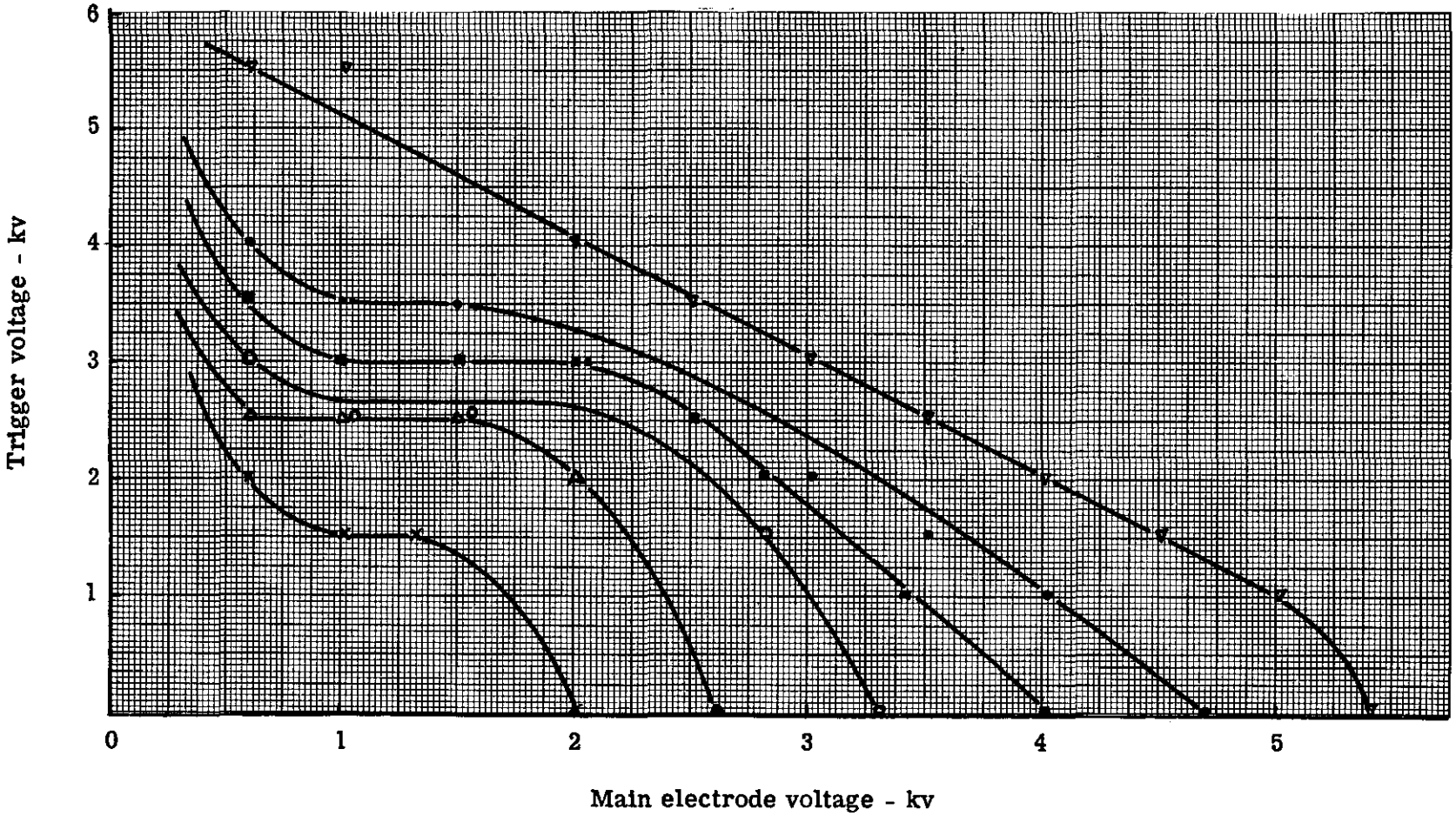

Fig. 88 -- Trigger voltage required for gap breakdown at a capacity level of 467 μμf -- for varying fill pressures

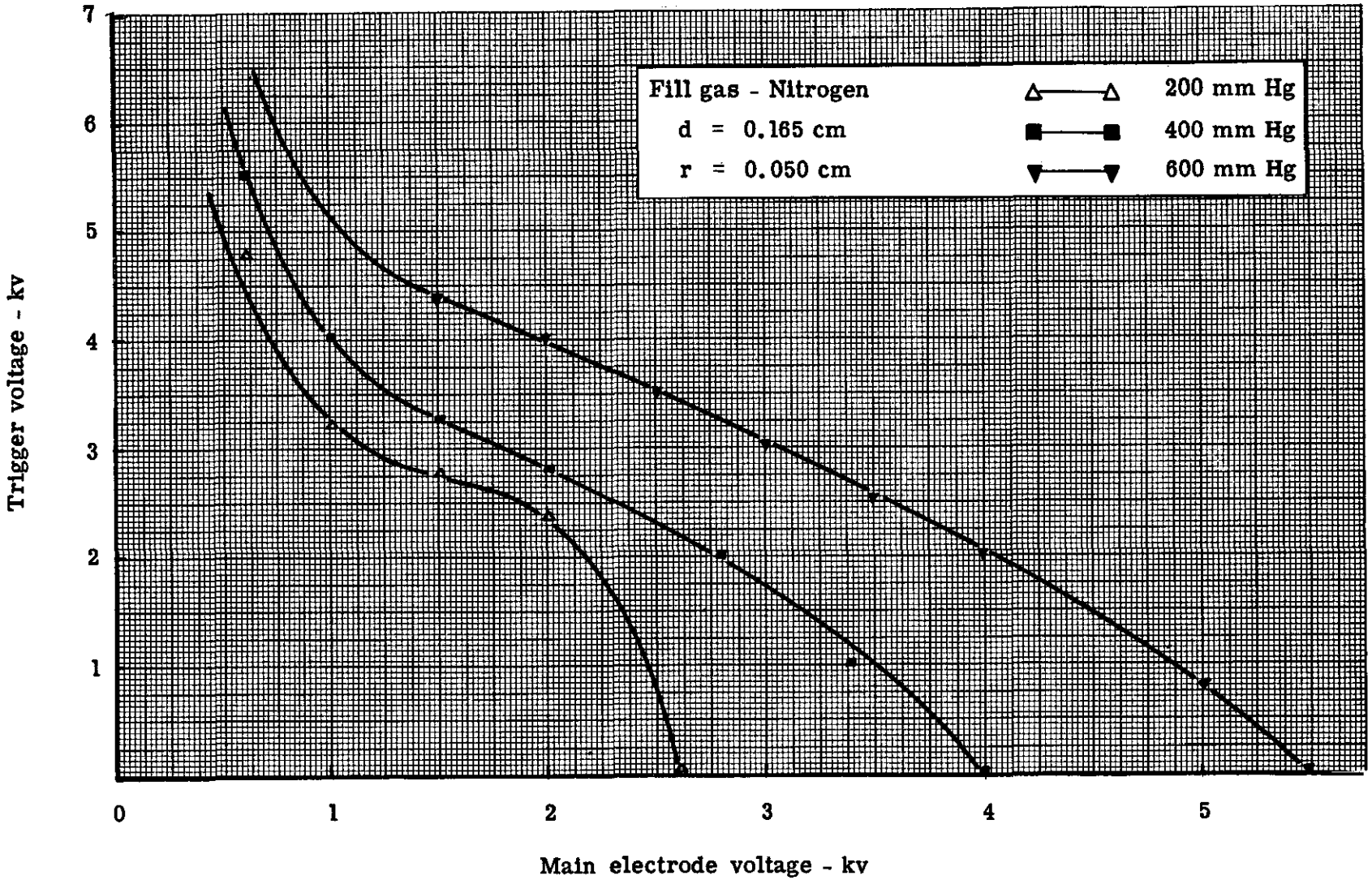

Fig. 89 -- Trigger voltage required for gap breakdown for varying fill pressure

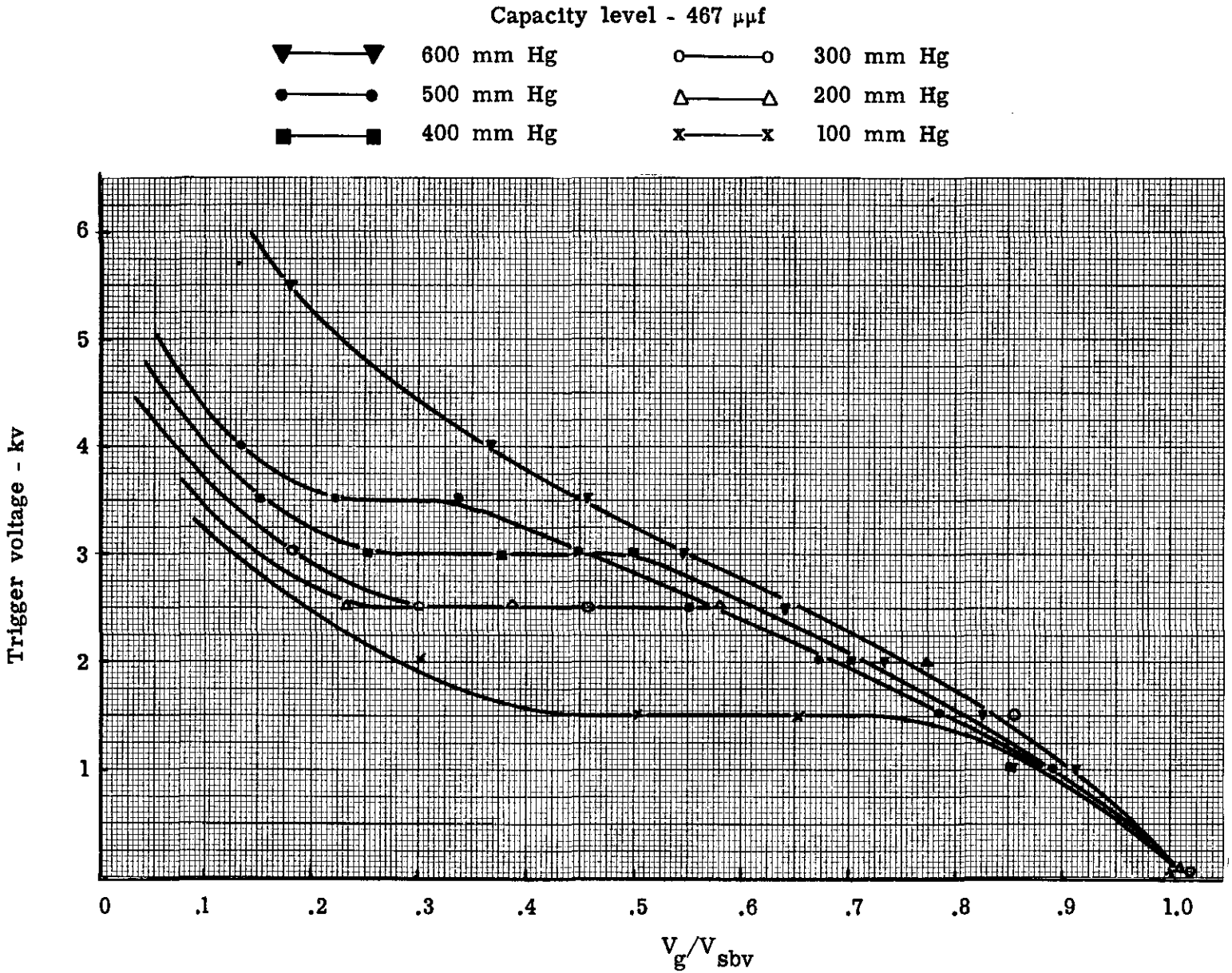

Fig. 90 -- Trigger voltage required for gap breakdown as a function of the ratio of gap voltage to static breakdown voltage -- for various fill pressures

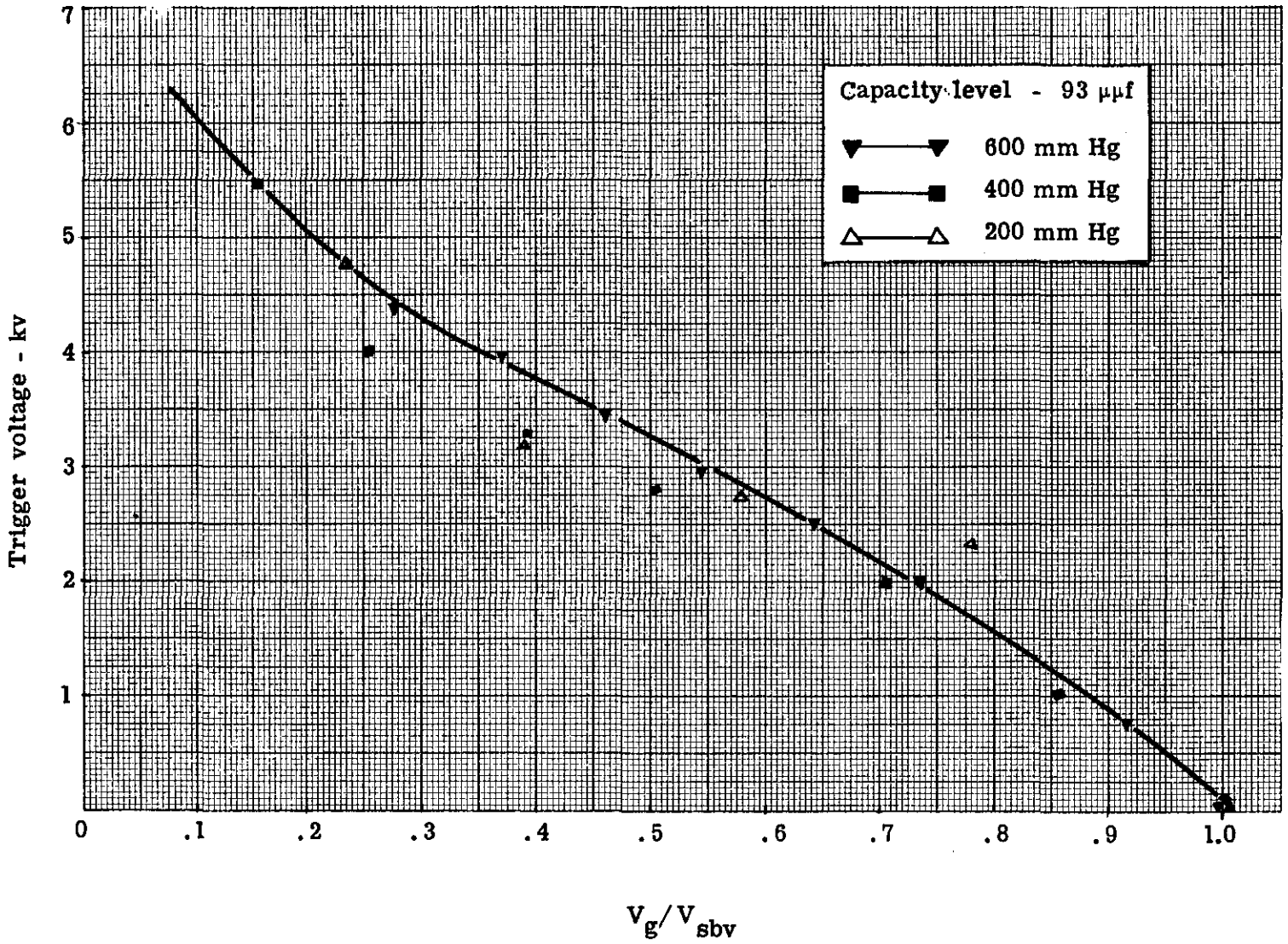

Fig. 91 -- Trigger voltage required for gap breakdown as a function of the ratio of gap voltage to static breakdown voltage -- for various fill pressures

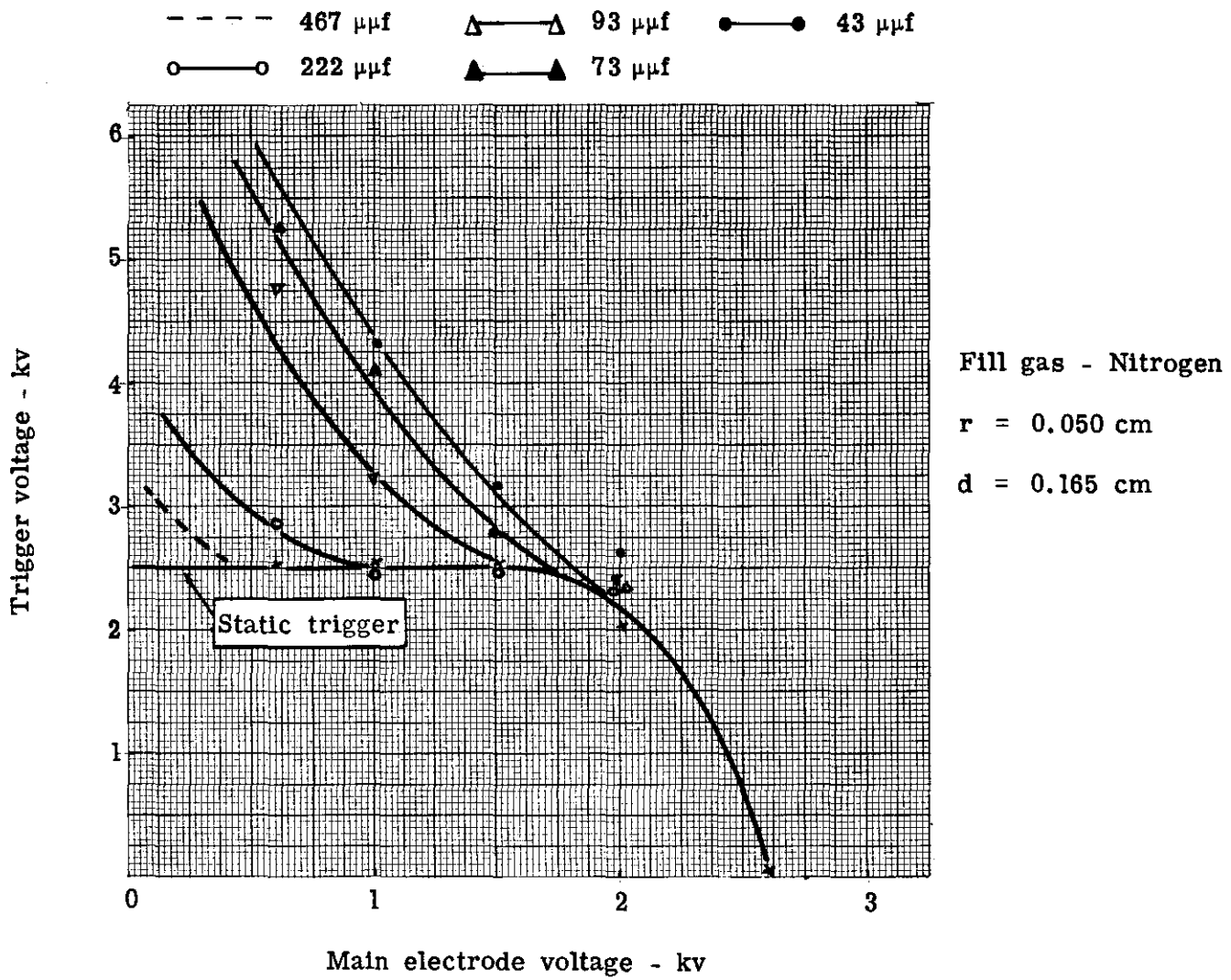

Fig. 92 -- Trigger voltage required for gap breakdown for varying trigger circuit capacity -- for pressure of 200 mm Hg (Mode A)

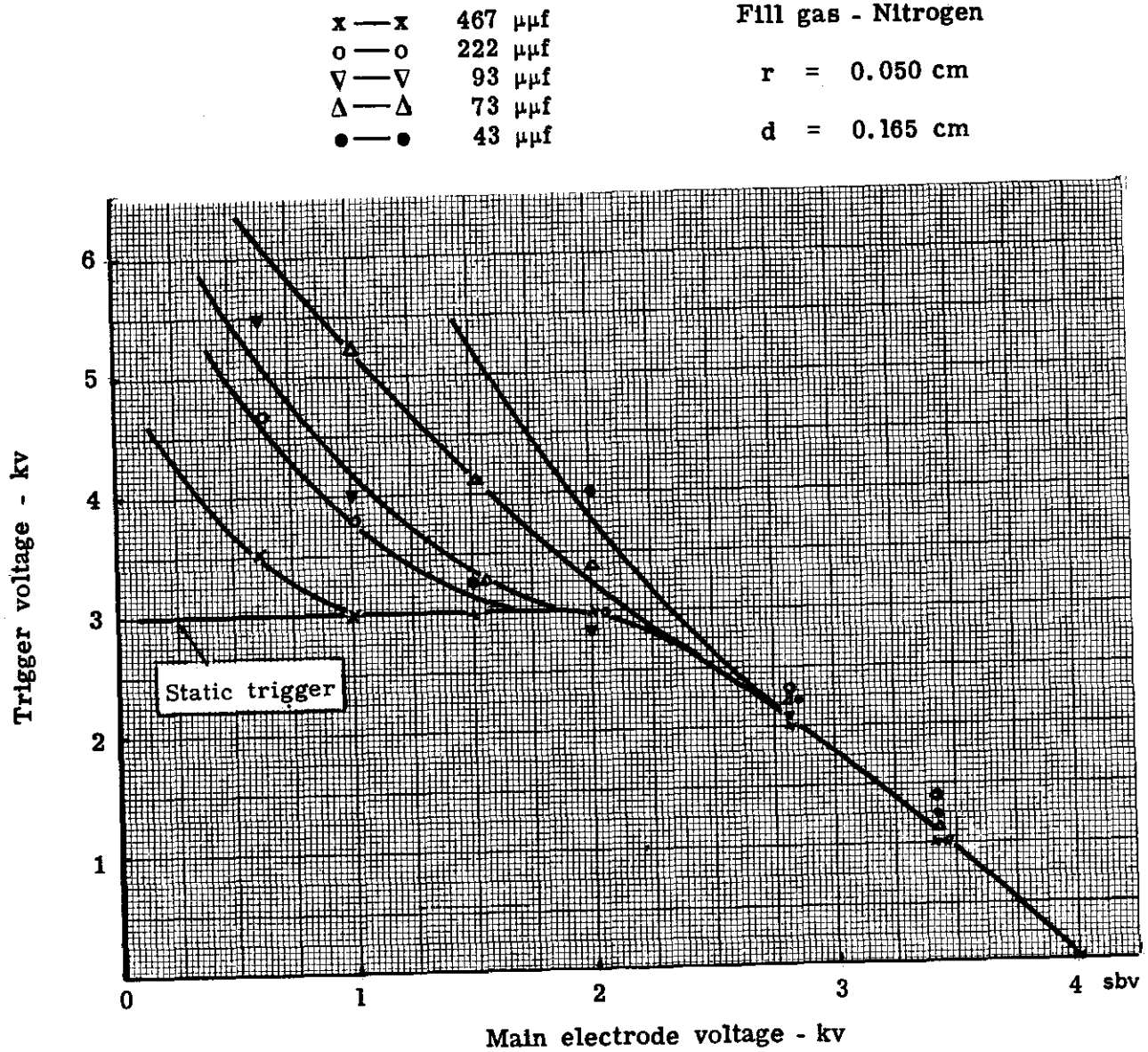

Fig. 93 -- Trigger voltage required for gap breakdown for varying trigger circuit capacity -- for pressure of 400 mm Hg (Mode A)

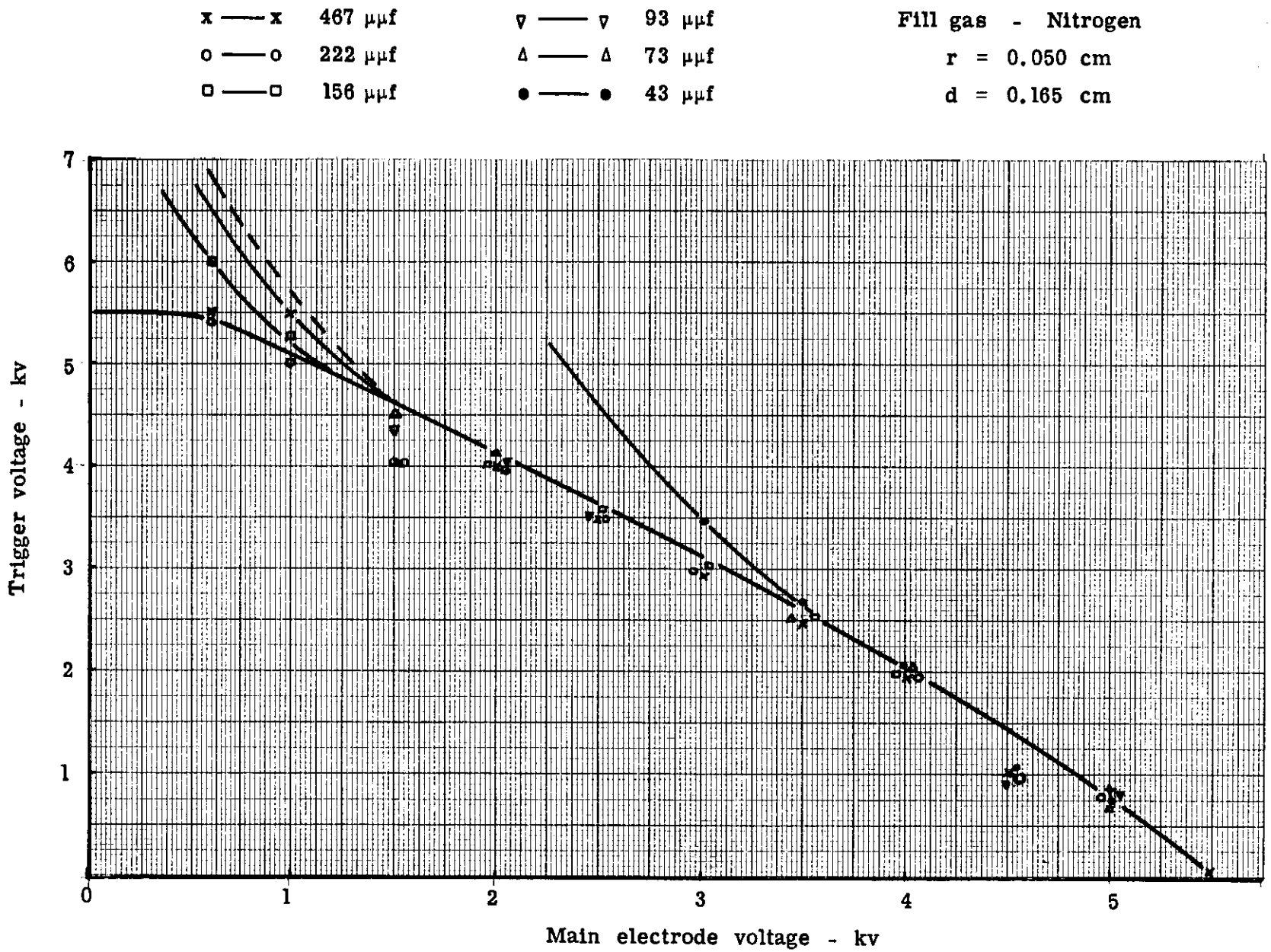

Fig. 94 -- Trigger voltage required for gap breakdown for varying trigger circuit capacity -- for pressure of 600 mm Hg (Mode A)

Mode C curves of Figs. 95 and 96 are for the same gap as Fig. 87, but for different fill pressures. It is clearly seen that as the fill pressure increases the product of the capacity level and the trigger voltage increases. This fact will be discussed in the next section.

Capacity-Voltage Product

From the results obtained in analyzing Modes A and C operation, it is obvious that the triggering operation is dependent upon some relation of the capacity-voltage product. Early data obtained during the analysis of the trigger requirements indicated that the capacity-voltage relation was a function of $1/2\ cv^2$ or energy. At the suggestion of S. Goldberg of EG&G, the input charge (capacity-voltage product) concept was studied in more detail. The input charge relation would agree more favorably with our results on the effect of trigger current flow and the ability to trigger the gap, since charge is related to current by the following expression,

$$cv = \int i dt \ .$$

It is not the input charge itself that controls triggering, but its contribution to the trigger current in conjunction with the impedance in the trigger discharge. For a constant trigger loop impedance, the interchange of capacity level and trigger voltage, in such a way that their product remains constant, results in reliable triggering for the range of combinations investigated. The dependence on input charge has also been reported by Sletten and Lewis[16] whose report was published after this present work was started.

In order to establish this relationship to the capacity-voltage product, the input charge in the region of cutoff for the gaps discussed in the preceding section were calculated. Only those points which were above the static trigger curve were considered. In this manner both the voltage and capacity were variables, and a better estimate of the charge could be made. The capacity-voltage product and the energy relation were tablulated for the different gap voltages, V_g, of the geometries shown in Figs. 84 and 85. In addition, the results of Figs. 88 to 96 were also tabulated in order to show the influence of pressure variation and differences of operating modes. These results are shown in Table VI.

A review of Table VI clearly shows the tendency toward the capacity-voltage product as opposed to the energy relationship. In a few cases, there appears to be a capacity-voltage combination that does not agree closely with other combinations at the same operating point. This discrepancy is believed to be due to differences in the internal impedances of the capacitors used, especially the inductance. This difference would then affect the trigger spark current which is considered to be the controlling influence on successful triggering.

There is also the problem of the current duration as well as the current amplitude and its effect on reliable triggering. If a minimum peak current for a certain minimum duration is required, then extremes of capacity or voltage may require a cv product different from the more nominal values.

Comparing the input charge as a function of the ratio of gap voltage to its static breakdown voltage for the different pressures of Mode A of Figs. 92, 93, and 94 results in the curve of Fig. 97. This curve shows that the normalized operating voltages for different pressures fall on the same curve and are then apparently independent of pressure for a fixed gap spacing. The required input charge is increased as the ratio of gap voltage to static breakdown voltage is decreased. The decrease in input charge is gradual until a ratio of approximately 0.3 is reached. Below a ratio of 0.3, the curve becomes steep requiring larger inputs for small reduction in the gap ratio.

Fill gas - Nitrogen

r = 0.050 cm

d = 0.165 cm

Δ——Δ 73 μμf

∇——∇ 93 μμf

o——o 223 μμf

x——x 467 μμf

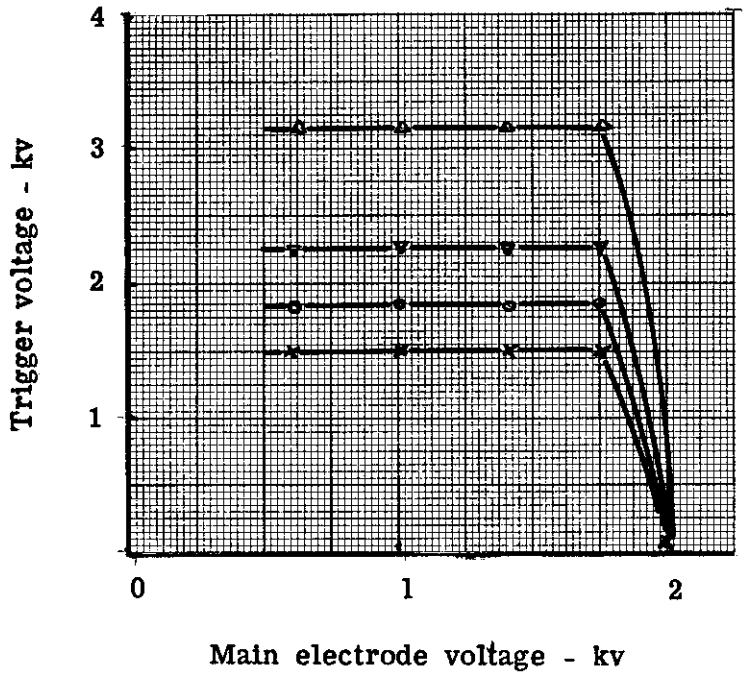

Fig. 95 -- Trigger voltage required for gap breakdown for varying trigger circuit capacity -- for pressure of 100 mm Hg (Mode C)

Fill gas - Nitrogen

r = 0.050 cm

d = 0.165 cm

● —— ● 43 μμf

▲ —— ▲ 73 μμf

Δ —— Δ 93 μμf

o —— o 222 μμf

x —— x 467 μμf

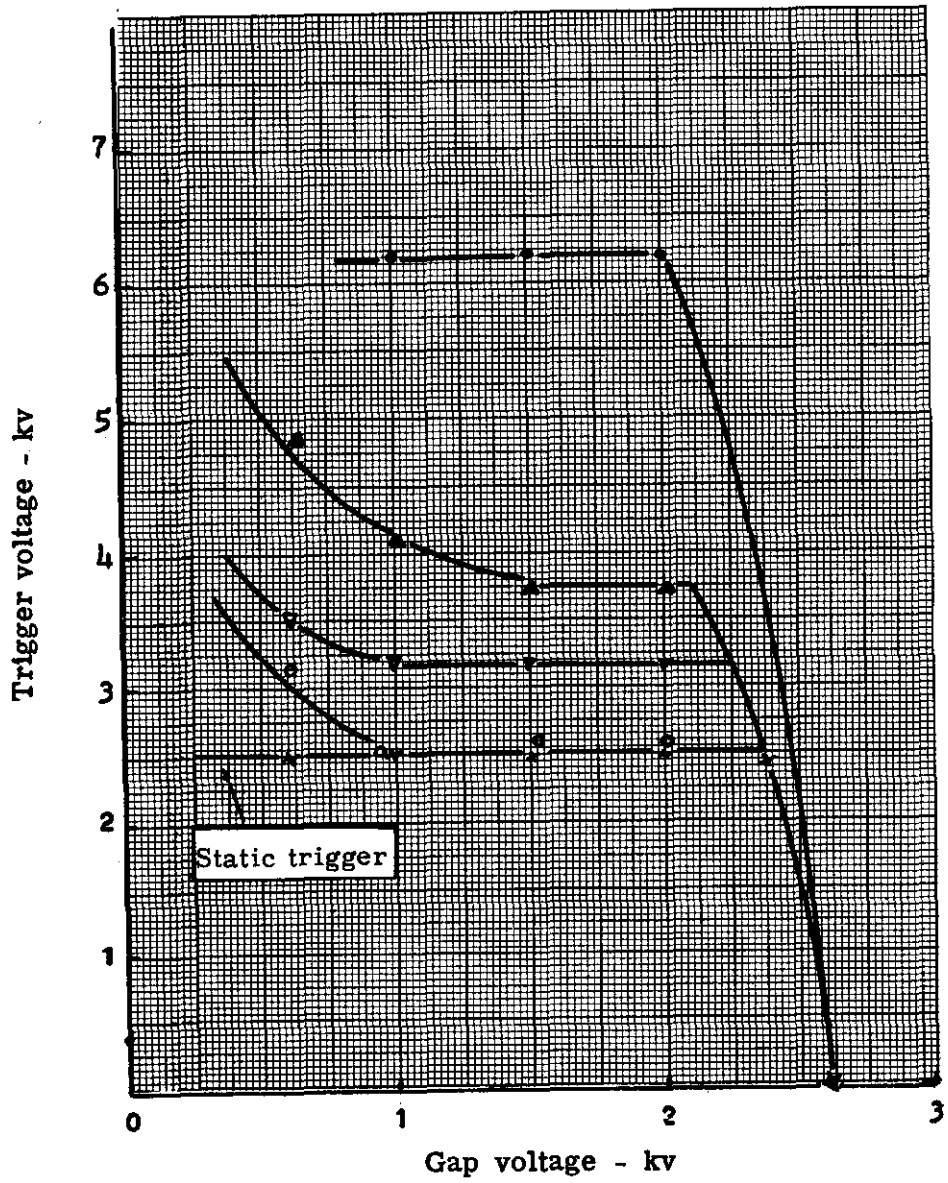

Fig. 96 -- Trigger voltage required for gap breakdown for varying trigger circuit capacity -- for pressure of 200 mm Hg (Mode C)

TABLE VI

Minimum Capacity-Voltage Product Required for Triggering

Data from Figures 87, 92, 93, 94, 95, and 96

Mode A*

		Capacity $\mu\mu$f	Voltage kv	Charge 10^{-9} coulomb	Energy ergs
P = 20 cm Hg	Vg = 600	73	5.25	383	10,100
		93	4.75	441	10,500
		222	2.80	630	8,800
	Vg = 1000	43	4.30	185	3,900
		73	4.10	300	6,100
		93	3.20	298	4,700
	Vg = 1500	43	3.15	136	2,100
		73	2.80	202	2,800
P = 40 cm Hg	Vg = 600	93	5.50	510	14,000
		222	4.70	1050	24,700
		467	3.50	1640	28,700
	Vg = 1000	73	5.20	380	9,800
		93	4.00	370	7,400
		222	3.75	830	15,556
	Vg = 1500	73	4.10	299	6,150
		93	3.25	302	4,907
	Vg = 2000	43	4.00	172	3,440
		73	3.35	245	4,120
		93	2.80	260	3,640
P = 60 cm Hg	Vg = 1000	93	5.50	510	14,025
		156	5.2	820	21,320
P - 10 cm Hg	Vg = 600 and greater	73	3.15	230	3,622
		93	2.25	209	2,340
		222	1.83	406	3,714

TABLE VI (continued)

Data from Figures 87, 92, 93, 94, 95, and 96

		Mode C			
		Capacity $\mu\mu f$	Voltage kv	Charge 10^{-9} coulomb	Energy ergs
P = 20 cm Hg	Vg = 600	73	4.80	350	8,400
		93	3.50	325	5,670
		222	3.15	700	11,025
	Vg = 1000	43	6.20	266	8,246
		73	4.10	300	6,150
		93	3.20	298	4,768
	Vg = 1500 and greater	43	6.20	266	8,246
		73	3.70	270	4,995
		93	3.20	297	4,736
P = 40 cm	Vg = 600	222	8.10	1800	72,900
		467	4.50	2110	47,475
	Vg = 1000 and greater	93	7.00	650	22,750
		156	3.50	546	9,550
		222	3.25	722	11,732

Data from Figure 85

		Mode A			
	Vg = 1500	48	4.25	204	4,335
		81	3.30	268	4,422
	Vg = 2000	32	4.50	144	3,240
		48	2.50	120	1,500

Data from Figure 84

		Mode A			
	Vg = 1000	127	3.28	414	6,789
		167	3.15	525	8,284
	Vg = 2000	39	3.50	136	2,380
		64	2.90	185.5	2,697

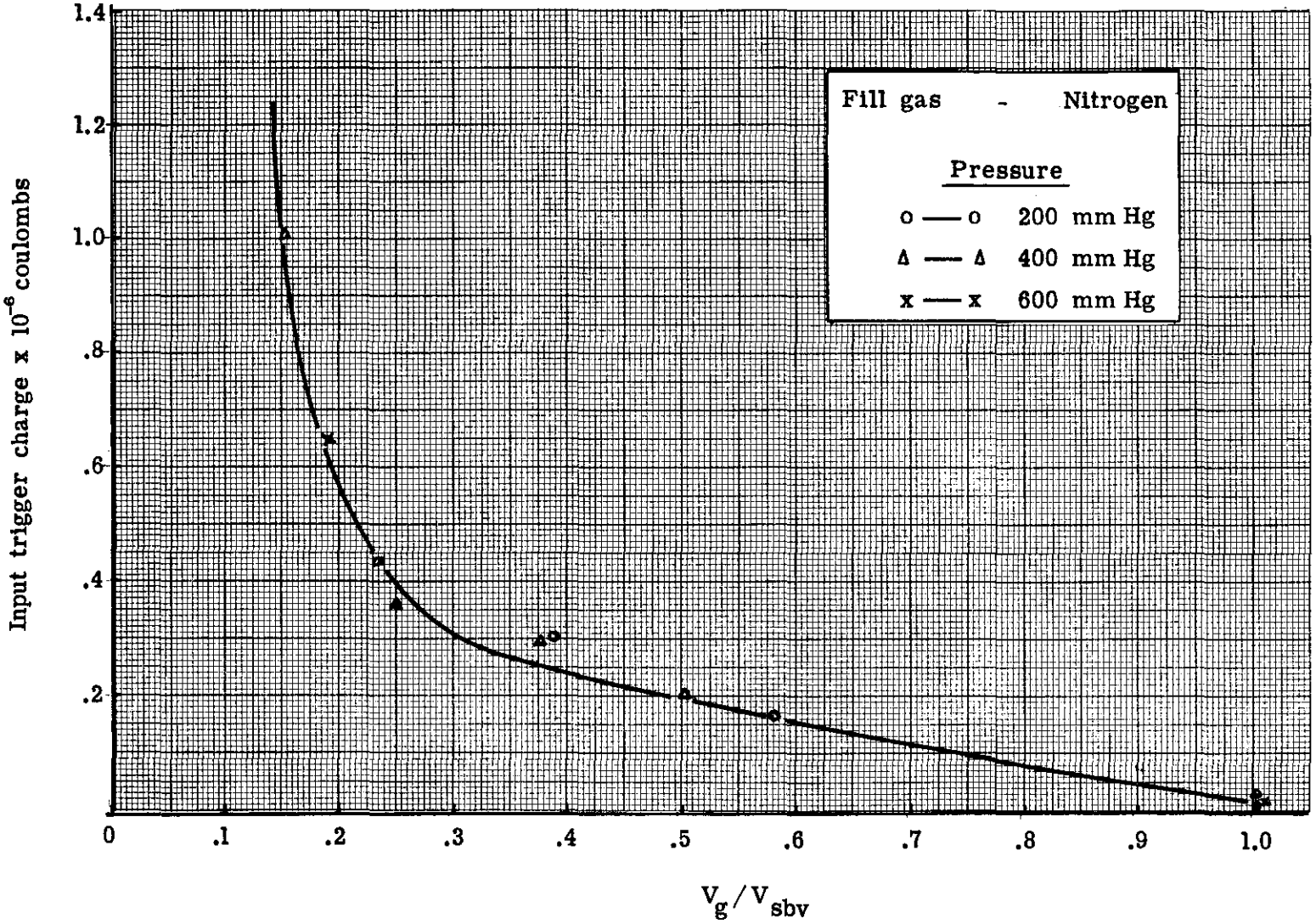

Fig. 97 -- Input charge required for reliable triggering -- Mode A operation

The normalized curve for Mode C is shown in Fig. 98. For Mode C the required input charge appears to be a function of pressure and, above cutoff, to be independent of the ratio of gap voltage to static breakdown voltage. As the pressure increases, the required input charge increases.

The static breakdown values for the various pressures were tablulated and the resultant static breakdown gradients were obtained. Each gradient was then divided by the corresponding pressure and α/p for each value of E/p was obtained from a curve similar to Fig. 18. In this manner, the α ionization coefficient for each pressure was obtained. The results of this analysis are shown in Table VII.

TABLE VII

Evaluation of the α Coefficient at Breakdown for Various Pressures for a Fixed Gap Geometry

Pressure mm Hg	V_{sbv} volts	E volts/cm	E/p volt/cm mm Hg	α/p ion pairs/cm mm Hg	α ion pairs/cm
200	2600	15,800	79.	0.32	64
300	3300	20,200	67.	0.21	63
400	4000	24,200	60.5	0.15	60
500	4700	28,500	57.0	0.12	60
600	5400	32,600	54.5	0.10	60

The results of this table show that the variation of pressure and the change in breakdown voltage for a fixed geometry system still result in an α of approximately 60. This is to be expected, since the discussion in Chapter II indicated that for a fixed geometry system, especially d being constant, that the product αd should equal a constant. If the product αd is a constant, then α must necessarily be a constant. The fact that $\alpha d = 10$ is approximately one half of the value for a uniform field ($\alpha d = 20$) is due to the nonuniform field of the geometry used in this experiment, consequently giving it an effective higher gradient than the applied voltage would suggest. If the α for a uniform field with a fixed spacing were calculated as before, the same constant value of α would be maintained for the different variations of pressures. The product αd would then equal 20. This is exactly the results obtained in calculating the breakdown curve of Fig. 39. For the various pressures at a fixed gap spacing, the value of α was 72. The product αd then equaled (72)(.279) = 20.

As mentioned before, the input charge required for reliable triggering was fairly low, down to an operating ratio of 0.3. Below this ratio the required input charge increased rather rapidly. If we now select an operating ratio of 0.3 for each pressure, we obtain the results shown in Table VIII. The values of E/p for such low values are not readily available in the literature and, therefore, are extrapolated values giving only an approximate value.

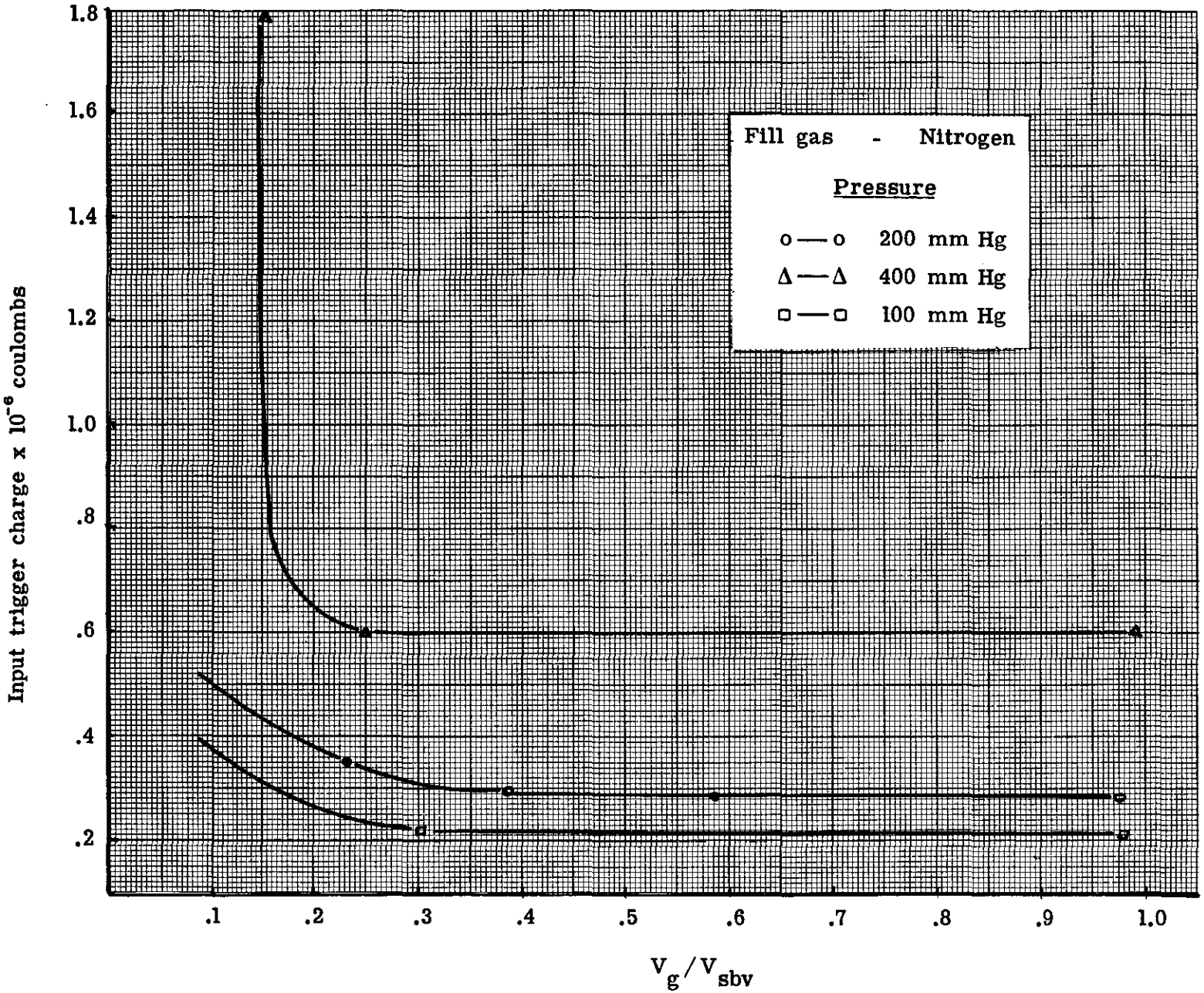

Fig. 98 -- Input charge required for reliable triggering -- Mode C operation

TABLE VIII

Evaluation of the α Coefficient at an Operating Ratio of 0.3 for Various Pressures for a Fixed Gap Geometry for Mode A Operation

Pressure mm Hg	V_g volts	E' volts/cm	E'/p volts/cm mm Hg	α'/p ion pairs/cm mm Hg	α' ion pairs/cm
200	780	4730	23.6	2.4×10^{-4}	4.8×10^{-2}
300	990	6000	20.0	8.7×10^{-5}	2.6×10^{-2}
400	1200	7300	18.2	4.8×10^{-5}	1.9×10^{-2}
500	1410	8550	17.0	3.2×10^{-5}	1.6×10^{-2}
600	1620	9820	16.2	2.5×10^{-5}	1.5×10^{-2}

From Table VIII, the values of α' then for a low operating ratio are all of the same order of magnitude, clearly showing that the ability to trigger is a function of the ratio α'/α for any given pressure in a fixed geometry. The results of Mode C at this point are not completely clear, indicating a more complex mechanism is operating.

Delay Time

After actuating S_1 of our equivalent circuit of Fig. 15 (page 11), we are next concerned with the parameters affecting the closure of S_2. As mentioned in the opening sections, the delay time is defined as the time from the start of the trigger spark current flow to the time of the main gap current flow. This time delay is in addition to any delay of the applied pulse in reaching the desired pulse breakdown value. If the total time delay for triggering is required to be low, then a fast rising pulse must be applied to the probe to reduce the probe breakdown time.

The main delay time (trigger current to main current) and pulse breakdown time are clearly shown in Figs. 99A and B. Figure 99A shows the delay time for Mode A operation of a typical gap. It shows the voltage to the probe, and the resultant collapse of the voltage at the point of breakdown. The probe potential has gone below the reference potential of the trigger electrode to the applied potential of 1300 volts of the main electrode, indicating that the trigger spark has formed to the main electrode. The traces were taken with two Tektronix 535 scopes, recording both the probe voltage and current flow simultaneously. In later experiments, a Tektronix Dual Beam, Model 551, scope was employed, thereby combining these traces into a single photograph per operation. A review of the current pulses shows the smaller trigger spark current followed by a considerable delay, and finally the larger main current flow. The average delay time for this gap is about 5 μsec with considerable delay time variation or jitter. Figure 99B shows the voltage and current for the same gap, but operated in Mode C. From these traces, we see that the trigger spark has formed to the trigger electrode, since the probe voltage has returned to the same voltage as the reference voltage of the trigger electrode. When

Probe No. 1

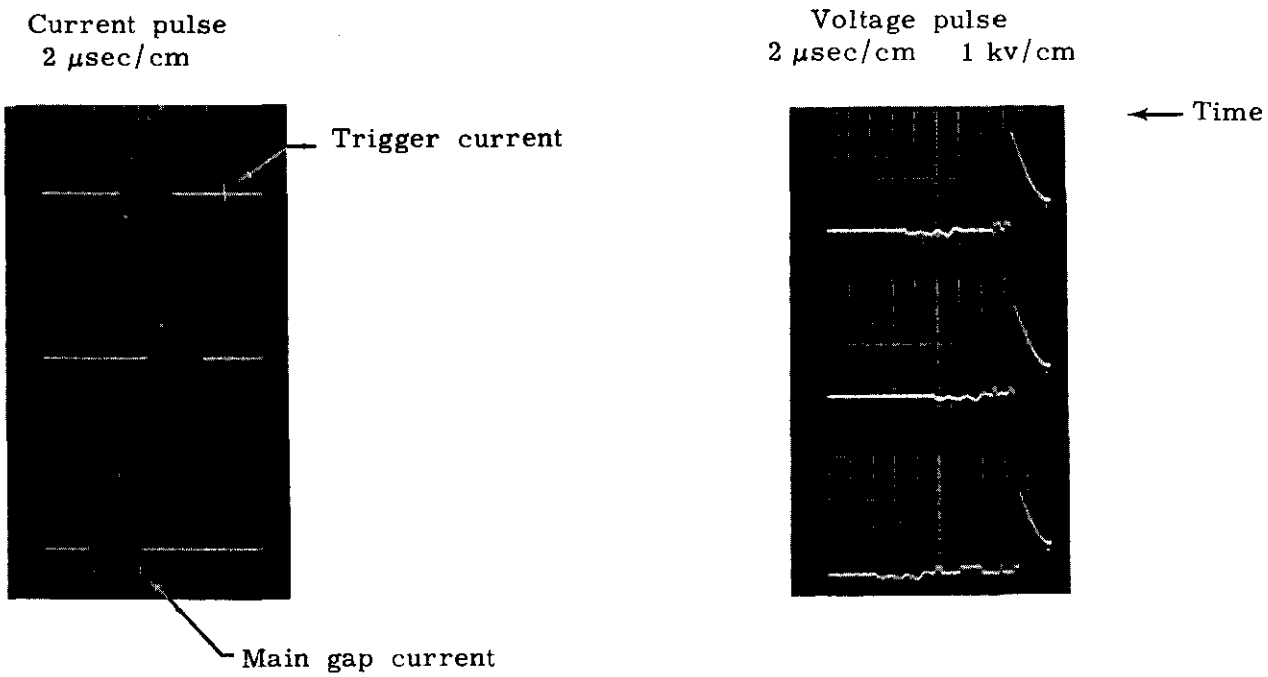

Probe No. 2

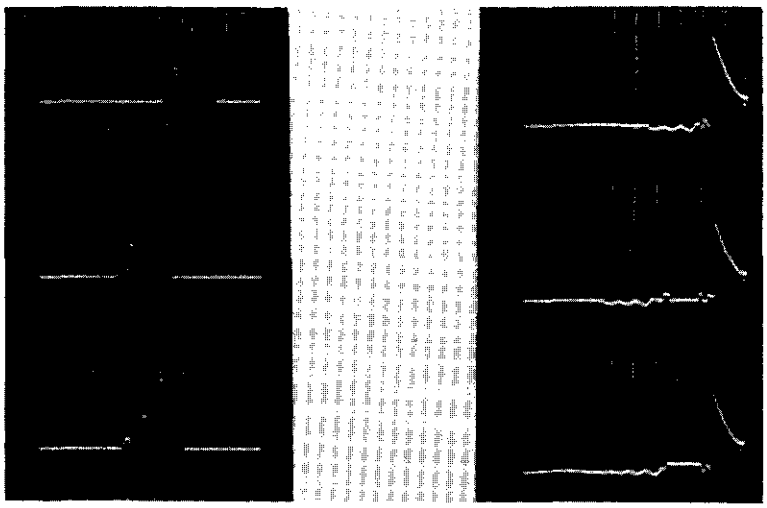

Fig. 99A -- Probe breakdown and delay time

Probe No. 1

Current pulse
2 μsec/cm

Trigger current

Voltage pulse
2 μsec/cm 1 kv/cm

Time

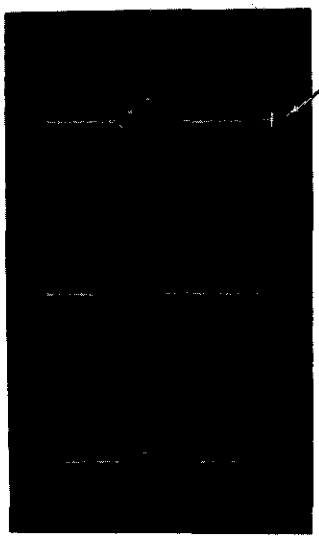

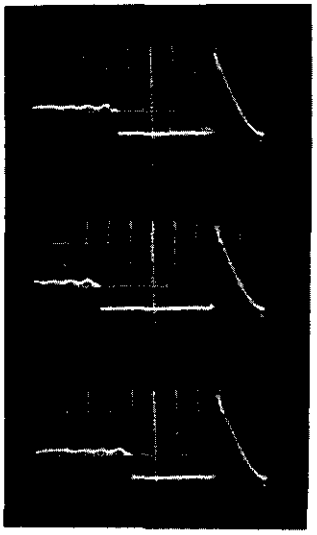

Probe No. 2

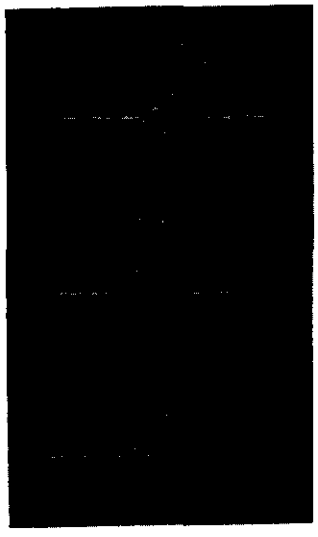

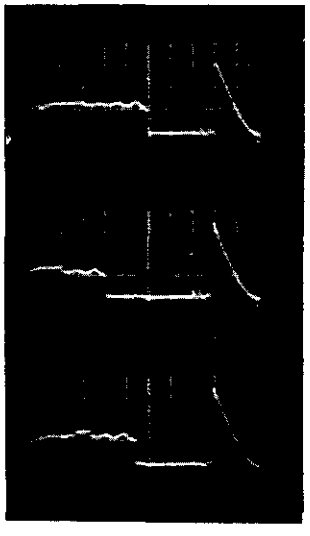

Fig. 99B -- Probe breakdown and delay time

the main gap breakdown occurs, both the probe and the trigger electrode suddenly rise to the applied potential of the main electrode (the trigger electrode was referenced at a negative high voltage while the main electrode was at ground potential).

This delay time for a fixed gap geometry and fill pressure is dependent upon the operating mode (polarity), applied gap voltage, and trigger input. Figure 100 is a good example of a typical delay curve for Mode C as a function of main gap voltage. As the main gap voltage increases the delay time decreases and also the jitter decreases. When the delay time becomes appreciable, the delay time approaches infinity asymptotically to the cutoff voltage of the gap. The cutoff voltage for the gap of Fig. 100 in Mode C operation is about 1200 volts for a fixed trigger input. If higher and higher applied gap voltages are used, delay times as low as 0.05 μsec or less can be achieved.

Figure 101 shows Mode C where values of shunt capacitance of 100 and 150 $\mu\mu$f were added to the output terminals of the transformer. This adds to the existing transformer distributed capacity, wiring capacity, and input capacity of the probe, and is the source that is immediately available in the trigger spark when the trigger discharges. The addition of lumped shunt capacitance to the output of the transformer, if appreciable, will of course load the transformer, and the output rise time of the probe now becomes slower. As shown earlier, the slower the rise time, the lower the breakdown voltage. Consequently, the amount of capacitance added should be such that the capacity level increases with no appreciable reduction of the probe breakdown voltage. Figure 101 shows that with increased capacity, the delay time is reduced considerably. Mode D (not shown) with increased capacity responds even more readily, dropping from 70 to 2-1/2 μsec delay time at 1500-volt gap voltage and 0.6 μsec delay at 2000-volt gap voltage.

In general, the effect of the operating mode or polarity is to control the minimum cutoff voltage of the gap. For a given gap with a relatively small gap spacing, the order of lowest cutoff is Modes A, C, B, and D, where Mode A has the lowest cutoff voltage and Mode D has the highest cutoff voltage. With regard to delay time, Modes C and D can have very long delay times near the region of cutoff, while Modes A and B usually have very short delay times. Some of these factors will be studied in more detail in the next chapter under Geometry and Other Design Factors.

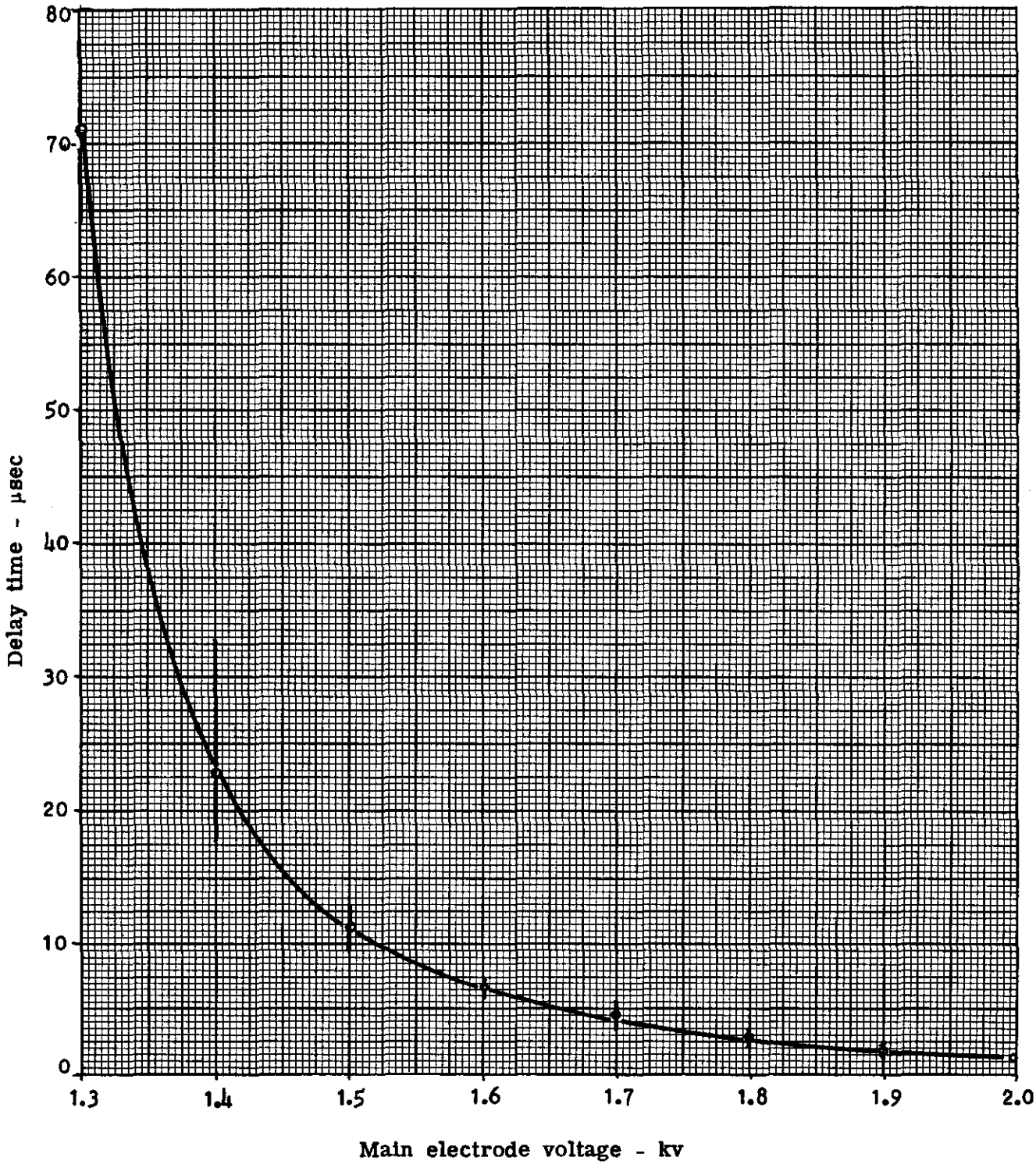

Fig. 100 -- Typical delay time curve for Mode C -- 0.5 μsec rise time pulse

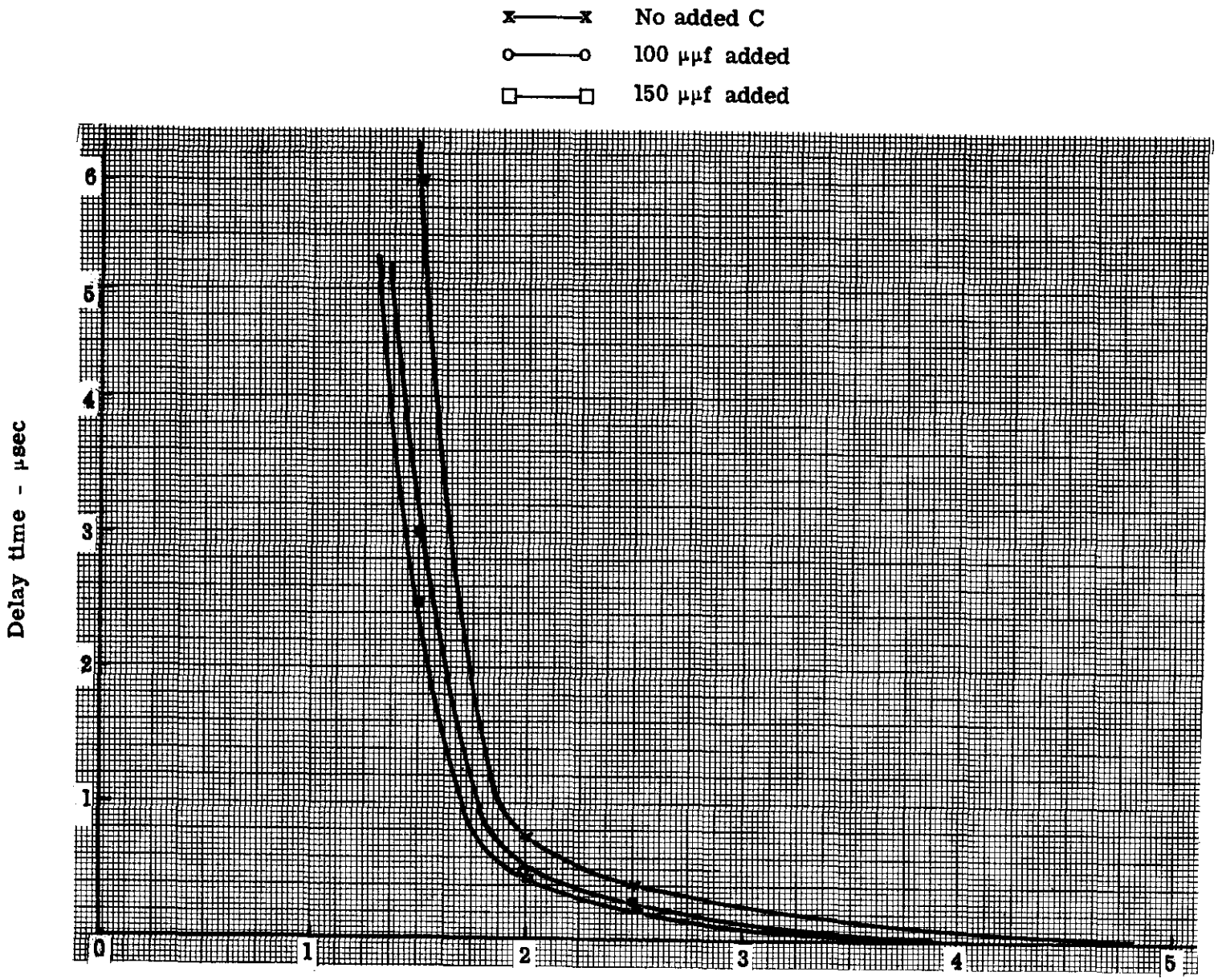

Fig. 101 -- Mode C Delay time for variations of transformer capacity

CH IV -- GEOMETRY AND OTHER DESIGN FACTORS

Up until the present development we have primarily considered only the triggering effects for a fixed gap geometry. In order to adequately design a triggered spark gap, we must also understand the influence of the geometry design factors such as the main gap spacing and the probe assembly configuration and their effect on the required trigger spark and the resultant delay time. Some of the observed effects of these factors will be discussed.

Spark Paths

In this study a typical probe geometry with a probe radius, r, of 0.046 cm and with a trigger hole radius, R, varying from 0.076 to 0.178 cm was employed. The radius of curvature of the main electrode and the trigger electrode was 0.475 cm. The gap assembly was mounted in a bell jar employing suitable supports. The gap spacing was controlled externally to the bell jar by use of a micrometer arrangement mounted on the main electrode and passing through the base plate of the bell jar through a bellows brazed to the base plate and to the micrometer mounting. The gas used was commercial dry nitrogen. The probe was inserted into the trigger electrode with an Alumina ceramic insulator surrounding the probe. The bond at the probe and at the trigger electrode was not continuous, providing a small void at each of these electrodes. The trigger source was a typical pulse transformer charging a 50 $\mu\mu$f capacitor connected to the probe through a 47 K ohm resistor. The open-circuit pulse voltage was approximately 5 kv with a rate of rise of 200 volts/μsec. The use of the relatively slow rate of rise of the pulse and the RC charging circuit was to provide as constant a triggering source as possible. The pulse transformer provides the voltage to the probe, the capacitor coupled with the probe provides the available charge that supplies the trigger spark, and the resistor limits the amount of primary current that can flow through the trigger spark once it has formed. This circuit is shown below in Fig. 102.

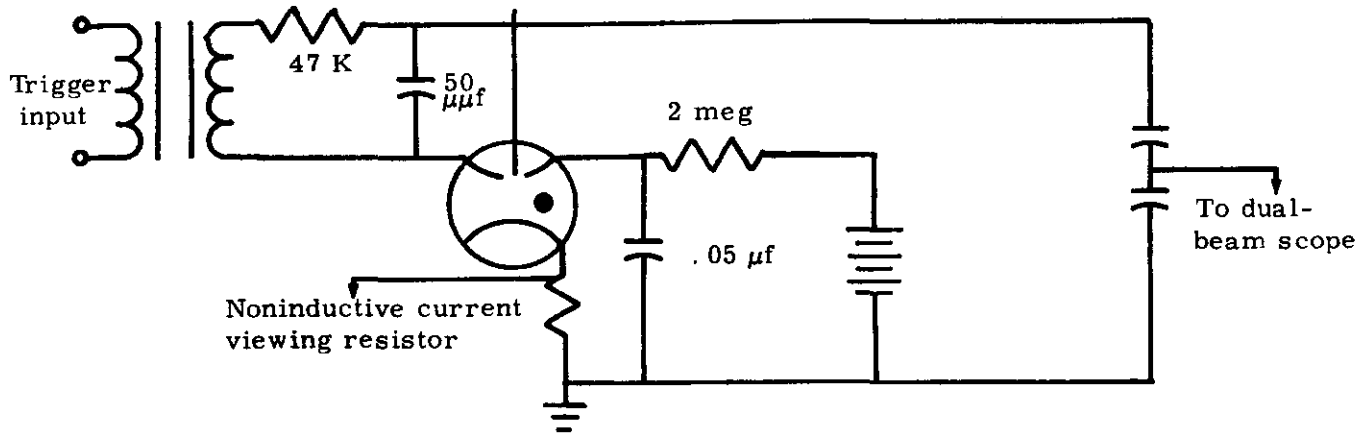

Fig. 102 -- Test circuit for obtaining cutoff and delay time characteristics

A current viewing resistor between the main electrode and ground and a capacity divider on the probe provided the means of observing delay time, probe breakdown voltage, and direction of the trigger spark whether it formed to the trigger electrode or to the main electrode. Typical waveforms were similar to those of Fig. 99B.

Prior to the dynamic triggering curves the static breakdown voltages were observed along with the path of the main gap breakdown. The gap capacitor was made small (.05 μf) in order to more clearly view the discharge path by limiting the light intensity of the spark. Observations on the spark path of the main gap static breakdown showed that the main gap would breakdown along a path forming an L-shaped path connecting the trigger electrode and main electrode via the trigger probe. This was especially true for the geometries having the larger hole radius, R . If R is made small compared to the gap spacing, d , the spark path may then be between the trigger electrode and main electrode directly. The impedance of the trigger circuit also influences the spark path as shown in Fig. 103.

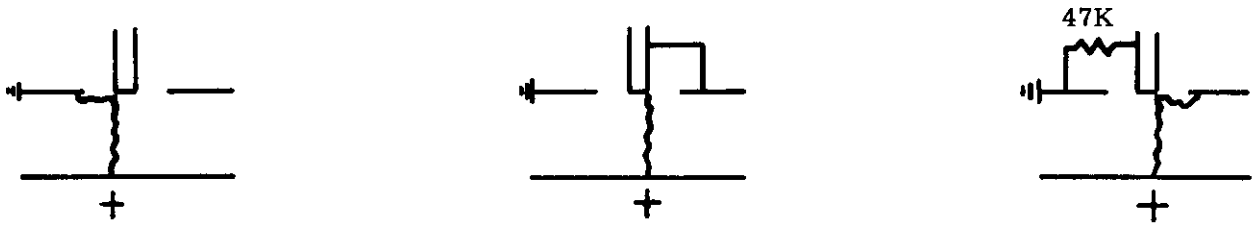

Fig. 103 -- Spark path at main gap breakdown

If the probe is left floating, it evidently assumes a potential by divider action and charge accumulation such that the field at the probe is intensified causing the breakdown to occur between the probe and main electrode. However, the floating probe is in reality a very high impedance, limiting the spark current that can flow, and the probe thereby assumes the potential of the main electrode less any drop in the spark, with the result that the probe then breaks down to the trigger electrode and the capacitor discharges along the low impedance path of main electrode to probe to trigger electrode. If the probe is then shorted directly to the trigger electrode, the spark again forms to the probe and, since there is now an external low impedance, the capacitor discharges completely through the probe. If a large resistor, 47 K, is now connected between the probe and the trigger electrode, the spark path again forms an L shape. If the capacitor being switched is large with a high applied voltage the discharge is blurred, but appears to form directly between main electrodes indicating that with a large discharge the L spark channel quickly expands and moves between the main electrodes forming the hypotenuse of the original discharge. It may also be that a new discharge is formed between the main electrode due to the irradiation of the initial L-shaped discharge. Extending this analysis to the static trigger tests discussed earlier, the similar L-shaped discharge occurs along with some additional shapes as shown in Fig. 104. The discharge path does not always remain the same, changing as a function of gap spacing and gap voltage, and trigger electrode geometry.

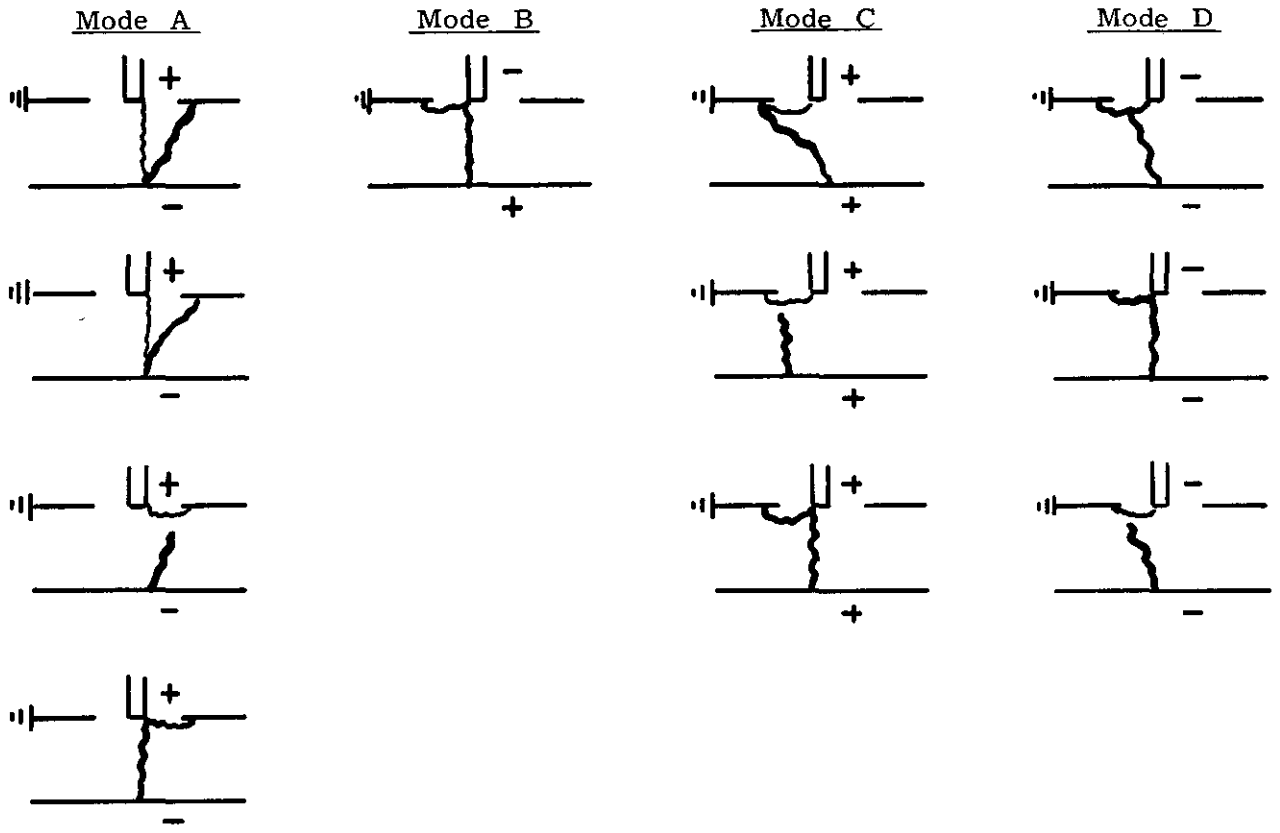

Fig. 104 -- Spark paths for static triggering for various operating modes

Mode A -- In Mode A, four distinct types of discharges can be observed depending on the operating conditions: (1) when the static trigger spark forms to the main electrode, the main spark forms from the cathode spot of the trigger spark to the trigger electrode thereby employing a common cathode spot for both discharges, (2) same as the preceding path, but where the main gap spark forms up the trigger spark channel a short distance then branches off on an independent path to the trigger electrode, (3) when the trigger spark forms to the trigger electrode, the main gap spark forms to the probe and then along the conducting path of the trigger spark, (4) same path as (3), except there appears to be a dark space near the probe side of the main spark and it forms toward the center or lowest point of the trigger spark which "bends" into the main gap spacing. This "bending" of the trigger spark into the main gap spacing occurs in most probe assembly geometries and appears to be one of the factors of the triggering mechanism. The amount of penetration into the main gap spacing increases as the trigger electrode hole radius, R , increases. It also appears to increase as the trigger spark input increases.

Mode B -- Mode B appears to have only one basic discharge path. Regardless of whether the trigger spark forms to the main electrode or to the trigger electrode, the main spark forms to the probe from the other electrode and then along the trigger spark path forming an L-shaped discharge.

Mode C -- Mode C has three basic discharge paths. In Mode C operation, the trigger spark always forms to the trigger electrode since the main gap field is a repelling field. The most repeatable and observed main spark path is from the cathode spot of the trigger spark on the trigger electrode directly to the main electrode. The other two variations occur along the trigger spark (with a dark space at the trigger spark) or at the probe.

Mode D -- Mode D also always has its trigger spark form to the trigger electrode since it has a repelling main gap field. The main gap spark then forms to the probe or to the trigger spark with or without a dark space in the main gap discharge.

The spark paths for dynamic triggering were studied next and are shown in Fig. 105.

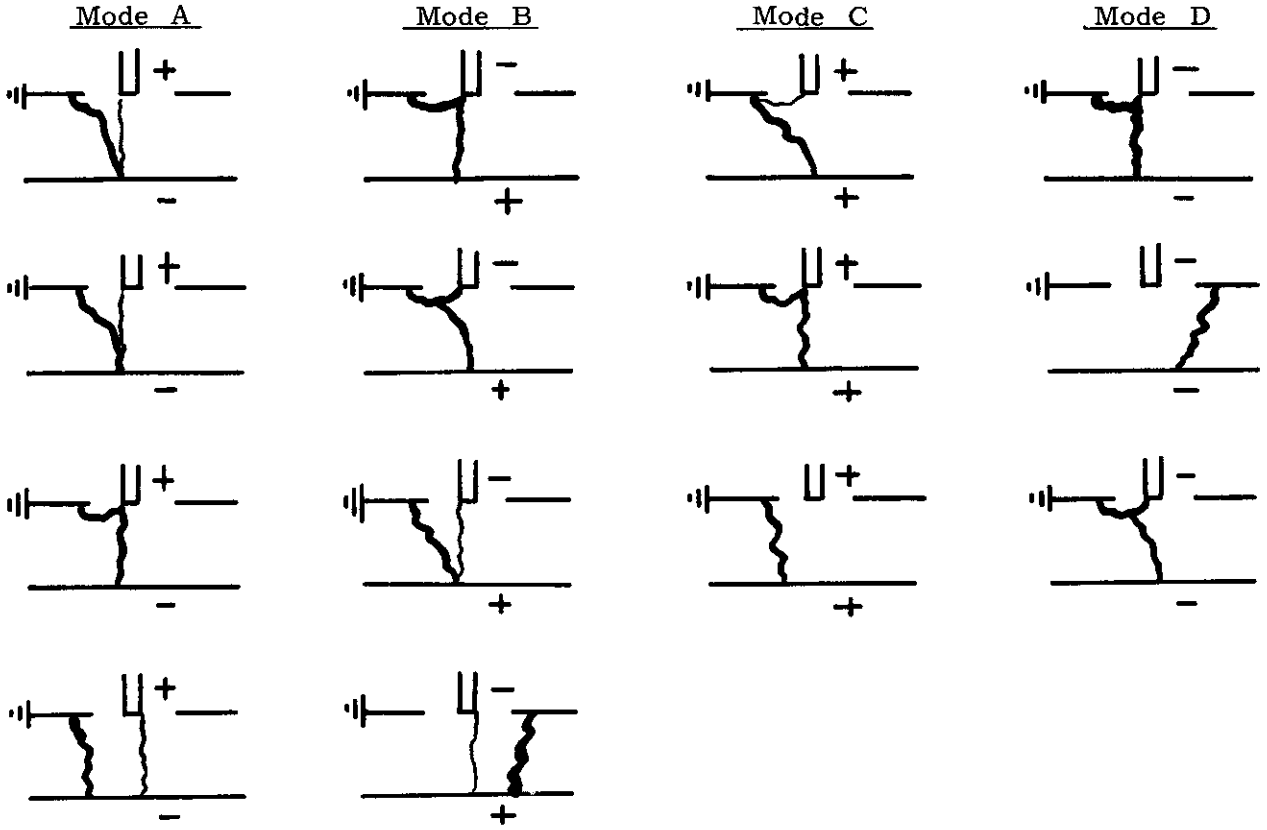

Fig. 105 -- Spark paths for dynamic triggering for various operating modes

The discharge paths of the dynamic triggering are essentially the same as for the static triggering except for the addition of a new path when the gap voltage, V_g, is well above the cutoff voltage, V_ℓ, and relatively close to static breakdown voltage, V_{sbv}. For Modes A and B, the main gap discharge occurs directly between the trigger electrode and main electrode immediately after or during the formation of the trigger spark evidently due to the intense irradiation of the main gap from the trigger spark. While in Modes C and D no trigger spark was observed by eye, but scope traces indicated that trigger current, probably corona current, flowed causing irradiation of the main gap and initiating main gap breakdown. At lower gap voltages close to the cutoff voltage, only Modes A and B still showed this pattern of the independent trigger spark and main gap spark. In addition, the delay times while small are measurable, which indicates a trigger mechanism based on the time dependence of the trigger spark and the resultant ionization products moving toward the region of the main gap. This pattern at low gap voltage was more prevalent when the trigger hole radius, R, was relatively large.

Studying Mode A in closer detail, the following discharge paths were observed as shown in Fig. 106:

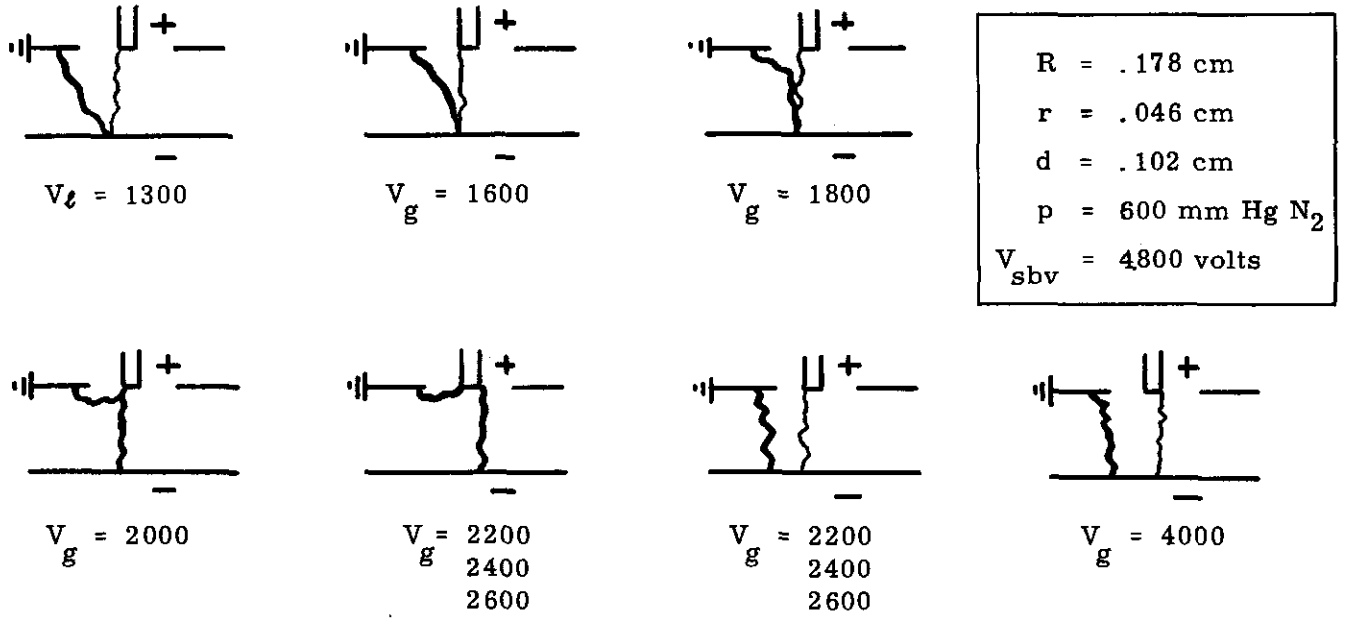

Fig. 106 -- Dynamic spark paths as a function of gap voltage for Mode A

For V_g of 1300 to 1800 volts, the trigger mechanism appears to depend on utilizing a common cathode spot for both the trigger spark and the main spark. For voltages of 2000 volts, the trigger mechanism is the result of the probe breaking down to the main electrode thereby placing the probe at main electrode potential less arc drop. This now places a voltage between the probe and the trigger electrode in excess of its static breakdown value which immediately breaks down, and the main discharge goes along the conducting paths from main electrode to probe to trigger electrode. Between gap voltages of 2200 to 2600, there are two possible modes that occur with equal frequency, the one just mentioned, or the one where the main spark goes from the trigger electrode to the main electrode directly. At higher gap voltages the direct path prevails.

Small Trigger Electrode Hole

In order to study the effects of probe geometry one trigger electrode with a small hole, R = .076, and one with a large hole, R = .178, were studied. Both geometries contained the same size probe, however; r = .046 cm. The probe geometry employing a small trigger electrode hole was chosen in order to always control the trigger spark to the trigger electrode even for small gap spacings.

With this geometry, the cutoff voltage, V_ℓ , for each mode of operation was determined for varying gap spacings and varying fill pressures. For each cutoff determination, the gap voltage was gradually increased until five successful triggerings were obtained out of five attempts. Successful triggerings could be obtained at gap voltages lower than cutoff, but the probability of triggering would be less than 100 percent and would follow a curve similar to that of Fig. 80. Modes B and C (positive main electrode) appeared to be the more consistent and repeatable in their cutoff voltages than were Modes A and D (negative main electrode).

The cutoff tests were conducted by employing a fixed gap spacing and then varying the fill pressure, or by setting a fixed fill pressure and then varying the gap spacing, or by varying both spacing and pressure while maintaining a constant static breakdown voltage. These cutoff determinations were made by a number of trials at many spacing and pressure combinations in order to establish the repeatibility of these cutoff points. The resulting data could be presented in a number of ways, but the most meaningful and convenient method is to plot cutoff as a function of the product of gap spacing and pressure and to compare it to the plot of the natural breakdown voltage which is also a function of pd. Figure 107 depicts such a plot.

Figure 107 shows that Mode B has the lowest cutoff voltage followed closely by Mode C, with Modes A and D the highest. Modes A and D are essentially the same. The significance of this curve shows that the minimum gap operating voltage or cutoff for any given mode is a function of the product of gap spacing and fill pressure as is the conventional static breakdown curve. Also, it shows that when the trigger spark forms to the trigger electrode, the cutoff voltage is lowest when the main electrode is positive (Modes B and C), and highest when the main electrode is negative (Modes A and D). If we plot these same cutoff curves as a percentage of the static breakdown voltage or ratio of cutoff voltage to static breakdown voltage, we obtain the curve of Fig. 108. This curve shows that for increasing pd products the cutoff ratio for all modes increases. At the higher pd values the cutoff ratio for Modes A and D begins to approach a constant value.

It should be pointed out that the cutoff voltage as a function of pd product only holds for a uniform field as does the typical Paschen breakdown. If the gap spacing is enlarged in relation to the radius of curvature of the main electrodes or to the probe hole in the trigger electrode, the generated field becomes nonuniform, and the interchange of gap spacing and fill pressure so that their product remains constant does not result in a constant cutoff voltage. For the case presently under discussion, the cutoff voltage increases slightly (about 200 volts) as the gap spacing is increased from 0.152 to 0.254 cm while holding the pd product constant.

In addition to the cutoff voltage of the gap, the time delay for the different operating modes as a function of the applied voltage, gap spacing, and fill pressure, is also of importance. A typical delay time curve taken for a fixed gap spacing and fill pressure as a function of gap voltage is shown in Fig. 109. The delay time is seen to increase exponentially with decreasing gap voltage. The delay time approaches infinity asymptotically to the gap cutoff voltage and is a good indication of when the cutoff voltage is near. In all modes near the cutoff voltage, the trigger spark was forming to the trigger electrode (as observed on a Tektronix 551 Dual Beam Scope) with long delay times of approximately 70 to 120 μsec. The delay times shown are averages taken from photographs of scope traces of several trials at each gap voltage. As mentioned earlier, the delay time variation or jitter decreases with increasing gap voltages. For the case of Mode A when the voltage becomes high enough, there is a transition region of gap voltages whereby the trigger spark could form to the main electrode as well as to the trigger electrode. In either case the main gap fired. However when the trigger spark formed to the main electrode, the delay time was very short < 0.2 μsec. As the main gap voltage was increased further, the delay time for the case of the trigger spark forming to the trigger electrode continued to decrease in the normal manner. When the gap voltage is sufficiently high, the trigger spark always forms to the main electrode and the delay time is very short.

As the gap spacing is increased, holding the pressure constant, the gap voltage required to give a constant delay time, say of 50 μsec, increases in about the same manner as does the cutoff voltage for an increasing pd product, since the cutoff voltage and delay time near cutoff are related when the trigger spark forms to the trigger electrode. Shown in Fig. 110 is the typical delay time curve of Mode C plotted on semilog paper as a function of gap voltage for variations of gap spacings at a constant fill pressure of 600 mm Hg of Nitrogen.

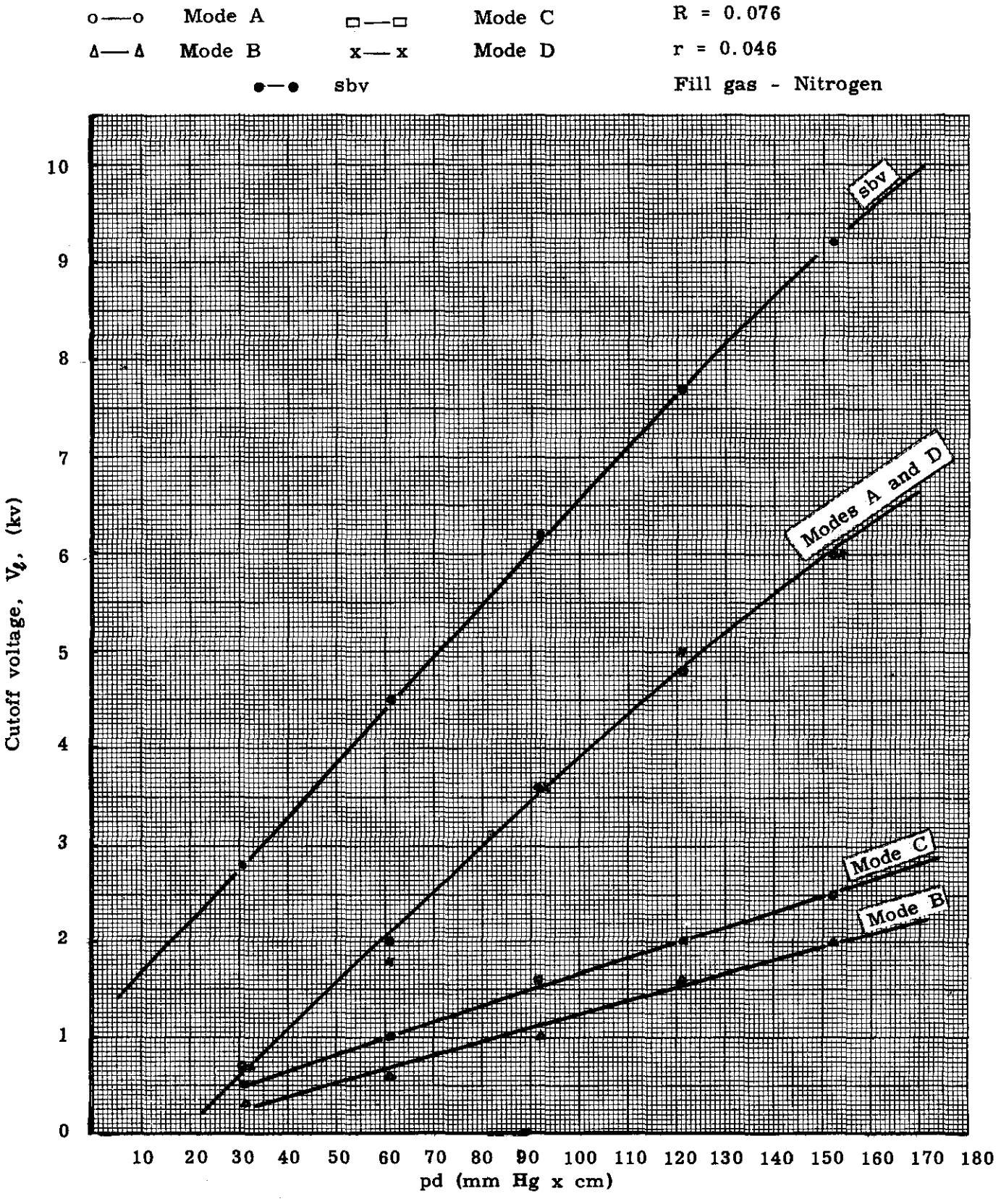

Fig. 107 -- Cutoff voltage as a function of pd product for large trigger electrode hole

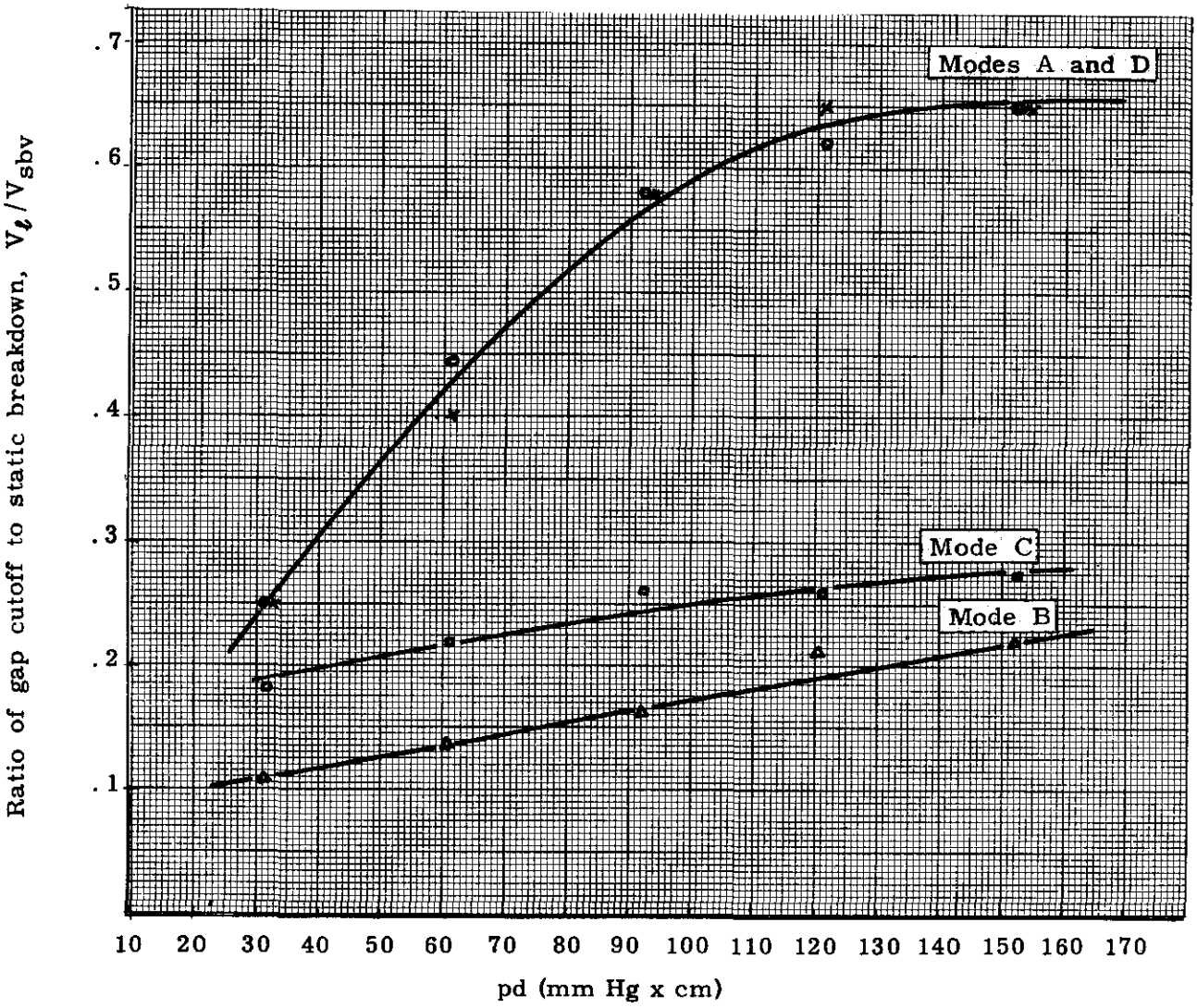

Fig. 108 -- Gap cutoff ratio, V_ℓ / V_{sbv}, as a function of pd product

d = 0.203 cm r = 0.050 cm p = 600 mm Hg

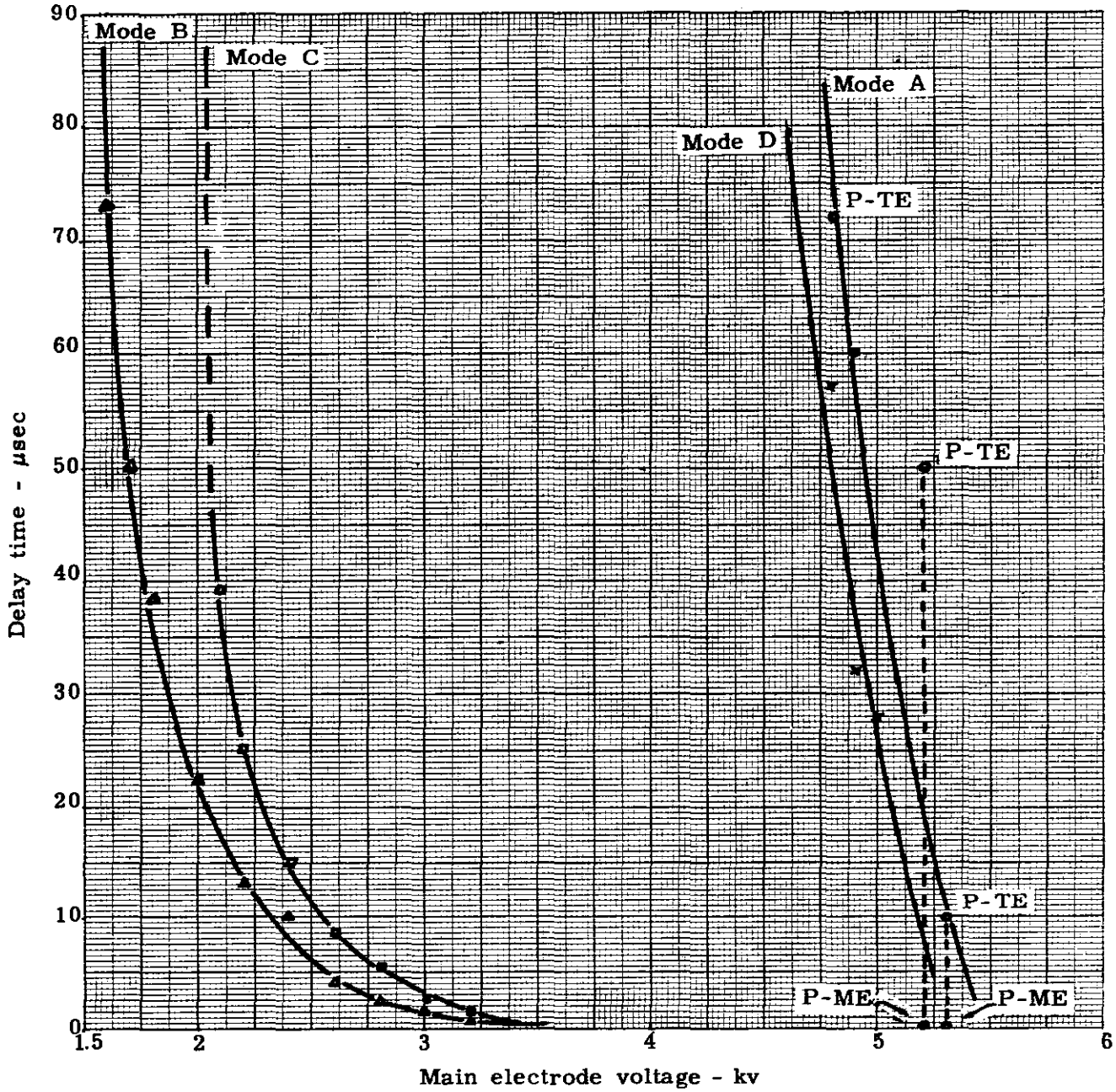

Fig. 109 -- Typical delay time curves in nitrogen for various operating modes for R = 0.076 cm

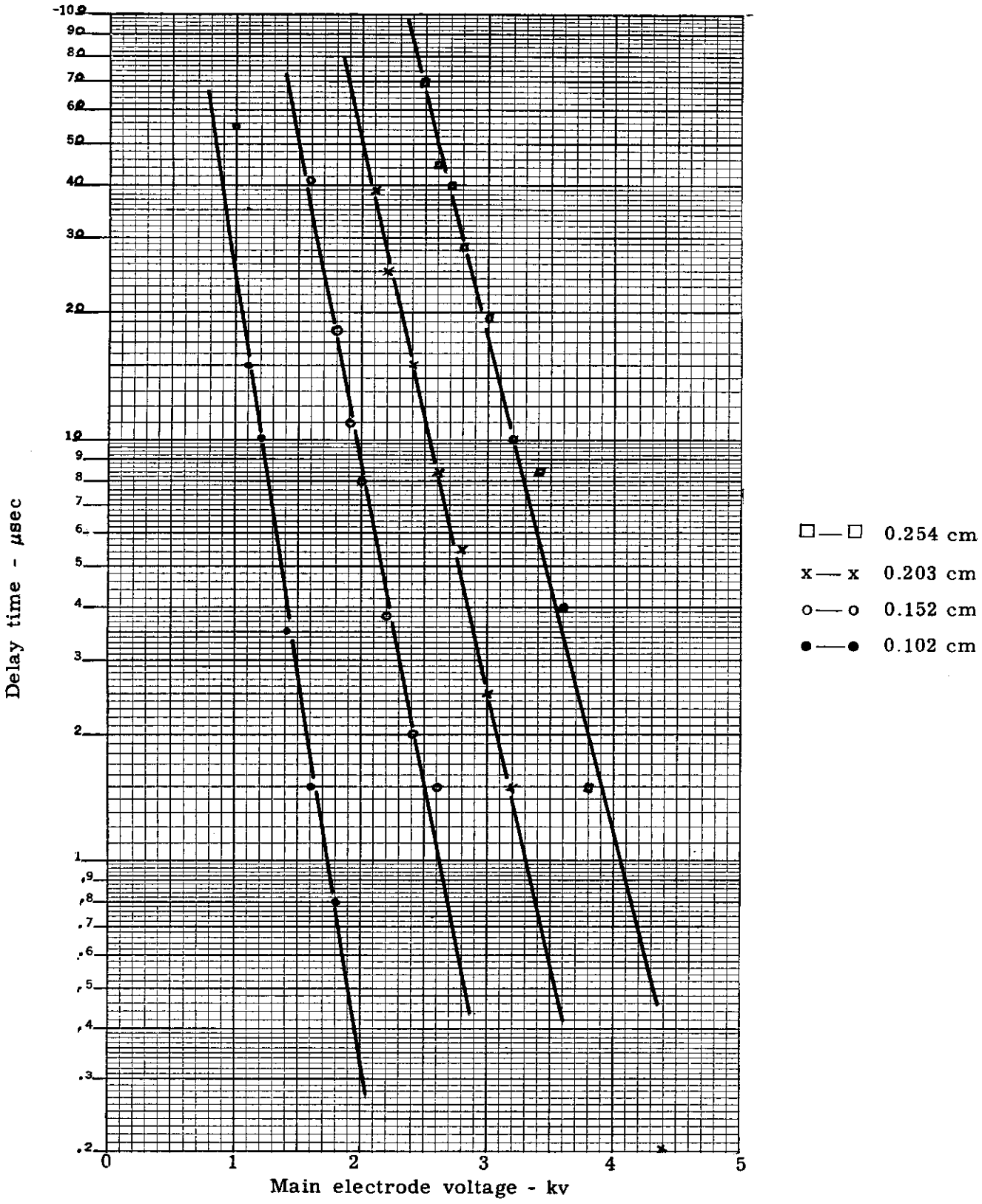

Fig. 110 -- Mode C delay time for various gap spacings at a pressure of 600 mm Hg of nitrogen (R = 0.076 cm)

If the delay curve of Fig. 110 is now normalized as a function of the gap operating ratio,

$$\frac{V_g}{V_{sbv}} ,$$

the curve of Fig. 111 is obtained.

This normalized curve of delay time as a function of

$$\frac{V_g}{V_{sbv}}$$

for different gap spacings shows good correlation, and also shows that the delay time of different gaps may be made approximately the same by operating them at the same operating ratio. There is, however, a tendency for the delay time to be slightly higher when the gap spacing is made large. Here again the nonuniform field becomes of importance since it also cause a deviation from the normal delay time as well as the previously considered cutoff voltage and static breakdown voltages. From the design point of view, the data indicate that if a high gap holdoff with a low cutoff voltage and low delay time is required, the main gap geometry should be made as uniform as possible.

If we assume such a uniform field condition we can, by Paschen's law, let V_{sbv} be a function of pd, and the gap operating ratio for delay time now can be expressed as

$$\frac{V_g}{V_{sbv}} \triangleq \frac{V_g}{f(pd)} = \frac{E}{p} \text{ volts/cm/mm Hg} . \qquad (53)$$

If we now replot Fig. 110 as a function of E/p, we obtain a universal curve which holds for various spacings at a constant pressure. Such a curve is shown in Fig. 112. A similar curve can also be obtained by holding the gap spacing constant (E = a constant) and by varying the pressure. This dependence of the delay time for different gap geometries and pressures on the main gap field divided by the fill pressure gives us a better understanding of the trigger behavior, and enables the design engineer to obtain better design estimates on the triggered gap parameters.

Large Trigger Electrode Hole

We next consider the opposite extreme of the trigger probe assembly where we now have a very large trigger electrode hole in order to cause the trigger spark to form to the main electrode more frequently. The experiment was performed exactly as before except that the radius of the trigger electrode hole is now 0.178 cm instead of 0.076 cm. The cutoff curves for this probe geometry are shown in Fig. 113. At high values of pd product where the trigger spark forms to the trigger electrode, the order of lowest cutoff (Modes B, C, A and D) is the same as for the preceding geometry. However at low pd products, the order of lowest cutoff changes to C, B, A, D and then to A, C, B, D. A comparison of these curves with Fig. 107 shows that the static breakdown curves and the cutoff curves for Modes C and D are unchanged, while the cutoff curves for Modes A and B have changed considerably resulting in the change of the order for cutoff. In addition, the cutoff points for Modes C and D were

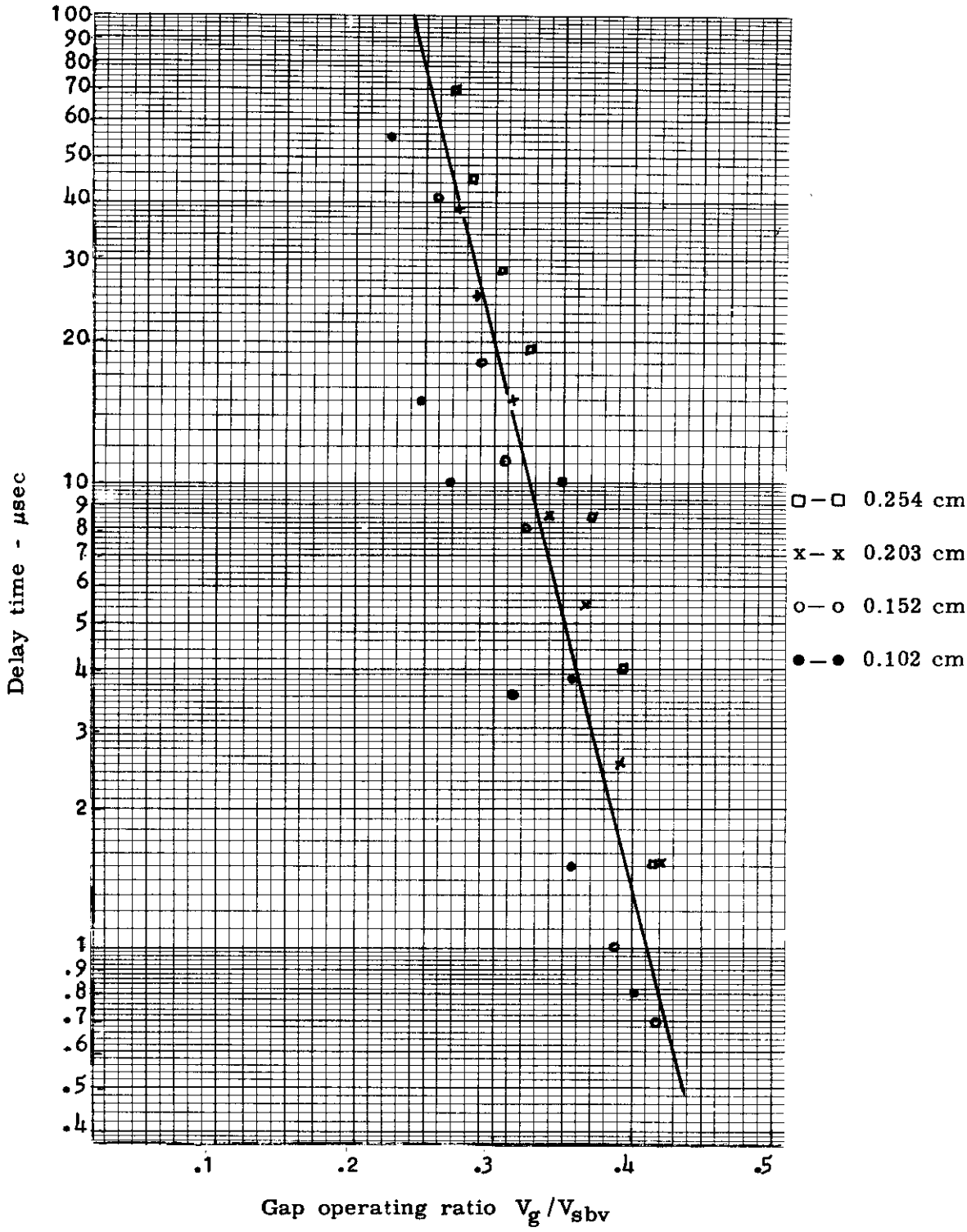

Fig. 111 -- Normalized Mode C delay time for various gap spacings as a function of gap operating ratio, V_g / V_{sbv} (P = 600 mm Hg - N_2, R = 0.076 cm)

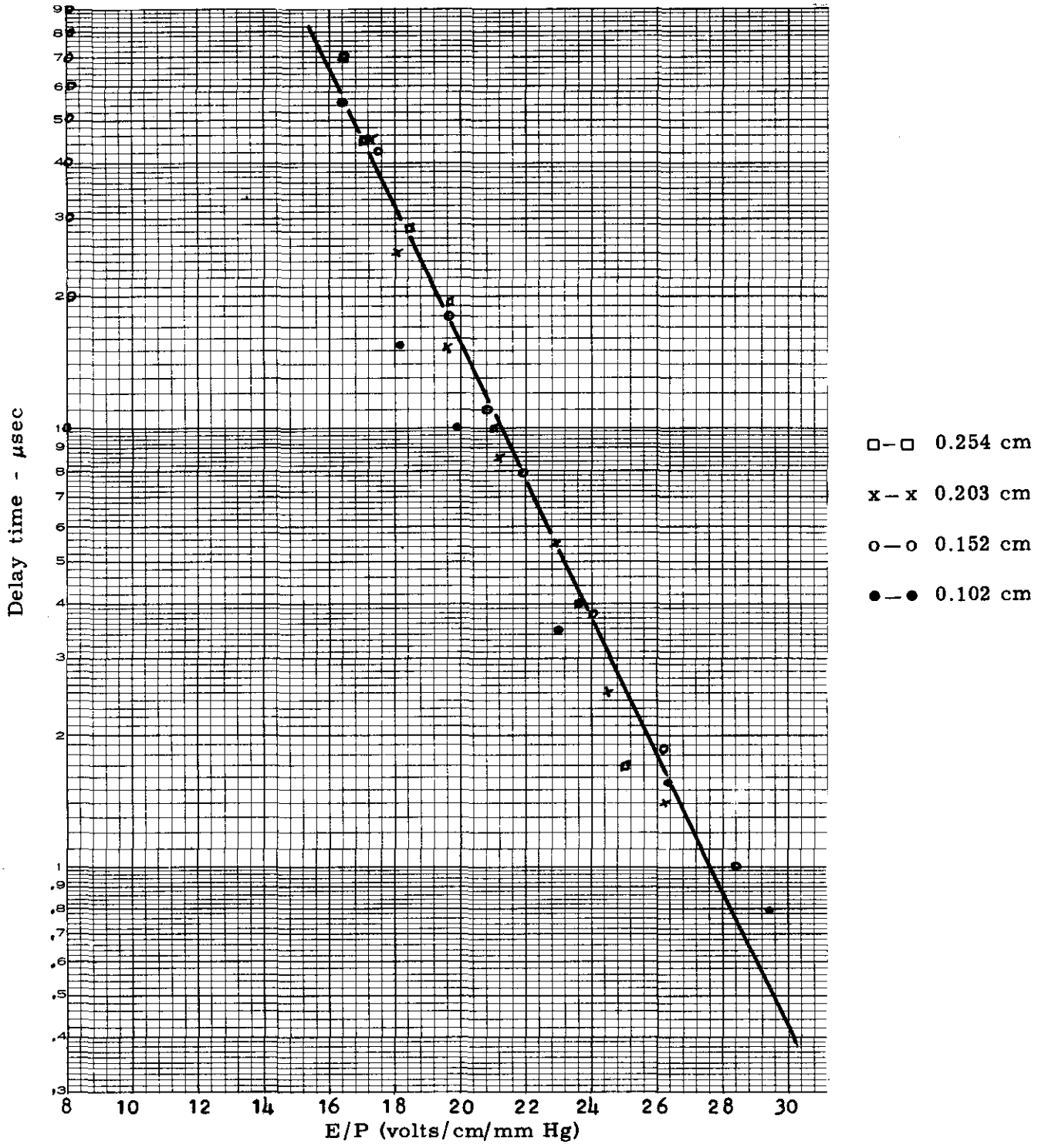

Fig. 112 -- Normalized Mode C delay time for various gap spacings as a function of E/P (P = 600 mm Hg - N_2 , R = 0.076 cm)

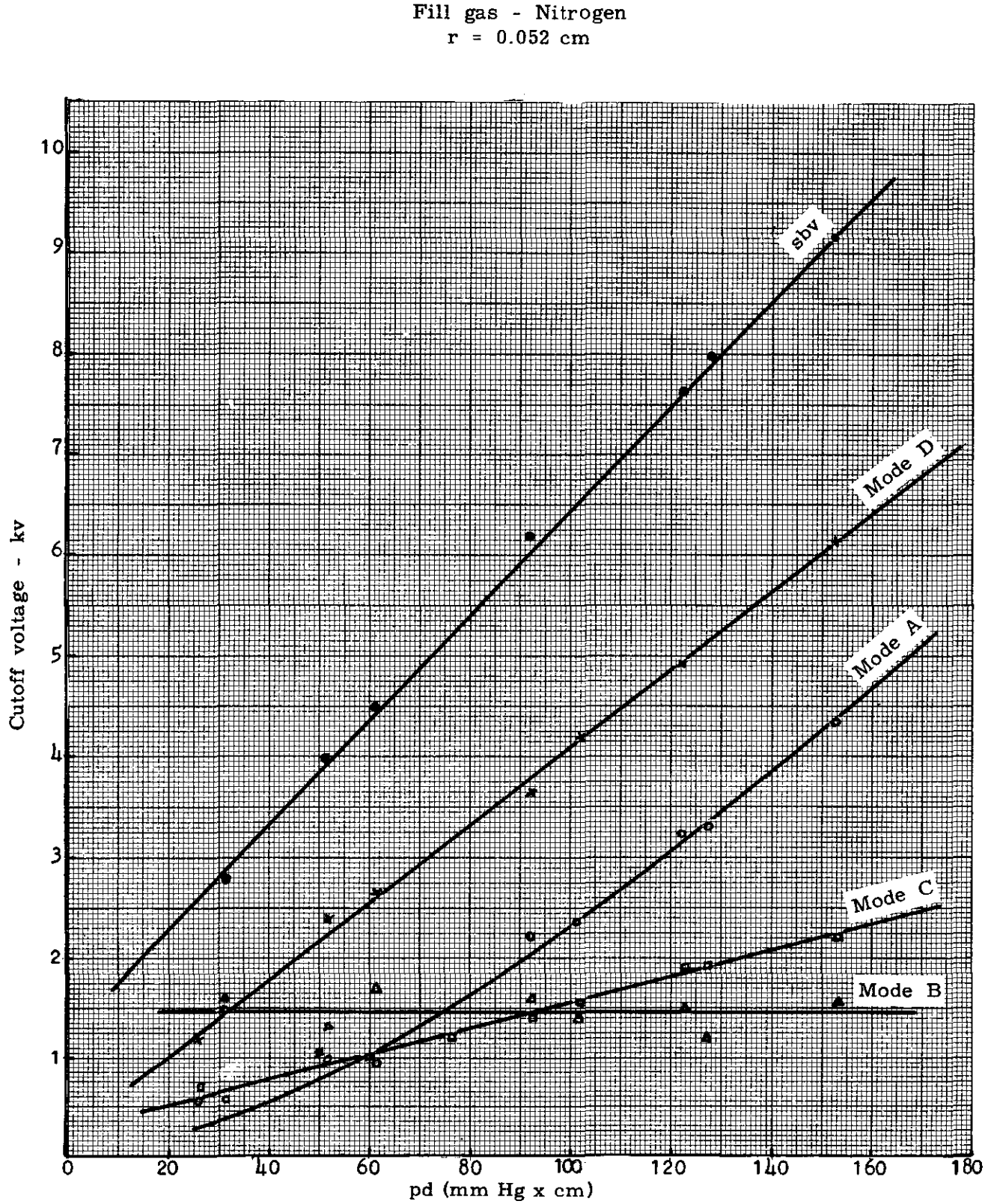

Fig. 113 -- Cutoff voltage as a function of pd for different operating modes (R = 0.178 cm)

fairly repeatable over a wide range of pressure and gap spacing variations, whereas Modes A and B showed a greater variation for both pressure and gap spacing variations. It is also significant that Mode A is much lower than Mode D for this geometry, whereas Modes A and D were the same in the preceding geometry. It is also interesting to note that when the gap spacing is made very large compared to the radius of curvature of the main electrode such that a nonuniform field is established, the cutoff values for the modes having an aiding field (Modes A and B) are unaffected, while the modes having a repelling field (Modes C and D) have an increase in their cutoff voltage.

The reason for Modes A and B shifting in their cutoff characteristics for an increase in the probe hole radius is not clearly understood; but since it occurs only for Modes A and B where there is a tendency for the trigger spark to form across the gap to the main electrode, it is felt that this direction of the trigger spark is beneficial to the triggering mechanism, especially Mode A. In support of this conclusion, many triggering situations for Mode A as viewed by scope traces have shown that near low cutoff voltages and in a trigger spark transition region, when the trigger spark formed to the main electrode, the gap fired. However, if the trigger spark formed to the trigger electrode, the gap failed to fire. If the trigger spark input is increased, if the gap voltage is increased, or if the gap spacing is large with a high gap voltage, then the gap may fire when the trigger spark forms to the trigger electrode. There is evidently an optimum arrangement whereby if the trigger electrode hole is made too large and the trigger spark forms to the main electrode the gap does not fire. This is the result of the large distance from the cathode spot on the main electrode to the trigger electrode. Figure 114 shows the variation of cutoff voltage for Mode A operation as a function of the trigger electrode hole radius, R , for different gap spacings at a constant fill pressure. The radius of curvature of the trigger electrodes and the size of the probe were the same. As Fig. 114 shows, the cutoff voltage decreases for Mode A as the trigger electrode hole radius increases. However, if the trigger electrode hole radius is increased further, the cutoff voltage again increases. For those cases where the trigger spark forms to the trigger electrode, the increase in trigger electrode hole radius tends to cause the trigger spark to "bow" out and extend into the main gap region and effectively reduces the main gap spacing.

The reason for Mode B becoming harder to trigger than Mode C is not clearly understood. While some of the triggering characteristics of the various modes have been studied and presented here, there still is a great need for additional research in this area, especially on the influence of the trigger spark path.

Typical delay curves for this geometry are shown in Figs. 115 and 116, which show the change of the order of cutoff for the different modes and the resulting delay times for two different spacing-pressure combinations. Figure 117 shows the transition of Mode B from a trigger spark path to the trigger electrode to a path where the trigger spark forms to the main electrode with the corresponding change in delay time. Figure 117 also shows the variation of delay time for Mode C for varying gap spacings at a fixed pressure, while Fig. 118 shows this variation with a fixed spacing and varying pressure. Figure 119 shows the normalized curve as a function of E/p for Mode C for variations in pressure. Figure 120 shows the delay time for all modes as a function of the gap operating ratio,

$$\frac{V_g}{V_{sbv}},$$

for pressure variations where the trigger spark is forming to the trigger electrode only.

o — o d = 0.254 cm

□ — □ d = 0.203 cm

x — x d = 0.152 cm

Δ — Δ d = 0.102 cm

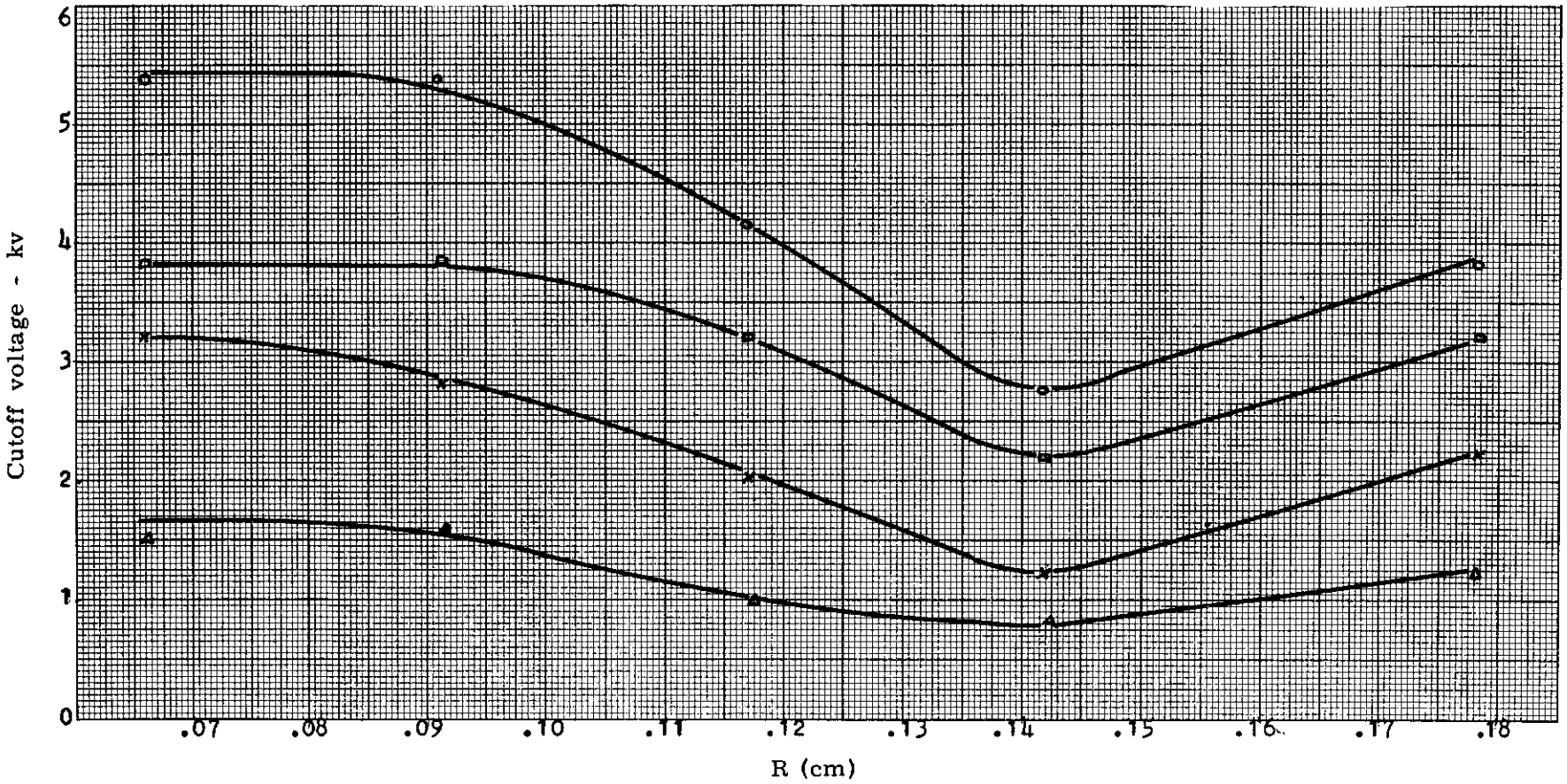

Fig. 114 -- Mode A cutoff as a function of trigger electrode hole radius, R , for variations of gap spacing - (p = 600 mm Hg - N_2)

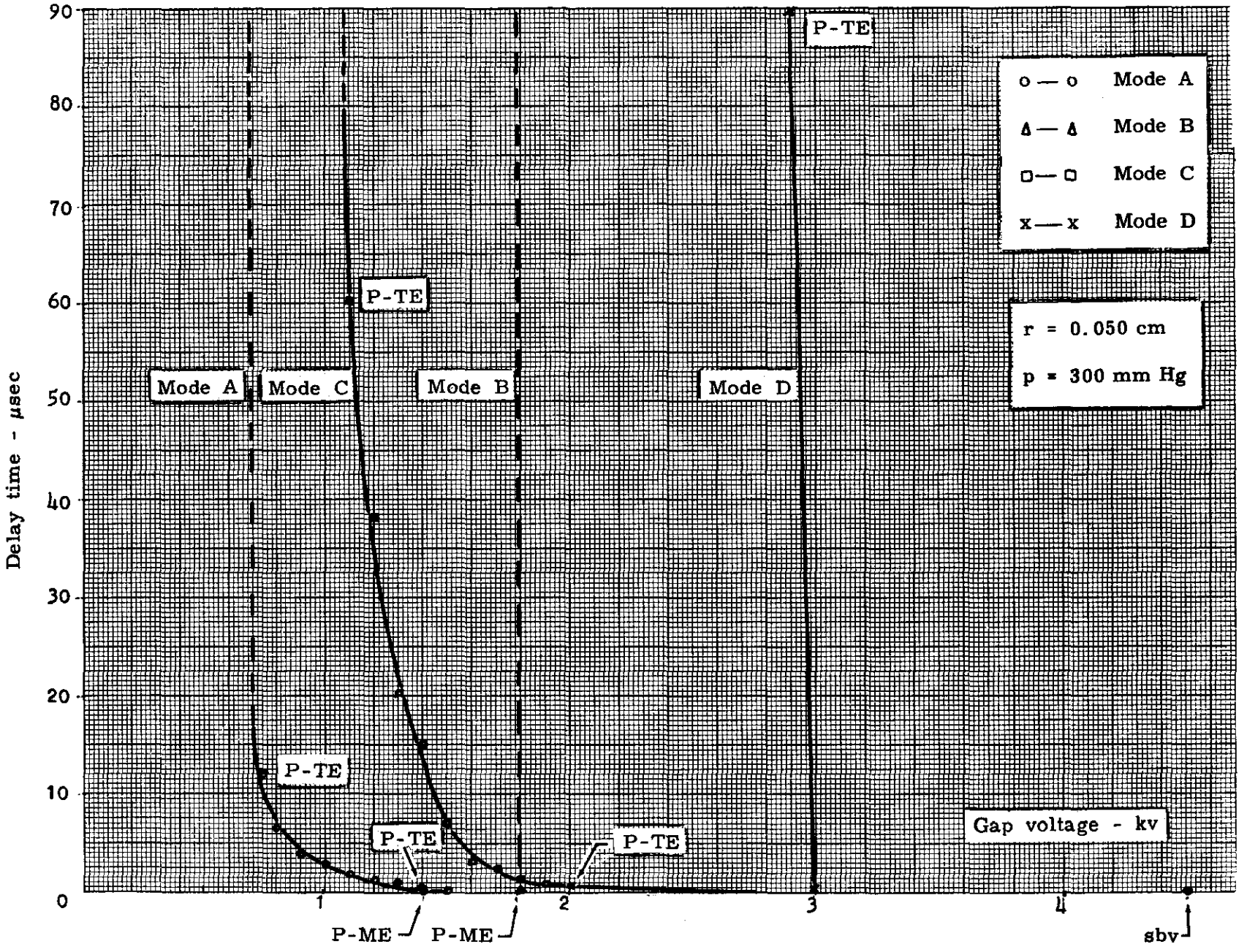

Fig. 115 -- Typical delay time curves in nitrogen for various operating modes for R = 0.178 cm, d = 0.203 cm

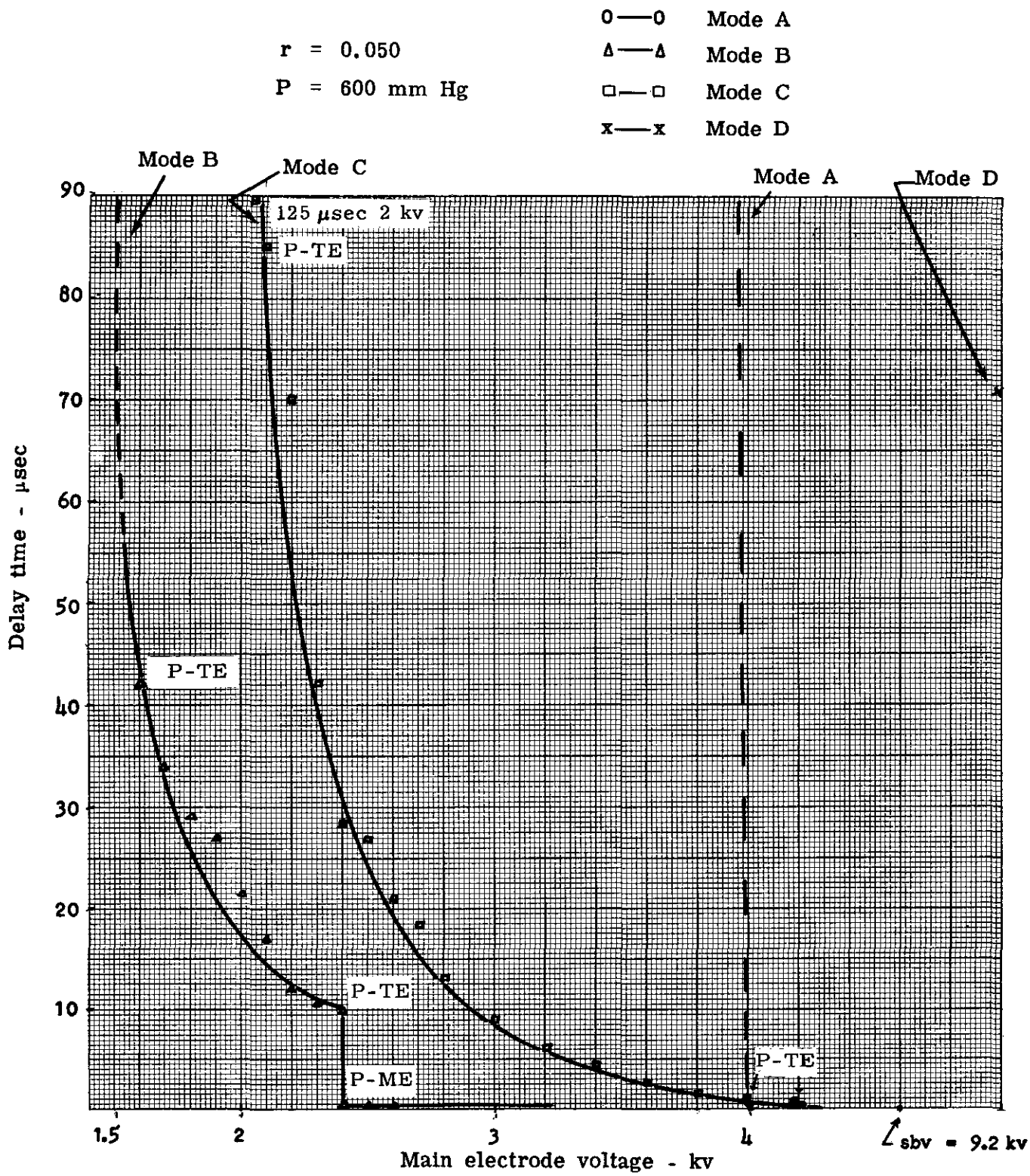

Fig. 116 -- Typical delay time curves in nitrogen for various operating modes for R = 0.178 cm, d = 0.254 cm

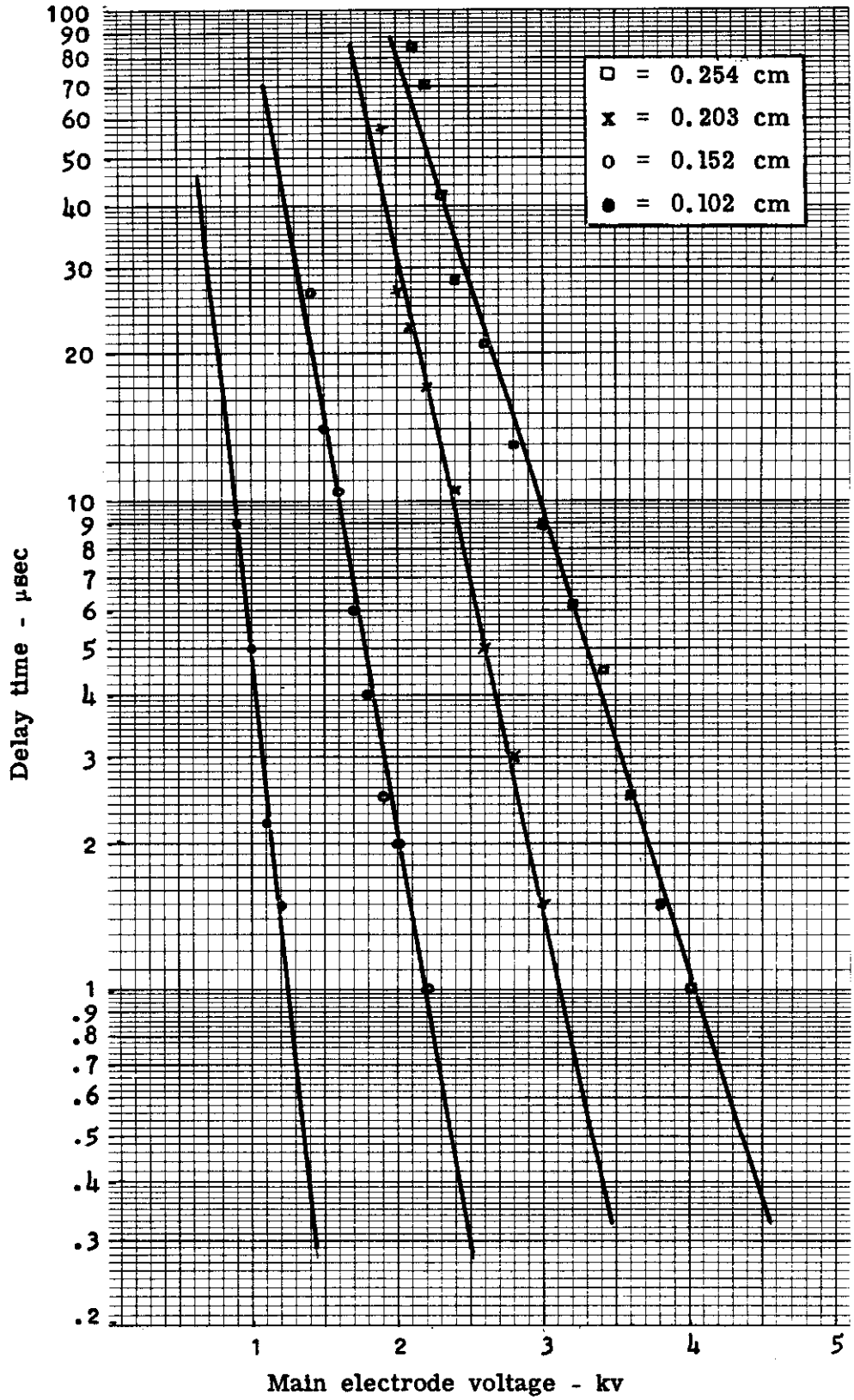

Fig. 117 -- Mode C delay time for various gap spacings at a pressure of 600 mm Hg of nitrogen (R = 0.178 cm)

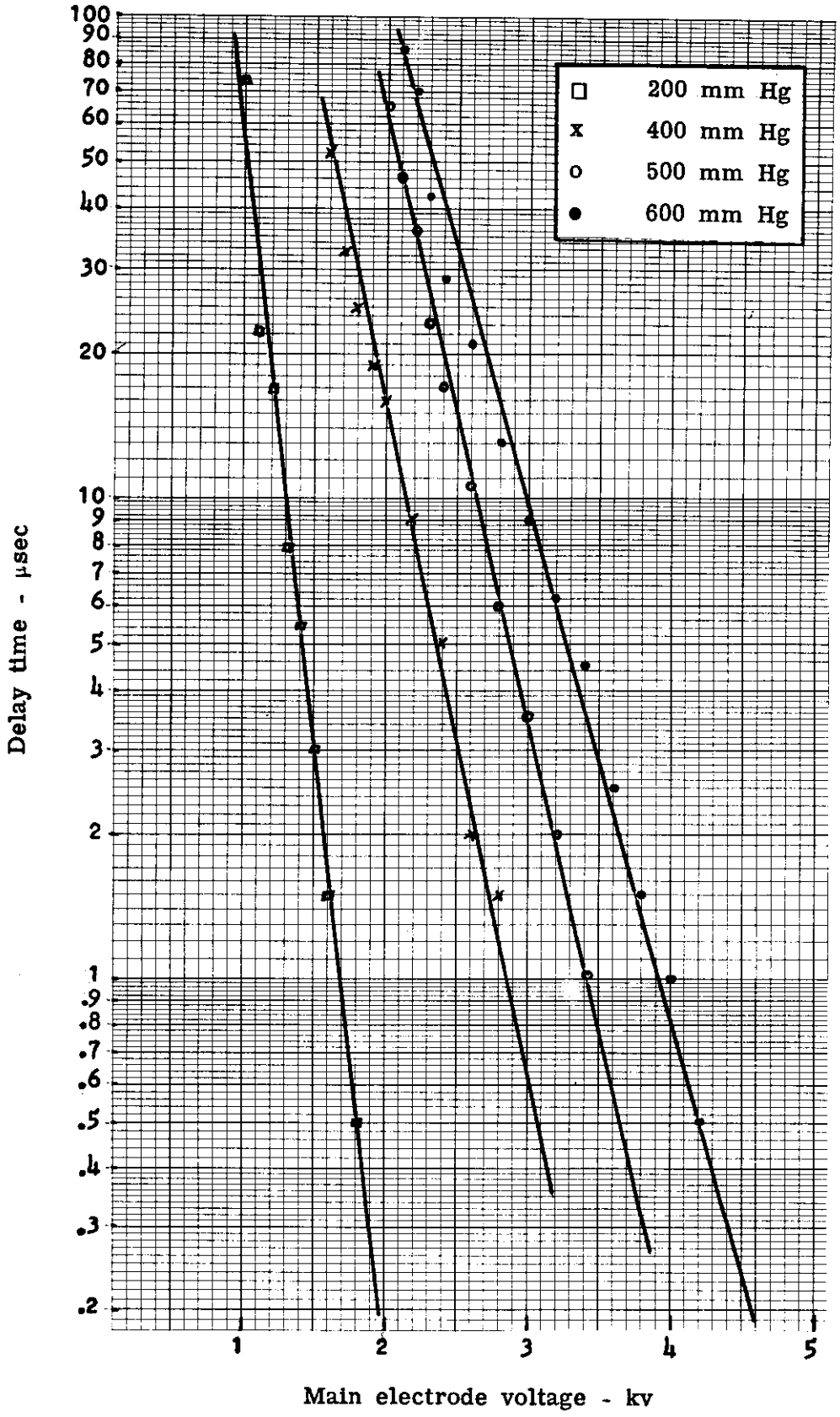

Fig. 118 -- Mode C delay time for various fill pressures of nitrogen at a gap spacing of 0.254 cm (R = 0.178 cm)

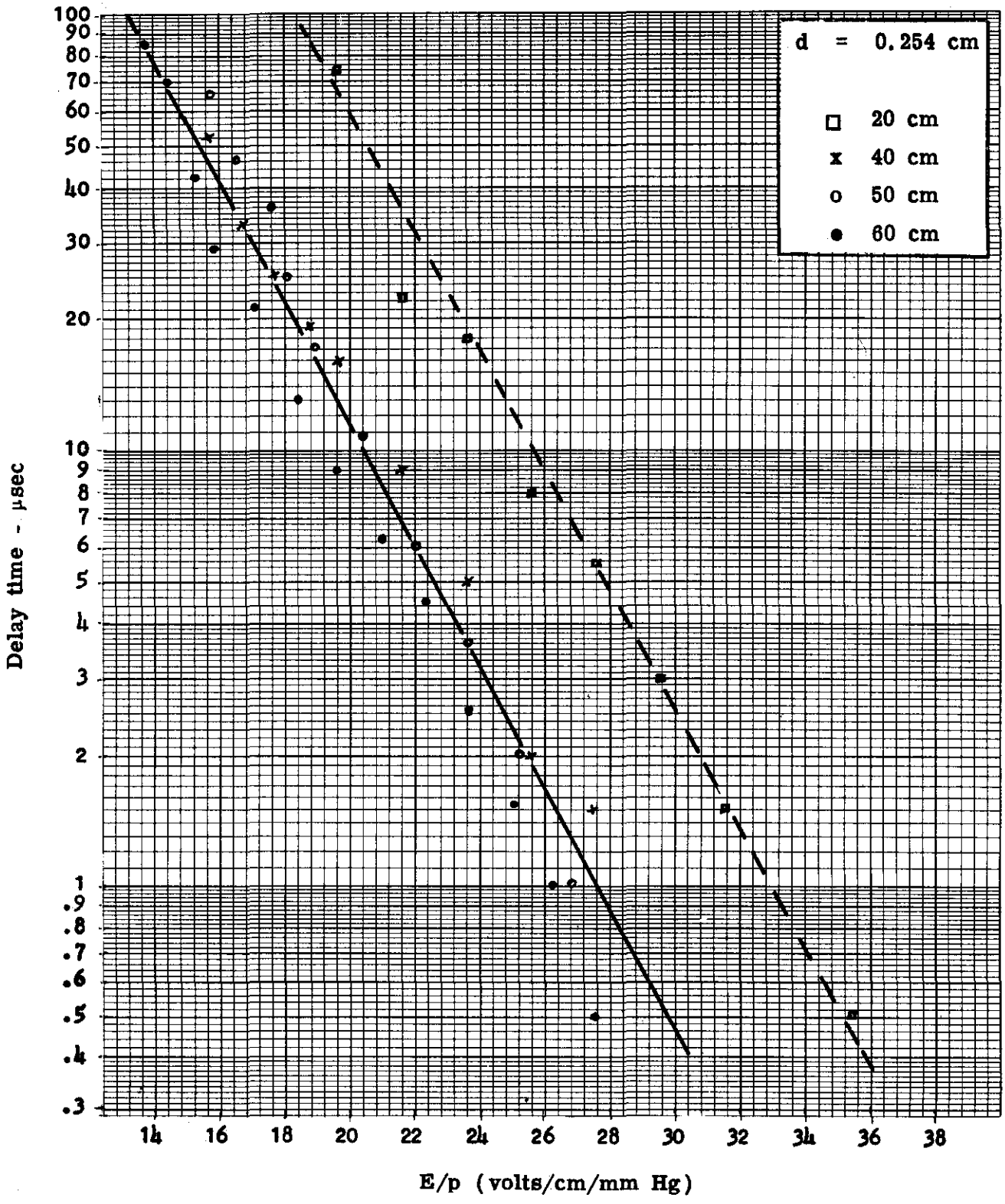

Fig. 119 -- Normalized Mode C delay time for various gap spacings as a function of E/p ($p = 600$ mm Hg - N_2, $R = 0.178$ cm)

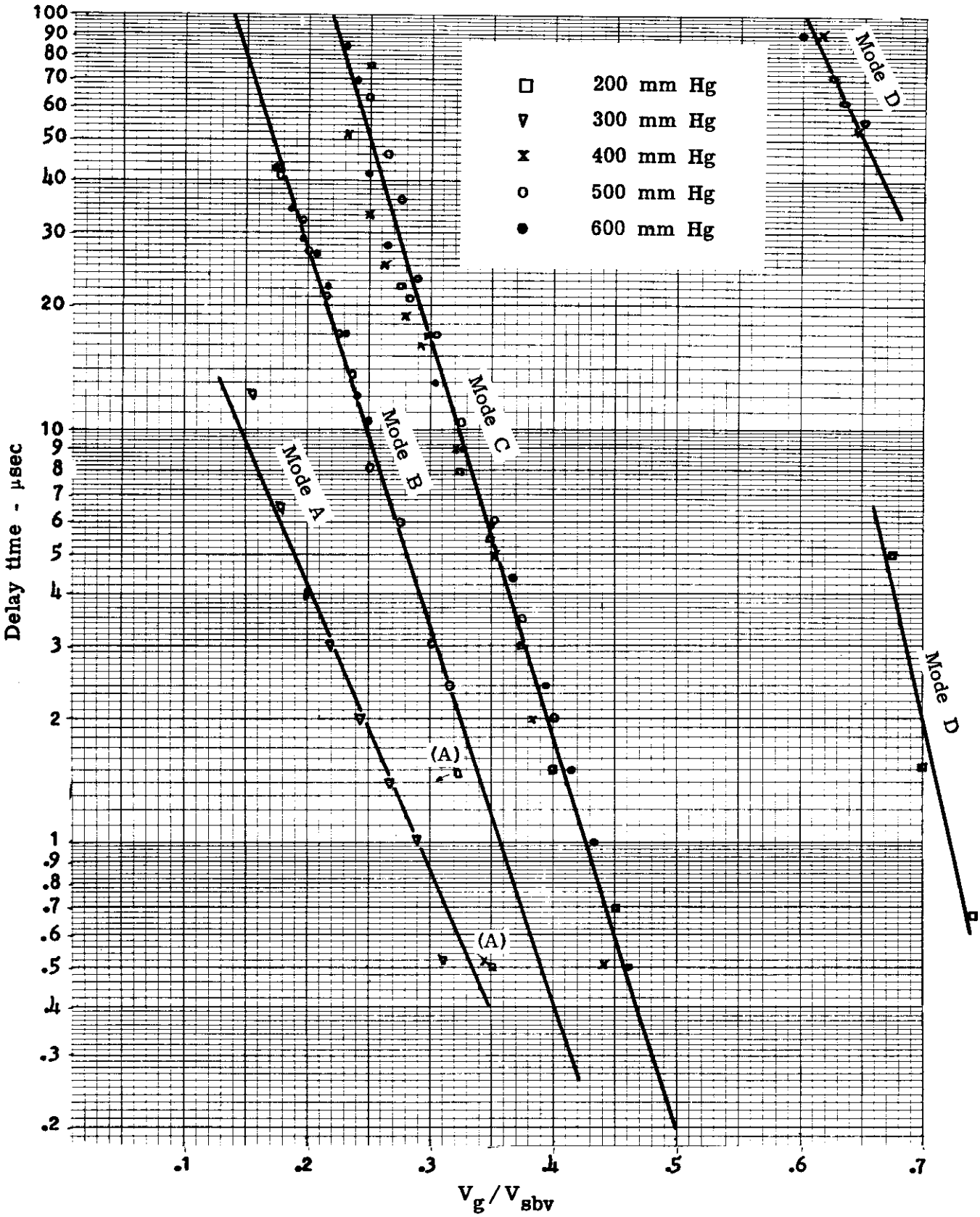

Fig. 120 -- Delay time for probe-to-trigger electrode trigger spark as a function of gap operating ratio, V_g/V_{sbv}, for a fixed spacing and variable pressure

Other Design Considerations

1. Probe Position -- If the probe is recessed into the trigger electrode and the probe insulator remains flush with the trigger electrode, it can be shown that the trigger pulse breakdown voltage is increased due to the increased probe-to-trigger electrode path length. This increase in breakdown voltage coupled with the trigger circuit capacitance increases the input charge to the trigger spark and, since the pd product of the end of the spark at the trigger electrode remains the same, the cutoff voltage is lowered.

If the insulator is also recessed into the trigger electrode along with the probe, the probe-to-trigger electrode breakdown remains unchanged, but the effective spacing of the trigger spark to the main electrode is increased. Thus the pd product has increased thereby linearly increasing the cutoff voltage of the main gap by a proportionate amount.

2. Triggering Rate -- In the region near cutoff, it has been observed in the course of this study that if the trigger attempts were rapid, approximately once a second, a trigger spark would form but the gap would not always fire. If the triggering rate were decreased say to 10-second intervals, the gap would fire every time. If the gap is operated above its cutoff curve, it is independent of the trigger interval. The fact that there is a time interval effect suggests that space charges in the gap or charge accumulations on the insulators or the gas temperature, or a combination of these factors influences the triggering mechanism.

3. Spark Irradiation of the Main Gap -- Several experiments were performed whereby the light of a two-electrode gap discharge in a sealed glass envelope placed immediately adjacent to the main gap region of the triggered gap was allowed to irradiate the volume between the main electrode. While there was an observed reduction in the gap breakdown voltage, the reduction was small and no way near the reduction observed during a normal triggering.

CH V -- THE MULTIPROBE GAP

The versatility of the triggered gap is greatly increased when the gap is supplied with more than one trigger probe. Since the main gap will fire due to the initiating of any trigger spark, any number of available triggering sources may be employed to perform the required trigger spark discharge. By use of a multiprobe arrangement, isolation between triggering sources is obtained. In general, the characteristics and requirements of the single probe gap apply to each probe of the multiprobe gap. There will be slight differences, however, due to the nonuniform field generated by the main electrodes and differences in the electric field distribution due to interaction of the trigger probe fields.

Typical Geometries

The insertion of more than one probe into a gap usually necessitates an asymmetrical main gap geometry. This type of geometry then generates a nonuniform field compared to the gaps having a single probe construction. Figure 121 shows a few typical gaps employing multiprobes in the trigger electrode assembly. Figure 121A and B shows the multiprobe gap, where the probes are inserted in the trigger electrode through individual holes. Figure 121C

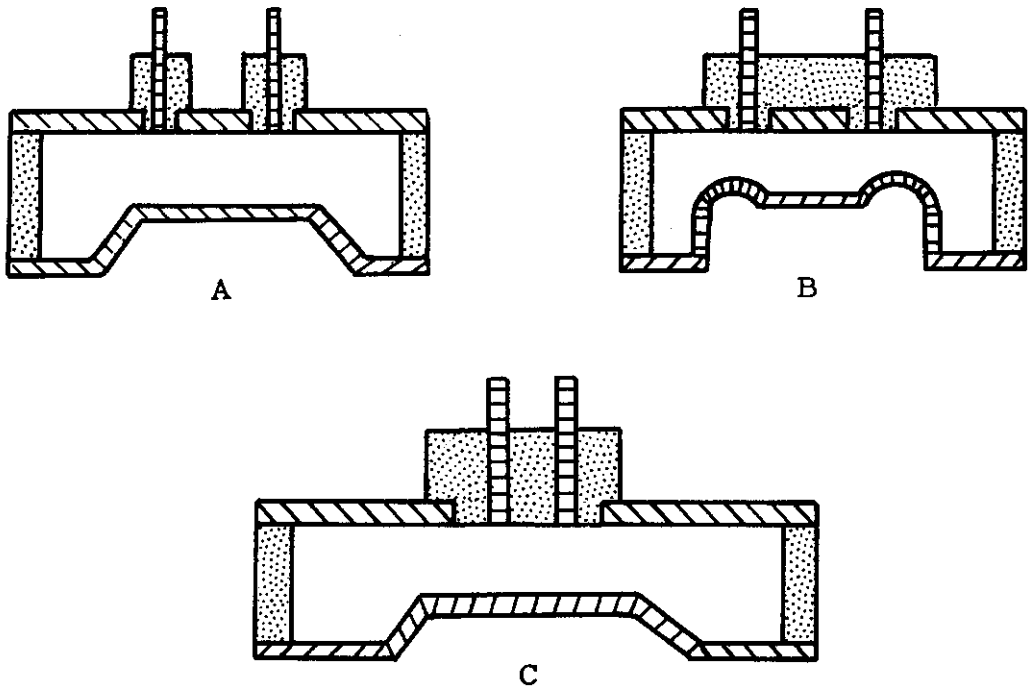

Fig. 121 -- Typical multiprobe spark gap designs

shows the probes inserted through one hole in the trigger electrode and separated within the common insulator. Where the probes are inserted individually in separate holes, the trigger electrode completely surrounds each probe thereby establishing a more uniform field with improved triggering than when the probes are inserted in a common insulator. The author has previously reported on a few of the characteristics of the multiprobe gap[18,19,20] and, in addition, multiprobe characteristics are discussed in some of the EG&G[21] technical reports.

The number of probes that may be inserted into the gap appear to be limited only by the practical need and by the imagination of the designer. Gaps with probes numbering up to as many as five have already been investigated with favorable results.

In addition to the above multiprobe gaps, it is also possible to construct a two-probe gap similar to the symmetrical single probe gap with hemispherical electrodes by essentially employing two trigger electrode geometries as shown in Fig. 122. Such a gap has been developed and gave a satisfactory performance.

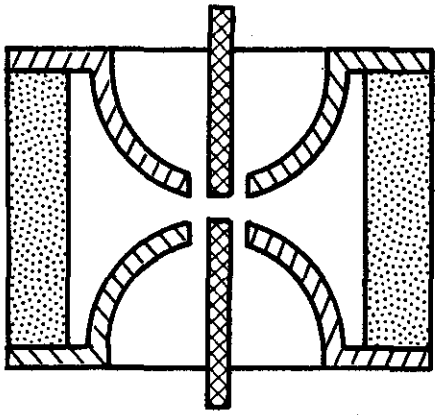

Fig. 122 -- Opposing probe spark gap

In analyzing the field distributions of the multiprobe gap, the use of an analog field plotter may be used to advantage since the main gap geometry usually results in the generation of nonuniform fields. Since the field in a multiprobe gap is usually nonuniform, the fill pressure is necessarily higher for a given gap spacing in order to achieve the same holdoff capability obtainable in a uniform field gap. This resultant increase in pressure for the multiprobe gap usually results in a slightly higher gap cutoff voltage.

CH VI -- PRACTICAL DESIGN CONSIDERATIONS

Breakdown Voltage

In the fundamental study of breakdown phenomenon, most observers reporting their results in the literature used a demountable spark gap where they could have access to the various electrodes. These investigators would utilize highly polished electrodes in their experiments. After each discharge or limited number of discharges they would disassemble their gap and repolish and condition the electrodes. In this manner they would be able to obtain very repeatable results from shot to shot. They also found that the varying light surrounding the gap had some influence. Some experiments were performed in a darkened enclosure while other experiments were performed with varying amounts of controlled light. This light, of course, would give rise to the photoelectric effect and the natural ionization level of the gas would be enhanced. Some investigators also noticed that when their system had been idle for some time that the first breakdown value obtained would be abnormally high and then all remaining shots would be quite repeatable and much lower. These high first readings were normally ignored as being of no importance to the experiment under consideration and were usually omitted.

In the design of a practical gap, all of these features are not under absolute control and must be taken into account. In a sealed spark gap the electrodes are not accessible and can not be polished after each discharge. Consequently, the electrodes begin to errode since the spark reaches molten temperatures at the surface of the electrode in the region of the arc. A gradual buildup of material will occur causing sharp discontinuties and therefore effecting the breakdown properties by a distortion of the field to a more nonuniform case. In addition, the gap spacing will vary slightly as the electrodes build up and errode away. For detailed information on suitable electrode materials, Reference 23 should be consulted.

In laboratory spark gap systems the electrodes are usually suspended in space, and there is no distortion of the field due to the proximity of major gap insulator surfaces. In practical gaps the insulator is present and will affect the breakdown characteristics either directly or by collection of contaminates or sputtered molten electrode material on the surface. The more the gap is allowed to breakdown and the larger the currents the gap passes, the greater is the amount of insulator contamination and electrode distortion.

The amount of surrounding light that may penetrate into the gap will vary from location to location and may affect the breakdown characteristic as noted above. In theoretical studies the dielectric or insulating gas is usually kept at a constant pressure and purity. In practical units traces of impurities may exist and the gas density may vary due to "clean up" after each discharge. Such impurities as water vapor are known to have a very decided effect on the gap breakdown values. In practical gaps it is usually very difficult to accurately control the gap spacing during assembly. In order to arrive at a constant breakdown value with such a varying spacing between gaps, the fill pressure is adjusted accordingly. These variations in gap spacings and fill pressure will affect the triggering and other static characteristics of the gap.

The omission of the high first reading cannot be accepted in practical gaps, but must be taken into account. Except for a nusiance factor in testing for this parameter, the high first reading is an advantage since it affords a higher holdoff capability. The reason for this behavior is suggested as follows--the Townsend equation for current to flow through a gas, and which is the basis for establishing the breakdown criterion, is repeated from Equation (1),

$$I = I_o e^{\alpha d} \qquad (1)$$

where, to emphasize again, I_o is the residual ion and electron current that exists due to external agents such as cosmic radiation, ultraviolet illumination, etc.

Obviously, if I_o were equal to zero, no current would flow, and consequently no multiplication of electron-ion pairs could occur to form the avalanche and cause breakdown. It is the source of electrons from I_o that enables this multiplication to occur. Whenever a discharge takes place, there is a small amount of residual ionization that remains for some time and adds to I_o and assumes repeatable breakdown values. When this residual discharge ionization reduces to zero after being idle for long periods of time, I_o is reduced and the probability for breakdown is also reduced, thereby resulting in an abnormally high breakdown value. This is similar to the discussion of impulse breakdown and the necessity of having sufficient initiatory electrons. The addition of radioactive material into the gap would then appear to give repeatable results because of a constant source of I_o masking out slight variations due to the other external agents. This is exactly what happens in practice. The addition of approximately 0.05 microcuries of Ni^{63} (Beta emitter) inside a typical sealed gap reduces the standard deviation, σ, of the breakdown voltage from a value of 148 volts to approximately 50 volts. While the addition of a stabilizing radioactive source influences the static breakdown voltage of the gap, it does not appear to influence the triggering characteristics to any degree.

Effect of Impurities in the Fill Gas

Investigations in our laboratory have repeatedly shown that if traces of water vapor and air are mixed in with the fill gas the breakdown curve is changed. Shown in Fig. 123 are the breakdown curves for 0.625-cm diameter spheres at a 0.625-cm spacing in Nitrogen and Helium and for 0.950-cm diameter spheres at a 0.254-cm spacing in Nitrogen. The breakdown curves were first run with traces of water vapor and air allowed to be present. The gaps were then evacuated and flushed through a cold trap several times before filling for testing.

In the case of Nitrogen, the removal of air and water vapor with its resultant lower breakdown strength will cause the breakdown value to rise. For Helium, the breakdown strength of air and water vapor are higher than Helium, consequently their removal would cause the breakdown value to be lowered. As we observed earlier, these results are in agreement with the results of gas mixtures.

Influence of the Main Insulator on SBV

Consider a practical spark gap design, as shown below, that utilizes an insulator of high dielectric constant to separate the two electrodes. The gas fill will be assumed to be air which

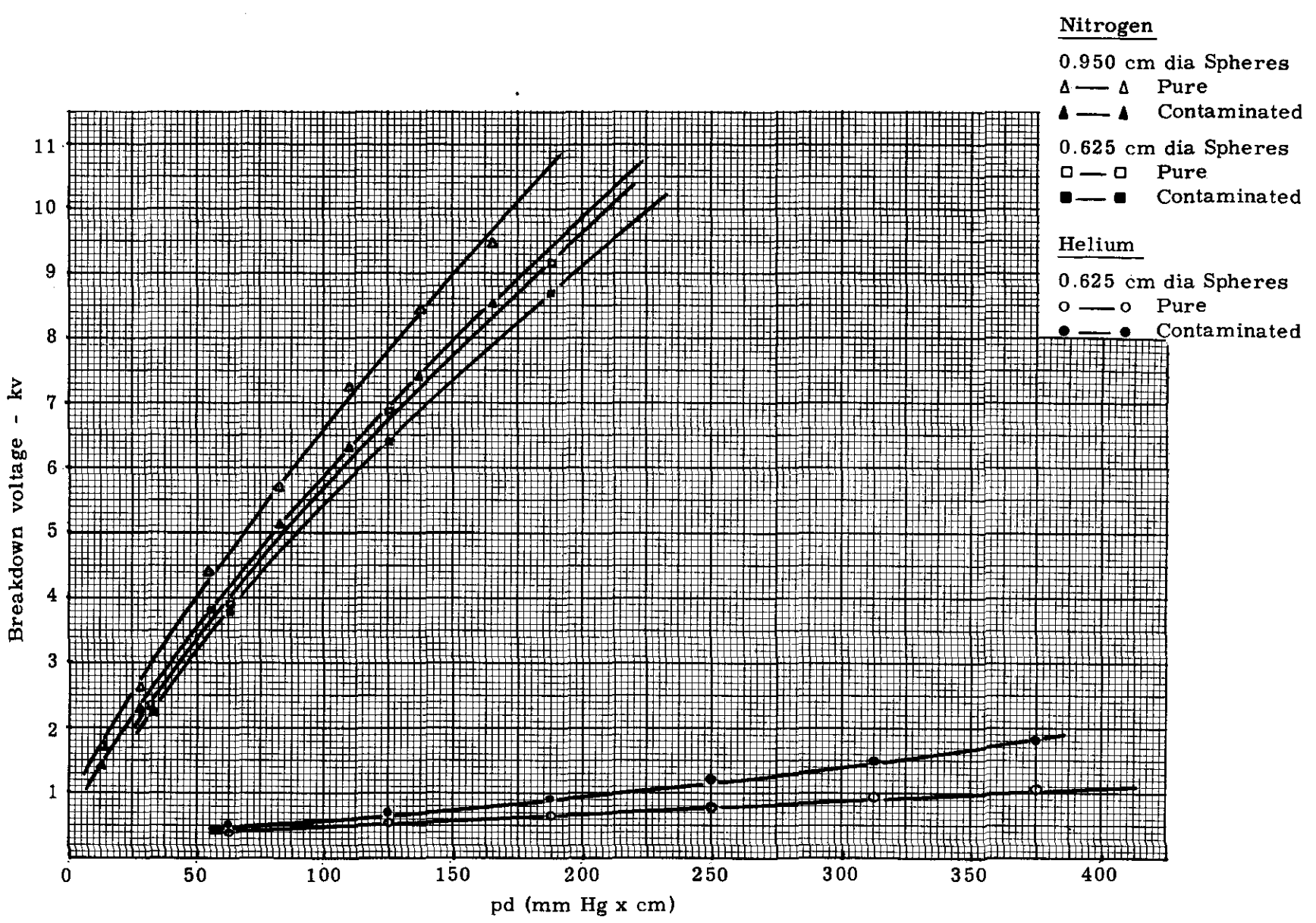

Fig. 123 -- Comparison of static breakdown voltage for pure and contaminated gases

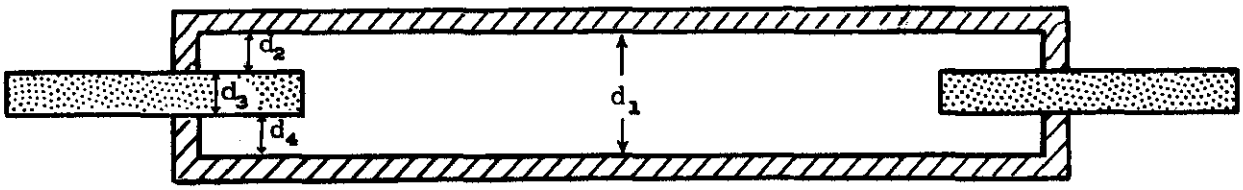

Fig. 124 -- Typical insulator arrangement

has a dielectric constant $K = 1$ and an approximate rupturing gradient of 31 kv/cm at atmospheric pressure. Assume the applied voltage to be 6 kv and the spacing d_1 to be 0.200 cm. The voltage gradient will then be 6 kv/0.200 cm or 30 kv/cm which is just below the rupturing voltage of 31 kv/cm; therefore, the gap at d_1 will not breakdown.

Now consider the area of d_2, d_3, and d_4 where the insulator projects into the gas fill. Assume the ceramic insulator is a high alumina ceramic which has a dielectric constant $K = 8.9$ and a rupture strength of 118 kv/cm. At this point the insulator of higher dielectric constant has increased the capacity of the combination and also increased the total flux and flux density in the air. An increase in flux density, therefore, results in an increase in gradient. The combination of the insulator with the air gaps can be considered as three capacitors in series with a corresponding division of voltages. The gradient at any point in a combination of n insulations in series is given by the following equation:[13]

$$E_x = \frac{V_x}{d_x} = \frac{V_{applied}}{K_x\left(\frac{d_1}{k_1} + \frac{d_2}{k_2} + \frac{d_2}{k_3} + \ldots . \frac{d_n}{k_n}\right)} \qquad (54)$$

for an example, the gradient across d_2

$$E_{d_2} = \frac{6}{1\left(\frac{.075}{1} + \frac{.050}{8.9} + \frac{.075}{1}\right)} = 38.6 \text{ kv/cm} .$$

Since 38.6 kv/cm is much greater than the rupture gradient for air, the air gaps d_2 and d_4 will break down. When these air graps break down, the main gap may then break down around the insulator due to a distortion of the field, and also because of the fact that the gap spacing at this edge has been effectively reduced to that of d_3 with the full applied voltage of 6 kv applied across this reduced spacing.

The main insulator is also subjected to the full applied voltage when the air gaps, d_2 and d_4, break down. With 6 kv across the 0.050-cm thick insulator, the gradient is 6 kv/.050 or 121 kv/cm, which is greater than the rupture strength of 118 kv/cm, and the insulator will also break down.

This example, while hypothetical, does point out that in the design of practical gaps, care must be exercised not to overstress the gas dielectric by the geometry of the insulator with respect to the main electrodes.

CH VII -- THEORETICAL CONSIDERATIONS OF THE TRIGGERING MECHANISM

Summary of Results

From the results of the previous sections the following summary of the triggering characteristics can be made:

1. The cutoff voltage is controlled by the input charge to the trigger spark.

2. Cutoff is a function of the pd product for uniform field conditions. Interchange of p and d such that the product remains constant results in the same cutoff voltage.

3. When the trigger electrode hole is small compared to gap spacing and when the pd product is large for gaps with a large trigger electrode hole, the cutoff is lowest when the main electrode is positive (Modes B and C) and highest when the main electrode is negative (Modes A and D). There is also a difference in cutoff due to the polarity of the probe, i.e., A and D, B and C.

4. Delay time decreases exponentially with increasing gap voltages and is found to be a function of E/p.

5. The trigger spark path for Modes C and D always forms to the trigger electrode while the trigger spark path for Modes A and B may form to either electrode depending upon the gap spacing, pressure, trigger electrode hole and gap voltage.

6. Evidence indicates that the main gap discharge takes a path from the trigger electrode to the main electrode via the trigger probe under certain operating conditions (primarily Modes B and D, occasionally Mode C, and also Mode A when the trigger spark goes to the trigger electrode).

7. The predominant main gap discharge path for Mode C is directly to the main electrode from the cathode spot of the trigger spark at the trigger electrode and, consequently, Mode C employs a common cathode spot.

8. The predominant main gap discharge path for Mode A when the trigger spark forms to the main electrode is directly to the trigger electrode employing a common cathode spot for both the trigger spark and the main spark discharge.

9. Delay times are much shorter for Modes A and B when the trigger spark forms to the main electrodes than when it forms to the trigger electrode.

10. When the trigger spark forms to the trigger electrode, the delay time for Mode B is lower than Mode C for the same applied gap voltage.

11. Delay times may be longer than the duration of the applied trigger pulse.

12. The cutoff voltages for Modes A and D are not precise, but rather are statistical in nature forming a distribution over a region of gap voltages where there are 0 percent firings to 100 percent firings. The cutoff voltages for Modes C and B appear to be more repeatable and precise.

General Conditions

The process of breakdown in the triggered gap at gap voltages below the breakdown voltage appears to be very complex. The fact that the process is not clearly understood is shown by the scarcity of reference material on the subject and by the different interpretations of the observed data when a triggering mechanism is suggested. The work of Sletten and Lewis[16] appears to give the best general explanation of the triggering mechanism available to date, and the following discussion is based on their proposal and adapted by the author to the gap type presently under consideration.

A lowering of the breakdown voltage of a two-electrode gap by intense irradiation of the gap has been studied extensively, and is found to be a function of the square root of the photoelectric current produced at the cathode by this irradiation.[1] However, it is well established that the maximum amount of lowering is about 10 percent of the breakdown voltage. Any mechanism suggested must account for the fact that a voltage lowering of 60 to 80 percent of the breakdown voltage can be obtained. The accepted mechanism of the natural breakdown of the gap has been shown to be due to the Townsend α process as discussed in Chapter II. While the value of α obtained at the cutoff voltage is too low to support cumulative ionization, it was shown that the minimum input charge to cause reliable triggering for various pressures at a fixed gap geometry was constant for a constant value of the ratio of α at cutoff to α at the static breakdown voltage. See Table VIII. Also the dependence of the minimum cutoff voltage on the product of gap spacing and fill pressure suggests that the triggering process is dependent on α, that the actual value of α is increased within the gap by space charge distortion of the applied electric field due to the trigger spark, and that there is a reduction of the effective pd product within the gap.

The work of Broadbent and Wood[22] on the thermally triggered spark gap and the later work by Broadbent[2] showing the similarity of the thermal gap to the trigatron have led to the suggestion that the triggering mechanism is caused by the lowering of the dielectric strength of the gas adjacent to trigger spark due to the heat liberated to the gas by the trigger spark, since the dielectric strength of the gas is inversely proportional to the gas temperature. A low density region is then generated near the trigger spark and thereby increases the value of α in that region. The fact that the cutoff voltage is determined by the input charge to the trigger spark supports this theory, since it can be shown emperically that the energy liberated by the passage of the spark can be given by the following equation:[23]

$$\omega = (.703 \times 10^{-6} + .420\, t - .0233 \times 10^{-6} t^2)\, di_p \qquad (55)$$

where

ω is in joules

t is the pulse duration in seconds

d is the gap spacing in mils

i_p is the pulse current in amps.

This equation clearly shows the dependence on the input charge since

$$CV = \int i\,dt .$$

The main products of the trigger spark as envisaged by Sletten and Lewis[16] are summarized below:

"(a) A local region of hot gas of low density corresponding to the spark channel which would be ejected into the main gap and would continue to move after the trigger discharge had ceased. The initial growth of the spark channel can be about 10^5 cm/sec or greater, and is accompanied by a shock wave. Behind this, the low-density region would tend to propagate at lower velocities.

"(b) Ionization products, electrons and positive ions. The electrons may not be so important as the relatively immobile positive ions which can produce important space charges. These charged particles may be ejected along with the hot-gas region.

"(c) Photons which will irradiate the main gap. These will be very important in insuring an initial supply of electrons, particularly at the opposing main electrode. The efficacy of spark illumination is well known.

"(d) Hot cathode spots, especially at the trigger cathode, which will continue to emit electrons for an appreciable time after the trigger discharge has ceased."

Evidently then a combination of all of these factors will influence α significantly to allow cumulative ionization to occur with the resultant breakdown of the gap.

Probe-to-Trigger Electrode Spark

Mode C

We will first consider the operation for Mode C. A suitable voltage pulse is applied causing a trigger spark to form between the probe and the trigger electrode. The trigger electrode then becomes the cathode spot. A low-density region is then generated near the trigger spark and begins expanding toward the main electrode. Electron avalanches are generated within the low-density region because of the lowered dielectric strength of the gas. The electrons are quickly swept out of this region and collected at the main electrode which acts as the anode. Also any photoelectrons produced in the space between the low-density region and the anode are swept into the anode. Within the low-density region the relatively immobile positive ions set up a positive space charge field. As the low-density region increases the space charge field behind it also grows forward causing a plasma-like extension of the cathode, provided that an electron source at the trigger electrode is maintained. This extension takes a definite time to form into the main gap spacing before the new effective pd product allows the rest of the remaining gap to break down in the normal manner. If the applied gap voltage is reduced, the time for the low-density region and cathode extension to reach a spacing suitable for breakdown at the new gap voltage is consequently increased. This plasma-like extension may form from the cathode spot on the trigger electrode and cut diagonally across the gap following behind the

propagating low-density region until it reaches the main electrode at the point of closest spacing to the initiating trigger spark or, depending upon the conductivity and extension into the main gap region of the original trigger spark, it may move back along this spark channel a ways and then down to the main electrode. Figure 125 shows a graphical representation of this action.

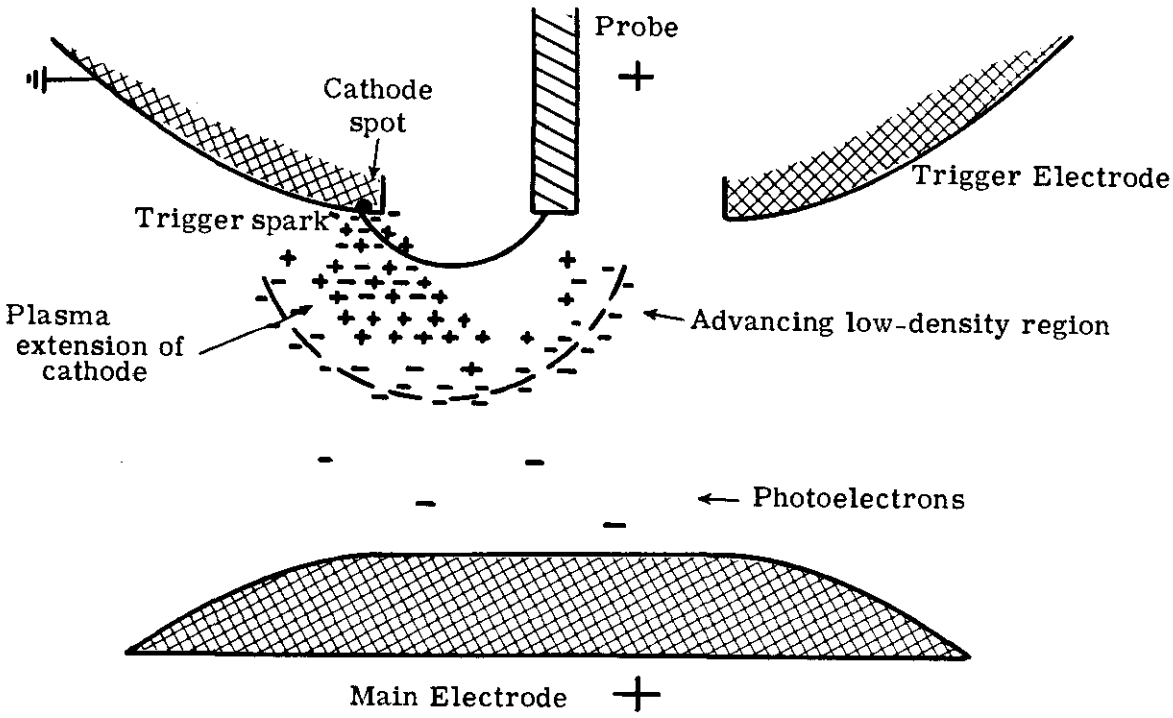

Fig. 125 -- Main gap breakdown mechanism

This model would account for the observed spark paths discussed earlier. Consequently, it also shows the dependence of the magnitude of the low-density region on cutoff. In addition to the author's results, it has also been shown by Sletten and Lewis that the cutoff voltage was a function of the input charge. They also found that if a resistance was inserted in the probe circuit the cutoff voltage was not altered since the total charge was unchanged, but that the delay time was increased. This increase in delay time was caused by the decrease in the rate of growth of the spark channel and, consequently, the low density region velocity.

Mode B

Mode B operation is then essentially the same for Mode C except that the plasma extension forms from the probe since it is now the cathode of the trigger discharge. There is a slight difference in Mode B compared to Mode C in that when the plasma extension is great enough so that the probe breakdown occurs to the main electrode, the probe voltage is now essentially that of the main electrode causing the probe-to-trigger electrode spacing to be overstressed and the main discharge then occurs from trigger electrode to main electrode via the trigger probe.

Because the total length of the plasma extension into the main gap is shorter for Mode B, and since a portion of the discharge path is covered by an immediate breakdown, the delay time for Mode B should be less than for Mode C, which is shown experimentally in Fig. 109. Also since the effective total length for Mode B is shorter, Mode B should have a lower cutoff.

Mode A

Again for Mode A, a low-density region is established near the trigger spark and electron avalanches are started in this region. The electrons are then swept into anode leaving a positive ion space charge region near the anode. As the low-density region progresses toward the main electrode, the positive space charge also progresses. Out in the main gap, photoelectrons generated by the trigger spark are swept into the low-density region and will produce further avalanches. The resulting electrons then proceed into the anode leaving an increased positive space charge behind. The field strength ahead of the advancing low-density region then builds up to a sufficient value so that a positive streamer bridging the main gap via the probe is obtained. This type of trigger mechanism would suggest that Mode A would be easier to trigger, since it would utilize the generated photoelectrons more effectively than when the main electrode was positive. This is borne out in experiment where the streamer mechanism is generally accepted to be operating (pd $>$ 150 mm Hg cm). However, for the general region discussed in this paper, the reverse cutoff order appears to be true. It would appear then that for values of pd $<$ 150 mm Hg cm, the Mode A trigger mechanism occurs at higher gap voltage because of the reduction of photoelectron generation at the lower gas pressures which causes this mechanism to be less effective, and the onset of the streamer, if one occurs, does not occur until the higher gap voltages are applied. When it does occur it should be more rapid than in Modes B and C. The fact that the cutoff voltage is statistical indicates that the process of triggering for Mode A is subjected to a more random process than is the cathode extension condition of Mode B and C. In the absence of an efficient number of electrons to feed into the advancing low-density region, and for long gap spacings where the low-density region peters out before crossing the gap, the space charge field fails to build up to a sufficient value to cause breakdown and no triggering occurs.

Mode D

The trigger mechanism of Mode D is essentially that of Mode A and follows the same pattern. For a small trigger electrode hole, the cutoff appears to be independent of probe polarity since the cutoff voltage remains the same for both Mode A and Mode D over the same range of pd products. When the trigger electrode hole is large Mode D cutoff is essentially unchanged, but Mode A cutoff becomes much lower and approaches the cutoff of Mode C. Sletten and Lewis have observed the same order of cutoff between Modes A and D, and suggest that in the region of cutoff where the attainment of adequate ionization for the beginning of a streamer in the deteriorating low-density region is difficult, that it is possible for the electron emission from the hot trigger cathode to inhibit this further. Conditions are then more favorable when the probe is positive because of the absence of electron emission. If the probe to trigger electrode spacing is small, there is no difference between Mode A and Mode D because of the proximity of the trigger cathode to the trigger anode where electron emission from either electrode inhibits development of the streamer. If the probe to trigger electrode spacing is large, Mode D is still unchanged since the probe is negative. However in Mode A, the probe is positive and the cutoff is consequently lowered because the streamer may still form in a region away from the hot trigger cathode.

Probe-to-Main Electrode Spark

In addition to the previous four possible triggering conditions, there are two additional possibilities when the trigger spark forms across the gap to the main electrode due to the aiding field's characteristic of Modes A and B.

Mode A

When the trigger spark forms to the main electrode, the main electrode becomes the common cathode spot for both the trigger spark and the main spark, and a trigger mechanism occurs similar to the plasma-like extension of the cathode discussed for Mode C operation. The trigger spark generates a low-density region that propagates radially outward from the trigger spark core. Electron avalanches then occur in this region, space charges arise, and with a hot trigger cathode, the cathode extension moves toward the trigger electrode behind the low-density region front. When the effective spacing and density becomes sufficiently reduced, the remainder of the gap then breakds down in the normal manner. The main spark may move directly toward the trigger electrode or it may move partly up the trigger spark and then over to the trigger electrode. In this method of main spark formation there may be a finite time delay, but it is usually much lower than Mode C.

If the gap voltage is high enough, the main spark may form by breaking down to the probe which after forming to the main electrode is now at main electrode potential. After breaking down to the probe, the main spark now breaks down to the main electrode over the previously ionized path of the trigger spark. The delay time for this sequence of events is of course very rapid (less than 0.1 μsec) for relatively low applied gap voltages.

Mode B

The operation for Mode B is essentially the formation of an L-shaped discharge due to the overstressing of the probe to trigger electrode gap after the trigger spark has formed to the main electrode. The time delay for this sequence is also very short. It should also be pointed out that operation in Mode A or B, where the trigger spark forms to the main electrode, allows the main gap capacitor to sustain the trigger spark after the original trigger spark has ceased, therefore enhancing triggering.

Conclusions

This paper has presented a more extensive study into the characteristics of the triggered spark gap in the holdoff voltage range from 3 to 10 kv than has been available to date. Considerable quantitative data have been presented to aid the engineer in the designing of the triggered spark gap for use as a circuit component, or as a laboratory tool. Much new qualitative data have been presented to further advance the theory of operation, and a suggested theory of the trigger mechanism has been given that incorporates and generally agrees with earlier suggestions reviewed from the literature.[4,2,16] There is still a need to obtain more data concerning geometry effects and the paths of the trigger spark and main spark, with their resultant influence on the cutoff voltage.

LIST OF REFERENCES

1. Craggs, J. D., Haine, N. E., and Meek, J. M., Proc IEE, Vol. 93, Part IIIA, p. 963, 1946.

2. Broadbent, T. E., British Journal of Applied Physics, Vol. 8, p. 37, January 1957.

3. Cullington, E. H., Chace, W. G., and Morgan, R. L., Electronics engineering edition Vol. 31, No. 15, p. 86, April 11,1958.

4. Gonz, J., and Goldberg, J., unpublished reports of Edgerton, Germeshausen, and Grier, Inc., under Sandia Corporation Contract 14-0850.

5. Kleen, Werner, Translation from Annalen der Physik, 1931.

6. Bethge, O., Translation from Annalen der Physic, 1931.

7. Zarem, A. M., Marshall, E. R., and Poole, F. L., Physical Review 72, p. 158, 194

8. Burkhardt, L. C., Dunaway, R. E., Mather, J. W., Phillips, J. A., Sawyer, G. A., Stratton, T. F., Stovall, Jr., E. J., and Tuck, J. L., Journal of Applied Physics, Vol. 28, No. 5, p. 519, May 1957.

9. Johnstone, J. H., Tele-Tech and Electronic Industries, August 1956.

10. Anderson, O. A., Baker, W. R., Colgate, S. A., Ise, Jr., J., and Pyle, R. V., Physical Review, Vol. 110, No. 6, June 15, 1958.

11. Llewellyn - Jones, F., Ionization and Breakdown in Gases, John Wiley and Sons, Inc. New York, 1957.

12. Meek, J. M., and Craggs, J. D., Electrical Breakdown of Gases, Oxford at the Clarendon Press, 1953.

13. Peek, F. W., Dielectric Phenomena in High-Voltage Engineering, McGraw-Hill Book Co., 1929.

14. Wheatcroft, E. R. E., Gaseous Electrical Conductors, Oxford at the Clarendon Press 1938.

15. Thomson, J. J., and Thomson, G. C., Conduction of Electricity Through Gases, Vol. 2, p. 506.

16. Sletten, A. M., and Lewis, T. J., Proceeding IEE, Vol. 104, Part C, pp. 54-61, August 1956.

17. Cobine, J. D., Gaseous Conductors, Dover Publications, Inc., New York, 1958.

LIST OF REFERENCES (continued)

18. Williams, T. J., Sandia Corporation Tech Memo 341-57(14), January 1958.

19. Williams, T. J., Sandia Corporation Tech Memo 85-58(14), April 1958.

20. Williams, T. J., Sandia Corporation Tech Memo 46-56(14), April 1956.

21. Israelsohn, J. M., EG&G Report No. 1641, performed on Sandia Corporation Contract 13-0542, July 1957.

22. Broadbent, T. E., and Wood, J. K., British Journal of Applied Physics, Vol. 6, p. 368, October 1955.

23. Glasoe, G. N., and Lebacqz, J. V., Pulse Generators, McGraw-Hill Book Co., Inc., New York, 1948.

ELECTRON DEVICES TID-4500 (14th Ed.)

	No. of Copies
Air Force Special Weapons Center	2
Albuquerque Operations Office	1
Armed Forces Special Weapons Project, Sandia	2
Bureau of Yards and Docks	1
Iowa State College	1
Massachusetts Institute of Technology	1
National Academy of Sciences	1
Naval Research Laboratory	3
National Academy of Sciences, Office of Technical Services, Washington	75
Rensselaer Polytechnic Institute	1
South Dakota School of Mines and Technology	1
Technical Information Service Extension, Oak Ridge	325
	414

DISTRIBUTION:
Dr. R. K. Moore, UNM (3)
H. Wallace, EG&G
L. Woolever, EG&G
S. Goldberg, EG&G
H. S. Dunkerly, GE, Schenectady
A. F. Bischoff, GEXM
R. F. Ling, GEXF
D. E. Marshall, Westinghouse, Elmira
P. A. Oddo, Bendix, Red Bank
C. J. Morris, Bendix, Kansas City
J. W. McQueen, GMX-7, LASL
E. H. Draper, 1200
L. D. Smith, 1260
G. H. Mauldin, 1263
R. A. White, 1263-1
L. A. Hopkins, Jr., 1400
T. S. Church, 1410
R. T. DePew, 1411
R. Creveling, 1413-2
H. E. Lenander, 1450
R. C. Reineke, 1451
T. J. Williams, 1451-2 (8)
W. T. Price, 2542
B. E. Arthur, 2543
J. H. Findlay, 5500
G. E. Hansche, 5130
R. S. Claasen, 5150
L. Gutierrez, 8140
W. C. Scrivner, 8150
C. R. Barncord, 8160
R. E. Dewhurst, 8233
R. K. Smeltzer, 4721-3
W. F. Carstens, 4723
T. F. Lonz, 4761-1 (10)

SECOND REPRINTING:
OTS (25)
R. C. Smelich, 3446-1 (5)

THIRD REPRINTING:
R. C. Smelich, 3446-1 (25)